

**CONTRACTED PHTHALOCYANINE MACROCYCLES**  
**Conjugation with Nanoparticles and the first synthesis of**  
***meso*-substituted Boron SubTriBenzoDiAzaPorphyrin Hybrids**  
**(SubTBDAPs)**



**Sonia Remiro Buenamañana**

A thesis submitted in fulfilment of the requirements for the degree of Doctor of Philosophy

**School of Chemistry**

**University of East Anglia, Norwich, United Kingdom**

**2015**

©This copy of the thesis has been supplied on condition that anyone who consults it is understood to recognise that its copyright rests with the author and that use of any information derived there from must be in accordance with current UK Copyright Law. In addition, any quotation or extract must include full attribution.

## **Declaration**

The research described in this thesis is, to the best of my knowledge, original except where due reference is made.

Sonia Remiro Buenamañana

**This thesis is dedicated to my beloved parents**

**Ismael Remiro Sastre and M<sup>a</sup> Teresa Buenamañana Sánchez-Migallón**

## Abstract

The first part of this thesis is concerned with the attachment of subphthalocyanines to quantum dots. The macromolecule was chosen as encapsulant due to its perfect curvature and interesting optical properties. CdSe quantum dots are well-known materials with size-dependent properties that makes them unique. Hence, some subphthalocyanines bearing functional groups with affinity for the CdSe surface were synthesised by means of cross-coupling reactions. Small nanoparticle size (2.6 nm) quantum dots have been synthesised, capped with a layer of oleic acid molecules that confers them stability, and characterised by means of UV-Vis, emission and NMR spectroscopies. The original ligands were replaced by ligand exchange processes monitored by  $^1\text{H}$ -NMR spectroscopy. The experiments consist of titrations of CdSe-OA solutions with known concentrations of the new ligand. In this work, titrations using 3-ethynylpyridine, benzyl alcohol and phenylacetic acid have been performed. Parallel results in our group, involving the herein synthesised subphthalocyanine bearing pyridyl – groups, towards the attachment to the nanoparticle's surface are also described. Subphthalocyanine bearing three carboxylic acids is demonstrated to be the most promising candidate for this project. However, attempts to synthesise such a molecule by direct approach strategies were unsuccessful. Experiments with sodium periodate-subphthalocyanine conjugates gave promising and encouraging results, opening the possibility of accessing subphthalocyanines with carboxylic acid groups by means of deprotecting silyl groups.

The second part of this thesis is based on the results obtained towards the first syntheses of hybrid structures whose structure lies between subphthalocyanines and subporphyrins, SubTriBenzoDiAzaPorphyrins (SubTBDAPs). The key intermediates are aminoisoindolene precursors that provide the methine bridge, and substitution with the *meso*-phenyl ring. Boron trichloride has been used in a two-step, one-pot reaction in a preliminary strategy to give access to the hybrids. However, trialkoxyborates are the preferred boron source; they provide the apical substituent, as well as act as Lewis acid and template. The latter synthesis is versatile and gives modest yields and highly pure materials, but most importantly allows control over the apical and the *meso*-substituents in one single step. The new hybrids exhibit interesting optical and rotational characteristics that have been fully investigated by means of UV-Vis, emission, NMR spectroscopies, variable temperature experiments and mass spectrometry. In this work the first crystal structures elucidated for a wide range of new hybrids are also presented.



## Acknowledgements

First of all I would like to thank my supervisor and mentor Prof Andrew N. Cammidge for his constant guidance, support and help during my PhD. He has encouraged me during all these years not only professionally but personally. One of the many things that I have learnt from him is that the most precious resource in research as well as in life, is time. I will always be grateful not only for his patience, but also his kindness, expertise and care. An excellent example of how a leader should be.

I would like to thank Prof Manfred Bochmann for his advice as my second supervisor and Prof David Russell for providing me with the necessary laboratory facilities and instrumentation. I must also thank UEA for funding these projects.

I am also thankful to Dr Colin MacDonald for his valuable help and advice with NMR spectroscopy. Dr David L. Hughes at UEA and, Dr G. J. Tizzard and Dr S. J. Coles at the UK National Crystallography Service are also acknowledged for collection and analysis of X-Ray data. I am also grateful to the EPSRC for mass spectrometry analysis and Prof P. Ballester for help with calculations.

I am also very grateful to Dr Alejandro Díaz Moscoso, Dr Isabelle Chambrier, Dr María Marín Altaba, Dr Hemant Gopee and Dr Teresa Quirós for their dedication, their endless help, the useful discussions, and most importantly their friendship. At UEA I must also thank all my friends and colleagues from lab 3.17 (past and present members) who have made these years unforgettable. Xiao, Rhoda, Tahani, Ateyah, Ross you have made my days (and nights) in lab very enjoyable and I will miss you! I would like to mention all colleagues from the organic department who have been fantastic and have made possible a wonderful environment.

I wish to thank all my friends (who are now more like family to me) from Norwich, especially Jay, Hanae, Flavia, Desi, Paulina, Aiste, Davide and my bros César and Victor, despite distance you will always have a place in my heart. It has been a pleasure to share so many good moments with you all. Also my friends from Spain who have supported me and have always believed in me, in particular, Raquel, Óscar, Pablo, Marta and Patri for being always there.

My deepest gratitude to all my family for their love, despite the big sacrifice that distance meant for all of us, they have always supported me and encouraged me to aim high, to give the best of myself and to follow my dreams. Especially my parents, who have sacrificed everything in life for us and to whom I owe everything. My sister and brother, Laura and Javier, have my gratitude for their unconditional love and support. A reminder to the ones that will see me ending this journey from a very especial place, my guardian angels, who would have been very proud (Alfonso, Currito, Teresa, Sole, Josefina, Emi).

I finally thank Dani for his love, help and for always believing in me. I could not have accomplished this PhD without him by my side. He guided me, encouraged me, and made me laugh and happy every single day, even during hard times. I feel very lucky for having shared this journey with him.

## Table of Contents

Declaration.....	I
Dedication.....	II
Abstract.....	III
Acknowledgements.....	IV
Table of Contents.....	V
List of Figures.....	IX
List of Schemes.....	XIV
List of Tables.....	XVIII
Abbreviations.....	XIX
Chapter 1: INTRODUCTION and AIMS – Porphyrinoids and Quantum Dots.....	1
1.1 Aims.....	1
1.2 Porphyrinoid Family.....	3
1.2.1 Porphyrins.....	3
1.2.2 Phthalocyanines.....	4
1.2.3 Properties and applications of Ps and Pc.....	6
1.2.4 Ring modifications.....	7
1.2.4.1 Subphthalocyanines.....	9
Selectivity in SubPc synthesis.....	10
Properties and applications.....	11
Latest advances.....	13
1.3 Nanoparticle Assembly.....	14
1.3.1 Quantum dots.....	14
1.3.1.1 CdSe nanocrystals.....	16
1.3.2 Hybrid nanoassemblies: Organic chromophores – QDs.....	17
1.3.2.1 QDs – Porphyrins.....	17
1.3.2.2 QDs – Phthalocyanines.....	19
1.3.2.3 QDs – Subphthalocyanines.....	20

Chapter 2: RESULTS and DISCUSSION.....	23
2.1 CdSe Nanoparticles.....	23
2.1.1 Synthesis.....	23
2.1.2 Characterisation.....	26
2.2 Subphthalocyanines.....	31
2.2.1 Surfactant design for ligand exchange purposes.....	31
2.2.2 Synthesis.....	32
2.2.2.1 Mechanism for SubPc formation.....	34
2.2.2.2 Reactivity.....	36
a) Ring expansion.....	36
b) Axial functionalisation.....	37
c) Peripheral functionalisation.....	38
2.2.2.3 Peripherally functionalised SubPcs.....	40
Sonogashira-Hagihara cross-coupling.....	41
Suzuki-Miyaura cross-coupling.....	48
2.2.3 Optical properties.....	50
2.3 Nanoparticle Conjugation.....	53
2.3.1 CdSe - 3-pyridyl SubPc QDs.....	53
2.3.2 NMR titrations.....	54
2.3.2.1 Analysis of 3-ethynylpyridine.....	55
2.3.2.2 Analysis of benzyl alcohol.....	57
2.3.2.3 Analysis of phenylacetic acid.....	59
2.3.3 Synthesis towards tricarboxylic acid - SubPc.....	60
2.3.3.1 Design of a suitable SubPc encapsulant.....	60
2.3.3.2 Literature survey.....	61
2.3.3.3 Direct cross-coupling strategy.....	62
2.3.3.4 Protected SubPc approach.....	64
2.4 Conclusions.....	71

Chapter 3: SubTriBenzoDiAzaPorphyrins (SubTBDAPs).....	72
3.1 Introduction.....	72
<i>Phthalocyanine – Porphyrin: tetrabenzoazaporphyrins</i>	
3.1.1 TBTAPs: tetrabenzotriazaporphyrins.....	74
3.1.1.1 <i>meso</i> -Substituted TBTAPs.....	76
3.1.1.2 Properties and applications.....	79
<i>Subphthalocyanine – benzoSubPorphyrins: SubTBDAPs hybrids</i>	
3.1.2 Aim of the project.....	81
3.1.3 Subporphyrins (SubPs).....	83
3.1.3.1 Reactivity and properties.....	84
3.1.3.2 Triphyrins: The exception.....	86
3.1.4 Benzosubporphyrins (BzSubPs).....	87
3.1.4.1 Properties.....	88
3.2 Results and Discussion.....	91
3.2.1 First steps.....	91
3.2.2 Optimisation of the conditions.....	98
3.2.3 Preliminary characterisation of SubTBDAP-OPh <b>134</b> .....	100
3.2.3.1 X-Ray diffraction.....	100
3.2.3.2 <sup>1</sup> H-NMR spectroscopy.....	101
Variable temperature experiments.....	102
3.2.3.3 Optical properties.....	107
3.2.4 Towards a more efficient SubTBDAP synthesis.....	108
3.2.4.1 Boron source - BORATES.....	108
3.2.4.2 Screening the conditions.....	111
3.2.4.3 Scope of the protocol.....	113
Apical functionalisation.....	113
Functionalisation at the new <i>meso</i> -site.....	117
Controlled synthesis of azaBODIPY derivatives.....	123

3.2.4.4 Preliminary mechanism study and an interesting intermediate..	126
3.2.4.5 Properties of SubTriBenzoDiAzaPorphyrins.....	129
Photophysical properties.....	129
Nuclear magnetic resonance.....	132
DFT calculations.....	135
3.3 Conclusions.....	135
Chapter 4: Experimental.....	137
4.1 General Methods.....	137
4.2 Fluorescence Quantum Yield.....	137
4.3 General procedures for the synthesis of SubPcs.....	138
4.4 Experimental details and characterisation: SubPc - CdSe project.....	139
4.5 Experimental details and characterisation: SubTBDAP project.....	157
4.5.1 Aminoisindolene precursors.....	157
4.5.2 SubTBDAPs.....	163
4.5.3 BODIPYs.....	173
4.5.4 X-Ray data.....	175
4.5.5 DFT calculations.....	183
References.....	185
Appendix - Publication.....	193

## List of Figures

Figure 1: Depiction of SubPc 3D structure.....	2
Figure 2: Controlled assembly of 1D hetero-nanoparticle arrays.....	2
Figure 3: Parent structures porphyrin <b>1</b> and phthalocyanine <b>2</b> .....	3
Figure 4: Absorption spectra of a) H <sub>2</sub> Ps, b) MPs, c) H <sub>2</sub> Pcs, and d) MPcs.....	6
Figure 5: Some examples of expanded porphyrins.....	8
Figure 6: Extended naphthalocyanine <b>10</b> , and expanded superphthalocyanine <b>11</b> .....	8
Figure 7: Ring contracted systems.....	9
Figure 8: I-SubPc-Cl <b>20</b> and its corresponding computational model (right) performed by Sigismund Melissen at the University of Rouen.....	12
Figure 9: Absorption (blue line) and emission spectra (pink line) of phenoxy- SubPc <b>21</b> .....	12
Figure 10: 3-Dimensional views of the SubPc macrocycle, and head-to-tail stacking into polarised columnar structures.....	14
Figure 11: Molecules that constituted the organic solar cell.....	14
Figure 12: (a) Energy bands of bulk semiconductor showing the continuity of conduction and valence band separated by a bandgap, $E_g$ . (b) For QD, the continuous bands become discrete atomic states with energies determined by the size of the nanoparticle.....	15
Figure 13: (Top) Change of photoluminescence (PL) emission colour with size for CdSe QDs excited under 365 nm lamp.(Bottom) Photoluminescence spectra of some CdSe QDs.....	16
Figure 14: (a) Face-on, and (b) face-off binding of the porphyrin to the nanoparticle surface.....	18
Figure 15: Proposed mechanism for the degradation of RhB catalysed by porphyrin-functionalised CdS nanocomposites under exposure to solar light.....	19
Figure 16: Structures of 1,2-dithiolane functionalised SubPcs <b>31</b> , <b>32</b> and <b>33</b> (top), and representation of the monolayers on a gold surface (bottom).....	22
Figure 17: UV-Vis spectra of CdSe nanocrystals, the label describes the absorption maxima and the calculated sizes.....	25
Figure 18: Emission spectra of various sizes CdSe nanoparticles, the label depicts emission maxima in nm.....	25
Figure 19: Absorption spectrum of CdSe QDs and representation of the HWHM.....	26
Figure 20: Photoluminescence spectrum, and TEM image of 2.68 nm averaged size CdSe nanoparticles.....	26

Figure 21: Free and bound oleic acid <sup>1</sup> H-NMR spectra.....	28
Figure 22: Integration of the ferrocene reference against the double bond protons of OA.....	29
Figure 23: Oleic acid performed on Chimera 1.9 software.....	30
Figure 24: Computational model of (2-pyridyl) <sub>3</sub> -SubPc-OPh <b>34</b> .....	31
Figure 25: Computational model of (3-pyridyl) <sub>3</sub> -SubPc-OPh <b>35</b> .....	32
Figure 26: Computational model of (Ph-CH <sub>2</sub> OH) <sub>3</sub> -SubPc-OPh <b>36</b> .....	32
Figure 27: <sup>1</sup> H-NMR of the by-product isolated during the SubPc formation.....	34
Figure 28: <sup>1</sup> H-NMR spectrum of I-SubPc-OPh <b>41</b> .....	40
Figure 29: MALDI-TOF spectrum of SubPc <b>41</b> .....	40
Figure 30: <sup>1</sup> H-NMR comparison before (A) and after (B) treatment of SubPc <b>22</b> with EDTA.....	44
Figure 31: <sup>1</sup> H-NMR of SubPc <b>35</b> .....	45
Figure 32: <sup>1</sup> H-NMR comparison before (A) and after (B) treatment of compound <b>48</b> with EDTA.....	47
Figure 33: UV-Vis spectra of axially substituted SubPcs <b>16</b> , <b>21</b> and <b>73</b> in dichloromethane.....	51
Figure 34: UV-Vis spectra of compounds <b>35</b> , <b>41</b> , <b>47</b> and <b>48</b> in dichloromethane.....	51
Figure 35: Absorption and emission spectra of (Ph-CH <sub>2</sub> OH) <sub>3</sub> -SubPc-OPh <b>36</b> .....	52
Figure 36: A) Experimental trend of some peripherally substituted SubPcs. B) Corresponding fluorescence spectra.....	53
Figure 37: The <sup>1</sup> H-NMR signal for alkene protons of OA capped CdSe QD upon addition of ODPa.....	55
Figure 38: Progress of the oleate proton signal on the <sup>1</sup> H-NMR upon addition of 3-ethynylpyridine.....	55
Figure 39: <sup>1</sup> H-NMR progression upon addition of pyridine derivative.....	56
Figure 40: Evolution of the alkene protons regions of the OA ligand upon addition of up to 20 equivalents of pyridine derivate.....	56
Figure 41: Progress of the <sup>1</sup> H-NMR spectra upon addition of 20 equivalents of 3-ethynylpyridine and comparison with the free ligand and unbound OA.....	57
Figure 42: Representation of the alkene signal upon addition of benzyl alcohol.....	58
Figure 43: <sup>1</sup> H-NMR spectra of the titration process of CdSe-OA with a solution of benzyl alcohol.....	58
Figure 44: Changes in the alkene protons of the OA upon addition of phenyl acetic acid.....	59

Figure 45: <sup>1</sup> H-NMR progression after additions of phenylacetic acid to CdSe nanoparticles.....	59
Figure 46: Representation of the QD – 3-pyridyl SubPc hypothetical conjugate.....	60
Figure 47: Computational model of the SubPc target compound <b>55</b> performed with Chimera 1.9.....	61
Figure 48: Different SubPc derivatives synthesised by Torres and colleagues.....	62
Figure 49: <sup>1</sup> H-NMR of pinacol boronic ester derivative <b>71</b> .....	66
Figure 50: MALDI-TOF spectrum of SubPc <b>69</b> .....	67
Figure 51: Structures of Pc, TBP and the hybrid macrocycles.....	72
Figure 52: Porphyrin <b>3</b> and tetrabenzoporphyrin (TBP) <b>77</b> structures.....	73
Figure 53: UV/Vis absorption spectra of the magnesium-metallated compounds Pc <b>95</b> , TBTAP <b>85</b> , <i>cis</i> -TBDAP <b>86</b> , TBMAP <b>87</b> , and TBP <b>88</b> in THF.....	80
Figure 54: Structures of nickel Pc and nickel TBTADAP.....	81
Figure 55: A representation of the desired hybrid compound's computational model, performed with Chimera 1.9 software, and parent macrocycles of the new hybrid.....	83
Figure 56: UV-Vis (solid lines) and emission (dashed lines) spectra of SubP-OMe <b>105</b> (red) and ZnTPP <b>107</b> (black).....	86
Figure 57: (Left) UV-Vis (black line) and emission (blue) spectra of OMe <b>113</b> in MeOH. (Right) picture of the green fluorescence of <b>113</b> irradiated at 355 nm.....	88
Figure 58: Absorption (solid line) and emission spectra (dashed line, upon excitation at 480 nm) of <b>118</b> in dichloromethane.....	89
Figure 59: Crystal structure of BzSubP-OH <b>112</b> (left) and BzSubP-SiPh <sub>3</sub> <b>120</b> (right).....	89
Figure 60: <sup>1</sup> H-NMR spectrum of phenyl isoindolene <b>131</b> in d <sub>6</sub> -DMSO.....	92
Figure 61: MALDI-TOF spectrum of the isolated SubPc-Cl <b>16</b> during the SubTBDAP formation and corresponding fragmentations.....	94
Figure 62: (Top) MALDI-TOF spectrum of the crude mixture depicting SubTBDAP-Cl <b>99</b> mass and its corresponding fragmentations. (Bottom) Theoretical and experimental isotopic pattern.....	95
Figure 63: (Left) Boron dipyrromethene (BODIPY) parent structure, with positions for further modification indicated, and aza-(dibenzo)BODIPY derivatives synthesised in our group (right).....	97
Figure 64: Absorption (red) and emission (green) spectra of the new BODIPY <b>135</b> formed as side product.....	98



Figure 65: Crystal structure of SubTBDAP-OPh <b>134</b> with a hydrogen-bonded water molecule. Thermal ellipsoids are drawn at the 50% probability level (left). View of the dimer unit (right), optimised structure by Dr David Hughes at UEA.....	100
Figure 66: <sup>1</sup> H-NMR spectrum of SubTBDAP <b>134</b> in CDCl <sub>3</sub> at 298K.....	101
Figure 67: Plane of symmetry in SubTBDAP macrocycle.....	102
Figure 68: Variable temperature <sup>1</sup> H-NMR spectra of hybrid <b>134</b> in CD <sub>2</sub> Cl <sub>2</sub> .....	103
Figure 69: Variable temperature COSY of hybrid <b>134</b> at 263K in CD <sub>2</sub> Cl <sub>2</sub> .....	104
Figure 70: Variable temperature NOESY of hybrid <b>134</b> at 263K in CD <sub>2</sub> Cl <sub>2</sub> .....	105
Figure 71: Estimated distances between <i>meso</i> - and apical rings with the phenoxy-ring lying completely perpendicular to the core.....	106
Figure 72: Picture of same fraction of a column chromatography under normal and UV light.....	107
Figure 73: Absorption and emission spectra of hybrid SubTBDAP-OPh <b>134</b> and SubPc-OPh <b>21</b> in dichloromethane.....	108
Figure 74: Borane derivatives employed in subporphyrin synthesis.....	109
Figure 75: <sup>1</sup> H-NMR of SubTBDAP-OMe <b>133</b> in CD <sub>2</sub> Cl <sub>2</sub> at 263K.....	114
Figure 76: Crystal structure of SubTBDAP-OMe <b>133</b> .....	115
Figure 77: Variable temperature <sup>1</sup> H-NMR of SubTBDAP-O <i>i</i> Pr <b>139</b> at 263K in CD <sub>2</sub> Cl <sub>2</sub> .....	116
Figure 78: X-Ray structure of SubTBDAP-O <i>i</i> Pr <b>139</b> showing two conformations of the isopropoxide-substituent.....	116
Figure 79: Crystal structure of SubTBDAP-OBu <b>140</b> .....	117
Figure 80: Expansion of <sup>13</sup> C-NMR spectrum of aminoisindolene-CF <sub>3</sub> <b>143</b> .....	119
Figure 81: Crystal structure of aminoisindolene <b>145</b> .....	119
Figure 82: Full VT <sup>1</sup> H-NMR spectrum of OMe-SubTBDAP-OMe <b>146</b> in CD <sub>2</sub> Cl <sub>2</sub> at 263 K (bottom) and expansion of the selected regions (top).....	121
Figure 83: VT COSY experiment showing cross peaks between <i>meso</i> -phenyl protons in hybrid <b>146</b> .....	121
Figure 84: Crystal structure of OMe -SubTBDAP-OMe <b>146</b> , where the phenyl group is tilted into two different conformations.....	122
Figure 85: Crystal structure of pyrenyl-azaBODIPY-OPh <b>151</b> . Three different views: (a) side, (b) top, and (c) front.....	125
Figure 86: UV-Vis and Emission spectra (exc. 490 nm) of pyrenyl-BODIPY-OPh <b>151</b> .....	126

Figure 87: MALDI-TOF spectrum showing the parent ion peak of trimer <b>152</b> .....	127
Figure 88: Crystal structure of trimer <b>152</b> showing hydrogen bond between N1–H1...N3.....	128
Figure 89: Structure of [6]helicene <b>153</b> and enantiomers.....	128
Figure 90: Comparison UV-Vis spectra of trimer <b>152</b> and dimer <b>138</b> in dichloromethane.....	129
Figure 91: Absorption and Emission spectrum of SubTBDAP-OMe <b>133</b> .....	130
Figure 92: Structure Rhodamine B and absorption and emission spectrum in MeOH.....	131
Figure 93: General R'-SubTBDAP-OR showing the assignment of the <i>meso</i> -protons regarding the shape of the hybrid.....	133
Figure 94: VT <sup>1</sup> H-NMR comparison of SubTBDAP hybrids in CD <sub>2</sub> Cl <sub>2</sub> at 263K. The legend describes the substitution of the molecule (axial, <i>meso</i> ) and the number of compound.....	134
Figure 95: Structure of capped subporphyrin <b>154</b> and its crystal structure.....	134
Figure 96: Theoretical chemical shift values calculated by DFT performed on SubTBDAP-OMe <b>133</b> (red), and experimental values (blue).....	135

## List of Schemes

Scheme 1: Adler and Longo synthetic route for the formation of <i>meso</i> -substituted porphyrins.....	4
Scheme 2: General procedure for symmetrical Pc formation .....	5
Scheme 3: The first synthesis of SubPc-Cl <b>16</b> .....	10
Scheme 4: Synthesis of I-SubPc-Cl <b>20</b> , showing the regioisomers <b>17</b> and <b>18</b> , and the corresponding enantiomers.....	10
Scheme 5: QD – Porphyrin conjugate which acts as oxygen sensor.....	18
Scheme 6: Self-assembly of SubPc metallosupramolecular cages.....	21
Scheme 7: Encapsulation of C <sub>60</sub> in the cage.....	21
Scheme 8: Most common synthetic routes to obtain CdSe nanoparticles.....	24
Scheme 9: The synthetic route followed in this work.....	24
Scheme 10: Synthesis of unsubstituted SubPc <b>16</b> .....	33
Scheme 11: First stage in the mechanism of SubPc formation and hydrolysis products.....	35
Scheme 12: Ring closing and reduction to achieve SubPc-Cl <b>16</b> .....	35
Scheme 13: Free-radical chain reaction during the reaction of SubPc formation under light.....	36
Scheme 14: Main SubPc functionalisation routes.....	37
Scheme 15: Synthesis of I-SubPc-Cl <b>20</b> .....	39
Scheme 16: Synthesis of phenoxy-SubPc <b>41</b> and appearance of the product.....	39
Scheme 17: Stephens and Castro cross-coupling reaction.....	41
Scheme 18: Basic representation of Sonogashira cross-coupling reaction.....	41
Scheme 19: Mechanism of Sonogashira cross-coupling reaction.....	42
Scheme 20: Synthesis of 2-Ethynylpyridine <b>45</b> .....	42
Scheme 21: Synthesis of (2-pyridyl) <sub>3</sub> -SubPc-OPh <b>34</b> .....	43
Scheme 22: Synthesis of (3-pyridyl) <sub>3</sub> -SubPc-OPh <b>35</b> .....	45
Scheme 23: Reaction pathway for the synthesis of (3-pyridyl) <sub>3</sub> -SubPc-(4-F-OPh) <b>48</b> .....	46
Scheme 24: Reaction path for the formation of (Ethynyl) <sub>3</sub> -SubPc-OPh <b>50</b> .....	47
Scheme 25: Suzuki-Miyaura coupling reaction and simplified catalytic cycle.....	48
Scheme 26: Synthesis of (Ph-CH <sub>2</sub> OH) <sub>3</sub> -SubPc-OPh <b>36</b> .....	49

Scheme 27: Synthetic conditions for the synthesis of (Ph-CN) <sub>3</sub> -SubPc-OPh <b>53</b> and (thiophenyl) <sub>3</sub> -SubPc-OPh <b>54</b> .....	50
Scheme 28: Two possible adsorption/ desorption mechanism.....	54
Scheme 29: Synthetic route to unsymmetrical SubPcs bearing a carboxylic acid at the periphery....	61
Scheme 30: Sonogashira reaction attempts with SubPc <b>20</b> and <b>41</b> and propiolic acid.....	63
Scheme 31: Suzuki coupling attempted reaction.....	63
Scheme 32: Retrosynthetic path towards protected (alkylCOOEt) <sub>3</sub> -SubPc-OPh <b>69</b> formation.....	64
Scheme 33: Esterification reaction of 11-bromoundecanoic acid.....	64
Scheme 34: Alkylation attempts to synthesise boronic acid <b>68</b> .....	65
Scheme 35: Synthesis of pinacol derivative <b>71</b> .....	65
Scheme 36: Suzuki-Miyaura cross-coupling between SubPc <b>41</b> and boronic ester <b>71</b> .....	66
Scheme 37: Synthesis of SubPc-(OPh-COOEt) <b>73</b> .....	67
Scheme 38: Hydrolysis test reactions performed with SubPc <b>74</b> .....	68
Scheme 39: Control experiments under deprotecting conditions. ....	69
Scheme 40: Protection step of 4-hydroxybenzoic acid as TIPS derivative <b>75</b> .....	69
Scheme 41: Synthesis of SubPc-(OPh-COOTIPS) <b>76</b> .....	70
Scheme 42: Deprotection step with sodium periodate.....	70
Scheme 43: Main synthetic routes for the synthesis of tetrabenzoporphyrins.....	73
Scheme 44: First syntheses of CuTBTAP <b>81</b> using phthalonitrile and different precursors.....	74
Scheme 45: Linstead's synthesis of MgTBTAP <b>82</b> .....	75
Scheme 46: a) Cammidge, Cook et al.'s octaalkyl-TBTAP <b>83</b> synthesis, and b) optimised synthesis of a series of tetrabenzozaporphyrin hybrids using varying equivalents of MeMgBr.....	75
Scheme 47: McKeown and Leznoff's synthesis of <i>meso</i> - aryl and alkyl-TBTAPs.....	77
Scheme 48: Synthetic path for the formation of <i>meso</i> -substituted TBTAPs.....	77
Scheme 49: Synthesis of <i>meso</i> -substituted TBTAPs <i>via</i> Grignard reagents, and subsequent functionalisation.....	78
Scheme 50: Synthetic path giving straightforward access to functionalised porphyrin-phthalocyanine hybrids.....	79
Scheme 51: Synthesis of <i>trans</i> -TBDAP.....	79

Scheme 52: (Route A) Optimised SubPc synthetic route. (Route B) Newly developed synthesis of TBTAPs in our group. (Route C) Synthetic strategy towards the target molecule: Hybrid Structure (SubTBDAP-Cl <b>99</b> ).....	82
Scheme 53: Kobayashi methodology for the synthesis of Subporphyrin <b>102</b> .....	83
Scheme 54: Different methodologies for subporphyrin synthesis.....	84
Scheme 55: Bromination of subporphyrin <b>104</b> and further functionalisation by means of cross-coupling reactions.....	85
Scheme 56: Hypothetical [14] triphyrin (1.1.1) <b>108</b> . Reported subpyriporphyrin <b>109</b> and reaction to give subporphyrin <b>110</b> .....	87
Scheme 57: First synthesis of BzSubPs by Osuka.....	87
Scheme 58: Synthesis of <i>meso</i> - phenyl BzSubPs by Kobayashi.....	88
Scheme 59: Published TBTAPs from our group following this protocol, and crystal structures of compounds <b>125</b> , <b>127</b> and <b>128</b> .....	91
Scheme 60: Two step synthesis of aminoisoindolene <b>131</b> .....	92
Scheme 61: Proposed copper-free Sonogashira cross-coupling reaction.....	93
Scheme 62: Proposed mechanism for the 5-exo-dig cycloisomerisation.....	93
Scheme 63: Synthesis of SubTBDAP-Cl <b>99</b> .....	94
Scheme 64: Two step, one-pot reaction for the formation of hybrid SubTBDAP <b>134</b> . Inset, highly coloured products under normal light (top) and the same compounds under irradiation with a 365 nm light (bottom) .....	96
Scheme 65: Unsuccessful attempts with boric acid and pinacol boronic ester.....	109
Scheme 66: Synthesis of SubTBDAP-OPh <b>134</b> using triphenyl borate, and side products.....	110
Scheme 67: Self-condensation reaction of aminoisoindolene <b>131</b> and crystal structure of dimer <b>138</b> .....	111
Scheme 68: Reaction attempts with dimer <b>138</b> towards the formation of SubTBDAP-type molecule.....	111
Scheme 69: Selective syntheses of SubTBDAP hybrids selectively functionalised at the apical position.....	113
Scheme 70: Reaction scheme for the formation of substituted aminoisoindolenes.....	117
Scheme 71: Versatile syntheses of SubTBDAP hybrid demonstrating selective functionalisation at the <i>meso</i> - and apical sites.....	120

Scheme 72: Controlled synthesis of azaBODIPY-OPh <b>135</b> under microwave irradiation.....	123
Scheme 73: Synthesis of pyrenyl-BODIPY <b>124</b> as Z –isomer.....	124
Scheme 74: Synthesis of pyrenyl-azaBODIPY-OPh <b>151</b> .....	125
Scheme 75: Reaction conditions and formation of intermediate <b>152</b> .....	127

## List of Tables

Table 1: Quantitative results regarding OA capping each nanoparticle.....	29
Table 2: Optical data for some subphthalocyanines.....	52
Table 3: Optimisation of the equivalents used in the reaction.....	99
Table 4: Different reaction conditions modified during the screening of the reaction; optimal conditions are highlighted.....	112
Table 5: Reaction of amidine <b>130</b> in conjunction with acetylenic precursors to form the products listed above and the corresponding yields obtained.....	118
Table 6: Summary of optical properties of SubTBDAPs.....	130
Table 7: Fluorescence quantum yields obtained for SubTBDAP hybrids.....	132
Table 8: <sup>11</sup> B-NMR chemical shifts of some SubTBDAP hybrids.....	132

## Abbreviations

A	absorbance
Abs	absorption
aq.	aqueous
a. u	arbitrary units
Å	Armstrong
Ar	aromatic/ aryl
asym	asymmetric
AFM	Atomic Force Microscopy
BzSubPs	Benzosubporphyrins
br	broad
NBS	N-bromosuccinimide
DCTB	2-[(2E)-3-(4-tert-Butylphenyl)-2-methylprop-2-enylidene]malononitrile
OBu	butoxy-
calc.	calculated
Ec	conduction band
COSY	Correlation Spectroscopy
DFT	Density Functional Theory
D	diameter
DABCO	1,4-Diazabicyclo[2.2.2]octane
DBU	1,8-Diazabicyclo[5.4.0]undec-7-ene
DDQ	2,3-Dichloro-5,6-dicyano-1,4-benzoquinone
DCM	dichloromethane
Et <sub>2</sub> O	diethylether
DME	1,2-dimethoxyethane
DMF	dimethylformamide
DMSO	dimethylsulfoxide
BINAP	2,2'-Bis(diphenylphosphino)-1,1'-binaphthalene



dppf	diphenylphosphinoferrrocene
dppp	diphenylphosphinopropane
dist.	distilled
d	doublet
dd	doublet of doublet
ddd	doublet of doublet of doublet
dt	doublet of triplet
DSSC	Dye-Sensitized Solar Cell
DLS	Dynamic Light Scattering
eT	electron transfer
eV	electron volt
Em	emission
E <sub>g</sub>	energy band gap
eq	equivalent
EtOAc	ethyl acetate
EDTA	ethylenediaminetetracetic acid
exc.	excitation
FET	Field-Effect Transistors
FT-IR	Fourier Transform-Infrared Spectroscopy
HWHM	half-width half-maximum
HDA	hexadecylamine
HPLC	High-Performance Liquid Chromatography
HOMO	Highest Occupied Molecular Orbital
HR	high resolution
ICP-OES	Inductively Coupled Plasma-Optical Emission Spectroscopy
IR	infrared
IQE	Internal Quantum Efficiency
<i>i</i> Pr	isopropyl-

<i>J</i>	coupling constant
K	Kelvin
LED	Light Emitting Diodes
LUMO	Lowest Unoccupied Molecular Orbital
MS	mass spectrometry
<i>m/z</i>	mass-to-charge
MALDI-TOF	Matrix Assister Laser desorption/ionisation-time-of-flight
M	metal
MeOH	methanol
OMe	methoxy-
MW	microwave
H <sub>2</sub> Pcs	metal-free phthalocyanines
H <sub>2</sub> Ps	metal-free porphyrins
MPcs	metallated phthalocyanines
MPs	metallated porphyrins
<i>m</i>	multiplet
NP	nanoparticle
NSI	NanoSpray Ionisation
Nc	naphthalocyanine
NMR	Nuclear Magnetic Resonance
NOESY	Nuclear Overhauser Effect Spectroscopy
<i>n.</i>	number
ODE	octadecene
ODPA	octadecylphosphonic acid
OA	oleic acid
OFETs	Organic Field Effect Transistors
OLEDs	Organic Light Emitting Diodes
OPV	Organic Photovoltaic

OTFT	Organic Thin Film Field-Effect Transistors
QDs	quantum dots
p	page
ppm	parts per million
nPe	<i>n</i> -pentyl-
PE	petroleum ether
PCBM	[6,6]-phenyl C <sub>61</sub> butyric acid methyl ester
OPh	phenoxy-
PDT	photodynamic therapy
PL	photoluminescence
Pcs	phthalocyanines
PCN	phthalonitrile
Ps	porphyrins
PCE	Power Conversion Efficiency
py	pyridine
QY	quantum yield
q	quartet
quat.	quaternary
RhB	rhodamine B
RT	room temperature
rpm	revolutions per minute
$\alpha$ -6T	$\alpha$ -sexithiophene
s	singlet
SEC	size exclusion chromatography
st	strong
SubNc	Subphthalocyanine
SubPc	Subphthalocyanine
SubPzs	SubPorphyrazines

SubPs	SubPorphyrins
SubTBDAP	SubTriBenzoDiAzaPorphyrin
sym	symmetric
TBDAP	TetraBenzoDiAzaPorphyrin
TBMAP	TetraBenzoMonoAzaPorphyrin
TBTAP	TetraBenzoTriazaPorphyrin
TBP	Tetrabenzoporphyrin
TBAF	tetra-n-butylammonium fluoride
TPP	TetraPhenylPorphyrin
THF	tetrahydrofuran
t	triplet
td	triplet of doublet
tt	triplet of triplet
TLC	Thin Layer Chromatography
TEM	Transmission Electron Microscopy
OTf	triflate
TFA	trifluoroacetic acid
TIPS	triisopropylsilyl
TMSBr	trimethylsilyl bromide
TOP	trioctylphosphine
TOPO	trioctylphosphine oxide
UV	ultraviolet
UV-Vis	ultraviolet-visible
VT	variable temperature
XPS	X-Ray Photoelectron Spectroscopy
XRD	Powder X-Ray Diffraction

## CHAPTER 1. INTRODUCTION and AIMS – Porphyrinoids and Quantum Dots

### 1.1 Aim of the project: *Subphthalocyanine - Nanoparticle self-assembly*

Nowadays chemists are achieving ever more control over the size, shape, composition and surface properties of nanocrystals, namely quantum dots (QDs). Latest advances in the field are pointing towards the development of "bottom-up" approaches utilising relatively simple building blocks. Understanding and engineering self-assembly<sup>[1]</sup> of nanoparticles could lead to multifunctional materials and devices, and application in different fields ranging from biomedical techniques to optoelectronic devices.<sup>[2], [3]</sup>

The controlled attachment of a known number of ligands, e.g. biomolecules, polymers, organic molecules, and chromophores, to these nanoparticles is a challenge in the field. Most of the publications in the literature are concerned with the inorganic core of the nanoparticle and the characterisation is mostly based on optical and physical techniques e.g. TEM, DLS, absorption and emission spectroscopies. Such techniques are not often enough to prove ligand binding to the surface of the nanocrystal, consequently the lack of investigation on this matter is a major drawback in the design of new nanomaterials with predetermined properties.

We are interested in developing a general protocol for generating QDs with one or two surface anchoring chromophores by exchange with the native ligands; the strategy focuses on the synthesis of small diameter (2-3 nm) nanoparticles. CdSe based nanoassemblies are perhaps the most studied systems because of their unique size-dependent properties, high extinction coefficients, high thermal and photochemical stability, and synthetic size and shape control of the particles.<sup>[4]</sup> In our general strategy, steric restriction on the maximum number of ligands on the surface is to be achieved by using large concave-shaped macrocyclic ligands.

The shape of the chosen surfactant plays the most important role on the design. Encapsulants with distinctly defined curvature, binding motifs, the possibility of peripheral functionalisation and a link-point for further assembly would be ideal.

We could consider calixarenes<sup>[5]</sup> for this aim; however their cylinder-shaped structure does not depict the right cavity size for our purpose, i.e. inner cavities of calix[4]arene, calix[6]arene, and calix[8]arene are 3.0 Å, 7.6 Å, and 11.7 Å, respectively. They are unsuitable also because they present too much conformational freedom, their syntheses are not straightforward, and the structures themselves offer few intrinsic interesting properties.

Due to its perfect curvature and remarkable optical properties, subphthalocyanine (SubPc) (Fig. 1) is the chosen molecule for this project. Moreover the synthetic versatility around the periphery allows defined binding geometries to be designed, the exotopic functionality opens the possibility of linking nanoparticles together in a parallel process (Fig. 2) to construct more complex and organised assemblies. From a synthetic point of view, the requirement is for subphthalocyanines

to have the appropriate functionality on the periphery in order to bind to the QD nanocrystal. The best ligands for surface attachment to CdSe will be discussed later on.

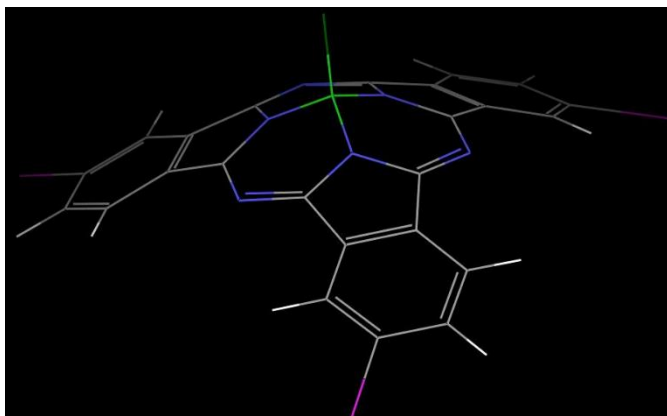


**Figure 1.** Depiction of SubPc 3D structure

In the long-term we envisage nanoparticles can be encapsulated and entrapment is then completed by chemical or photochemical reaction to lock the structure closed. In Figure 2 is an example where different nanoparticles are encapsulated in parallel processes leading to locked structures with complementary apical link-groups. –A-B-A-B-A-B- assembly is then assured in the final construction. In addition the concept could be simplified leading to homo-nanoassemblies.

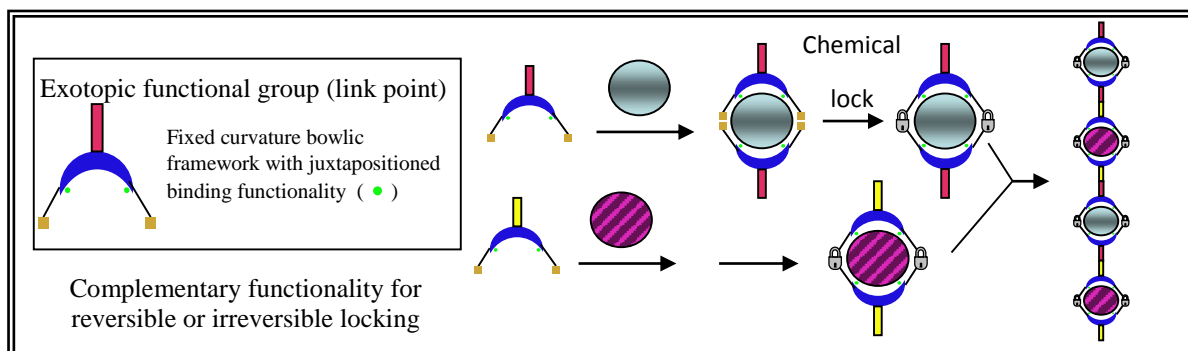


**Figure 2.** Controlled assembly of 1D hetero-nanoparticle arrays

A vast number of different molecules have been attached to various QDs, but despite their good photophysical properties, to the best of our knowledge the binding of subphthalocyanines to nanoparticles remains unexplored. This thesis describes our attempts to bring these two fascinating fields together, by means of the investigation of the synthesis, properties, ligand design and architecture of novel subphthalocyanine compounds.

## 1.2 Porphyrinoid Family

The centre of our investigations are subphthalocyanines that are members of the porphyrinoid family. These oligopyrrole structures are ubiquitous in both nature and everyday life. The general class is illustrated by the two structurally related planar macrocycles porphyrin **1** (four pyrrole units linked by methine bridges), and phthalocyanine **2** (four isoindole units linked by nitrogen bridges). These important chromophores are the parent structures of an enormous family of macrocycles and have triggered thousands of publications, covering their design, synthesis, properties and applications, and research effort continues to increase.<sup>[6]</sup> The synthesis of porphyrins (Ps) and their analogues, phthalocyanines (Pcs), are principally based on the use of templates to aid the cyclisation process.

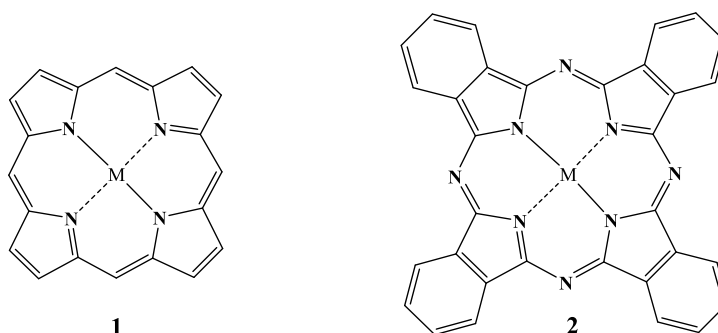


**Figure 3.** Parent structures porphyrin **1** and phthalocyanine **2**.

They possess some advantages with respect to other types of electro- and photoactive compounds which arise from their 18  $\pi$ -electron aromatic structure, specifically, high molar absorption coefficients and fast energy and/or electron transfer donor abilities to electron acceptor counterparts. Thus, porphyrinoids are widely used as molecular components in artificial photosynthetic systems, both for energy- and electron- transfer processes.<sup>[7]</sup>

### 1.2.1 Porphyrins

Porphyrins are an important family of naturally occurring pigments; they are deep purple in colour (name originated from the Greek porphura = purple). Crucial to the main function of porphyrins and porphyrin-like compounds in nature is their ability to bind metal atoms, which act as centres for significant biochemical events.<sup>[8]</sup> Thus, protoporphyrin-IX in heme complexes iron which, in haemoglobin and myoglobin, reversibly binds oxygen so that it can be transported around the body (haemoglobin) or stored in muscle tissue (myoglobin). This dye-molecule confers red colour to blood.

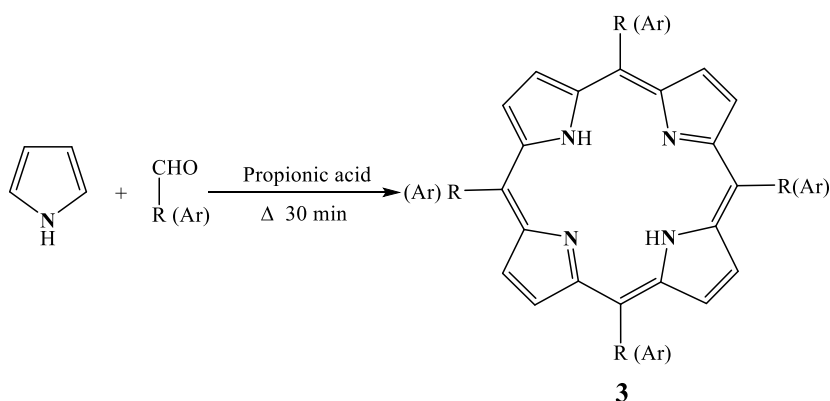
Another example from nature is chlorophyll; the bound metal in this case is magnesium, and this pigment gives rise to the green colour in plants. Here, the function of the macrocycle is to capture photons of light from the sun. The excited electrons are transported by proteins to begin the work of generating the high energy molecules necessary for turning carbon dioxide into carbohydrates. The

water molecules coordinated to the chlorophyll are oxidised very rapidly to oxygen.<sup>[9]</sup> Without any doubt they deserve the name that Professor Sir Alan R. Battersby used to refer to them: *Pigments of life*.<sup>[10]</sup>

### Generalities

Interestingly, the macrocyclic tetrapyrrole structure of porphyrins was first suggested in 1912 by Küster. At the time, Hans Fisher, thought that such a ring was too large to be stable. This structure was finally accepted in 1929, when Fisher and colleagues achieved their classical total synthesis of heme.<sup>[9], [11]</sup> It forms a planar macrocycle, containing two pyrrolic protons in the inner core, and four nitrogen atoms that can act as dianionic ligand to coordinate with metal ions to form metalloporphyrins.

There are many synthetic procedures available to prepare this macrocycle. The most famous pyrrole polymerization route to obtain symmetrical porphyrins involves the synthesis of tetraphenyl porphyrins (TPP) **3**, reacting pyrrole and an aldehyde (Scheme 1). The first procedure was reported by Rothmund,<sup>[12]</sup> but it was developed by Adler and Longo afterwards,<sup>[13]</sup> and finally optimised for unsymmetrical porphyrins by Lindsey.<sup>[14]</sup>

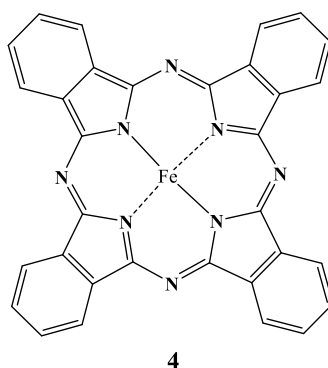


**Scheme 1.** Adler and Longo synthetic route for the formation of *meso*-substituted porphyrins.

### 1.2.2 Phthalocyanines

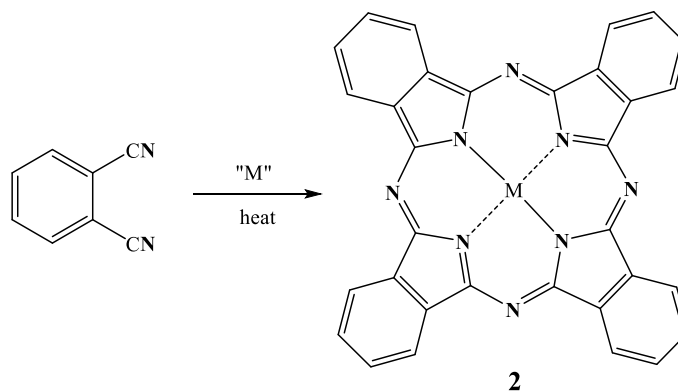
Unlike porphyrins, Pcs are man-made and represent one of the most studied macrocyclic systems. They were first observed in the early 20<sup>th</sup> century, but most importantly in 1928, during the industrial production of phthalimide from ammonia and molten phthalic anhydride.<sup>[15]</sup> A dark blue impurity was recognised as iron (II) tetrabenzotetraazaporphyrin (phthalocyanine **4**). This highly stable material contained iron in its cavity (derived from the vessels in which the reaction was carried out), and it could not be removed even by treatment with concentrated sulphuric acid. Due to their thermal, chemical and photochemical stabilities, Pcs are mainly used as dyes in the textile and paper industries.<sup>[16]</sup>





### Generalities

The macrocyclic core is formed by four isoindoline units, linked together by N-bridges. 18  $\pi$ -electrons are conjugated in this aromatic system in which the central cavity is big enough to accommodate a large number of different metals. A variety of functionalisation reactions can also be performed on the periphery. Symmetrical Pcs **2** are made by cyclotetramerisation reaction of 1,3-diiminoisoindoline or phthalonitrile (Scheme 2).<sup>[17]</sup> More challenging is the preparation of unsymmetrical Pcs. The most used route involves statistical tetramerisation of two different substituted phthalonitriles or diiminoisoindolines.<sup>[18]</sup> The understanding of phthalocyanines became more accessible thanks to Lindstead and co-workers, when they carried out a series of experiments and crystallographic studies.<sup>[19]</sup>



**Scheme 2.** General procedure for symmetrical Pc formation.

Pcs are generally planar molecules. However, introduction of steric hindrance can cause some more complex molecules to deviate from planarity. For example, Cook et al.<sup>[20]</sup> demonstrated the non-planarity of some non-peripherally substituted metal-free Pcs, the higher steric hindrance around the benzenoid rings leads to a saddle shaped conformation that translates into a reduced photostability compared to planar structures. A slight concave curvature is also obtained for Pcs metallated with Sn or Pb.

### 1.2.3 Properties and applications of Porphyrins and Phthalocyanines

Their strong light absorption makes porphyrins and Pcs very colourful materials, hence they have been widely used as pigments and dyes. Porphyrins show an intense (Soret) band between 390–425 nm, and between two and four very weak (Q) bands between 480–700 nm, depending on the molecule's substitution and whether it is metallated or not.<sup>[21]</sup>

Pcs have characteristic Soret bands in the UV region (320–370 nm) and Q bands in the visible-light region (670–690 nm). This absorption confers on them an intense blue or green colour. The absorption spectra can be tuned by non-peripheral substitution, benzoannulation, metallation, etc. Metal-free phthalocyanines (H<sub>2</sub>Pcs) show a Q-band split in two, compared to the single Q-band for metallated phthalocyanines (MPcs), owing to the lower symmetry of H<sub>2</sub>Pcs (D<sub>2h</sub>) than MPcs (D<sub>4h</sub>).<sup>[17]</sup> The lower symmetry of metal-free porphyrins (H<sub>2</sub>Ps) also affects the number of Q-bands, going from four Q-bands for H<sub>2</sub>Ps to two bands for metallated porphyrins (MPs). UV-Vis spectra showing the above described effect are represented in Figure 4.

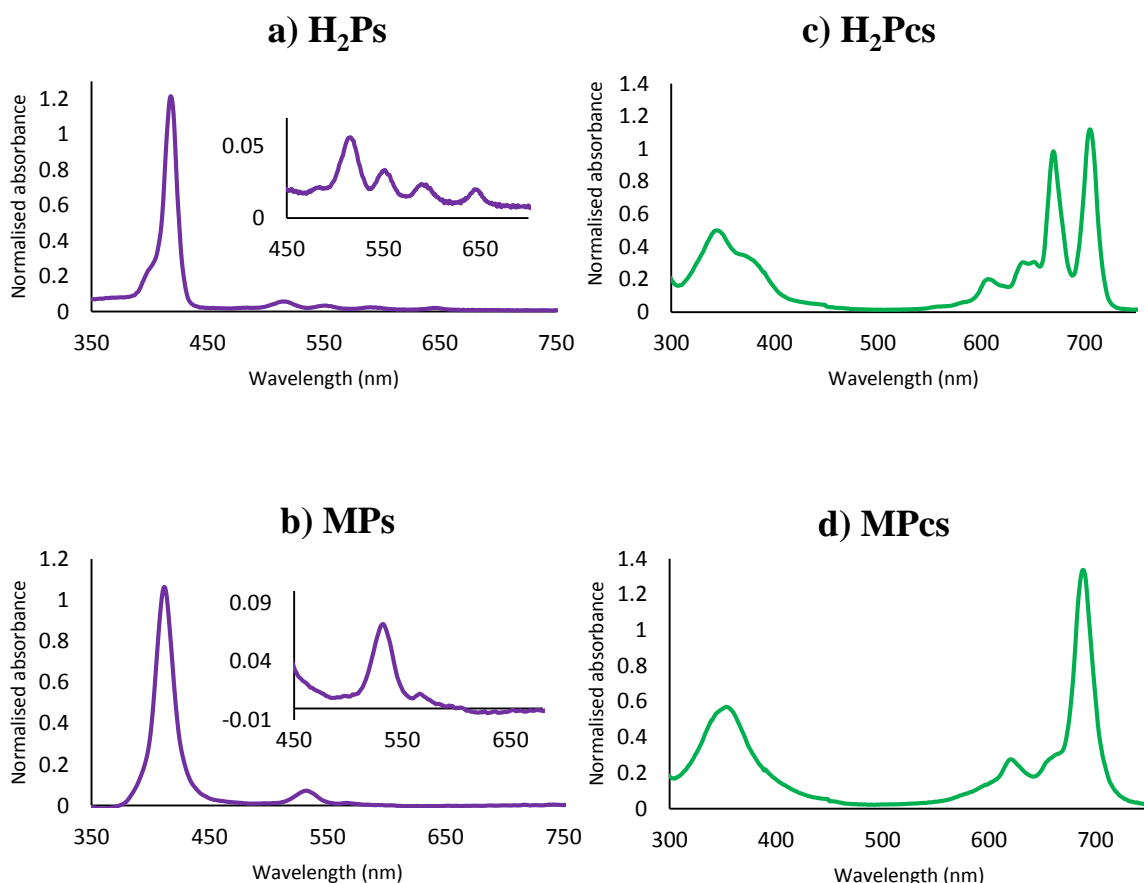
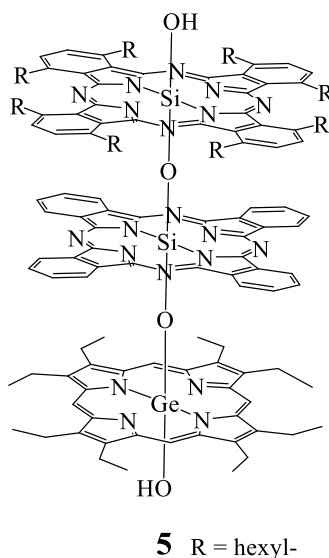


**Figure 4.** Absorption spectra of a) H<sub>2</sub>Ps, b) MPs, c) H<sub>2</sub>Pcs, and d) MPcs.

The absorption profiles are therefore complementary. Porphyrins and phthalocyanines can be combined and one approach from our group<sup>[22]</sup> is the combination of both chromophores in a single structure, for example the heteroligand, heterometalloid Pc/Ps triad **5**. Interestingly, this arrangement results in light absorption from the UV through to near-IR wavelengths.



Substituted and unsubstituted phthalocyanines have found applications in industrial catalysis, photosensitizers for photodynamic cancer therapy, markers for bioimaging, antibacterial composites, materials for ink-jet printing, chemical sensors, semiconductors, functional polymers and liquid crystals, light-harvesting modules for dye-sensitized solar cells and organic photovoltaics, nanotechnology, and non-linear optics.<sup>[18],[23]</sup> Thanks to their synthetic versatility, chemical robustness and tunable optical properties, porphyrinoids have found applications in a variety of fields such as optical communication, data storage, sensors, etc.<sup>[24]</sup>

#### 1.2.4 Core modifications

The modification of the macrocyclic porphyrinoid core has prompted rising synthetic efforts, with the literature describing progress towards the controlled synthesis of new derivatives (normally aromatic) with different properties and uses.<sup>[25]</sup> In general the manipulation of porphyrin-like structures has proved most straightforward for ring-expanded systems, with synthetic strategies based on well-established polypyrrole building protocols.<sup>[26]</sup>

The chemistry of expanded porphyrins began in 1966 after the serendipitous discovery of **sapphyrin 6** by Woodward et al.<sup>[27]</sup> Sapphyrin is a pentapyrrolic macrocycle, which exhibits a similar UV absorption to porphyrins and maintains aromatic features with 22  $\pi e^-$ .

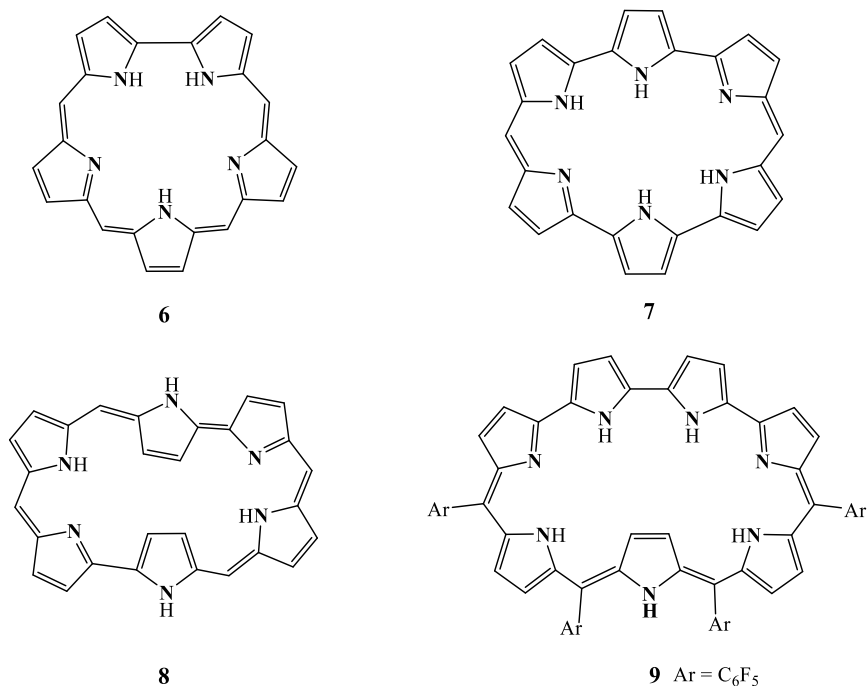


**Figure 5.** Some examples of expanded porphyrins.<sup>[26]</sup>

There are some notable examples of expanded porphyrins such as, **amethyrin 7** and **rubyrin 8** (two hexapyrrolic structures), or **heptaphyrin 9**, amongst others (Fig. 5). All these enlarged porphyrins share some characteristics: they possess a flexible  $\pi$ -conjugated electronic system, good stability, high aromaticity and unique photophysical properties.<sup>[26]</sup> Although significant discoveries have been made in this field, this chemistry is in its primitive stage and more work is required.

A considerable variety of Pc analogues has been achieved through modifications at one or more of the benzenoid rings, in particular through fused ring modifications,<sup>[28]</sup> like **2,3-naphthalocyanine 10** (Nc). Fundamentally ring altered phthalocyanine structures are much rarer, although there are some examples of expanded systems such as the “**superphthalocyanine**” **11**. The strategy here was to increase the ionic radius of the template allowing a greater number of subunits to coordinatively cyclise, thus the reaction of phthalonitrile and uranyl chloride yielded an expanded cyclic five isoindole unit complex.<sup>[29]</sup>

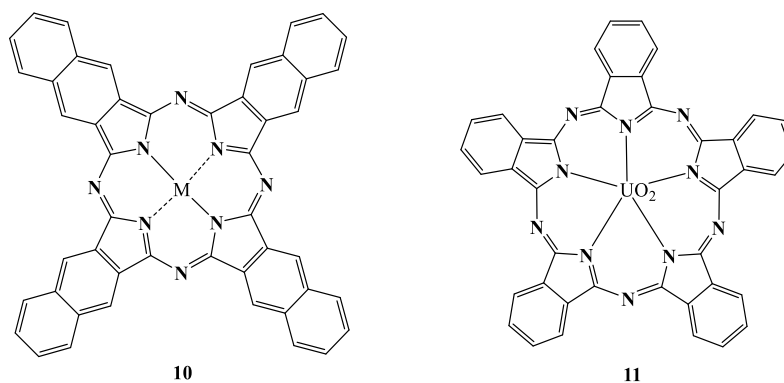


**Figure 6.** Extended naphthalocyanine **10**, and expanded superphthalocyanine **11**.

Comparatively less investigation has been focused on contracted porphyrins or Pcs, Figure 7. The most important structures can be classified as **subphthalocyanines** (SubPcs **12**), **benzsubporphyrins** (BzSubPs **13**), **subporphyrazines** (SubPzs **14**), and **subporphyrins** (SubPs **15**).

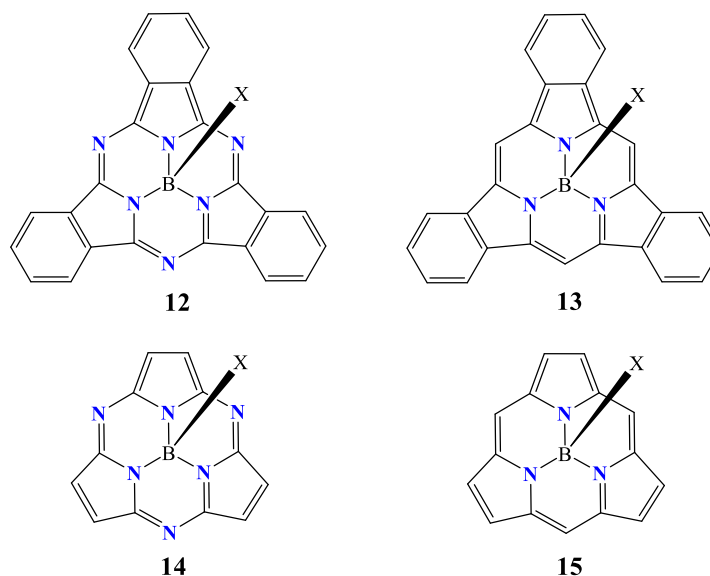
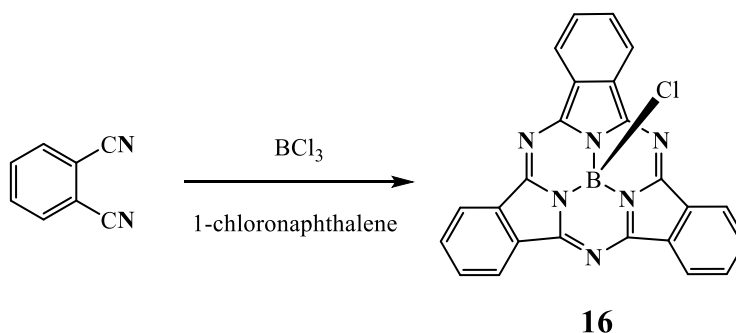


**Figure 7.** Ring contracted systems.

These subporphyrinoids contain three pyrrole or isoindole units. They adopt a bowl-like structure accommodating a tetrahedral boron in their central cavity. They also display a Hückel aromatic delocalised 14  $\pi$ -electron system. This exceptional arrangement results in rather unique optical and electronic properties.<sup>[30]</sup> These important macrocycles will be described in following sections.

#### 1.2.4.1 SubPhthalocyanines (SubPcs)

This macrocycle is the lowest homologue of phthalocyanine-like macrocycles, and it is the subject of a rapidly expanding research effort. Its serendipitous discovery was made in 1972 by Meller and Ossko<sup>[31]</sup> when they were trying to obtain boron phthalocyanine. The cyclisation reaction of phthalonitrile in the presence of boron trichloride in chloronaphthalene at 200 °C did not produce the cyclotetramerisation product. Instead, they observed the formation of a purple product whose analysis demonstrated the formation of chlorosubphthalocyanine **16**. Boron is too small to fit as a single atom into porphyrins or phthalocyanines, but forms a stable complex as a result of the cyclotrimerisation, Scheme 3.

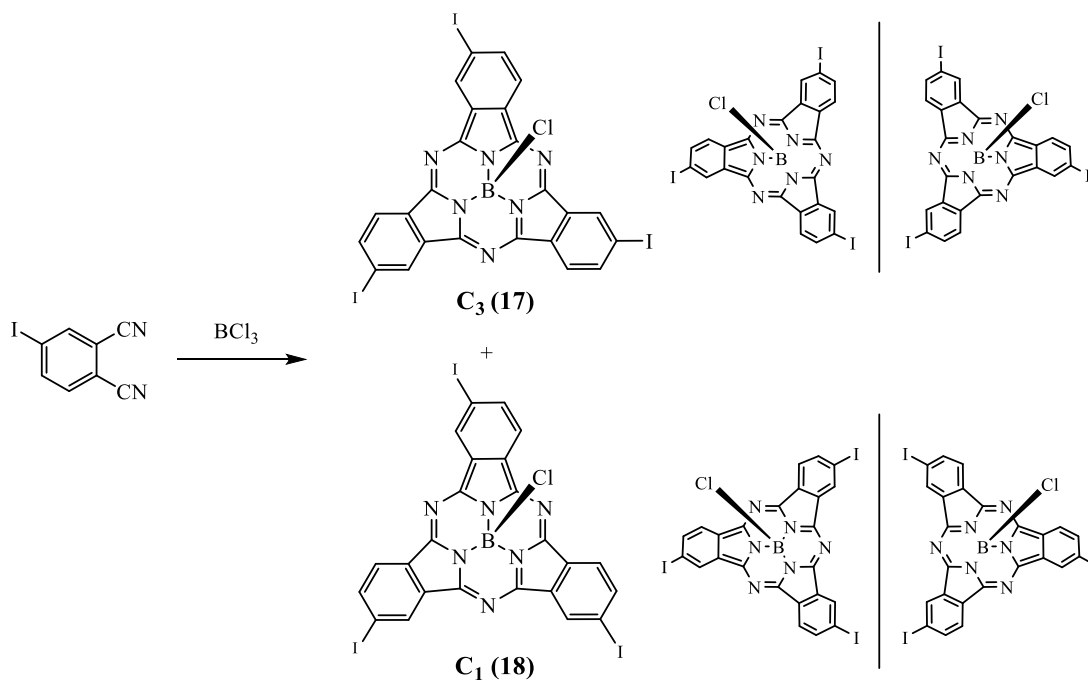


**Scheme 3.** The first synthesis of SubPc-Cl **16**.

The energetically most favourable situation for an aromatic ring system is a planar conformation but this requirement cannot be fulfilled in this case due to the tetrahedral boron hosted in the cavity. This semimetal stabilises the overall structure by coordinating with three nitrogens and an additional ligand, forming the basal plane and the apical position, respectively. In this manner, the boron subphthalocyanine adopts a non-planar, bowl-like structure.<sup>[32]</sup>

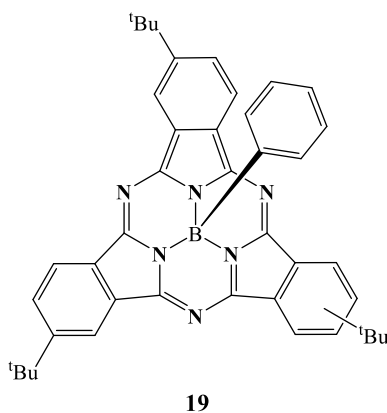
### Selectivity in SubPc Synthesis

Single SubPcs are obtained when the synthesis is carried out starting from highly symmetrical phthalonitriles. However, when phthalonitriles that lack  $C_{2v}$  symmetry are used as starting materials, mixtures of two SubPc regioisomers with  $C_3$  (**17**) and  $C_1$  (**18**) symmetries (each of which is chiral and the result is a racemic mixture of two enantiomers) are obtained. Exemplifying this selectivity, the synthesis of I-SubPc-Cl **20** from 4-iodophthalonitrile is represented in Scheme 4.



**Scheme 4.** Synthesis of I-SubPc-Cl **20**, showing the regioisomers **17** and **18**, and the corresponding enantiomers.<sup>[32]</sup>

Hanack and co-workers reported the separation of the C<sub>1</sub> and C<sub>3</sub> structural isomers of (*tert*-butyl)-SubPc-Ph, **19** by HPLC for the first time.<sup>[33]</sup> The most common way of achieving this separation is by column chromatography on silica gel.



### ***Properties and Applications***

Subphthalocyanines are the most studied macrocycles of the subporphyrinoid family, their properties and applications are well known.<sup>[30],[32]</sup> One of the advantages of SubPcs over Pcs is their better solubility in most common organic solvents. This results in a lower or null tendency to aggregate in solution, therefore SubPcs show <sup>1</sup>H-NMR spectra with very sharp peaks, contrasting those obtained for Pcs that are often broader due to their propensity to form aggregates.<sup>[34]</sup>

Unlike the planar or nearly flat structure of Pcs, the main feature of subphthalocyanines is their cone-shaped geometry, the macrocyclic core is acutely rigid being independent of the axial or peripheral substitution in the molecule. See Figure 8 for a 3 dimensional representation.

On the other hand, they are less stable than their parent molecule. Their photostability depends on the substitution. SubPcs are stable in the solid state, while they tend to decompose in solution in the presence of light. It is already known that I-SubPc-Cl **20** is one of the most stable derivatives. Interestingly, the photostability of polymeric films (polystyrene and polymethylmethacrylate) doped with differently functionalised SubPcs has been recently investigated.<sup>[35]</sup> The results reveal that the nature of the peripheral substituents strongly influences the stability of the SubPc material exposed to sunlight. Thermogravimetric studies carried out by Torres, Samios et al.<sup>[36]</sup> suggest that SubPcs have high thermal stability, with the loss of the axial group the first degradation event. Temperatures at which these molecules start to decompose increase depending on the axial substituent (Br < OH < OPh ~ Cl), whereas peripheral functionalisation seems not to play a notable role in this process.

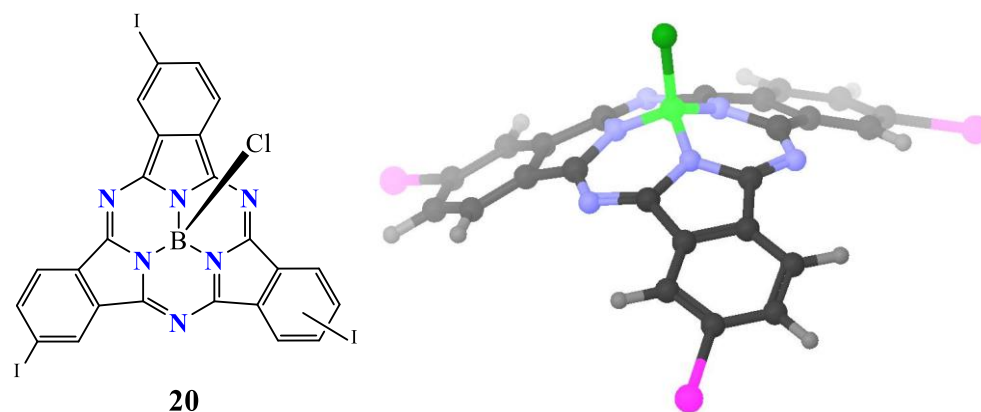


**Figure 8.** I-SubPc-Cl **20** and its corresponding computational model (right) performed by Sigismund Melissen at the University of Rouen.

One of the most attractive features of SubPcs is their unique optical properties.<sup>[32],[30]</sup> They are mostly bright pink materials and this trait is displayed in a very characteristic UV-Vis spectrum that shows a Soret and a Q band as observed in other aromatic macrocyclic compounds with aza substitution. The Soret band is the weaker band appearing in the region 260–370 nm and the Q band shows stronger absorbance intensity in the 460–560 nm region. Both absorptions are blue-shifted with respect to Pcs transitions ( $\lambda_{\text{max}} = 300\text{--}400$  and  $600\text{--}800$  nm) as a result of the decrease of the  $\pi$ -conjugation system from 18 to 14  $\pi e^-$ . Their non-planarity may lead to the decrease in the molar extinction coefficients for SubPcs that range from  $5$  to  $6 \times 10^4 \text{ dm}^3 \text{ mol}^{-1} \text{ cm}^{-1}$  with respect to the  $\epsilon$  values of Pcs that vary from  $8$  to  $24 \times 10^4 \text{ dm}^3 \text{ mol}^{-1} \text{ cm}^{-1}$ . Emission and fluorescence spectra of SubPc-OPh **21** is shown in Figure 9.

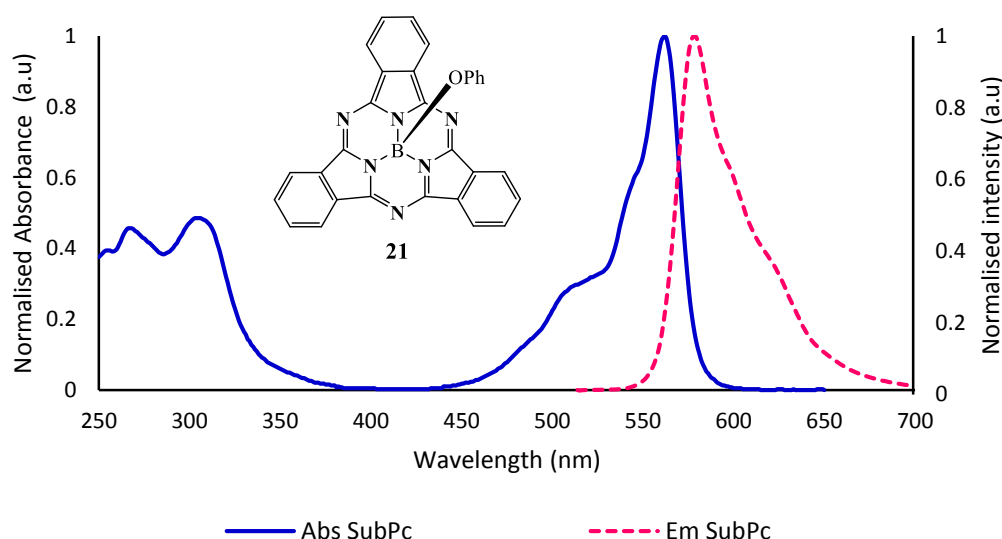


**Figure 9.** Absorption (blue line) and emission spectra (pink line) of phenoxy- SubPc **21**.

Subphthalocyanines are fluorescent molecules ( $\lambda_{\text{max}} = 575\text{--}670$  nm). In most cases, the emission is a mirror image of the Q absorption band. As their parent molecule, they display a very small Stokes shifts (typically around 10–15 nm), pointing out the small change in the geometry of



the excited state regarding the ground state. SubPcs also have higher triplet and singlet oxygen quantum yields, all these factors together with the fact that they do not aggregate, have prompted further investigations into their use as photosensitizers in photodynamic therapy (PDT).<sup>[32],[37],[38]</sup>

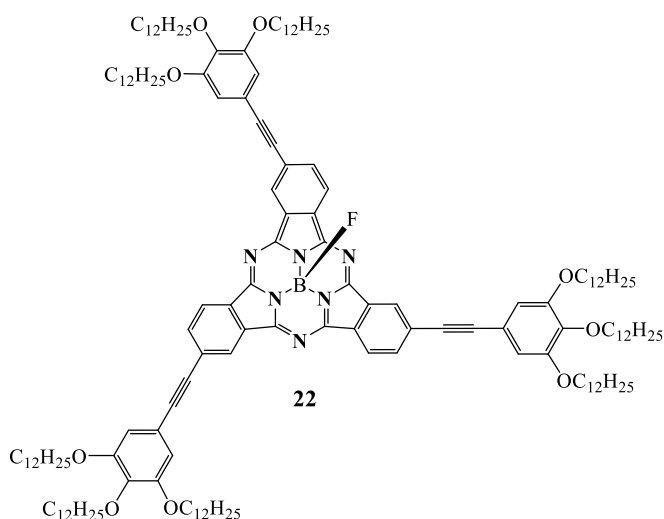
Thanks to its unique opto-electronic and nonlinear optical properties they have found increasing potential in a number of applications such as Organic Field Effect Transistors (OFETs), Organic Light Emitting Diodes (OLEDs), optical information recording media, dyes, anion sensors, etc.<sup>[30],[32],[39]</sup>

### Latest advances

In 2014, a variety of SubPc dimers were synthesised and developed for high efficiency catalysis in Lithium/thionyl chloride (Li/SOCl<sub>2</sub>) batteries.<sup>[40]</sup> The results showed that the stored energy and the capacity of the batteries whose electrolytes contain these compounds as catalysts were increased by approximately 21.4% - 33.1% and 15.7% - 32.7% than that of the battery in the absence of them. Decréau and colleagues<sup>[37]</sup> showed the versatility of SubPcs reporting the first successful use of water-soluble subphthalocyanines as efficient fluorophores for the *in vitro* fluorescence imaging of cells.

Very recently Torres, González-Rodríguez, Etxebarria and co-workers,<sup>[41]</sup> have demonstrated the self-assembly of axial dipolar subphthalocyanine molecules in the presence of electric fields, leading to uniaxially oriented columnar liquid crystalline materials that exhibit permanent polarisation.

Their strategy relied on the introduction of a highly electronegative atom, such as fluorine, linked to the central boron at the apical position, SubPc **22**. This generates a strong axial dipole in the molecule, and its arrangement as columnar liquid crystals that exhibit permanent polar order along the columnar axis upon application of electric fields. Interestingly, when such electric field is removed or reversed, the polar order remained unaltered for weeks, which makes this novel material interesting for device applications. Figure 10 depicts the result of the polarised columnar stacking.



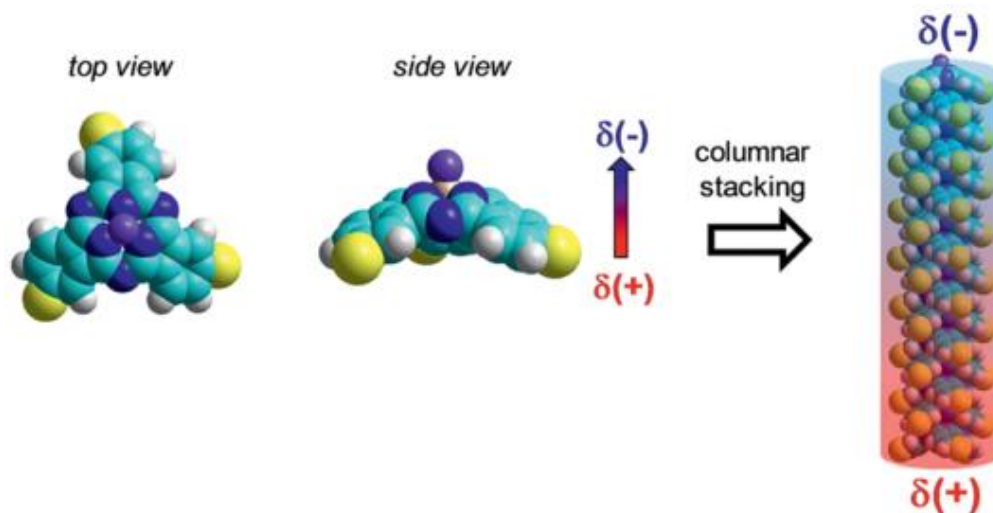


**Figure 10.** 3-Dimensional views of the SubPc macrocycle, and head-to-tail stacking into polarised columnar structures.<sup>[41]</sup>

One of the most exceptional applications of these chromophores is as small molecules in Organic Photovoltaic (OPV) solar cells, where they have been investigated as donor and as acceptor materials,<sup>[30],[39]</sup> giving rise to outstanding results regarding power conversion efficiency (PCE) and internal quantum efficiency (IQE).<sup>[42]</sup> Very recently, Cnops et al.<sup>[43]</sup> reported a major breakthrough in this area; they developed small-molecule organic solar cells with non-fullerene electron-accepting materials. The device was constituted by two acceptors, SubPc-Cl **16** and Subphthalocyanine **23** (SubNc), and a donor,  $\alpha$ -sexithiophene **24** ( $\alpha$ -6T), Figure 11. An unprecedented PCE of 8.4% was reported for fullerene-free organic solar cells establishing a record efficiency for evaporated single-junction OPV devices.

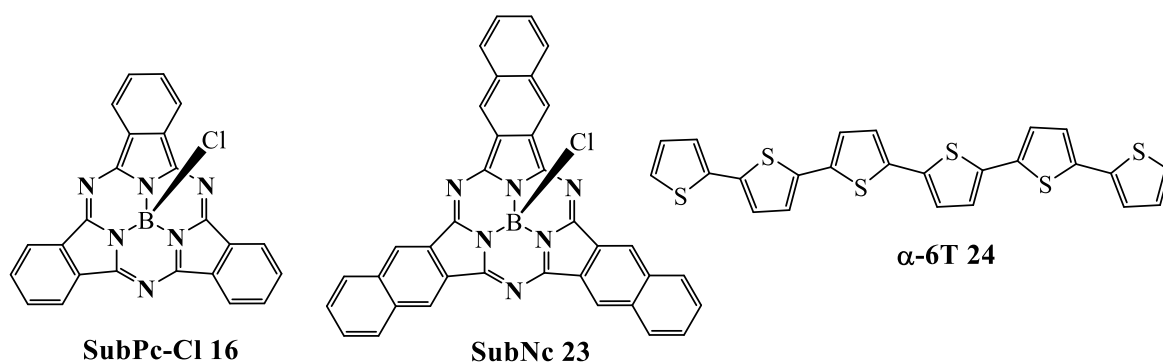


**Figure 11.** Molecules that constituted the organic solar cell.<sup>[43]</sup>

## 1.3 Nanoparticle Assembly

### 1.3.1 Quantum Dots

Inorganic semiconductor nanoparticles, quantum dots (QDs), are spherical nanomaterials that are zero dimensional relative to the bulk semiconductor. Composed of approximately 100 – 1000 atoms each, and typically with a diameter less than 10nm, QDs are promising candidates in

nanotechnology, and especially they have been widely used as energy devices, due to their unique optical and electronic properties, such as high quantum yield, narrow, tunable and symmetric emission spectra, broad absorption spectra, long-term photostability, high surface area, and high chemical stability.<sup>[44], [45]</sup>

The ability to tailor the electronic structure, optical, and magnetic properties of materials without changing the chemical composition, simply by modifying the size of the nanoparticles, is a key feature and opens interesting opportunities for device applications.<sup>[2]</sup>

One of the most important features of QDs is their size-dependent band gap, i.e. different colour emission depending on the size. This is due to the *quantum confinement effect*.<sup>[46]</sup> When a semiconductor absorbs light, an electron is promoted from the full valence band to the empty conduction band (Fig. 12). The minimum energy required to excite an electron is dictated by the energy band gap,  $E_g$ . The loss of the electron then creates a hole in the valence band, which gives rise to the electron-hole pair named exciton, and it is characterised by the distance known as the exciton Bohr radius. The electron will then return to the valence band recombining with the hole, losing energy in the form of light (fluorescence).

When the size of the QD is comparable or smaller than the Bohr radius, the exciton is then created within spatial limitations, meaning that the energy required to confine such exciton is higher. In essence, as the size of the nanoparticle decreases, the band gap energy becomes wider, therefore the absorption and emission maximum wavelengths decrease, appearing blue-shifted in the spectrum.

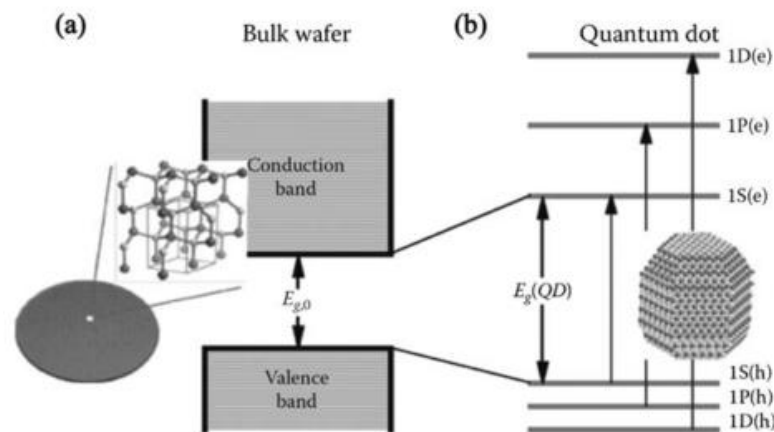


**Figure 12.** (a) Energy bands of bulk semiconductor showing the continuity of conduction and valence band separated by a bandgap,  $E_g$ . (b) For QD, the continuous bands become discrete atomic states with energies determined by the size of the nanoparticle.<sup>[47]</sup>

This control over the photoluminescence of the material, together with the fact that replacing bulk materials for QDs decreases the production costs, and they can be easily synthesised in a wide variety of shapes, such as spheres, prisms, rods, wires, etc.<sup>[48]</sup> contributed to the increased number of applications.<sup>[2],[49]</sup> They have been implemented in a wide range of devices,<sup>[44],[45]</sup> e.g. light emitting

diodes (LED), photodetectors, field-effect transistors (FET), memory elements and magnetic data storage, sensors and photosensitisers, among others.<sup>[50]</sup>

### 1.3.1.1 Cadmium selenide nanocrystals

Cadmium selenide (CdSe) QD is found to be of great interest due to its well-known physical properties, the ready availability of precursors, its tunable band-gap energy that covers almost the full spectral range (Fig. 13), and the remarkable narrow size distribution controllable during the synthetic process. They have already proved to be excellent components for a variety of applications, such as in optically pumped lasers, photovoltaic cells, telecommunications, and biomedicine.<sup>[4]</sup>

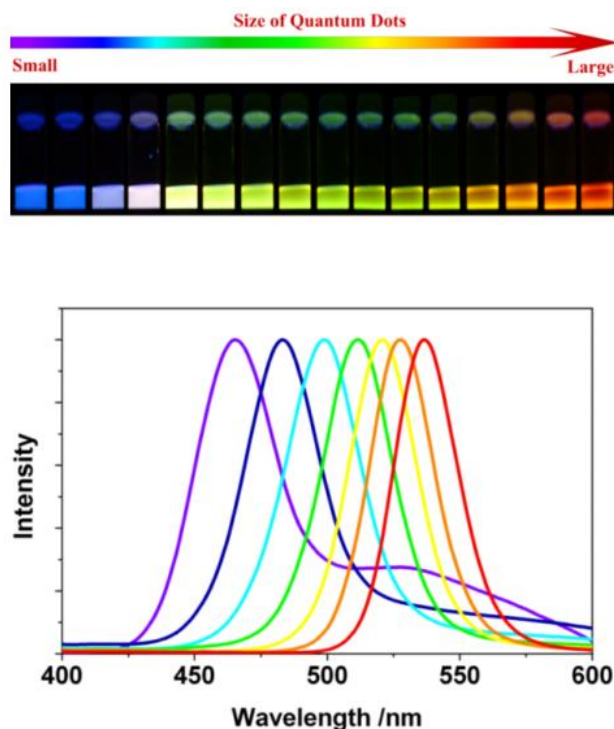


**Figure 13.** (Top) Change of photoluminescence (PL) emission colour with size for CdSe QDs excited under 365 nm lamp. (Bottom) Photoluminescence spectra of some CdSe QDs.<sup>[51]</sup>

The inorganic core is formed by cadmium and selenium, it exists in two natural crystal structures, namely the hexagonal wurtzite and the cubic zinc-blende structures.<sup>[52]</sup> Due to the high surface-to-volume ratio of QDs, the nanocrystals' surface has important effects on the optical properties. During the charge recombination process, defects and dangling bonds on the surface can occur, these deformations diminish the photoluminescence intensity and chemical stability of the semiconductor. Therefore the control over the growth is of utmost importance. Accordingly these inorganic nanoparticles are stabilised by a layer of inorganic or organic surfactants<sup>[50]</sup> (passivating ligands) attached to their surface. Due to previous knowledge in our group, this work will be focused on organic capping ligands.

Examples of organic alkyl capping ligands include phosphine oxides, phosphonic acids, phosphines, thiols, thiophenes, fatty acids and amines.<sup>[53]</sup> This inorganic-organic combination also

opens the potential toward more advance and complex materials. However, controlling the number of functionalities per nanoparticle still remains a challenge.

The optical spectroscopy and structural characterisation of the nanoparticles (XPS, XRD, DLS and TEM) in the literature, is mainly concerned about the inorganic core<sup>[52], [54]</sup> and the optical and electrical effect that changes on the interface trigger.<sup>[55]</sup> Just a few reports are truly motivated by the understanding of how surface chemistry works, and the demonstration of ligand binding by means of full characterisation by solution and/or solid-state NMR spectroscopy of this organic part.<sup>[56]</sup>

### 1.3.2 Hybrid nanoassemblies: Organic chromophores - QDs

Porphyrins and Pcs are chosen to an increasing extent for supramolecular systems, because of their above mentioned interesting optical and electronic properties that can be tailored by various modifications on the molecules' architectures. They are also chemically stable structures that possess the ability to self-assemble on surfaces as well as in solution, which makes them promising components in the field of bionanotechnology. In the sections below some examples of such hybrid-porphyrinoid combinations already existing in the literature will be described. Investigations on self-assembled nanostructures containing organic ligands are exponentially increasing, especially those concerning porphyrin – nanocrystals.<sup>[57]</sup> This scientific interest in porphyrins is mainly triggered by the fact that they are naturally occurring materials, hence ideal models for mimicking the photochemical processes *in vivo*.

#### 1.3.2.1 Quantum Dots - Porphyrins

The attachment of porphyrins to the inorganic surface results in the QD photoluminescence quenching.<sup>[58]</sup> The self-assembly is a competing process with capping ligand dynamics, ligand exchange dynamics and surface functionalisation is the focus of multiple studies.<sup>[1b]</sup> Such chromophore/QD pairs are promising building blocks for more advanced nanocomposites with potential applications in biology and medicine,<sup>[59]</sup> optical sensors,<sup>[60]</sup> and light harvesting devices.<sup>[61]</sup>

Shaikh et al.<sup>[62]</sup> studied the binding affinity of porphyrin (based on number and type of linker moieties) to gold nanoparticles (Au NP), performing UV-Vis and fluorescence titration experiments, amongst other techniques. The type of conformations of porphyrins binding to nanoparticles can be described as face-on binding, when the molecule lies flat on the surface (Fig. 14 a), and face-off binding, when the molecule is linked perpendicularly to the surface of the nanoparticle (Fig. 14 b). They carried out studies with four amino-substituted and two amino-groups present in porphyrins, revealing that there was much stronger porphyrin photoluminescence quenching for the tetra-amino functionalised porphyrin. The emission quenching is normally indicative of the attachment of porphyrins to the QD's surface.<sup>[1b]</sup>

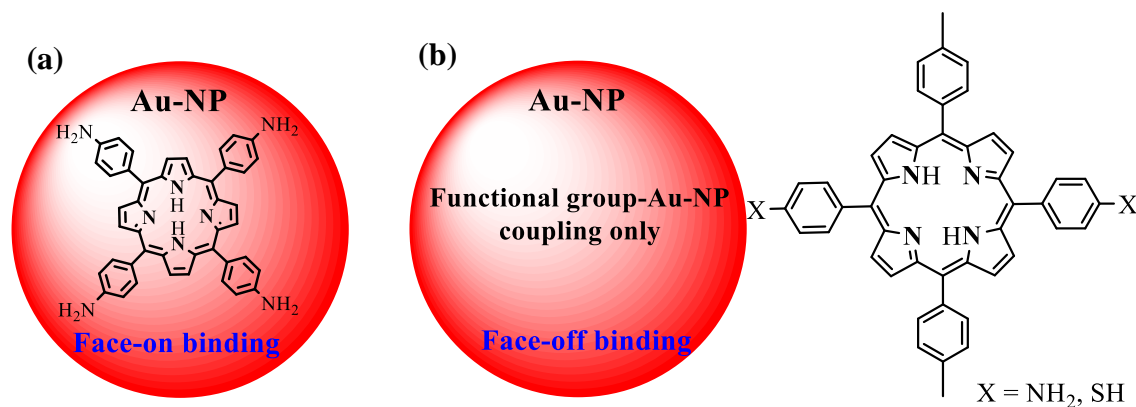
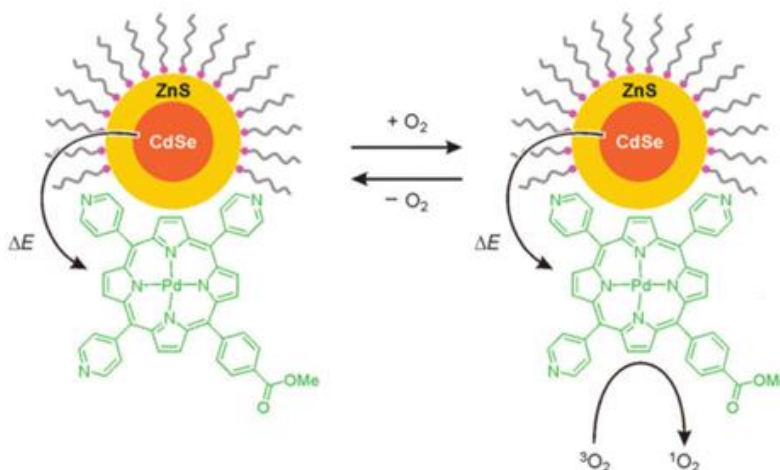


**Figure 14.** (a) Face-on, and (b) face-off binding of the porphyrin to the nanoparticle surface.<sup>[62]</sup>

Thiol-functional groups have higher binding affinity to gold surfaces compared to amino-groups, hence, they also investigated the interaction of thiol-functionalised porphyrins with Au-NP. A comparison study between the two amino- and two thiol-substituted porphyrins Au-NP revealed similar emission quenching. Although, it is not possible to demonstrate the configuration of porphyrin binding, nor measure binding constants from fluorescence studies, they concluded that binding depends on the number rather than type of functional group on the porphyrin molecules, possibly owing to the face-on and face-off binding of porphyrins to the surface.

A recent publication<sup>[63]</sup> describes how the quantum yield of photoinduced electron transfer (eT) is enhanced from a zinc porphyrin (ZnP) derivative that acts as a donor to a CdSe QD as the acceptor. As a result of linking both materials by a phenyl bis (dithiocarbamate) molecule, there is an increase in the binding affinities, regarding to the QD-ZnP without the use of such linkage.

Bawendi, Nocera et al.<sup>[64]</sup> synthesised palladium porphyrins bearing *meso*-pyridyl substituents that bind to the surface of QDs developed to detect oxygen in organic solvents. In the assembly the QD acts as an antenna for light absorption. Upon excitation of the QDs, the energy is transferred to the porphyrin, which is then emitted. The emission of the porphyrin is quenched by oxygen, whereas the insensitivity of the QD's emission towards O<sub>2</sub> serves as internal standard to establish a ratiometric signal response, Scheme 5.



**Scheme 5.** QD – Porphyrin conjugate which acts as oxygen sensor.<sup>[64], [65]</sup>

Photocatalytic degradation of organic pollutants (e.g. organic dyes) is a promising procedure for environmental purification, considering the substantial amount of coloured waste water that is generated by industries using dyes in their production processes. Accordingly, Liu et al.<sup>[66]</sup> investigated the photocatalytic activity for the degradation of Rhodamine B (RhB), an industrial pollutant. In the presence of a porphyrin functionalised CdS nanoassembly, the degradation efficiency of RhB was enhanced under exposure to solar light.

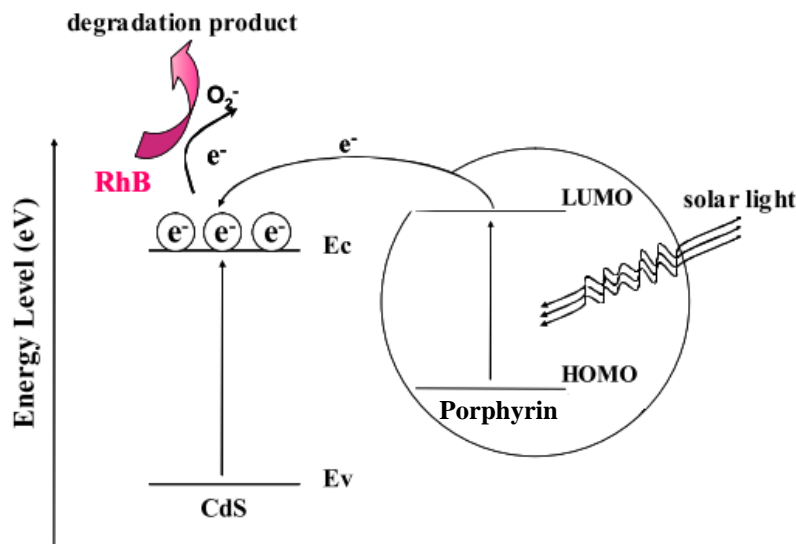


**Figure 15.** Proposed mechanism for the degradation of RhB catalysed by porphyrin-functionalised CdS nanocomposites under exposure to solar light.<sup>[66]</sup>

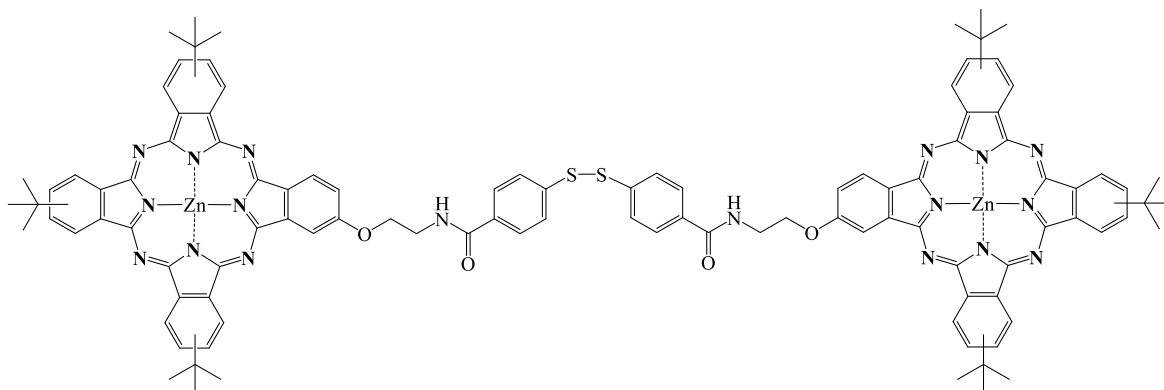
The authors proposed a possible mechanism for the degradation, and it is represented in Figure 15. In the nanoconjugate, porphyrin acts as the light-harvesting agent. When the porphyrin-CdS photocatalyst is irradiated under solar light, the electrons of the porphyrin can be excited from the highest occupied molecular orbital (HOMO) to the lowest unoccupied molecular orbital (LUMO). Because of the matching energy bands between CdS and porphyrin, the electrons at the LUMO energy level of the porphyrin can transfer to the conduction band (Ec) of CdS. The excited electrons react then with absorbed  $O_2$  producing  $O_2^{\bullet-}$  which subsequently oxidises RhB.<sup>[66]</sup>

### 1.3.2.2 Quantum Dots - Phthalocyanines

Nowadays, there is a growing interest in the mechanism involved in energy transfer between inorganic semiconductor nanoparticles (donor) and organic chromophores (acceptor).<sup>[67]</sup> This understanding together with the synthetic control of the nanoassemblies, could lead to the optimisation of the QD-dye pair properties and their application in diverse fields such as in oxygen reduction reactions,<sup>[68]</sup> bioimaging and targeted photodynamic therapy (PDT),<sup>[69]</sup> fluorescence-based sensors,<sup>[70]</sup> and photovoltaic applications.<sup>[71]</sup> Very recently Sastre-Santos et al.<sup>[72]</sup> reported the enhancement of power conversion efficiency of CdSe QD sensitised solar cells up to 45%. This outstanding efficiency is achieved by passivation of the surface with an unsymmetrically substituted



zinc phthalocyanine which, after rupture of the dimeric structure **25**, is covalently bonded to the nanocrystal by a sulphide group.



**25**

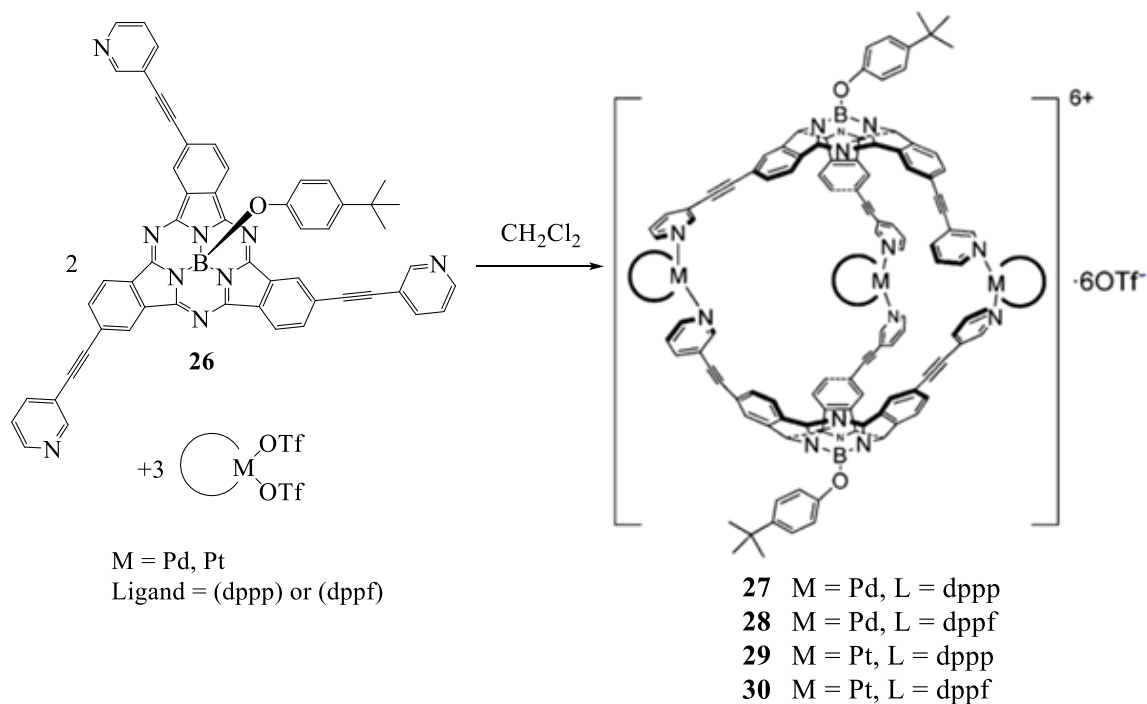
Antibody–zinc phthalocyanine–gold nanoparticle conjugates have been synthesised and applied for the first time by Russell et al.<sup>[73]</sup> as photosensitiser for photodynamic cancer therapy. This photoactive drug, is used to target and destroy tumours upon irradiation with red or near-infrared light due to the production of singlet oxygen. Their results show that the phthalocyanine derivative is essential for the production of singlet oxygen.<sup>[74]</sup> After irradiation at 633 nm, the nanoparticle conjugate induced cell death of approximately 95-98% of cancer cells.<sup>[75]</sup>

### 1.3.2.3 Quantum Dots - Subphthalocyanines

As previously discussed, a vast range of compounds have been attached to different QDs, to form nanoassemblies, including porphyrins and Pcs, but despite their promising properties to the best of our knowledge the coupling of quantum dots with subphthalocyanines to form a new class of hetero-nanoassemblies, remains unexplored.

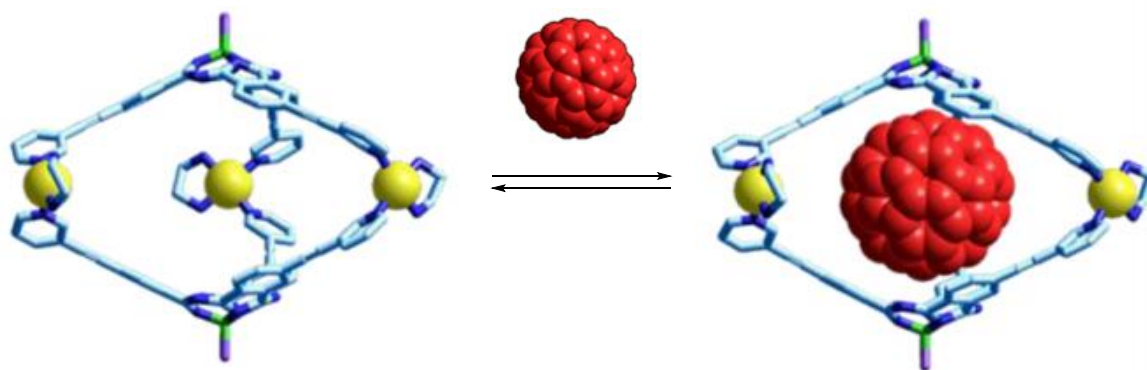
However, the curve-shaped structure of SubPcs has prompted their use as building blocks for the construction of homodimeric capsules.<sup>[76]</sup> Remarkable work led Torres and co-workers<sup>[77], [78]</sup> to build  $C_3$  symmetric SubPc  $M_3L_2$  cages capable of encapsulating  $C_{60}$  fullerene within its walls. In their work, the capsules **27-30** were obtained treating SubPc **26** bearing three ethynylpyridyl-groups with the corresponding Pt or Pd acceptors in a 2:3 ratio. In this reaction, represented in Scheme 6, diphenylphosphinopropane (dppp) and diphenylphosphinoferrrocene (dppf) were chosen as ligands, and Pd (II) and Pt (II) were employed as coordinating centres.





**Scheme 6.** Self-assembly of SubPc metallocsupramolecular cages.<sup>[78]</sup>

Their investigations involved a variety of host-guest experiments, whereby the possible guests (pentacene, ferrocene carboxylic acid,  $C_{60}$ ,  $C_{70}$ , and  $C_{60}$ -PCBM ([6,6]-phenyl  $C_{61}$ butyric acid methyl ester)), could interact via  $\pi$ - $\pi$  stacking with the host. Their results demonstrated that the encapsulation with pentacene or ferrocene carboxylic acid does not occur. However, the supramolecular cages formed adducts in a 1:1 ratio with  $C_{60}$ ,  $C_{70}$  and their PCBM-type derivatives, Scheme 7. They quantified the  $\pi$ - $\pi$  interactions between the fullerenes and the SubPc walls of the capsules determining the binding constants and the stoichiometry of the resulting adducts, concluding that fullerenes are suitable guests for the SubPc capsules.



**Scheme 7.** Encapsulation of  $C_{60}$  in the cage.<sup>[30]</sup>

The organisation of SubPcs<sup>[30]</sup> in the solid state, in thin films, in liquid crystalline phases, on surfaces or within nanoporous materials, is a promising object of study towards the development of novel organic-based materials. In this sense, Torres and co-workers<sup>[79]</sup> reported for the first time, the formation of self-assembled monolayers of 1,2-dithiolane-substituted SubPcs on gold surfaces.

For this purpose, they synthesised SubPcs **31** and **32** bearing the 1,2-dithiolane functionality at the apical position, and the peripherally substituted derivative **33** (Fig. 16). They first monitored

the monolayer formation by cyclic voltammetry, a gold electrode was immersed into a solution of the SubPc derivative in acetonitrile or THF, allowing the mixture to stir overnight. SubPc **33** showed the best self-assembled monolayer stability, according to the authors, owing to the increased number of S-Au bonds per molecule.

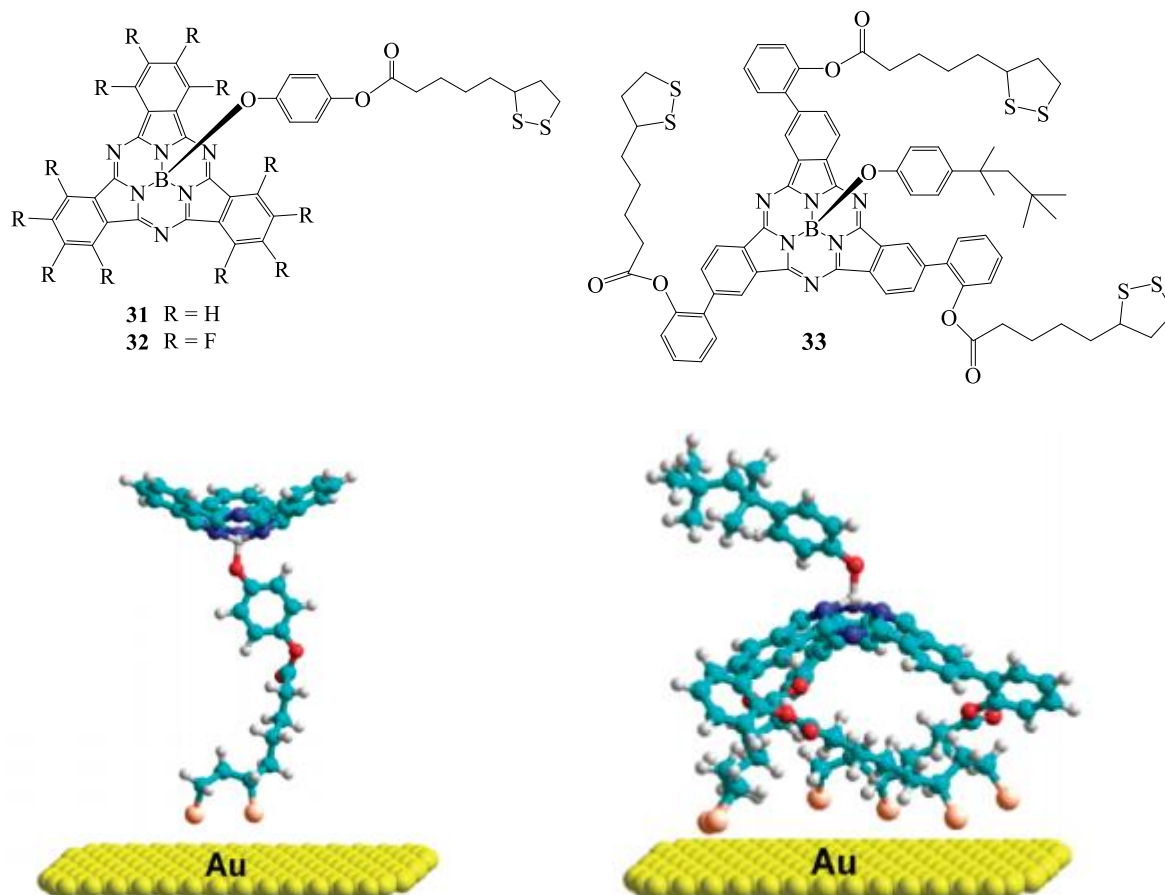


**Figure 16.** Structures of 1,2-dithiolane functionalised SubPcs **31**, **32** and **33** (top), and representation of the monolayers on a gold surface (bottom).<sup>[79]</sup>

They also prepared self-assembled monolayers on silicon substrates covered with a gold layer, by exposing them to a solution of the SubPcs derivatives in acetonitrile overnight. The substrates were studied by several techniques, such as X-Ray Photoelectron Spectroscopy (XPS), Atomic Force Microscopy (AFM) or water contact angle goniometry. The characterisation of the SubPc self-assembled monolayers confirmed that all SubPcs form stable, densely packed monolayers on gold surfaces, Figure 16.

## **CHAPTER 2. RESULTS and DISCUSSION – Subphthalocyanines and Conjugation with Nanoparticles**

### **2.1. CdSe Nanoparticles**

#### **2.1.1 Synthesis**

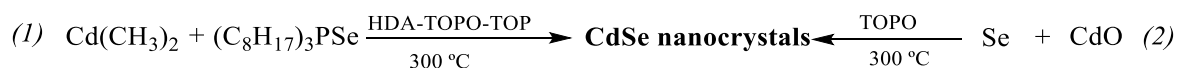
Over the past decades, chemists have been dedicated to search for the appropriate combination of precursors, surfactants, solvent and reaction conditions to achieve a reproducible method to synthesise high quality nanoparticles. Due to the enormous growth of their applications, the utilisation of QDs with uniform shape, size, composition and surface morphology is of paramount importance.

The outcome of all this research effort has been the accomplishment of reproducible methodologies which allow the use of simple equipment and inexpensive reagents, giving rise to high-quality materials with tunable properties. Generally, the techniques for synthesis of QDs are classified as top-down or bottom-up approaches.<sup>[50]</sup> Nanoparticle formation normally involves the following stages: nucleation from homogeneous solution, growth of the nuclei obtaining a colloidal dispersion and isolation of the particles with the desired size. The hot-injection technique allows temporal separation of the nucleation step from the growth of the nuclei, achieving a narrow size distribution.<sup>[2]</sup>

This protocol was first introduced by Murray and co-workers,<sup>[80]</sup> and it is based on the rapid injection of the precursors into a hot solvent with the subsequent temperature drop. Nucleation and growth steps take place in solution in the presence of organic surfactant molecules, which adhere onto the surface of the crystals. Most common surfactants are long-chain carboxylic acids and phosphonic acids, alkanethiols, alkyl phosphines, alkylphosphine oxides, and alkylamines.<sup>[2]</sup>

The syntheses are carried out at high temperatures to decrease defects on the surface. Coordinating solvents control the growth process, stabilising the colloidal dispersion and passivating the semiconductor QD surface. However, non-coordinating solvents such as octadecene (ODE), provide the best quality nanocrystals with nearly monodisperse size and shape according to Peng et al.<sup>[81]</sup> In a colloidal solution, the particle growth stage is consistent with the Ostwald ripening mechanism, which implies diffusion of material from small particles to the largest ones. Consequently, particle size increases with time and size can be selected by periodical extraction of samples from the reaction vessel.<sup>[80]</sup>

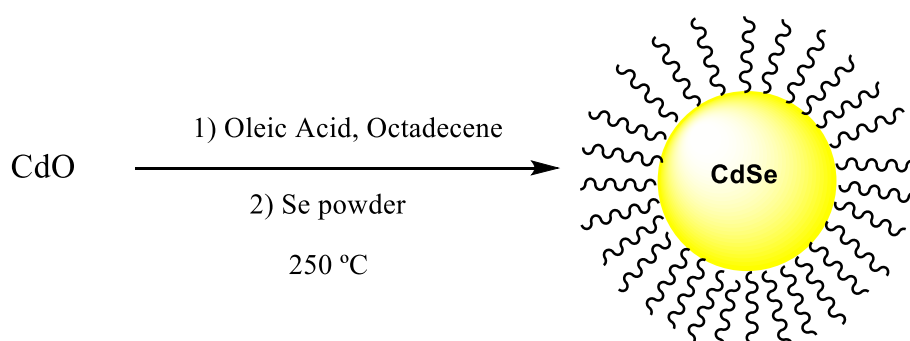
Murray et al.<sup>[80]</sup> reported the synthesis of cadmium chalcogenide nanocrystals using dimethyl cadmium  $\text{Cd}(\text{CH}_3)_2$  as cadmium source. The synthesis takes place at elevated temperature in the presence of trioctylphosphine (TOP), trioctylphosphine oxide (TOPO) and hexadecylamine (HDA) as stabilising agents. Selenium is provided by TOPSe (Scheme 8, (1)).



**Scheme 8.** Most common synthetic routes to obtain CdSe nanoparticles.

Although synthetic route (1) provides high-quality and monodisperse nanocrystals, dimethyl cadmium is pyrophoric, extremely toxic, expensive, unstable, etc. Peng et al.<sup>[82]</sup> replaced the use of this reagent by CdO; this one pot reaction is reproducible, simple and avoids the use of a glove box. Nanocrystals obtained with this method (Scheme 8. (2)) are close to monodisperse and represent a greener synthesis toward the synthesis of high-quality QDs.

Due to previous knowledge in our group,<sup>[83]</sup> and further optimisation of Yu et al.'s<sup>[81]</sup> protocol by our group, the synthesis outlined in Scheme 9 was followed in the current work.



**Scheme 9.** The synthetic route followed in this work.

Oleic acid was added to a solution of CdO in octadecene. The solution was heated under inert atmosphere up to 250 °C until a clear solution was observed. The mixture was cooled down, selenium powder was added the solution was re-heated to 250 °C. Aliquots were taken very frequently and immediately cooled down and quenched with toluene, absorption and emission spectra were recorded to monitor the growth of the CdSe nanocrystals. Figure 17 depicts the absorption spectra of samples going from 475 (yellow nanoparticles) to 542 nm (dark orange).

The size of the nanoparticles were calculated from the formula<sup>[84]</sup> where  $\lambda$  is the wavelength in nm of the absorption maxima. The legend in Figure 17 illustrates the calculated sizes of all aliquots taken during the reaction process, and range from 2.2 to 3.0 nm.

$$D(\text{nm}) = 59.60816 - 0.54736\lambda + 1.8873 \times 10^{-3}\lambda^2 - 2.85743 \times 10^{-6}\lambda^3 + 1.62974 \times 10^{-9}\lambda^4$$

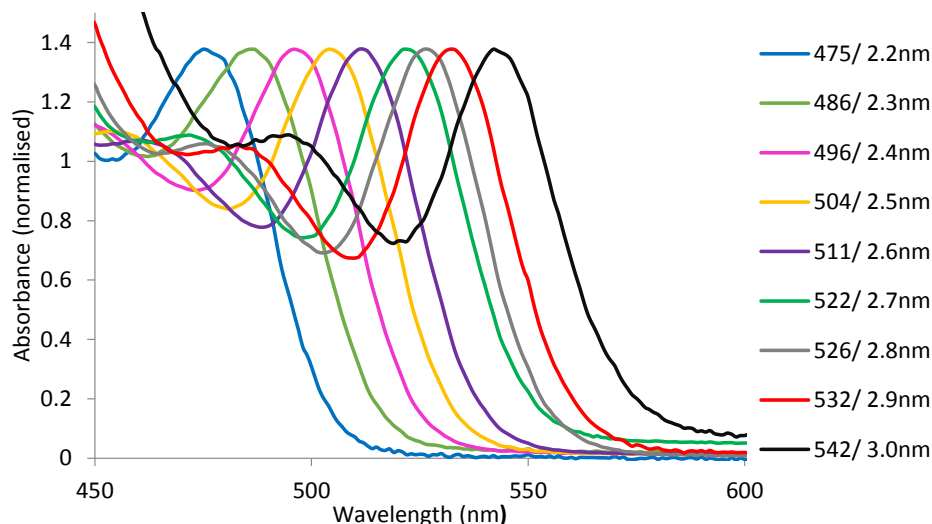


**Figure 17.** UV-Vis spectra of CdSe nanocrystals, the label describes the absorption maxima and the calculated sizes.

Photoluminescence spectra of the respective samples were also recorded (Figure 18). The samples show green fluorescence at 491 nm in the case of the smallest particles (2.2 nm) and orange fluorescence at 552 nm for the larger ones (3 nm).

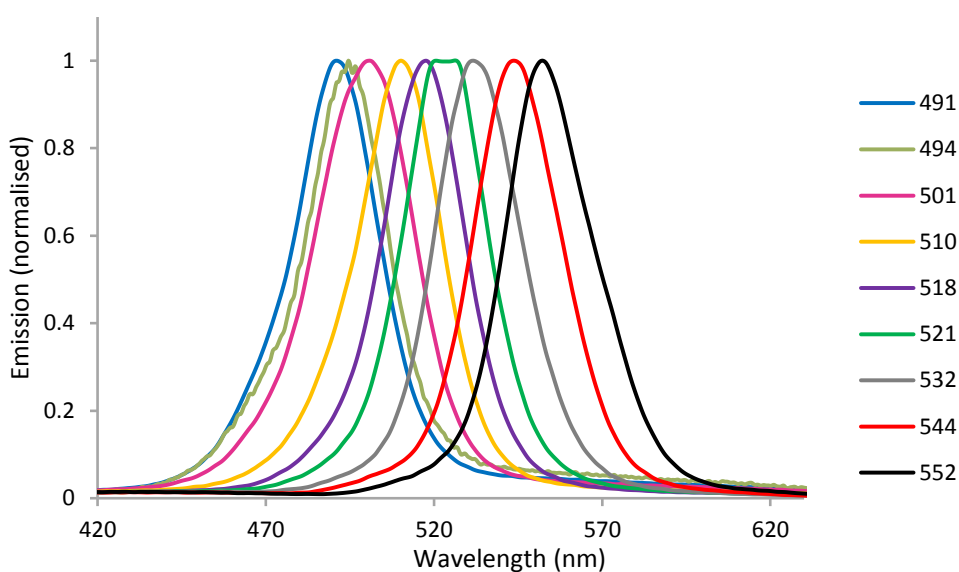


**Figure 18.** Emission spectra of various sizes CdSe nanoparticles, the label depicts emission maxima in nm.

Samples were extracted from the reaction vessel within a few minutes of each other, and the above illustrated optical measurements demonstrate the rapid growth of the particles, which often makes it challenging to terminate the reaction at the desired size. The same reaction protocol was repeated in order to synthesise small size nanoparticles; the process was followed checking the emission colour of aliquots irradiating with an UV lamp at 366 nm. When the required absorption/emission characteristics were observed, the reaction mixture was cooled down first in a cold water bath and then in ice to avoid any possible glassware damage due to the sudden drop in

temperature. Toluene was added immediately after that. Due to this relatively slow cooling the nanoparticles kept growing giving slightly larger sized particles than what was initially observed under the UV lamp. The crude mixture was then treated with acetone in order to selectively precipitate the unreacted starting material. The orange solution containing pure CdSe QDs was transferred to centrifuge tubes where subsequent washes with methanol and toluene facilitated the formation of a thick orange oil, this resultant oil was treated with isopropanol and hexane followed by centrifugation as many times as needed to finally obtain a free flowing orange powder.

### 2.1.2 Characterisation

Optical characterisation of the orange isolated NPs showed an absorption band at 512 nm (Fig. 19) and an emission band at 526 nm. The narrow band obtained might be attributed to a monodisperse size distribution for the nanocrystals (Fig. 20). Following equation (p 24) the size of the nanoparticles was calculated to be 2.6 nm.

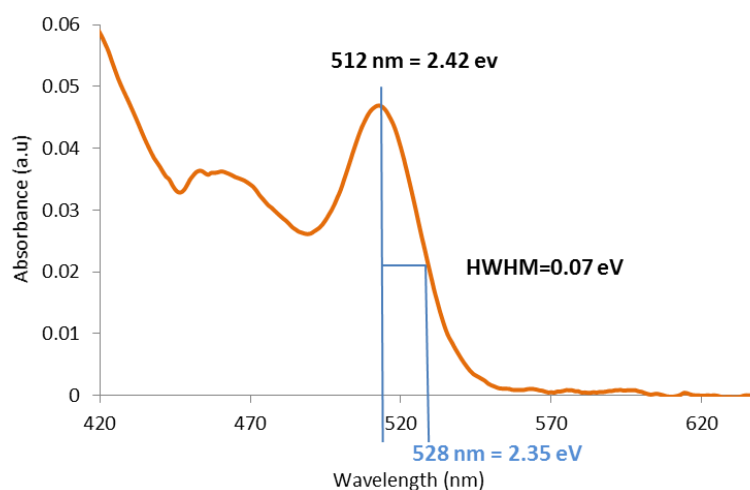


**Figure 19.** Absorption spectrum of CdSe QDs and representation of the HWHM.

A transmission electron microscopy (TEM) image represented in Figure 20 illustrates typical  $\sim 2.6$  nm spherical CdSe QDs.

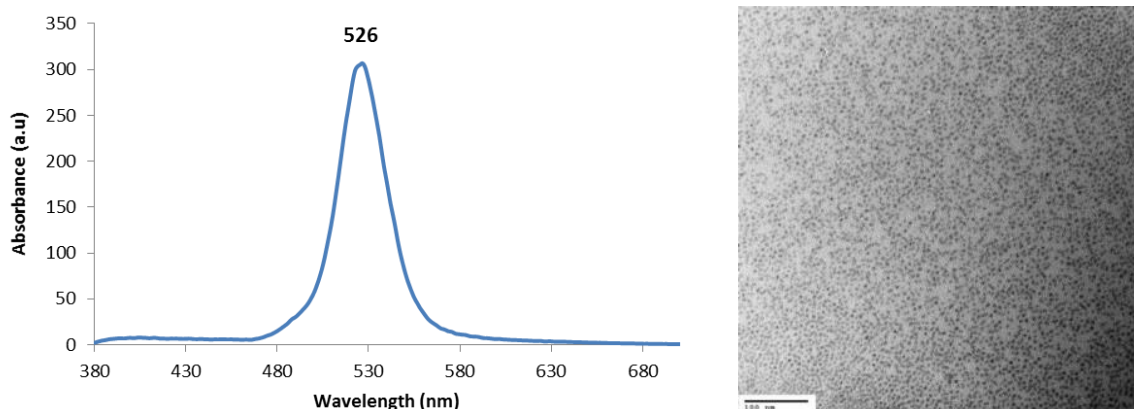


**Figure 20.** Photoluminescence spectrum on the left, and TEM image<sup>[83]</sup> of 2.68 nm averaged size CdSe nanoparticles on the right (picture courtesy of Dr Chiranjib Banerjee).

For many applications and also for our purpose it is essential to determine the concentration of QDs in the solution; gravimetric methods are not suitable for accurate measurements when working with nanocrystals due to the difficult identification of the number of ligands on the surface and their variability under different conditions. Accordingly considerable discrepancies regarding this matter can be found in the literature.<sup>[85]</sup>

The molar extinction coefficient ( $\epsilon$ ) is a parameter that has allowed scientists to calculate concentrations of nanocrystals in the media by their relationship in the Beer-Lambert law.

$$A = \epsilon c l$$

In equation,  $A$  is the absorbance for a given sample,  $c$  is the molar concentration (mol/L) of the same sample,  $l$  is the path length which in our case will always be fixed at 1 cm, and finally  $\epsilon$  is the molar extinction coefficient (L/ mol cm). This optical method is widely accepted as the most convenient way to determine particle concentrations.

Peng et al.<sup>[85]</sup> reported the experimental determination of the extinction coefficient for the first absorption peak energies for CdTe, CdSe and CdS nanocrystals. Their results show that the molar extinction coefficient at the band-edge increases with size of the nanoparticles; this parameter seemed independent of the nature of the capping ligands, the refractive index of the solvents, the fluorescence quantum yield, and the protocol followed for the synthesis of QDs.

Mulvaney et al.<sup>[84]</sup> established new size-dependent first absorption peak and molar extinction coefficient calibration curves, based on TEM, inductively coupled plasma-optical emission spectroscopy (ICP-OES), and UV-Vis absorption spectroscopy. Unlike Peng et al. who based their  $\epsilon$  calculations on small aliquots that were extracted from the reaction mixture, Mulvaney et al. isolated full reaction batches for all sizes, allowing perhaps a more thorough removal of unreacted starting material. In this work all calculations are performed based on Mulvaney's calibration formulae.

The molar extinction coefficient was calculated from the exponential function below,<sup>[84]</sup> where  $E_{1S}$  is the first absorption peak energy in eV. UV-Vis absorption spectra of our synthesised 2.6 nm CdSe QDs (Figure 19), shows the first absorption peak at 512 nm, which after conversion gives a value of 2.42 eV. Consequently, the molar extinction coefficient for our CdSe nanocrystals is  $1.63 \times 10^5 \text{ M}^{-1} \text{ cm}^{-1}$ .

$$\epsilon_{1S} (\text{M}^{-1} \text{ cm}^{-1}) = 155\,507 + 6.67054 \times 10^{13} \exp\left(-\frac{E_{1S}}{0.010551}\right)$$

The next step was to determine the concentration of particles in the solution, and subsequently calculate the molecular weight of our CdSe QDs. The modified Beer-Lambert law equation<sup>[84]</sup> was followed. The only value left to compute was the half-width-half-maximum of the first absorption peak on the low energy side,  $\Delta E_{1S, HWHM}$ . Figure 19, represents how a value of 0.7 eV is obtained from the absorption spectrum.



$$[CdSe](M) = \frac{Abs}{l(cm)\epsilon_{1s}(M^{-1}cm^{-1})} \times \frac{\Delta E_{1s,HWHM}(eV)}{0.06}$$

A concentration of  $3.36 \times 10^{-7}$  M of CdSe in the cuvette is accordingly obtained *via* optical measurements, equation 4. Working with a stock solution of known concentration finally allowed us to calculate the molecular weight of our CdSe nanoparticles as 101 000 g/mol.

So far the inorganic core of the nanocrystal has been characterised but, as previously discussed, the capping ligands constitute a very important part of the overall QDs, influencing their properties and applications. Consequently, Figure 21 depicts  $^1\text{H-NMR}$  comparison spectra. Free oleic acid (OA) (top) shows very sharp and well-resolved peaks with the expected chemical shifts and splitting; assignment<sup>[86]</sup> of all signals is also illustrated. The bottom spectrum shows broad signals of the bonded OA to the surface of the QD. It is worth noting the disappearance of the signal B, these are the closest protons to the nanoparticles' surface, hence the ones that are more affected by the chemical environment on the surface which can lead to shifts or even disappearance of the signals.<sup>[87]</sup>

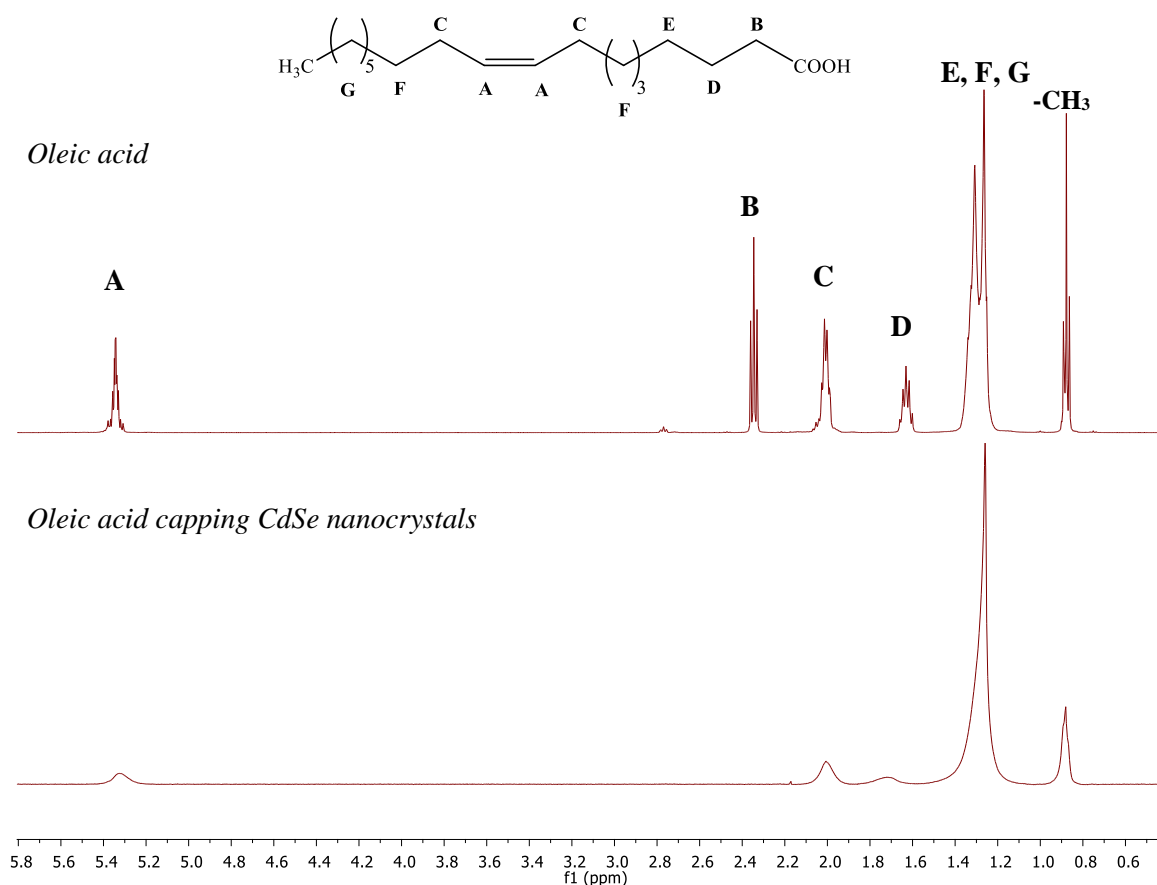


**Figure 21.** Free and bound oleic acid  $^1\text{H-NMR}$  spectra.

This broadening effect on the solution NMR spectra of capped nanoparticles is widely accepted and has been the focus of some studies.<sup>[87]</sup> There are two different models<sup>[88],[89]</sup> in the literature that explain this feature; one interpretation is based on the slow motion of the nanocrystals,



and the other is concerned with the inhomogeneity of the chemical environment of the surface ligands.

In addition to this broadening, there is also a complete absence of the acidic protons of the oleic acid groups at 11 ppm (which are omitted in the Figure 22 for clarity), strongly supporting the formation of the ligand – QD pair. In order to calculate the number of ligands that are attached to the surface, a quantitative  $^1\text{H-NMR}$  spectrum was recorded using ferrocene as internal reference.

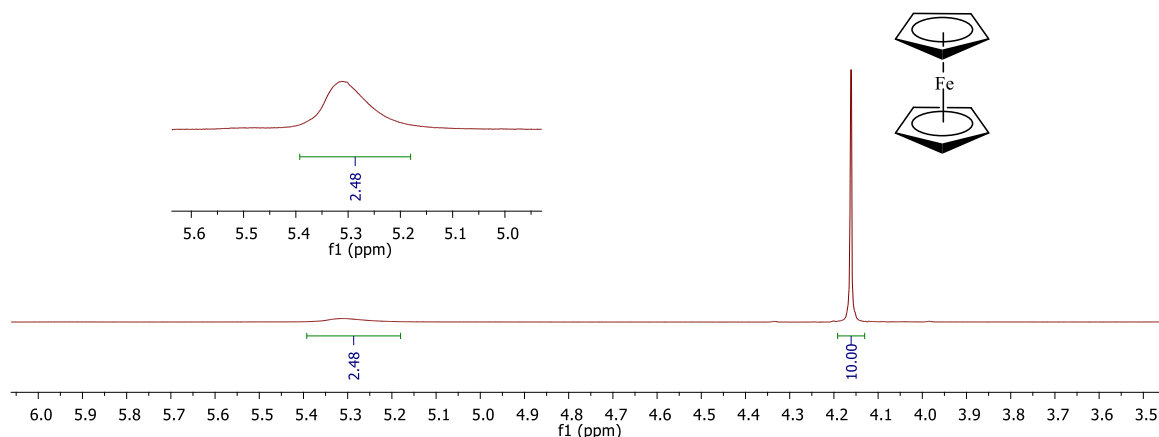


**Figure 22.** Integration of the ferrocene reference against the double bond protons of OA.

Integration of the 10 protons of the ferrocene molecule against the double bond signal of the oleic acid molecule (in this case 2.48), gives us  $1.34 \times 10^{-5}$  moles of OA. Taking into account the molecular weight of OA (282.46 g/mol), the relationship between these parameters allows us to calculate the number of molecules of OA and CdSe in each sample (see table 1). In essence, each nanoparticle is formed by 37% of OA capping ligands and a 63% corresponds to the CdSe inorganic core on average. This experiment was repeated several times obtaining similar values, therefore it can be concluded that the average number of molecules of OA capping each quantum dot is 213.

Experiment	Molecules of OA	Molecules of CdSe	% of OA	% of CdSe	Molecules of OA capping each NP
1	$8.1 \times 10^{18}$	$4.0 \times 10^{16}$	36	64	200
2	$8.3 \times 10^{18}$	$4.2 \times 10^{16}$	36	64	198
3	$8.8 \times 10^{18}$	$3.5 \times 10^{16}$	41	59	251
4	$8.4 \times 10^{18}$	$3.8 \times 10^{16}$	38	62	221
5	$8.4 \times 10^{18}$	$4.3 \times 10^{16}$	36	64	195
6	$8.3 \times 10^{18}$	$3.9 \times 10^{16}$	37	63	213

**Table 1.** Quantitative results regarding OA capping each nanoparticle.

These results show that the numbers fluctuate in each experiment, perhaps due to a sum of errors; from the precision of the balance, to the integration technique of the broad  $^1\text{H-NMR}$  signal.

The numbers are similar within the experimental error, therefore an average is reported in order to get a rough quantitative understanding on the structure of the synthesised quantum dots.

To study if these results are in accordance with the size of the QD, the capping ligand was modelled on a 3D software, calculating that the distance between each oxygen of the carboxylic acid is 0.22 nm (Figure 23).

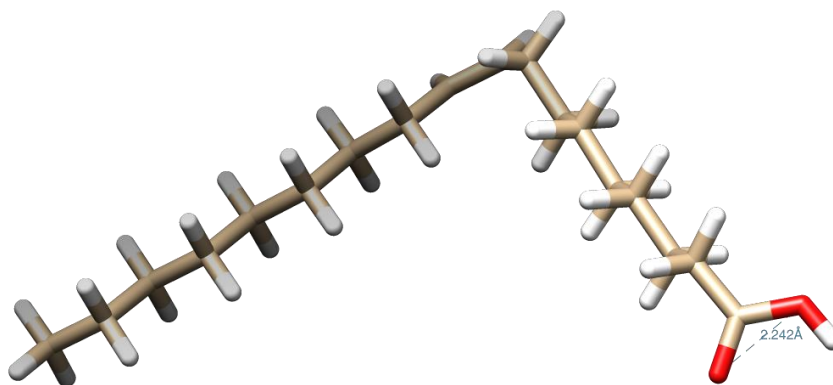


**Figure 23.** Oleic acid performed on Chimera 1.9 software.

If this distance is considered as the diameter of a circle, then the area of that circle ( $A = \pi \cdot r^2 = 0.0394 \text{ nm}^2$ ), would be approximately the surface that each ligand would need in order to be accommodated on the QD. This takes into account that 2.6 nm is the diameter of our QDs and considering the shape of the CdSe nanocrystals as a sphere. The formula of the surface area of a sphere ( $S = 4\pi \cdot r^2$ ) gives us an approximate total surface of 21.24 nm<sup>2</sup> for the synthesised QD.

Assuming that all nanoparticles adopted a wurtzite crystal structure, and based on previous studies,<sup>[84]</sup> QDs synthesised with this protocol are rich in cadmium. Taylor, Kippeny, and Rosenthal<sup>[90]</sup> calculated that CdSe nanocrystals are formed by an average Cd/Se ratio of 1.2:1. They also concluded that the excess of Cd is on the surface of the crystal and on average, 70% of the nanocrystal surface is Cd, while 30% is Se. Interestingly, they obtained a larger TOPO coverage (70%) than previously reported, owing to their consideration of the shape of the QD as hexagonal prism instead of a sphere. Taking their results into account then only a 14.87 nm<sup>2</sup> of our previously calculated surface would be covered by Cd sites, and considering a maximum of 70% coverage a figure of 264 molecules of OA on the surface is theoretically obtained. Hens et al.<sup>[91]</sup> reported 175 ± 15 OA ligands per 3.5 nm size CdSe QDs, the anionic ligands would also balance the charges of the excess of Cd<sup>2+</sup> on the surface resulting in overall neutral QDs.

These simplified calculations do not take into consideration repulsion forces and spatial limitations due to hinderance between the long aliphatic chains of OA; but as previously noted these are approximations in order to get better understanding on the surface of these nanoparticles, therefore our experimentally calculated coverage of 213 OA molecules per QD seems reasonable.

## 2.2 Subphthalocyanines

### 2.2.1 Surfactant design for ligand exchange purposes

Chemical modification of nanocrystal surfaces is an important area of study that is exponentially attracting the attention of worldwide scientists. This interest is fundamentally due to the impact that the organic ligand shell produces on the properties of the overall material.<sup>[2]</sup> Achieving a controlled modification of the surface by ligand exchange has proved to be an important resource towards, for example, functionalisation with biomolecules or tuning the conductivity of nanoparticle arrays amongst others.<sup>[91]</sup>

Ligand exchange provides an interesting tool to manipulate the surface of a nanocrystal, by means of the replacement of the original ligands used during the synthesis, by another desired ligand with high affinity towards the QD. Widely accepted capping ligands owing to their great affinity for the CdSe surface are, pyridine, alkylamines, and thiophenes. Thiols, carboxylic acids, phosphonic acids and phosphine oxides are considered the strongest ones,<sup>[49]</sup> whereas the most frequently used surfactants are trioctylphosphine oxide, dodecanethiol, oleylamine, hexadecylamine, and phosphonic acids.<sup>[2], [92]</sup>

The ligand exchange process involves treatment of the nanoparticles with a large excess of the replacement ligand, this partially or completely exchanges the original surface molecules. Interestingly, due to the effect of mass action, the new ligand could have lower affinity to QD surface than the surfactant to exchange.<sup>[2]</sup> For instance, when CdSe nanocrystals coated with TOPO are refluxed in pyridine, although pyridine is a weaker surfactant this excess results in the displacement of TOPO ligands.<sup>[53]</sup>

Our work aims to synthesise SubPc molecules bearing promising ligands for nanoparticle capture or surface attachments, such as pyridine or alcohols. The ligand design could be an important matter for future applications, therefore the orientation of such ligands was studied by modelling the target compounds in a computational program, Chimera 1.9. Figures 24 and 25 illustrate the direction of the lone pair of the nitrogen atoms in the pyridyl-ligands. In case of the (2-pyridyl)<sub>3</sub>-SubPc-OPh **34** the coordination is pointing towards the centre of the cavity having an average distance of around 1.7 nm, perhaps large enough to encapsulate small nanoparticles, Figure 20.

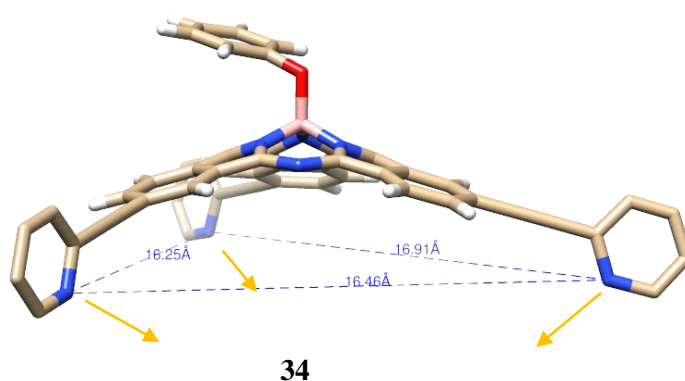


**Figure 24.** Computational model of (2-pyridyl)<sub>3</sub>-SubPc-OPh **34**.

On the other hand, (3-pyridyl)<sub>3</sub>-SubPc-OPh **35** has the same concave shaped structure typical for subphthalocyanines but the lone pairs of the N are available for coordination to the desired quantum dot in a different way, represented in Figure 25. In this case the chromophore could be accommodated sitting atop the quantum dot's surface or merely on a flat surface.

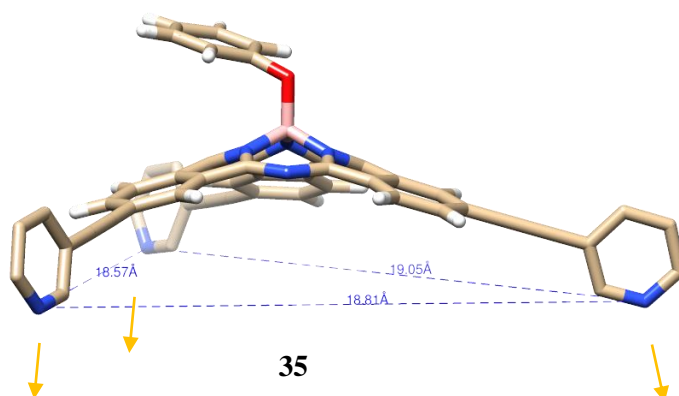


**Figure 25.** Computational model of (3-pyridyl)<sub>3</sub>-SubPc-OPh **35**.

Thiophenes are promising ligands for surface attachment to gold nanoparticles, whereas amines and alcohols proved to be better for capping nanoparticles, such as silicon or CdSe. Figure 26 illustrates the computational model of the target molecule bearing 3-hydroxy groups at the periphery, (Ph-CH<sub>2</sub>OH)<sub>3</sub>-SubPc-OPh **36**. Three-dimensional structures helped visualisation of the cavity sizes and especially assisted the design process, whereby the position of each substituent in the rings plays an important role.

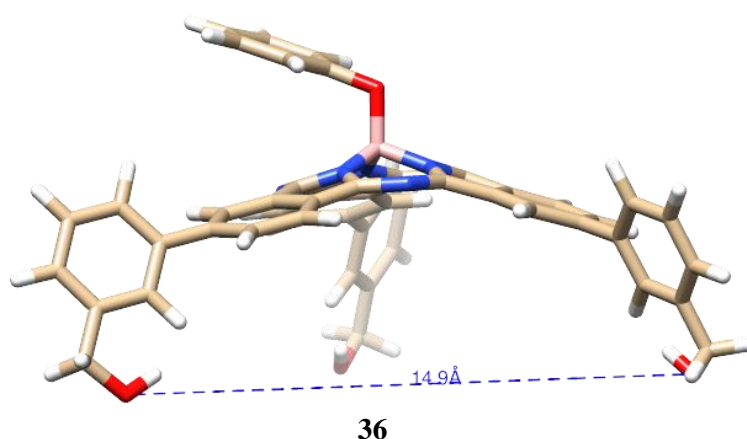


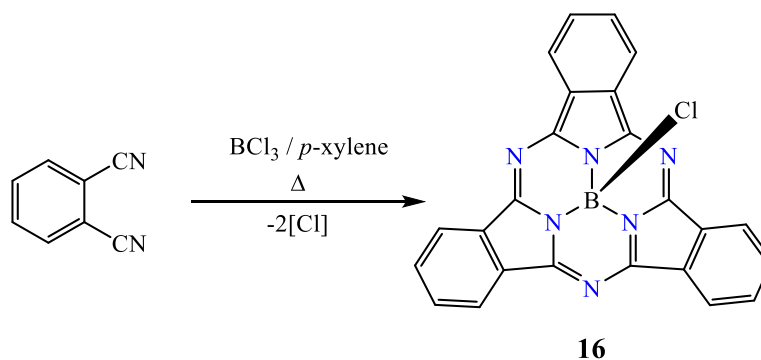
**Figure 26.** Computational model of (Ph-CH<sub>2</sub>OH)<sub>3</sub>-SubPc-OPh **36**.

### 2.2.2 Synthesis

Subphthalocyanines are typically synthesised in good yields by cyclotrimerisation reaction of phthalonitrile derivatives and a boron trihalide,<sup>[32]</sup> in the presence of a high boiling solvent such as 1-chloronaphthalene. In these reactions the boron reagent acts as Lewis acid and template. Hitherto, SubPcs without metal or with different central atom are unknown. BCl<sub>3</sub> is the most widely used boron source due to the good yields obtained and better stability of the chlorosubphthalocyanines formed owing to the higher stability of the B-Cl bond compared to the

B-Br bond. However, the handling of this moisture sensitive and gaseous reagent compromised the reproducibility and the performance of the reaction.

Torres et al.<sup>[93]</sup> described a new high yielding protocol for SubPc formation that involves a high aromatic boiling solvent such as *p*-xylene, the reported procedure is simple and straightforward thanks to the utilisation of a readily available solution of BCl<sub>3</sub> in *p*-xylene, Scheme 10. This allows the addition of precise quantities of boron trichloride and the two equivalents of chlorine released during the formation of the SubPc **16** can be efficiently consumed by this solvent,<sup>[94]</sup> avoiding chlorinated by-products.<sup>[95]</sup>



**Scheme 10.** Synthesis of unsubstituted SubPc **16**.

Their experiments showed that an excess of BCl<sub>3</sub> is required and a maximum yield of 82% is obtained when one equivalent per starting phthalonitrile is added. This procedure was reproduced in order to synthesise SubPc-Cl **16**. Accordingly, 1 equiv. of BCl<sub>3</sub> from a commercial 1M solution in *p*-xylene was added to phthalonitrile under an argon atmosphere, (the method does not require the addition of any extra solvent). However, after 1 hour refluxing and a purification process that consisted of flushing the resultant crude mixture with argon (to remove any possible unreacted boron trichloride) and a soxhlet extraction with toluene, less than 20 % yield of the unsubstituted SubPc **16** was finally isolated.

The main product was isolated as an off-white solid but unfortunately it did not correspond to the desired SubPc. Its <sup>1</sup>H-NMR spectrum, illustrated in Figure 27, shows two multiplets typical for an AA'BB' pattern at around 7.8 ppm and a broad singlet; this characteristic spectrum was indicative of the formation of phthalimide, possibly owing to the presence of adventitious water or oxygen in the reaction. Two bands at around 3180 cm<sup>-1</sup> for the -NH and a strong band at 1745 cm<sup>-1</sup> owing to the C=O in the IR spectrum were the final evidence that confirmed the structure of phthalimide.

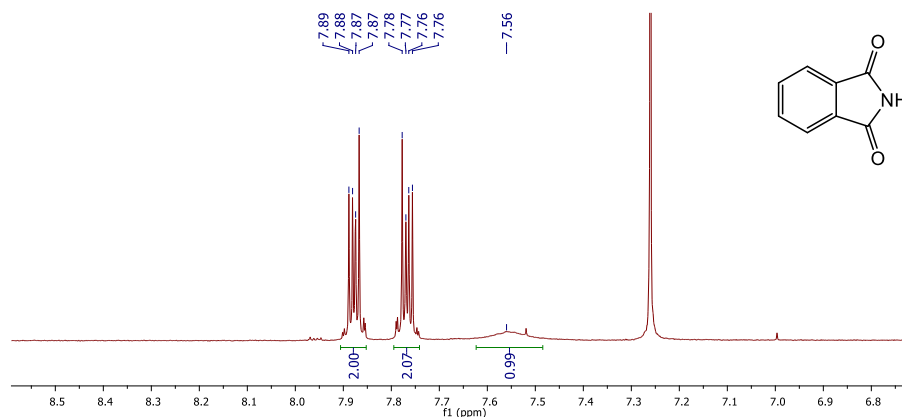


**Figure 27.**  $^1\text{H-NMR}$  of the by-product isolated during the SubPc formation.

This reaction was repeated with similar outcome, the formation of a black tar was indicative of the fast decomposition of the macrocycle. Different reagent ratios were tested, varying also the amount of solvent added in the reaction, time and purification process. Better results were observed when starting from a recrystallised phthalonitrile, but the yields were only slightly improved. The best results were obtained following a modified procedure based on Kennedy et al.'s<sup>[96]</sup> protocol, which involved the use of a large amount of solvent resulting in less decomposed material and less phthalimide formed. In this procedure, phthalonitrile was dissolved in *p*-xylene,  $\text{BCl}_3$  was added dropwise and the reaction mixture was brought to reflux gently over a period of 30 minutes and heated for further 3 hours. After evaporation of the solvent, the resultant solid was washed with cold hexane and subsequently extracted in a soxhlet apparatus with chloroform. The product was then isolated as a pink solid in 41% yield.

The optimal conditions for the formation of subphthalocyanines were established in this manner, allowing this protocol to be followed in all subsequent SubPc reactions described in this thesis.

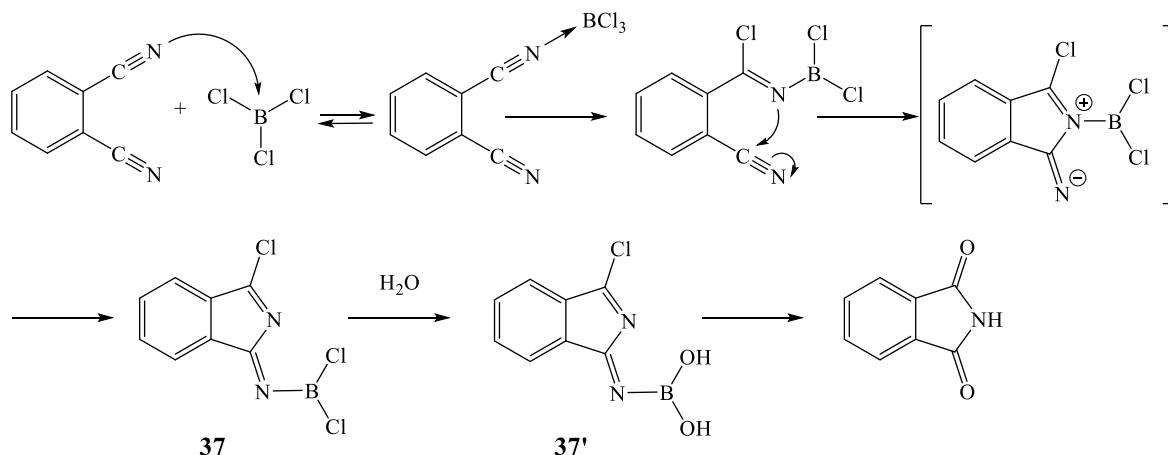
### 2.2.2.1 Mechanism for SubPc formation

The mechanism involved in subphthalocyanine formation has prompted some hypotheses.<sup>[97]</sup> In 2007 Torres et al. revealed the first mechanistic study of chloro-SubPc formation from phthalonitrile and  $\text{BCl}_3$  in *p*-xylene.<sup>[98]</sup>

There are two main stages involved in the mechanism of this reaction, the first concerning the oligomerisation of the phthalonitrile reactant to form the skeleton of the macrocycle, and the second one implying the reduction of the system in order to form the final SubPc system.

Torres et al.'s investigations suggested that the rearrangement of the initial phthalonitrile- $\text{BCl}_3$  adduct produces (1*Z*)-3-chloro-*N*-(dichloroboryl)-1*H*-isoindol-1-imine **37** (Scheme 11), which subsequently hydrolyses to form compound **37'** under adventitious moisture

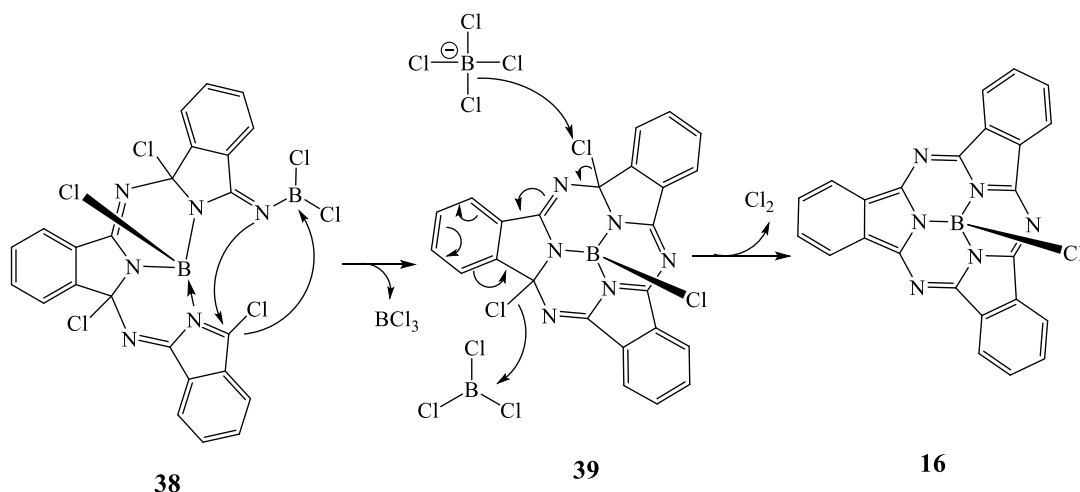
present during the isolation process, and then to the corresponding phthalimide. The hydrolysis products were confirmed by  $^1\text{H-NMR}$  spectroscopy.



**Scheme 11.** First stage in the mechanism of SubPc formation and hydrolysis products.

It is widely accepted that the initial step during the oligomerisation process is a desymmetrisation of the precursor such as phthalonitrile or 1,3-diiminoisoindoline, into a species that is both nucleophilic and electrophilic, such as compound **37**.

The progressive build-up of this species presumably occurs around a boron atom acting as the template in order for the cyclisation to proceed, leading to open trimer structure **38**. Quantum-chemical computations<sup>[98]</sup> suggested that the proposed reaction steps leading to the formation of the SubPc-precursor macrocycle **39** are exothermic or at least kinetically allowed. Once the macrocycle is formed, a reductive step occurs liberating chlorine in the form of  $\text{Cl}_2$ , Scheme 12.



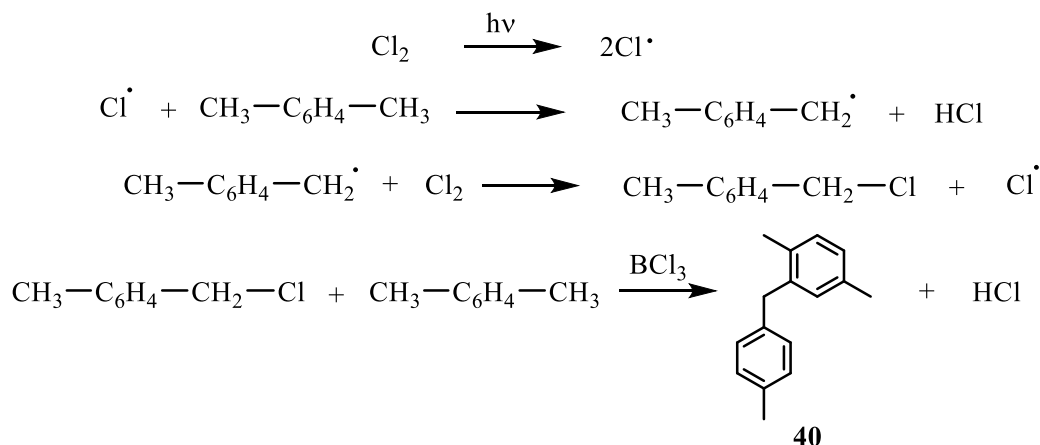
**Scheme 12.** Ring closing and reduction to achieve SubPc-Cl **16**.

The detachment of chlorine from **39** (Scheme 12) is assumed to be facilitated by the gain of conjugation in going from the precursor to the final product SubPc-Cl **16**.

It has been observed that when the reaction is left at reflux for a prolonged period of time, peripherally halogen-substituted SubPc by-products are formed.<sup>[95]</sup> However the addition of alkylaromatic solvents to the reaction seemed to reduce this chlorination.<sup>[99]</sup> Torres et al. investigated

this further,<sup>[98]</sup> and it was observed that reactions carried out in *p*-xylene under exposure to light gave rise to by-product **40**. A possible free-radical chain reaction responsible for this process is represented in Scheme 13.

When working under light exposure, photolysis of the Cl<sub>2</sub> produced during the macrocyclisation process would give rise to free-radical chlorine atoms that react very fast with xylene by hydrogen-abstraction. The benzylic chlorination of *p*-xylene would then occur, followed by a Friedel-Crafts reaction with another molecule of solvent catalysed by boron trichloride to produce 1,4-dimethyl-2-[(4-methylphenyl)-methyl]benzene **40**.



**Scheme 13.** Free-radical chain reaction during the reaction of SubPc formation under light.<sup>[98]</sup>

However, chlorinated products such as 2,5-dimethylchlorobenzenes or 1-chloromethyl-4-methylbenzene were not detected, suggesting that Cl<sub>2</sub> disappears efficiently through the chain reaction, and all the chlorine is eventually lost as HCl. The authors concluded that the use of aromatic solvents such as *p*-xylene or toluene, would influence a protective effect of the product SubPc and precursors, leading to an improve yield.<sup>[93]</sup>

### 2.2.2.2 Reactivity

SubPcs are synthetically versatile molecules whose reactivity may be classified in three main groups (see Scheme 14): a) ring-expansion reactions, imply ring-opening and recyclisation reaction to incorporate an additional isoindole unit to form low-symmetry A<sub>3</sub>B phthalocyanines, b) axial reactivity, which concerns the apical B-X group, and b) peripheral reactivity, regarding the introduction of functional groups at the benzenoid ring positions.

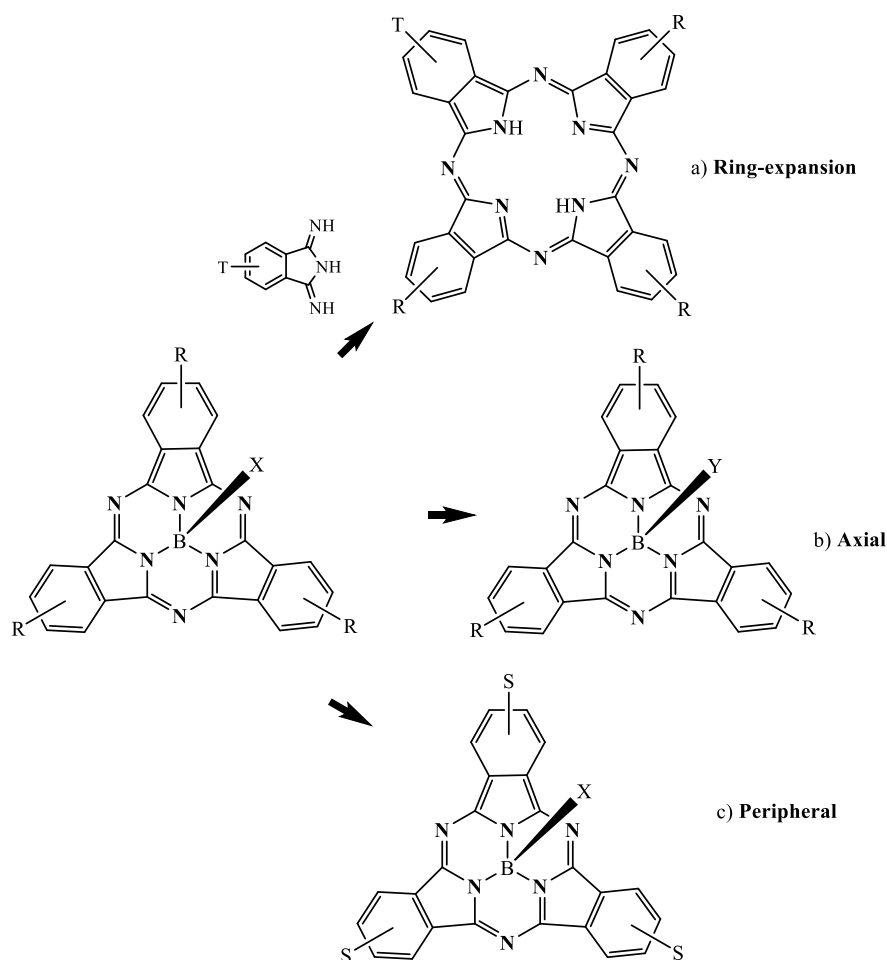
#### a) Ring-expansion reactions

Strategies for the synthesis of unsymmetrical Pc are mainly based on statistical condensation reactions of two different phthalonitriles, giving complicated mixtures that cannot be readily separated by chromatographic techniques. In 1990, Kobayashi et al.<sup>[100]</sup> published the first method



for the synthesis of such challenging unsymmetrical Pcs from SubPc precursors, the strained arrangement in the subporphyrinoid macrocycle could presumably facilitate the ring-expansion to take place, leading to reasonable yields and high selectivity.

Interestingly, other unsymmetrical Pcs became synthetically more available through the contribution of van Lier and colleagues,<sup>[101]</sup> when they reported the first synthesis of unsymmetrical SubPcs and their subsequent ring opening leading to complex structures which are difficult to prepare *via* alternative methods. The ring-opening route has promise for designing new unsymmetrical peripherally-modified Pcs.<sup>[102], [32]</sup>



**Scheme 14.** Main SubPc functionalisation routes.

#### b) Axial functionalisation

The functionalisation at the boron atom in SubPcs is the most used method to build more complex structures, and a straightforward way of varying its properties. For instance, replacing the halogen atom by alkylated pyridinium substituents leads to water soluble molecules, promising candidates for biological applications.<sup>[103]</sup> Or attaching less labile substituents can enhance thermal, optical, and chemical stability.<sup>[104]</sup> The halogen atom (X) in the axial position (Scheme. 14) can be replaced by nucleophiles, such as alcohols, alkylmagnesium bromides, phthalimides, phosphates,

phosphonates, etc.<sup>[39]</sup> as well as undergoing other ligand exchange reactions.<sup>[30]</sup> Axial replacement reactions typically require high temperatures, which can lead to decomposition *via* ring-opening.

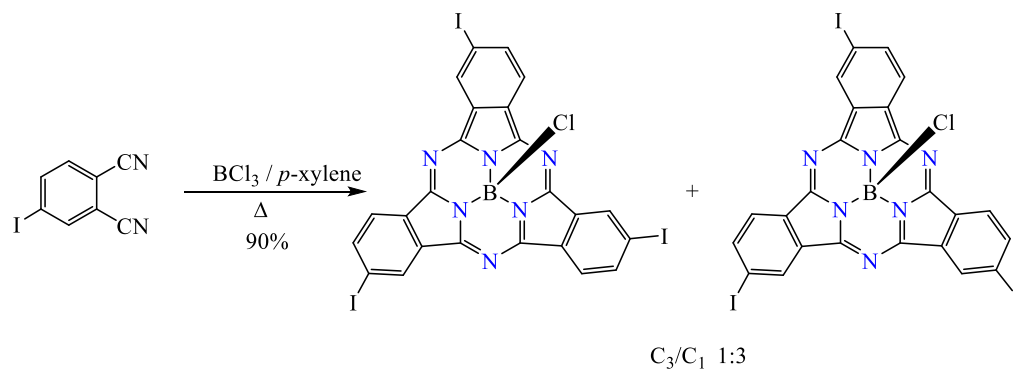
This issue was overcome in a recent publication by the irreversible replacement of the chlorine ligand to obtain a “SubPcB<sup>+</sup>” species, with a weakly coordinating triflate (OTf<sup>-</sup>) anion.<sup>[105]</sup> The activated triflate-SubPc intermediate shows considerable reactivity towards nucleophilic attack, which allows reaction at room temperature to form a wide range of new axially-substituted SubPcs, with increased yields and performance of the reactions.

### c) Peripheral functionalisation

Peripheral functionalisation refers to any modification occurring on the benzenoid rings of the macrocycle. These hydrogens are available for substitution by introduction of the appropriate groups into the phthalonitrile starting material or by post modification.<sup>[39]</sup> However, SubPcs tend to decompose in the presence of strong nucleophiles, acids and bases, and due to the harsh conditions required for their formation, there is a limitation on the kind of functional groups that can be introduced from phthalonitrile precursors, most typical are halogens, nitro, alkyl, thioethers or sulphones.<sup>[30]</sup> The use of other functional groups such as thiols, amines, carbonyl derivatives, etc. is restricted due to their reactivity with the boron halides used during the synthesis.

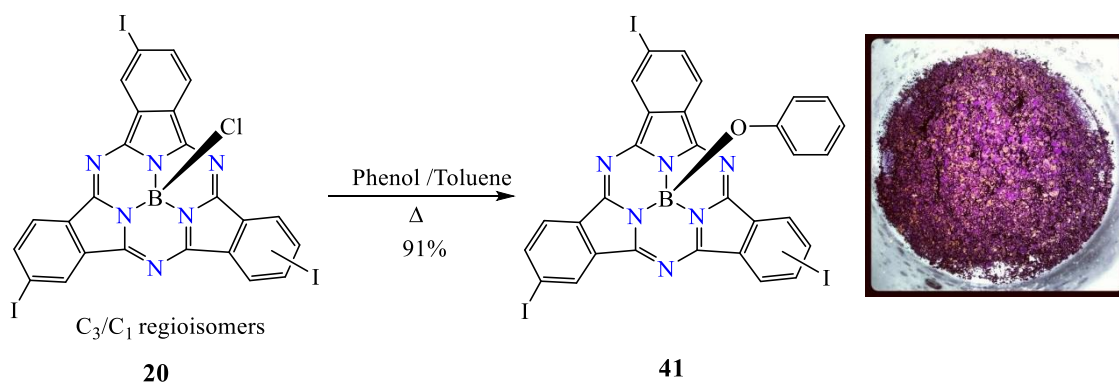
Metal-catalysed cross-coupling reactions are the most frequently employed methodology to functionalise SubPcs at the benzenoid positions once the macrocycle has been formed.<sup>[30]</sup> In our investigations towards the synthesis of possible ligands for nanoparticle attachment, mild cross-couplings were chosen to be suitable for the introduction of the appropriate substituents. It is commonly known that iodoarenes are usually the best-suited precursors in palladium-catalysed reactions; they have also been the most widely and successfully used derivatives in SubPc cross-couplings such as Stille, Suzuki or Sonogashira reactions.<sup>[30]</sup> Therefore I-SubPc-OPh **41** was chosen as the common starting material.

The synthesis began by refluxing (in xylene) commercially available 4-iodophthalonitrile in the presence of BCl<sub>3</sub> under an argon atmosphere for 3.5 hours, using the previously described optimised conditions for SubPc-Cl **16** synthesis (Scheme 15). As expected, its TLC showed a mixture of regioisomers. Column chromatography of the crude product yielded considerable amounts of axially hydroxy-substituted SubPc due to the hydrolysis of the B-Cl bond. Low yields were obtained after such separation. Considering the tediousness of the purification and the fact that for the purpose of this project the presence of both isomers does not present an issue, all compounds were carried on through the syntheses as a mixture of regioisomers. Hence, after a simple work up, which only required washing the crude material with cold methanol, a purple solid was obtained in a 90% yield as a 1:3 mixture of the C<sub>3</sub>/C<sub>1</sub> regioisomers.



**Scheme 15.** Synthesis of I-SubPc-Cl **20**.

Due to the instability of chloro-SubPcs owing to the weak B-Cl bond, and due to the improved stability and solubility of the resulting SubPc, and the easy and high-yielding protocols available in the literature,<sup>[93]</sup> phenol was chosen as the substituent for the apical position in our SubPc synthetic strategy. Following a reported protocol,<sup>[106]</sup> I-SubPc-OPh **41** was synthesised by addition of an excess of phenol to a solution of I-SubPc-Cl **20** in toluene (Scheme 16). The resulting mixture was refluxed until completion, which occurred after 27 hours. The crude material was subsequently washed with cold methanol and hexane to remove unreacted phenol, and the pure product was obtained as a bright purple solid (Scheme 16) in a 91% yield.



**Scheme 16.** Synthesis of phenoxy-SubPc **41** and appearance of the product.

Due to their low tendency to form aggregates, SubPcs display well-defined <sup>1</sup>H-NMR spectra, with very sharp peaks and defined chemical shifts. Protons on the fused benzenoid rings for compound **41** (Fig. 28) are located on the region 9.2 – 9.8 ppm, with the expected splitting. The three signals corresponding to the protons of the phenoxy- axial ligand are situated at a region from 5.4 to 6.8 ppm, and appear shielded owing to the effect of the strong core ring-current. The more upfield-shifted peak corresponds to the protons closest to the SubPc core.

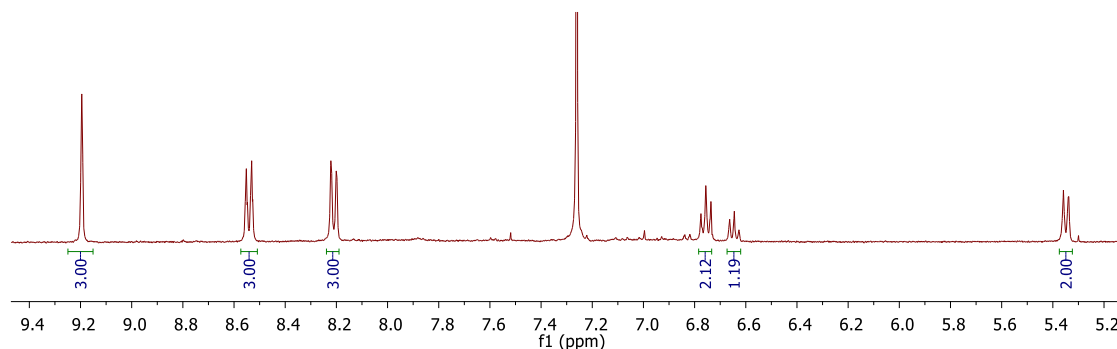


**Figure 28.**  $^1\text{H-NMR}$  spectrum of I-SubPc-OPh **41**.

Mass spectrometry of SubPcs normally shows the molecular ion peak, and very often protonated species such as in case of SubPc **41** (Figure 29). The fragmentation corresponding to the loss of the axial ligand (773 m/z) is present most of the time and it is very often the base peak, possibly owing to the fact that the boreniun cation ( $\text{SubPcB}^+$ ) “flies” better in MALDI-TOF mass spectrometry. It is also quite common to see the appearance of the hydroxy-SubPc ion peak (790 m/z), showing the easy hydrolysis of such compounds.

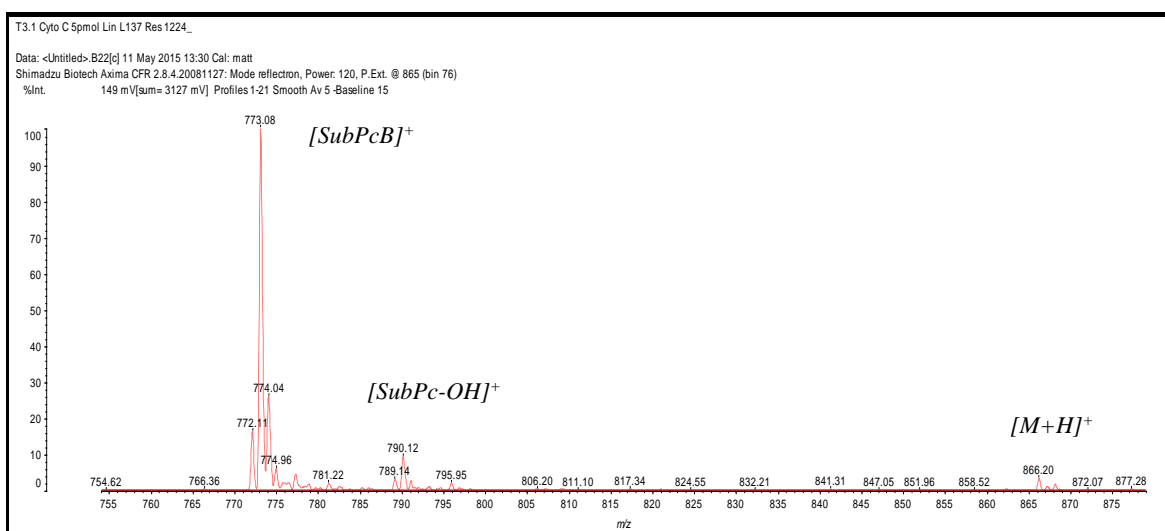


**Figure 29.** MALDI-TOF spectrum of SubPc **41**.

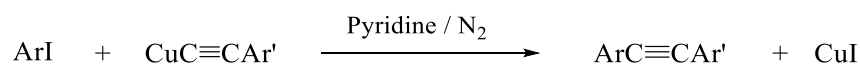
### 2.2.2.3 Peripherally functionalised SubPcs

The formation of carbon-carbon bonds is an important tool for the construction of complex materials, and metal-catalysed-cross-coupling reactions have been widely used by chemists as mild and selective ways of linking building blocks, in the fields of natural products, pharmaceuticals, liquid crystals, polymers and organic semiconductors.<sup>[107]</sup> This work is based on two important cross-coupling reactions chosen because of their versatility, the easy and fast set up of the reactions, the compatibility and stability of SubPcs towards conditions involved in the synthetic processes, and especially they offer an elegant and effective way of introducing three ligands in one single step in

the SubPc macrocycle. Accordingly, pyridyl- ligands were to be introduced by means of a Sonogashira cross coupling, and hydroxy-, nitrile-, and thiophenyl- ligands by Suzuki coupling.

### ***Sonogashira-Hagihara cross-coupling***

In 1963, Stephens and Castro reported the coupling of copper (I) arylacetylenes with iodoarenes or iodoalkenes in refluxing pyridine, Scheme 17.<sup>[108]</sup> Although it is a high yielding synthesis, there were some scope limitations due to the harsh reaction conditions and the complications associated with the copper acetylide synthesis.



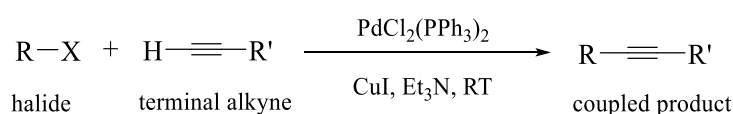
**Scheme 17.** Stephens and Castro cross-coupling reaction.<sup>[108]</sup>

To overcome such difficulties, Sonogashira, Hagihara and Tohda<sup>[109]</sup> reported in 1975 a very mild Pd-Cu catalysed cross-coupling reaction of sp<sup>2</sup>-C to sp-C atoms. This important reaction provides an ideal tool towards the synthesis of acetylenic derivatives and it has been further developed by Sonogashira and others<sup>[110]</sup> since then. It has arguably become the most used way of coupling terminal alkynes to sp<sup>2</sup> carbons.<sup>[107]</sup> This catalytic process requires the use of a palladium (0) complex, and it is performed in the presence of base and copper iodide as a co-catalyst (Scheme 18).

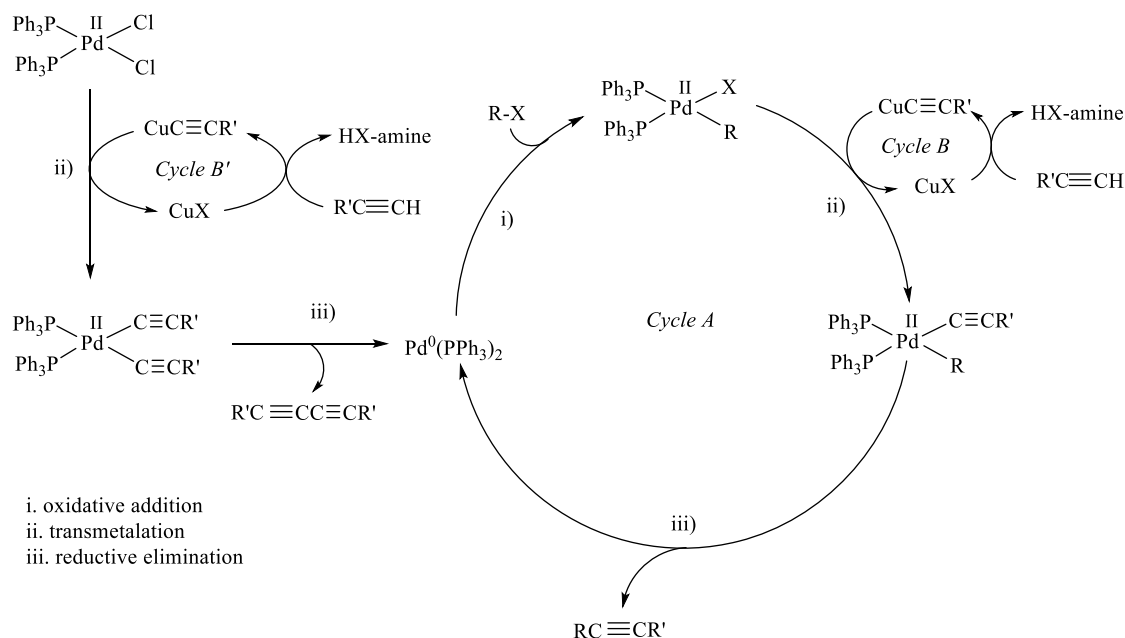
The mild conditions frequently employed (normally room temperature) is an advantage as the reaction can be used with thermally sensitive compounds. The absence of oxygen in these reactions is of utmost importance to prevent the formation of homocoupling compounds from the terminal alkyne. An aprotic amine should be used as solvent in this kind of reaction with SubPcs, the contrary could lead to ring opening and decomposition of the framework.

The use of a stable and soluble Pd (II) derivative such as bis(triphenylphosphine)palladium (II) chloride instead of a Pd (0) species is preferred. The generation of the active palladium (0) catalyst occurs after a transmetalation step with the copper acetylide (generated from a terminal alkyne, base and copper iodide, Scheme 19. *Cycle B*'), and a reductive elimination step of the homocoupled- diacetylide species, Scheme 17.

The overall mechanism of the reaction is outlined in Scheme 19. and consists of the oxidative addition of the organic halide giving a palladium (II) intermediate that undergoes transmetalation with the alkynyl copper (generated in *Cycle B*). Reductive elimination with coupling of the two organic ligands gives the product and regenerates the palladium (0) catalyst (Scheme 19. *Cycle A*).

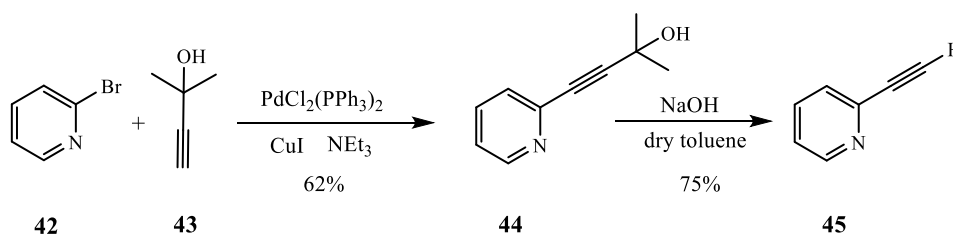


**Scheme 18.** Basic representation of Sonogashira cross-coupling reaction.



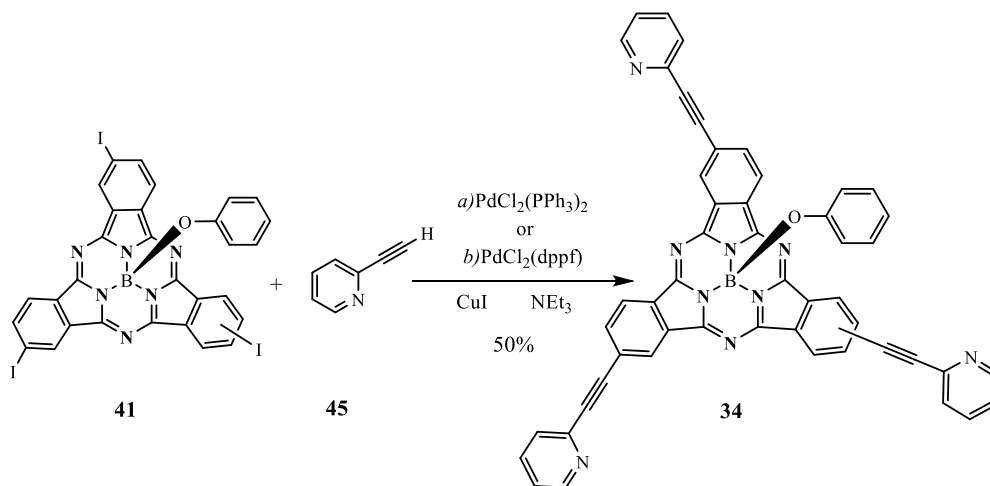
**Scheme 19.** Mechanism of Sonogashira cross-coupling reaction.<sup>[110]</sup>

First of all, the acetylenic pyridyl-substrate **44** was synthesised following a modified literature procedure.<sup>[111]</sup> 2-Bromopyridine **42** was mixed with the alkyne derivative **43**, 3% mol of the palladium catalyst and the co-catalyst CuI in dry triethylamine (Scheme 20). The suspension was stirred at room temperature for 6 hours, after which the reaction was complete. After work up, the crude mixture was subjected to column chromatography using ethyl acetate and the pure product **44** was obtained as yellow crystals in a 62% yield.



**Scheme 20.** Synthesis of 2-Ethynylpyridine **45**.

The deprotection step was carried out following literature conditions,<sup>[111]</sup> whereby a mixture of **44** was mixed with an excess of sodium hydroxide and heated under reflux in dry toluene until completion. After cooling the mixture and work up, 2-ethynylpyridine **45** was isolated as an orange oil in a 75% yield, without any other purification process required.



**Scheme 21.** Synthesis of (2-pyridyl)<sub>3</sub>-SubPc-OPh **34**.

Scheme 21 illustrates the attachment of 2-pyridylethynyl groups to the SubPc macrocycle, by means of a Sonogashira cross-coupling reaction. Literature conditions were applied<sup>[103]</sup> (Scheme 21. *a*) involving the use of freshly distilled triethylamine in the presence of catalytic amounts of PdCl<sub>2</sub>(PPh<sub>3</sub>)<sub>2</sub> and CuI. Unlike in the reported procedure, the reaction did not proceed at room temperature so the reaction was subsequently heated up to 90 °C under argon in a sealed tube. After several hours a very faint purple spot corresponding to the product was observed on the TLC, together with other fluorescent spots that could not be identified by mass spectrometry. The reaction yield was extremely low, resulting mostly in decomposition of the macrocyclic ring, easily identified due to the loss of purple colour during the reaction process.

The reaction was then attempted changing the catalyst to PdCl<sub>2</sub>(dppf) (Scheme 21. *b*). In this case the mixture was heated up gently to 70 °C to decrease thermal decomposition. After 7 hours the reaction was finished and the solvent was evaporated under reduced pressure. The resultant product was extracted with ethyl acetate and column chromatography was necessary in order to remove small amounts of mono- and di- substituted SubPc products. The desired trisubstituted (2-pyridyl)<sub>3</sub>-SubPc-OPh **34** was obtained as a purple solid in a 50% yield.

The <sup>1</sup>H-NMR spectrum of the product is presented in figure 30 (A). Three sets of signals corresponding to the phenoxy- group on the apical position appear at 6.8 – 5.4 ppm. As previously discussed the ring current of the convex face is responsible for the upfield-shift of these peaks. Their chemical shift remained unchanged compared to the starting material I-SubPc-OPh **41**. Some of the peaks that correspond to the pyridyl- ligands appear very broad (see Figure 30, A), this effect could suggest the possible coordination of the pyridyl-nitrogens to a metal. Copper iodide was used as co-catalyst in the reaction, so it seems possible that N-Cu coordination occurred. Copper induces a large broadening on the NMR signals of nearby protons influenced by its large quadrupole moment,<sup>[112],[113],[114]</sup> sometimes even resulting in undetectable signals, as in the case of copper (II) proteins.<sup>[115]</sup>

EDTA is, by far, the most widely used chelating agent in industrial applications due to its excellent sequestering performance and low cost.<sup>[116]</sup> It is composed of four carboxyl and two amino

groups, and it forms a stable chelating complex with cations in a 1:1 ratio regardless of the charge of the cation. Consequently, SubPc **34** was washed with a solution of EDTA in water twice. Figure 30. (B) illustrates the NMR spectrum after this treatment; the signals corresponding to the pyridyl- ligands get sharper and well-defined, suggesting the successful removal of the metal.

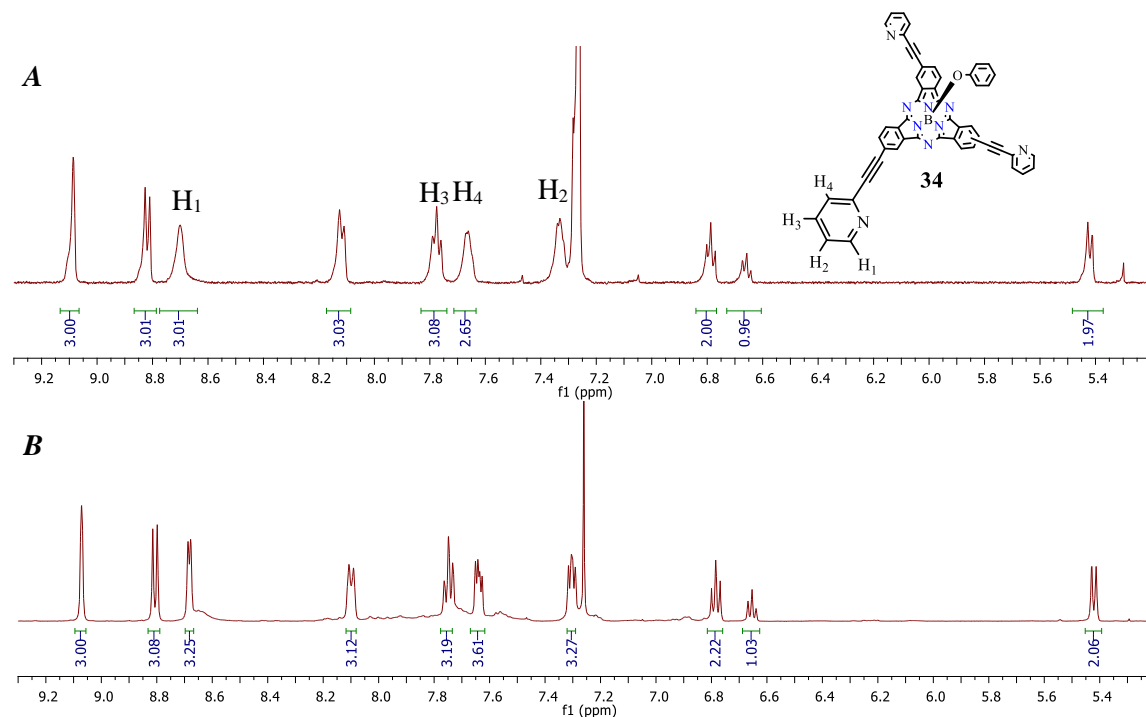
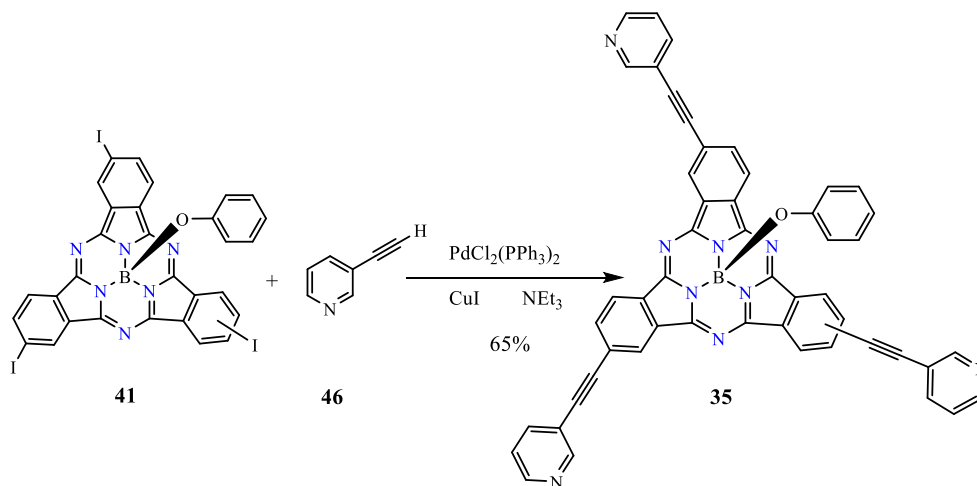


**Figure 30.**  $^1\text{H-NMR}$  comparison before (A) and after (B) treatment of SubPc **22** with EDTA.

The next target compound having pyridine-type substituents in the periphery was (3-pyridyl) $_3$ -SubPc-OPh **35**. Literature conditions<sup>[103]</sup> outlined in scheme 22 were employed. In order to avoid as much decomposition as possible, the reaction was initially carried out stirring at room temperature, but unfortunately after 42 hours there was still starting material remaining, plus mono- and di- substituted products but no sign of the required product. The starting material was getting consumed but only very slowly, so the mixture was subsequently warmed up to 40 °C. After 7 days there was still starting material present. The temperature was increased up to 50 °C which resulted in reaction completion, after a further 9 hours. At this stage there were just traces of other products on the TLC. The solvent was evaporated and the crude mixture was subjected to a column chromatography using ethyl acetate. After recrystallisation in DCM the product **35** was isolated in 65% yield as a dark purple solid. It has been demonstrated in our hands that these reactions show better performance under mild conditions, with both subphthalocyanines **34** and **35** synthesised improving the previously reported yields.





**Scheme 22.** Synthesis of (3-pyridyl)<sub>3</sub>-SubPc-OPh **35**.

A very similar pattern is seen in the <sup>1</sup>H-NMR spectrum for SubPc **35**; noteworthy is the singlet at 8.87 ppm corresponding to the proton in 2- positions of the pyridyl rings, Figure 31.

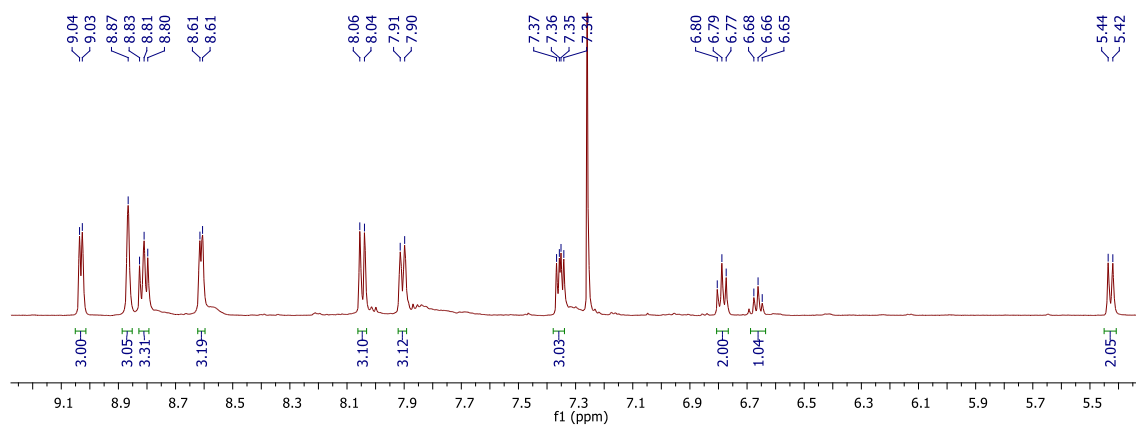
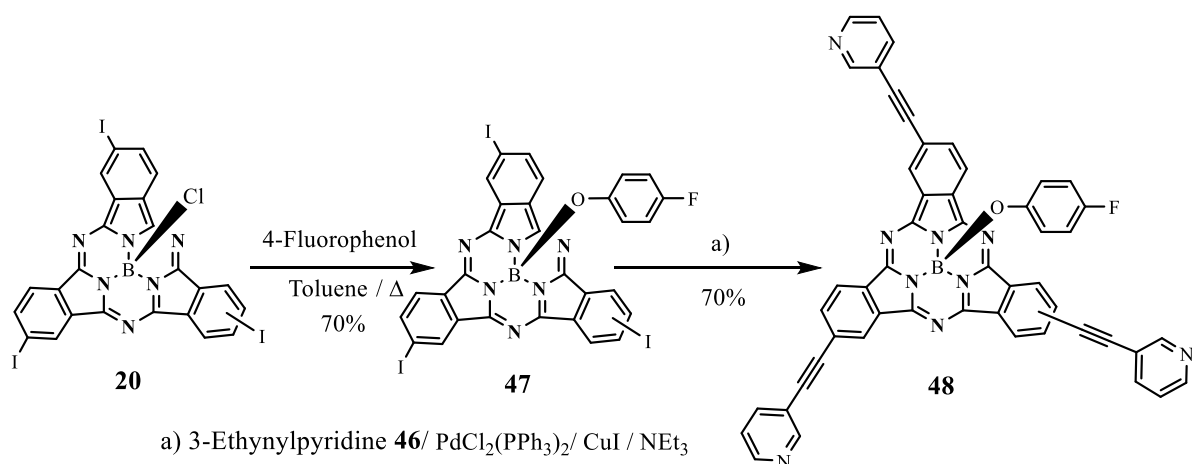


**Figure 31.** <sup>1</sup>H-NMR of SubPc **35**.

To demonstrate interchange of the apical group, novel SubPc **48** was chosen to be the next synthetic target. To achieve it, 4-fluorophenol was reacted with I-SubPc-Cl **20** in refluxing toluene. After 24 hours all starting material was consumed, the solvent was evaporated and the resulting crude residue was washed with cold MeOH and hexane. Filtration gave the pure compound as a purple solid in 70% yield.



**Scheme 23.** Reaction pathway for the synthesis of (3-pyridyl)<sub>3</sub>-SubPc-(4-F-OPh) **48**.

3-Ethynylpyridine **46** was then grafted at the periphery of SubPc **47**, as illustrated in Scheme 23, by reacting it under the previously developed Sonogashira conditions. The mixture was heated up to 50 °C in a sealed tube under argon for 11 hours. The required compound was the most intense spot on the TLC and there were only faint spots corresponding to the di-substituted macrocycle. Hence, the solvent was evaporated and the crude mixture was purified by column chromatography, obtaining the pure (3-pyridyl)<sub>3</sub>-SubPc-(4-F-OPh) **48** in a 70% yield.

The <sup>1</sup>H-NMR spectrum of **48** is depicted in Figure 32. In the spectrum A it can be observed that some peaks are missing. It was previously mentioned that the interaction with copper metal can result in undetectable signals in the NMR. In this case there are two broad and featureless peaks potentially corresponding to the pyridyl protons at around 8.7 and 7.5 ppm. The same treatment with EDTA was applied for this compound. The bottom NMR spectrum (Fig. 32 B) illustrates how the peaks appear after the treatment for copper removal. The 4-fluorophenoxy ring appears at a region from 5.4 to 6.5 ppm and depicts two expected sets of signals owing to its symmetry. Interestingly, the closest protons to the more electronegative atom, i.e. fluorine, appear downfield shifted and show experimentally a triplet with a <sup>3</sup>J = 8.8 Hz, due to the similar coupling constant values with the neighbouring proton and fluorine.

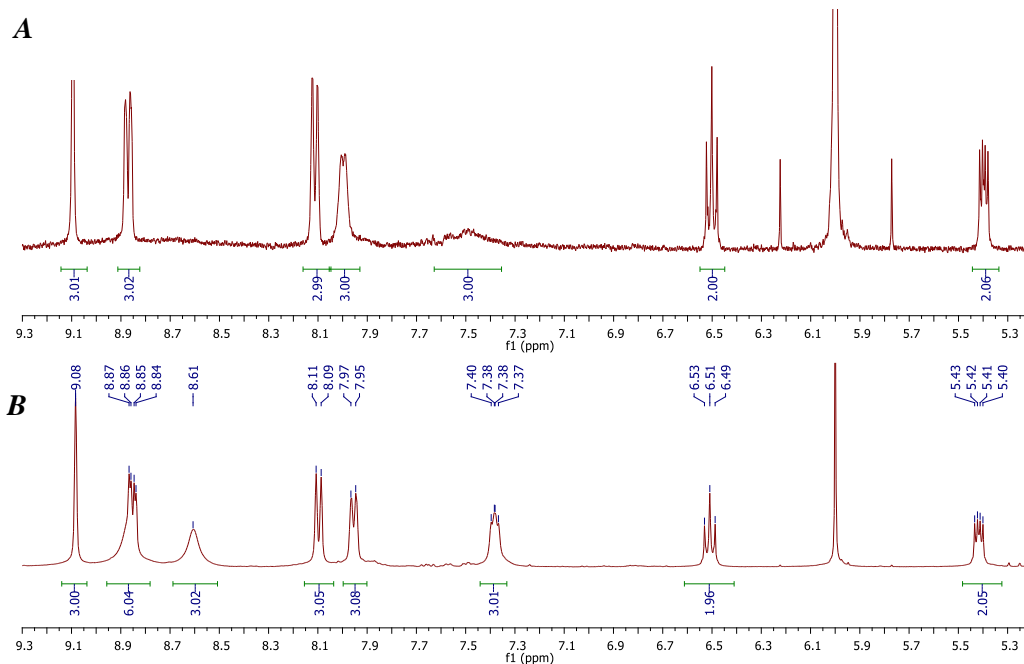
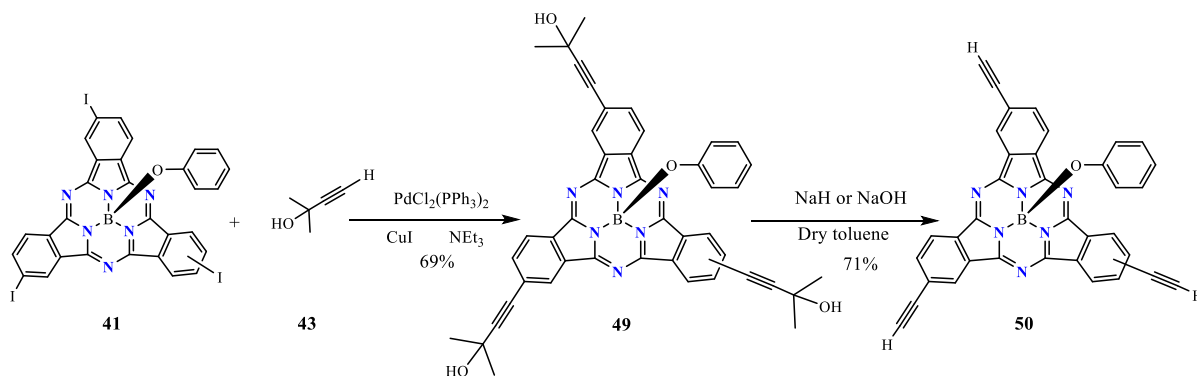


**Figure 32.**  $^1\text{H-NMR}$  comparison before (A) and after (B) treatment of compound **48** with EDTA.

Our interest goes beyond synthetic research efforts, but to synthesise SubPc derivatives that can be subjected to subsequent derivatisation towards more complex systems with interesting and unique properties. To give access to such compounds in our group, SubPc **50** was the next target to accomplish. This molecule was synthesised by Torres and co-workers<sup>[117]</sup> by means of Stille cross-coupling reaction, however due to the above described optimisation process of Sonogashira conditions, the former coupling method was selected.

We selected the commercially available 2-methylbut-3-yn-2-ol **43** as the protected acetylene starting material. Coupling of this alkynol with iodo-SubPc **41** was carried out in the presence of catalytic amounts of palladium catalyst and copper (I) iodide. This reaction proceeded smoothly under stirring at room temperature, and was complete after 25 hours. After an aqueous work up and a chromatographic purification, (alkynol)<sub>3</sub>-SubPc-OPh **49** was isolated as a dark purple solid in 69% yield.



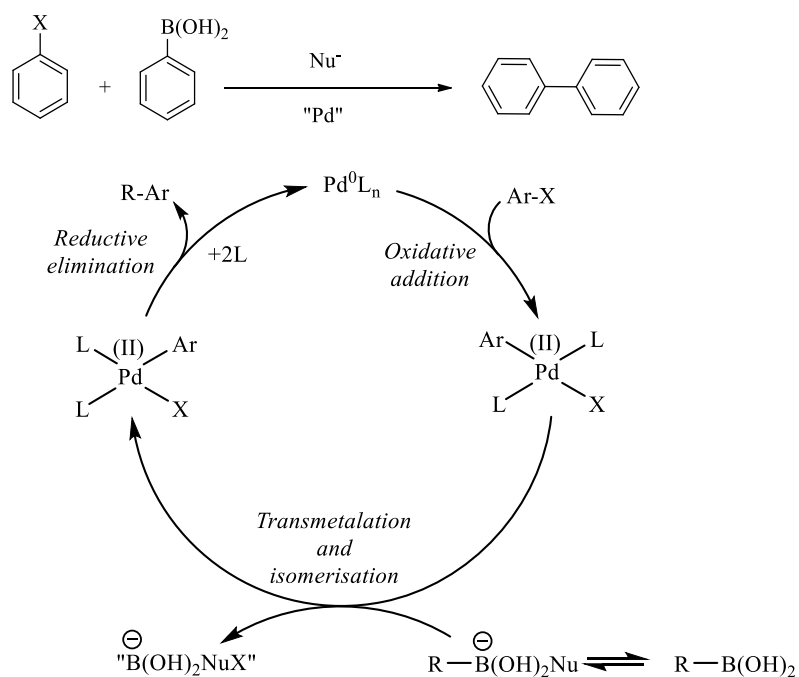
**Scheme 24.** Reaction path for the formation of (Ethynyl)<sub>3</sub>-SubPc-OPh **50**.

Deprotection of SubPc **49** was attempted using NaH, both as a 60% dispersion in oil and pre-washed with hexane to remove the oil. After refluxing in dry toluene the reaction led to decomposition or unreacted starting material was recovered, respectively. NaOH was then used as a base, and after 5 hours refluxing mostly product was formed (there was very small amount of di-deprotected product). (Ethyneyl)<sub>3</sub>-SubPc-OPh **50** could be isolated in a 64 % yield as purple solid. This SubPc brings many synthetic possibilities such as the coupling to another SubPc giving capsule-like compounds, as well as grafting other type of macrocycles to combine properties of both systems just two examples of the paths that this compound may offer.

### Suzuki-Miyaura Cross-Coupling

In 1981 Suzuki and Miyaura<sup>[118]</sup> reported the palladium-catalysed cross-coupling reaction of phenylboronic acid with haloarenes. The reaction proceeded smoothly in the presence of bases giving the corresponding biaryl compounds in good yields. The Nobel Prize in Chemistry was awarded to the authors in 2010, for the discovery, the continuous development and outstanding contributions on this important reaction over the past years.<sup>[119]</sup>

The coupling reaction and the mechanism involved are outlined in Scheme 25. An aryl halide undergoes oxidative addition to the active catalyst Pd(0), the second aryl group is subsequently transferred in the transmetalation step, from the boronate complex to the aryl palladium intermediate. The boronate complex involved in this process is obtained from the reaction between the boronic acid and a nucleophile, normally a base added to the reaction. Interestingly, this reaction can be carried out using trihydroxy- boronate salts as active species in the catalytic cycle, without any other nucleophile/base required.<sup>[120]</sup> The last step is the reductive elimination of the desired coupled product and the regeneration of the Pd (0) species ready to commence another catalytic cycle.

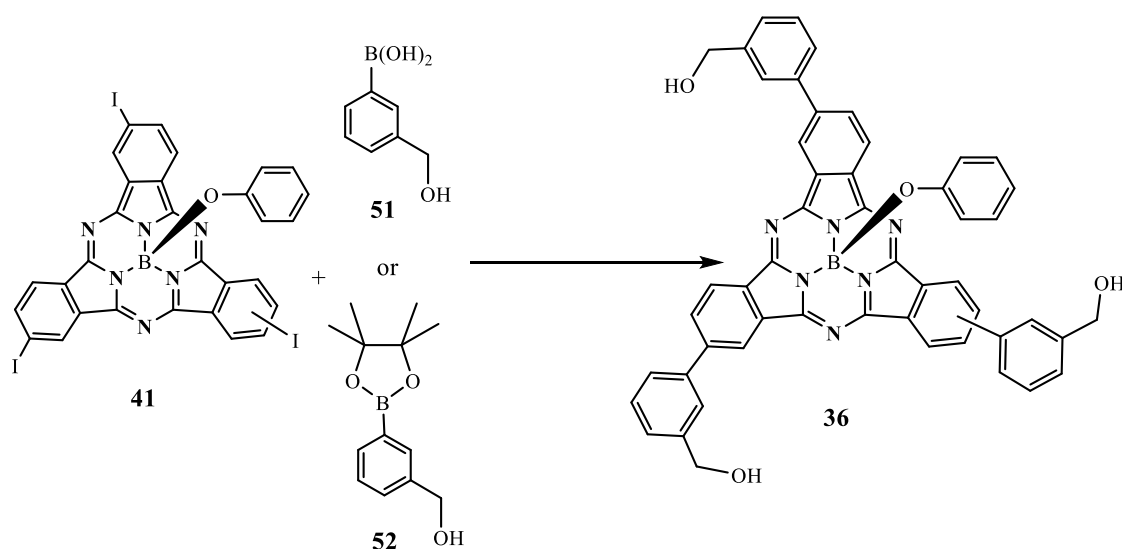


**Scheme 25.** Suzuki-Miyaura coupling reaction and simplified catalytic cycle.<sup>[120]</sup>

The selection of the appropriate reagents when working with sensitive materials like SubPcs is of major importance. Although the most commonly used catalyst for this reaction is Pd(PPh<sub>3</sub>)<sub>4</sub>, in which palladium is already in its oxidation state 0 to begin the cycle, this reagent is known to be air and light sensitive which could prove not to be easy to handle. Hence PdCl<sub>2</sub> and PPh<sub>3</sub> were used instead, the active catalyst will be generated after reacting with boronic acid reagent and therefore be ready to commence the coupling between the two desired units. Regarding the base, SubPcs are unstable in the presence of strong bases and nucleophiles, which would lead to the instant decomposition of the macrocyclic ring. Torres et al. [117] used CsF as a suitable base for Suzuki cross-couplings obtaining high yields as a result of the good stability of the macrocycle towards it.

The synthetic method used to prepare (Ph-CH<sub>2</sub>OH)<sub>3</sub>-SubPc-OPh **36** bearing alcohols- in the periphery for future nanoparticle or surface attachment is outlined in Scheme 26. I-SubPc-OPh **41** was refluxed in dry DME in the presence of an excess of 3-(hydroxymethyl)phenylboronic acid **51** and the above mentioned reagents. The reaction proceeded extremely slowly, after 52 hours starting material, mono- and di- substituted SubPcs, and only traces of the desired product were observed on the TLC.

The synthesis was then slightly modified. Pinacol boronic esters are well-known reagents in Suzuki-Miyaura reactions, hence reactant **52** was used as coupling agent. This reagent was prepared by refluxing 3-(hydroxymethyl)phenylboronic acid **51** acid with pinacol in a 1:1 ratio for 5 hours. After evaporation of the solvent under reduced pressure, the resulting crude product was filtered through a silica pad using 4:1 PE/EtOAc as solvent system. Product **52** was obtained in 71% yield as a white solid. The above described Suzuki conditions were then applied with this reactant using same equivalents, but after 3 hours the reaction showed signs of decomposition.

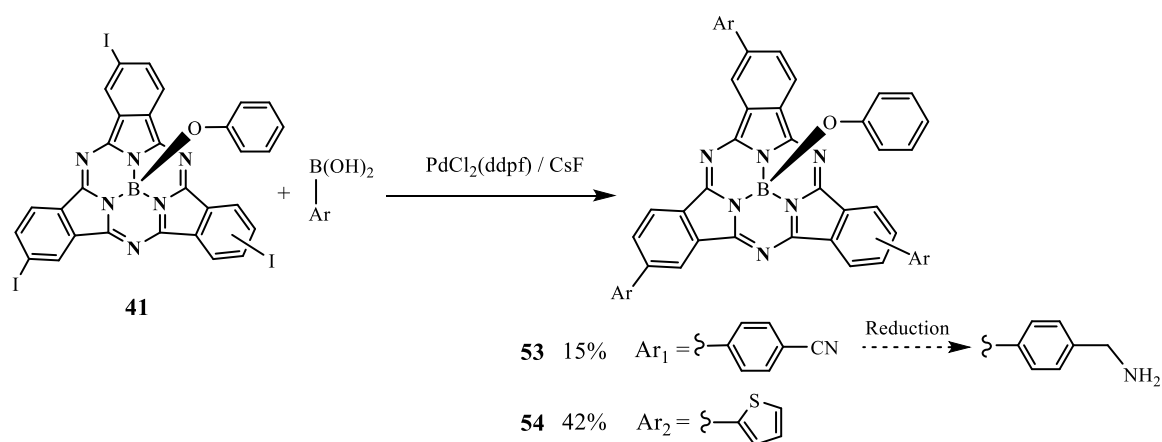


**Scheme 26.** Synthesis of (Ph-CH<sub>2</sub>OH)<sub>3</sub>-SubPc-OPh **36**.

It was noticed in both Suzuki reactions considerable amounts of triphenylphosphine oxide were formed. This was confirmed by <sup>1</sup>H-NMR and MALDI-TOF analysis, with a peak at 279 m/z corresponding to the protonated parent ion. Although these reactions were always carried out scrupulously under inert atmosphere and using degassed DME, the oxidation of triphenylphosphine

must have occurred due to oxygen or water accidentally present in the reaction. It was decided to avoid the use of triphenyl phosphine ligands, therefore PdCl<sub>2</sub>(dppf) was the chosen catalyst due to high yields and good performance in cross-couplings found in the literature.<sup>[121]</sup> This reaction was carried out in a sealed tube heating I-SubPc-OPh **41**, an excess of the boronic acid **51**, 9% mol of PdCl<sub>2</sub>(dppf) and CsF in DME, up to 100 °C. The reaction was completed within 9.5 hours, after which time the solvent was evaporated and the crude residue subjected to a column chromatography. Recrystallisation of the product from a mixture of DCM and hexane gave the pure (Ph-CH<sub>2</sub>OH)<sub>3</sub>-SubPc-OPh **36** as a dark purple solid in 72% yield.

Similar Suzuki reactions were used to prepare a range of ligand substituted SubPcs. (Ph-CN)<sub>3</sub>-SubPc-OPh **53** (precursor to amines) and (thiophenyl)<sub>3</sub>-SubPc-OPh **54** were chosen, with syntheses giving modest yields (Scheme 27).



**Scheme 27.** Synthetic conditions for the synthesis of (Ph-CN)<sub>3</sub>-SubPc-OPh **53** and (thiophenyl)<sub>3</sub>-SubPc-OPh **54**.

### 2.2.3 Optical properties

Absorption spectra of SubPc show two main components; a Q band in the region from 250 to 380 nm that corresponds to the S<sub>0</sub> → S<sub>1</sub> transition within Gouterman's four-orbital model,<sup>[122]</sup> and the B or Soret Band corresponding to the S<sub>0</sub> → S<sub>2</sub> transition around 570 nm, Figure 33. These bands appear blue-shifted compared to those of phthalocyanines (λ<sub>max</sub> = 300-400 and 600-800 nm) as a result of a decrease in the number of π-electrons in the aromatic conjugated system from 18 to 14.

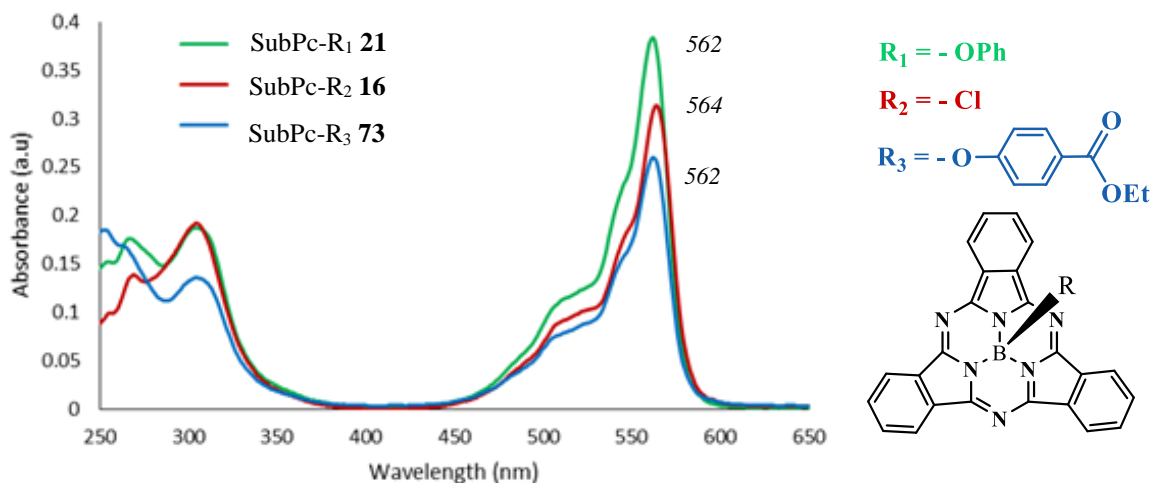


**Figure 33.** UV-Vis spectra of axially substituted SubPcs **16**, **21** and **73** in dichloromethane.

Extinction coefficients of the Q bands for SubPcs synthesised in this work are in the range of  $(5 - 9) \times 10^4 \text{ M}^{-1} \text{ cm}^{-1}$ . These values are smaller than those of Pcs ( $8\text{-}24 \times 10^4 \text{ M}^{-1} \text{ cm}^{-1}$ ) possibly attributable to their nonplanar nature.

Figure 33 shows the absorption spectra of SubPcs **16**, **21**, and **73**. The position of the Q bands seem not to be affected by the axial substituent. This is even more obvious when comparing two similar systems, such as the 3-pyridyl substituted SubPc **35** and **48** with phenoxy or 4-fluorophenoxy axial substituents, respectively. Figure 34 depicts the spectra of these molecules comparing them to their respective iodo-substituted SubPcs. It can be observed that the position of the bands is not influenced by modification of the axial substituent. However there is a bathochromic shift of around 16 nm when changing the peripheral substituent from an iodine to the 3-pyridyl groups.

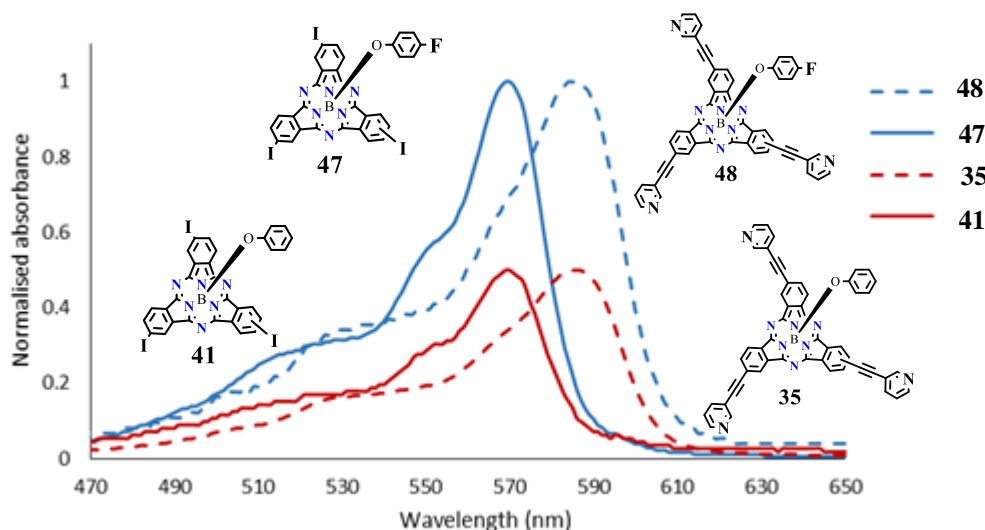


**Figure 34.** UV-Vis spectra of compounds **35**, **41**, **47** and **48** in dichloromethane.

Table 2 shows a summary of some optical data for the subphthalocyanines synthesised in this work. At first glance, peripheral substitution appears to have a more noticeable effect on both

the Q absorption band and the emission maxima, and as expected, fluorescence maxima shift paralleling those of the Q band.

SubPc n.	Axial, (Periphery) <sub>3</sub>	Abs Qband $\lambda_{\text{max}}$ (nm)	Emission $\lambda_{\text{max}}$ (nm)	Stokes Shift (nm)
16	Cl, –	564	577	13
21	OPh, –	562	575	13
20	Cl, I	572	583	11
41	OPh, I	569	580	11
34	OPh, 2-pyridyl	586	598	12
35	OPh, 3-pyridyl	586	599	13
48	(4-F-OPh), 3-pyridyl	586	598	12
47	(4-F-OPh), I	570	581	11
49	OPh, Alkynol	579	590	11
50	OPh, Ethynyl	576	587	11
36	OPh, (Ph-CH <sub>2</sub> OH)	576	588	12
53	OPh, (Ph-CN)	578	594	16
69	OPh, AlkylCOOEt	583	597	14
54	OPh, Thiophenyl	590	604	14
73	(OPh-COOEt), –	562	575	13

**Table 2.** Optical data for some subphthalocyanines.

In general, SubPcs show very intense pink fluorescence, the examples illustrated in table 2 show an emission band at a region from 575 to 604 nm. Emission takes place from the lowest excited state S<sub>1</sub> to the ground state S<sub>0</sub>, as a result emission bands are normally mirror images of the Q band in SubPcs, Figure 35. Very small Stokes Shifts are also observed for these rigid macrocycles, which range from 11 to 16 nm, suggesting small geometric distortion of the excited state regarding the ground state.

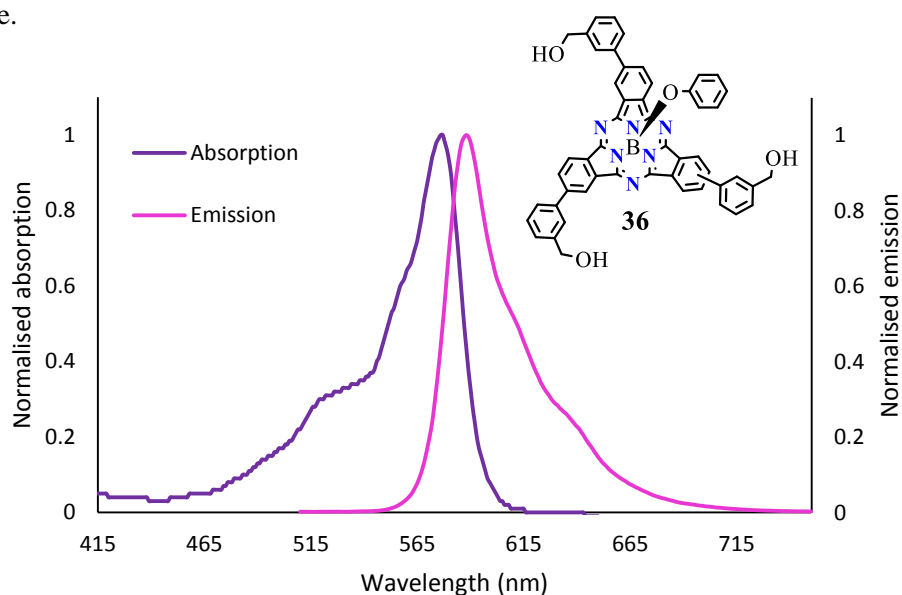


**Figure 35.** Absorption and emission spectra of (Ph-CH<sub>2</sub>OH)<sub>3</sub>-SubPc-OPh **36**.

Aside from the already mentioned red-shift when acetylene groups are introduced in the macrocycle, an interesting trend was noticed when comparing the wavelength of both absorption and emission (table 2) regarding the functional group. Apart from other factors that may influence the



experimentally obtained wavelengths, there is a tendency of shifting towards shorter wavelengths with higher electronegativities of the atoms that form the periphery, Figure 36.

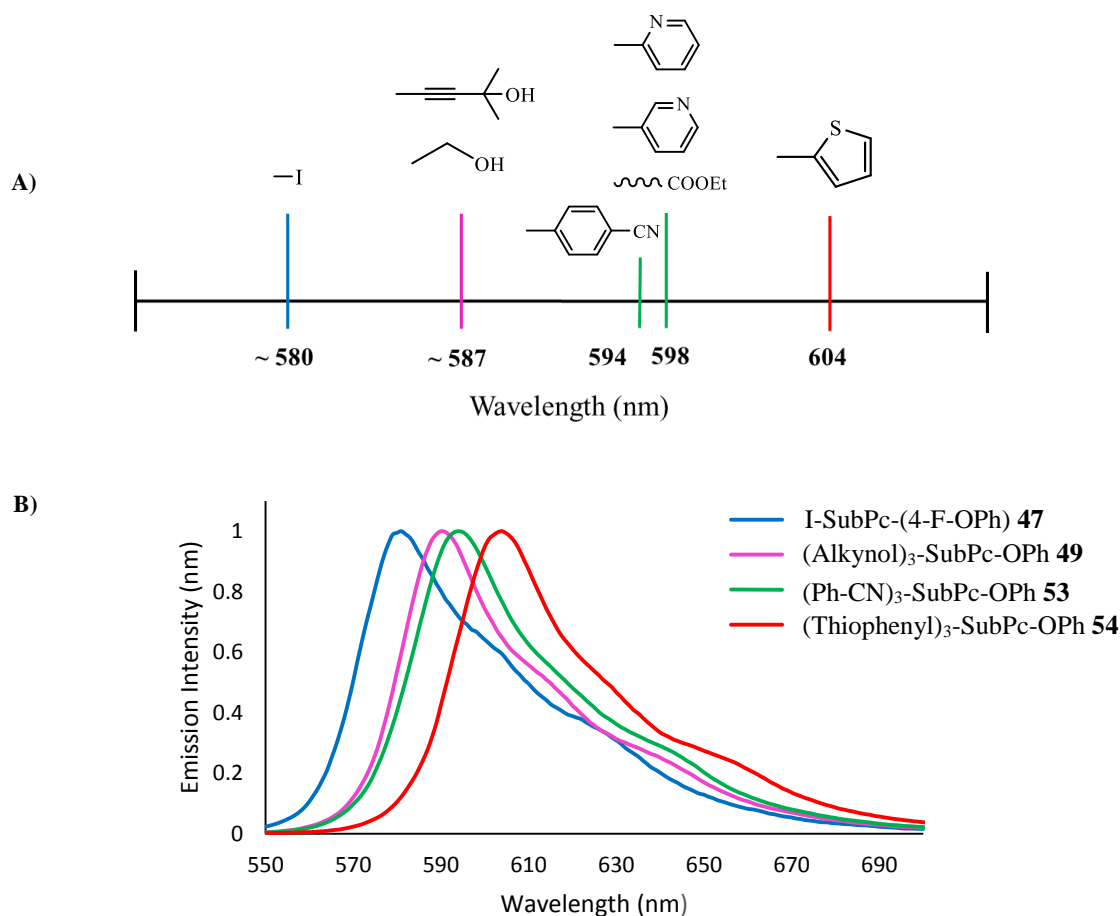


**Figure 36.** A) Experimental trend of some peripherally substituted SubPcs. B) Corresponding fluorescence spectra.

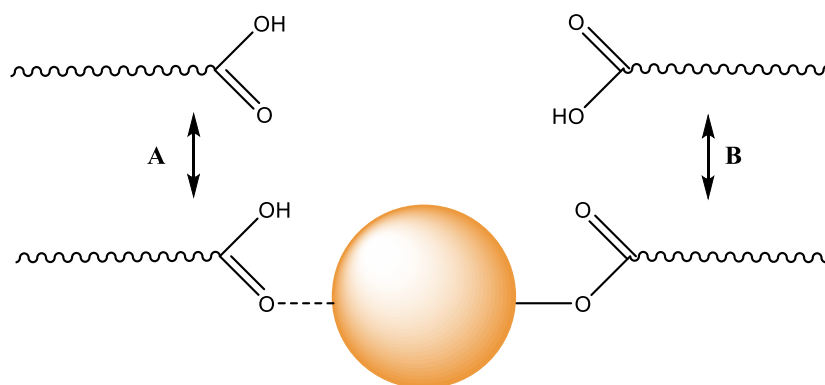
## 2.3 Nanoparticle Conjugation

### 2.3.1 CdSe – 3-pyridyl-SubPc QDs

Parallel experiments carried out in our group by Dr Isabelle Chambrier, demonstrated that the binding of the (3-pyridyl)-SubPc-OPh **35** synthesised in this work does not occur. It was believed that SubPc ligand bearing three pyridyl- functionalities was a potentially good surfactant to perform ligand exchange. However, no shift or sharpening of any monitored signal was noticed during the <sup>1</sup>H-NMR spectra upon titration of CdSe nanoparticles with a solution of this compound, suggesting that SubPc **35** does not effectively bind to the surface of the QD.

Hens et al.<sup>[91]</sup> used NMR solution technique in order to analyse the organic interface of CdSe QDs synthesised using oleic acid as surfactant. As soon as excess OA was added to the solution, they observed the exchange between free and bound ligands by NMR spectroscopy. The NMR spectra are indicative of a two-step exchange process, where free OA ligands get tangled through an intermediate state with the ligand shell prior its incorporation as bound ligands.

Scheme 28 represent two types of exchange mechanism, reaction **A** involves the replacement of bound OA by free OA breaking a dative bond. To fully understand this adsorption process, they performed an experiment whereby deuterated OA (replacement of the carboxylic acid hydrogen by deuterium) was added to a solution of CdSe-OA. They observed a small intensity of the alkene resonance compare to the one where OAs from the surface were exchanged by protonated OA, the authors concluded that the exchange of bound ligands for free ligands does not release protons from the QD surface. This strongly indicated a ligand shell made out of oleate ions instead of oleic acid molecules, the mechanism of adsorption/ desorption taking place is indicated in Scheme 28. **B**, and it involves a bond breaking.



**Scheme 28.** Two possible adsorption/ desorption mechanism.<sup>[91]</sup>

More importantly, this experiment carried out by Hens and colleagues demonstrated that the exchange process involves a proton transfer between excess oleic acid molecules and bound oleate ions. Meaning that if no protons are supplied to the oleate surfactants, the ligands do not readily come off. This remarkable work could explain the experiments carried out in our group with the 3-pyridyl SubPc. As previously mentioned SubPc **35** failed to desorb the oleate ligands on the surface of the QD probably due to the absence of protons supplied during the titration.

### 2.3.2 NMR Titrations

NMR spectroscopy is a particular interesting technique for the characterisation and study of the capping process of semiconductor nanocrystals, due to a wealth of chemical and structural information that this tool provides.<sup>[88]</sup> Hens et al. used  $^1\text{H}$  and  $^{31}\text{P}$  NMR in order to compare the binding strength of oleic acid and phosphonic acid to CdSe QDs. Titrations of synthesised QDs with excess oleic acid did not induce desorption of phosphonic species, whereas desorption of OA succeeded upon addition of an excess of phosphonic acid. In general, the signals of bound ligands appeared shifted and broadened compared to free ligand. They also monitored the alkene resonance of OA concluding the desorption of OA and its replacement by octadecyl phosphonic acid when a sharp signal was observed in the  $^1\text{H}$ -NMR spectrum (Fig. 37).<sup>[123]</sup>

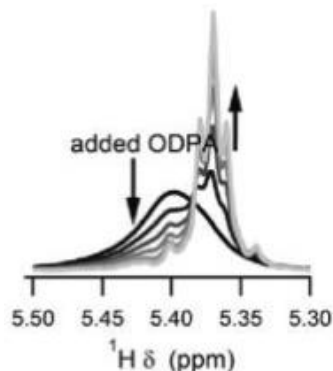


**Figure 37.** The  $^1\text{H}$ -NMR signal for alkene protons of OA capped CdSe QD upon addition of ODP.<sup>[123]</sup>

### 2.3.2.1 Analysis of 3-ethynylpyridine

Our SubPcs were designed and synthesised with pyridyl and alcohol ligands/binding groups attached. Following the preliminary results with pyridyl SubPc we decided to investigate ligand exchange using simple 3-ethynylpyridine and benzyl alcohol. As before, they were tested by means of  $^1\text{H}$ -NMR spectroscopy. The aim was to analyse and monitor the ligand exchange process with the original OAs that are capping the surface of the nanocrystals. Dzhagan et. al analysed the influence of pyridine ligand on the structure of the CdSe nanocrystals by Raman and optical absorption spectroscopy, nuclear magnetic resonance and transmission electron microscopy.<sup>[124]</sup> They observed a downfield shift of the pyridine peaks compared to signals of free pyridine molecules, concluding that pyridine efficiently replaces OA ligands. However based on the analysis of the NMR spectra, they postulated that both OA and pyridine molecules are bound to the surface of the nanocrystal after pyridine treatment, concluding that the replacement occurs but only partially.

Consequently, a known concentration solution of our CdSe nanoparticles in  $\text{CDCl}_3$  were placed in the NMR tube, a solution of 3-ethynylpyridine in  $\text{CDCl}_3$  was gradually added and  $^1\text{H}$ -NMR spectra were recorded after each addition. Figure 38 represents the signal of the alkene protons of the OA upon progressive addition of up to 2 equivalents of the ligand, the signal remains broad, a decrease in the intensity is observed due to the dilution effect, and a very slight downfield shift is also noticed.

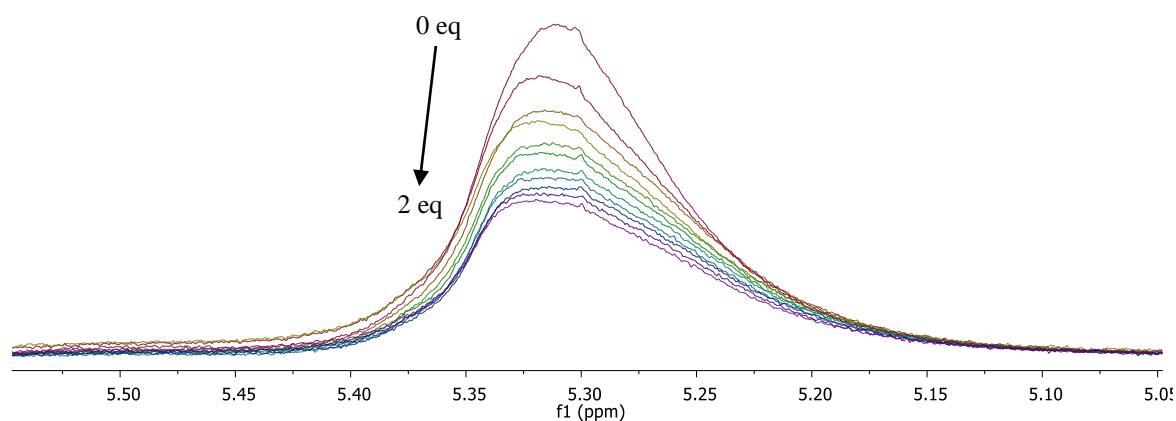


**Figure 38.** Progress of the oleate proton signal on the  $^1\text{H}$ -NMR upon addition of 3-ethynylpyridine.

Protons in the aromatic region corresponding to the pyridyl-group and the OA signals do not show any noticeable change, suggesting that the addition of 2 equivalents of pyridine derivative do not induce the release of the OA ligands, Figure 39.

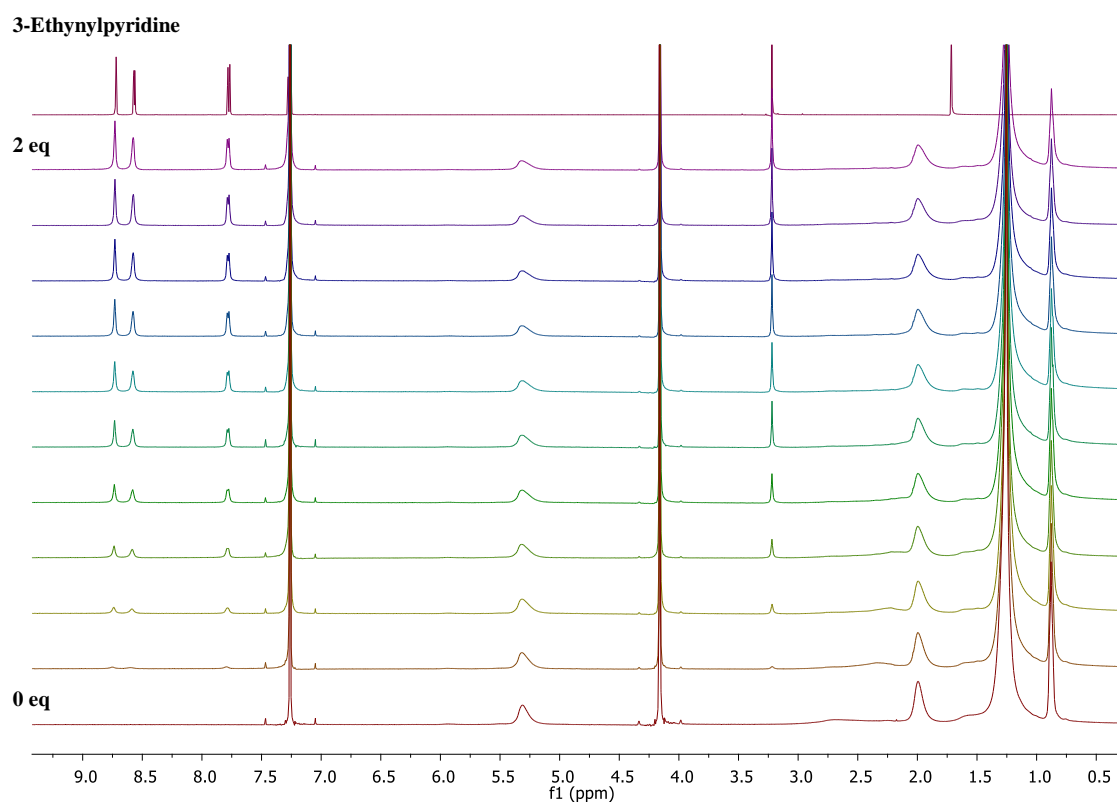


**Figure 39.**  $^1\text{H-NMR}$  progression upon addition of pyridine derivative.

Another titration was then carried out adding progressively up to 8 equivalents of 3-ethynylpyridine. A representation of the oleate protons (Fig. 40) show a moderate downfield shift as well as a slight sharpening of the signal upon addition of 8 equivalents. This excess might be releasing OA from the surface but the effect is not very evident, therefore up to 20 equivalents of the ligand was then added to the mixture. This large excess causes a sharper resonance to appear due to the free oleic acids in the solution.

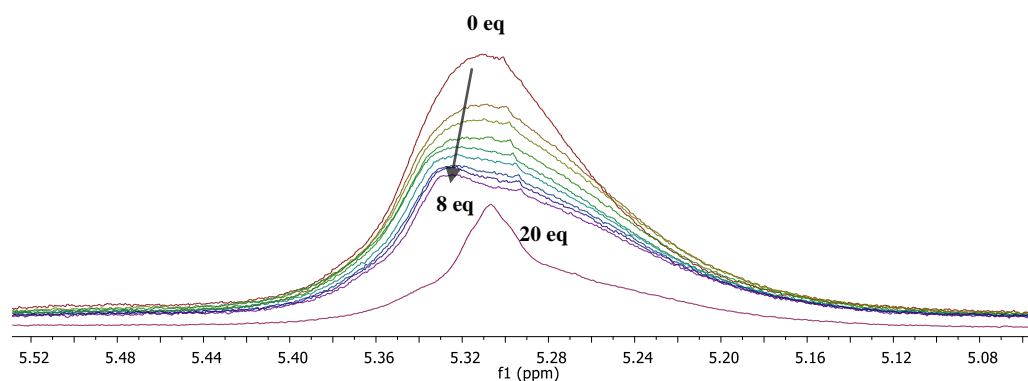


**Figure 40.** Evolution of the alkene protons regions of the OA ligand upon addition of up to 20 equivalents of pyridine derivative.

A clear upfield shift is obtained for the pyridyl protons as more of it is added to the solution (Fig. 41). The oleate protons were also monitored. Apart from the obvious sharpening of the alkene signal previously discussed, it is worth noting the appearance of a signal (\*) corresponding to the closest protons to the carboxylic acid as more ligand is added, due to the release of OA from the surface.

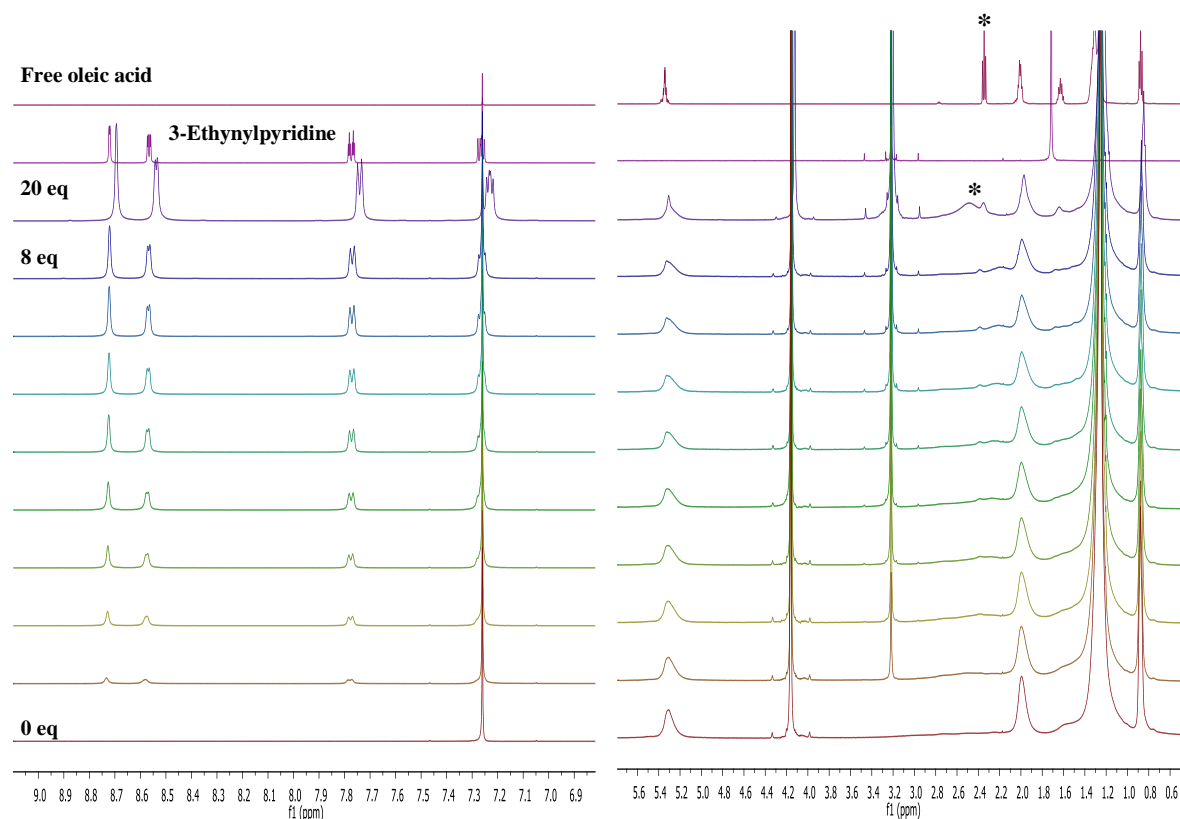


**Figure 41.** Progress of the  $^1\text{H}$ -NMR spectra upon addition of 20 equivalents of 3-ethynylpyridine and comparison with the free ligand and unbound OA.

The coordination of a ligand to the nanoparticles' surface is a dynamic process, the ligands adsorb and desorb. Due to the higher affinity of OA to CdSe QD, the pyridine derivative has to compete with the released oleic acids in solution at lower concentration. However, it has been demonstrated by NMR spectroscopy that a high excess of pyridine can effectively replace the oleate ligands on the surface of CdSe, although it shows very poor affinity.

### 2.3.2.2 Analysis of benzyl alcohol

The binding of benzyl alcohol was also tested, since a SubPc bearing this kind of functionality was successfully accomplished. Accordingly, a known solution of CdSe-OA in  $\text{CDCl}_3$  was titrated with gradual amounts of the alcohol up to 2 equivalents. Figure 42 illustrates the little or null effect that the additions of alcohol have on the alkene signal. An excess of up to 10 equivalents was then added in order to replace all oleate ions from the surface by mass action, but only very slight changes were observed.

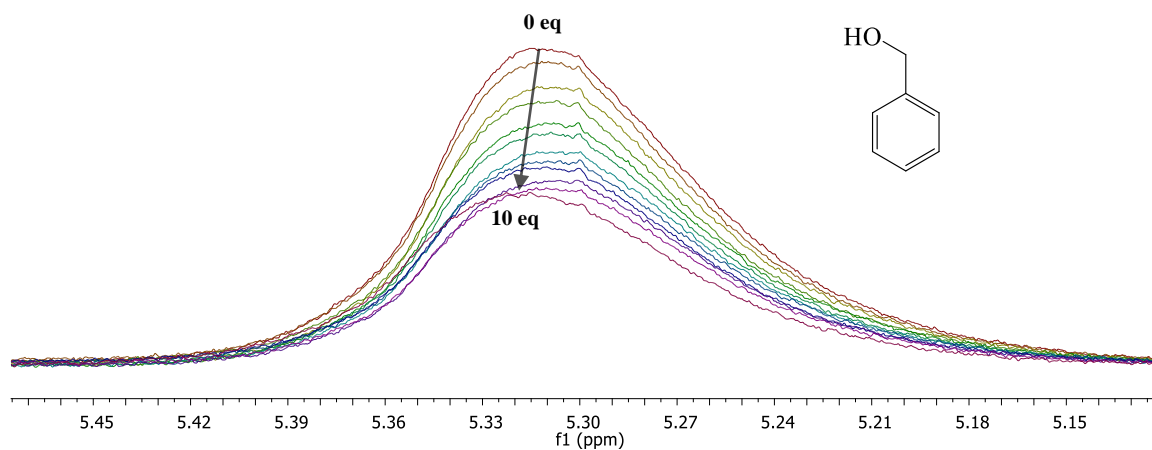


**Figure 42.** Representation of the alkene signal upon addition of benzyl alcohol.

All signals were monitored by NMR spectroscopy and Figure 43 depicts an expansion of the regions of interest where the aromatic area is not shown for clarity. There is no noticeable change on the benzylic- protons compared to the free ligand, in this case there is no sign of the peak corresponding to the protons closest to the  $-\text{COO}^-$  (\*), suggesting the very poor-binding nature of this ligand.

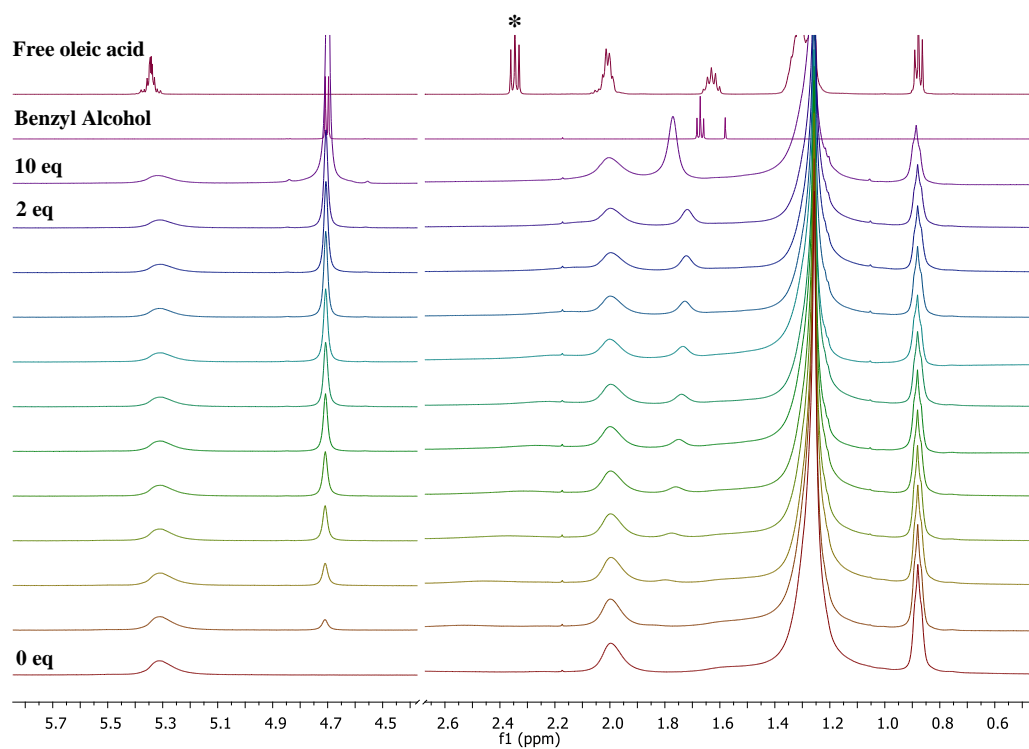


**Figure 43.**  $^1\text{H}$ -NMR spectra of the titration process of CdSe-OA with a solution of benzyl alcohol.

### 2.3.2.3 Analysis of phenylacetic acid

It is already known that one of the best ligands for ligand exchange purposes due to their good affinity for CdSe nanocrystals are carboxylic acids.<sup>[91]</sup> Consequently, a solution of the QD in  $\text{CDCl}_3$  was titrated with phenylacetic acid and  $^1\text{H-NMR}$  spectra were recorded after each addition.

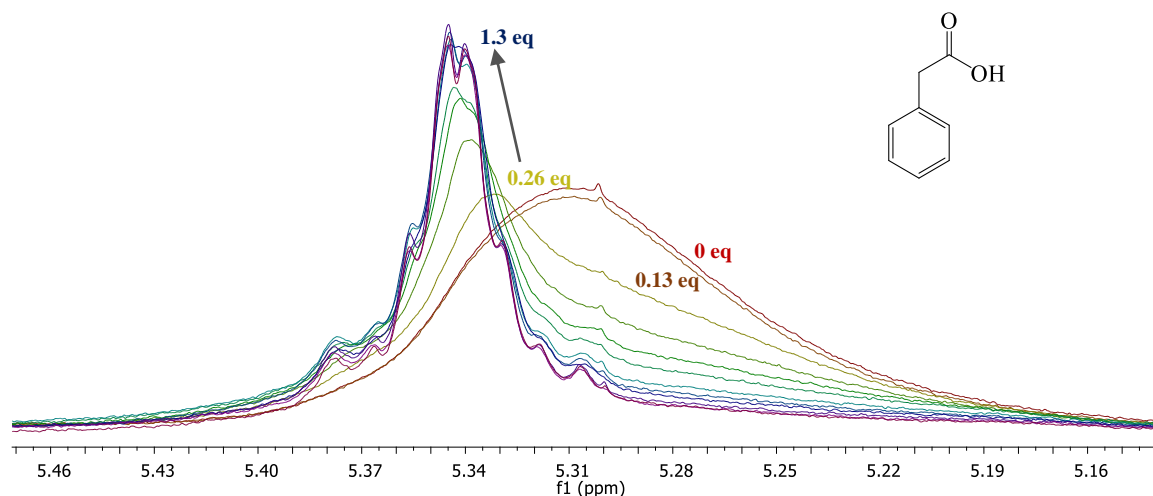


**Figure 44.** Changes in the alkene protons of the OA upon addition of phenyl acetic acid.

After addition of 0.26 equivalents of the carboxylic acid the signal of the alkene protons (Fig. 44) begins to shift downfield, the progressive addition of small amounts trigger an obvious sharpening of the peak. After the addition of approximately 1 equivalent, the signal is as sharp and resolved as the free oleic acid, suggesting that the original capping ligands have been replaced by the new ligand.

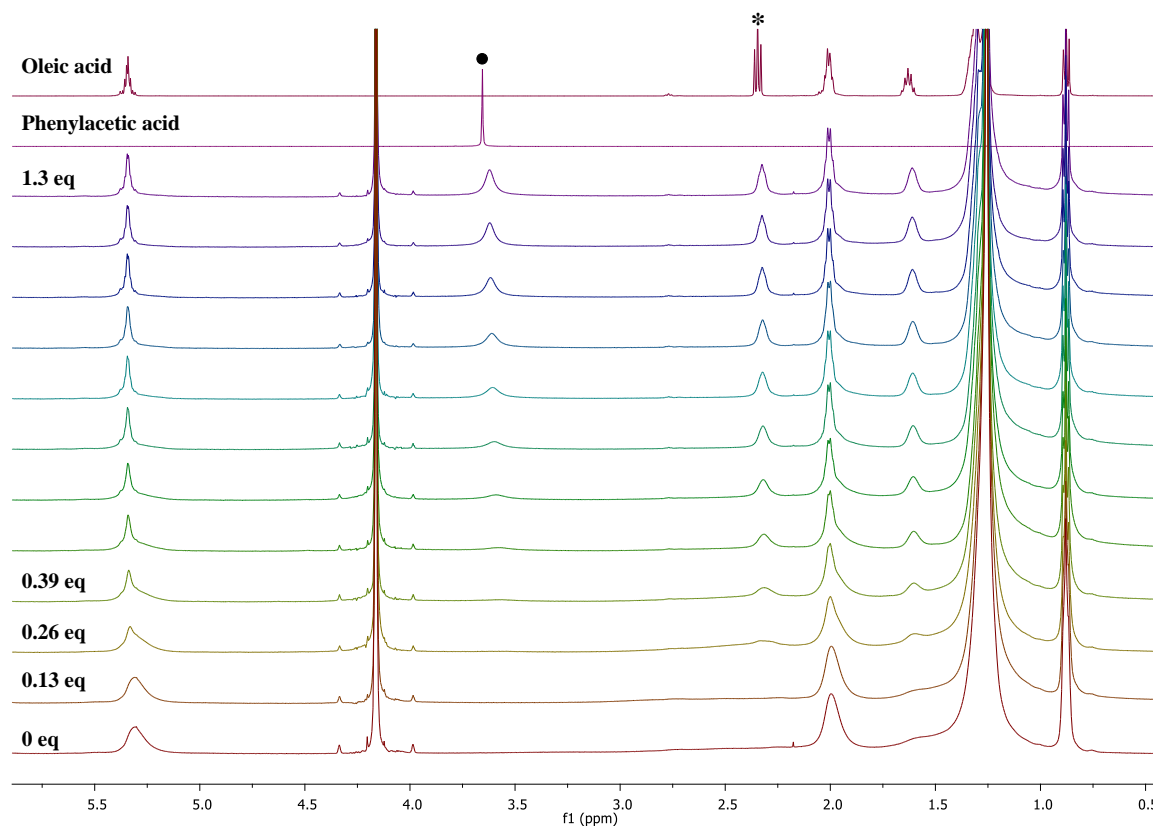


**Figure 45.**  $^1\text{H-NMR}$  progression after additions of phenylacetic acid to CdSe nanoparticles.

0.26 equivalents of phenylacetic acid seem sufficient to begin observation of the replacement of oleate ligands from the nanoparticle surface, as the  $-\text{CH}_2$  signal (\*) begins to appear, demonstrating its high affinity for the CdSe surface (Fig. 45). The benzylic- protons were also monitored (●) showing a very broad signal compared to the free compound, suggesting its bonded nature.

These NMR experiments allowed us to discriminate between bound and free ligands. Despite previous reports, the results showed that our initial SubPcs, with appended pyridyl and benzyl alcohol binding groups, would be unsuitable for nanoparticle encapsulation. The expected successful results with the carboxylic acid ligand demonstrated that it is one of the best capping ligands for CdSe QDs, hence a SubPc bearing three carboxylic acids on the periphery would be the ideal molecule for this project. This tridentate molecule has the potential to bind to the surface in a very effective way, the curved shape of the SubPc makes it ideal to capture the nanoparticle or even to encapsulate it.

### 2.3.3 Synthesis towards tricarboxylic acid – SubPc

#### 2.3.3.1 Design of a suitable SubPc encapsulant

We recognised that other factors could influence the binding efficiency of our designed tripodal ligands. CdSe nanoparticles synthesised in this work have a long aliphatic OA ligand shell that could be acting to protect the surface toward the ligand exchange, perhaps for constrained molecules such as SubPc it is really difficult to access the  $\text{Cd}^{2+}$  binding sites. Figure 46 illustrates how in the SubPc – QD conjugate, the pyridyl groups would have to displace or bypass the ligand shell barrier in order to reach the nanoparticle's surface.

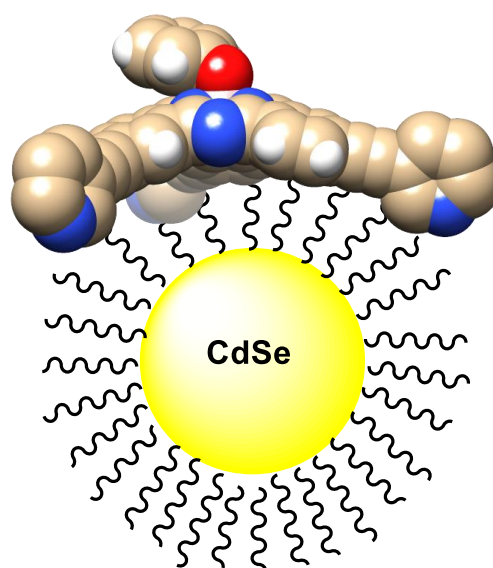


**Figure 46.** Representation of the QD – 3-pyridyl SubPc hypothetical conjugate. (Out of scale representation for clarity).



Taking into account these plausible problems, we turned our attention to building a SubPc molecule with three long chains, designed in order to facilitate its way through the shell. Figure 47 depicts a three dimensional representation of the target compound (alkylCOOH)<sub>3</sub>-SubPc-OPh **55**, the cone-shaped structure has a large concave cavity of approximately 3.4 nm from oxygen to oxygen to trap small QDs, obviously the long chains are flexible enough to easily modify that size in order to suit the nanoparticle.

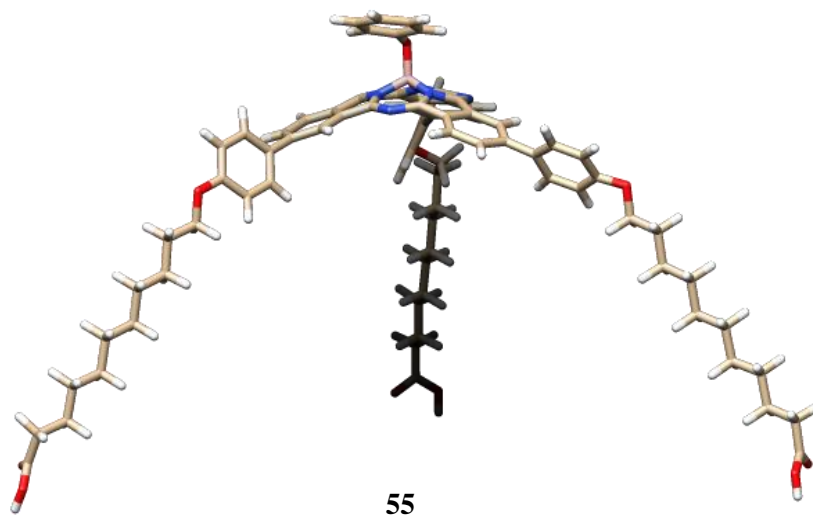
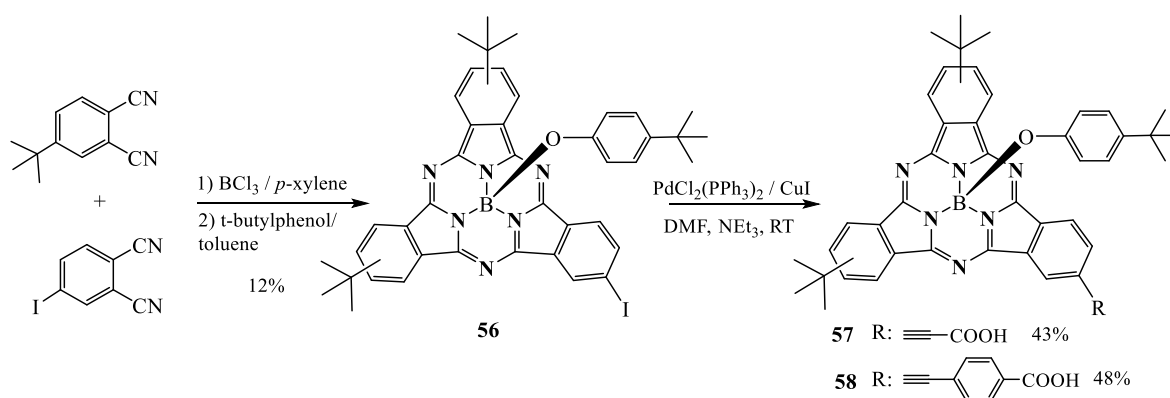


**Figure 47.** Computational model of the SubPc target compound **55** performed with Chimera 1.9.

### 2.3.3.2 Literature survey

Just very recently, Torres et al.<sup>[125]</sup> reported a series of SubPc molecules bearing one carboxylic acid group at the periphery. Cyclisation reaction of two phthalonitriles gave rise to unsymmetrically substituted SubPc **56**. The second step involved a Sonogashira cross-coupling reaction at room temperature obtaining a mixture of isomers that could not be separated by column chromatography, Scheme 29.



**Scheme 29.** Synthetic route to unsymmetrical SubPcs bearing a carboxylic acid at the periphery.

They also reported the synthesis of a series of mono-carboxylic acids functionalised at the apical position of the SubPc, illustrated in Figure 48.

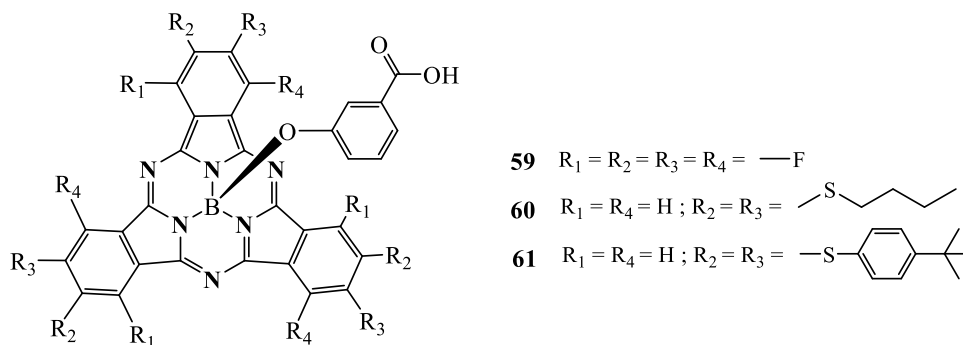


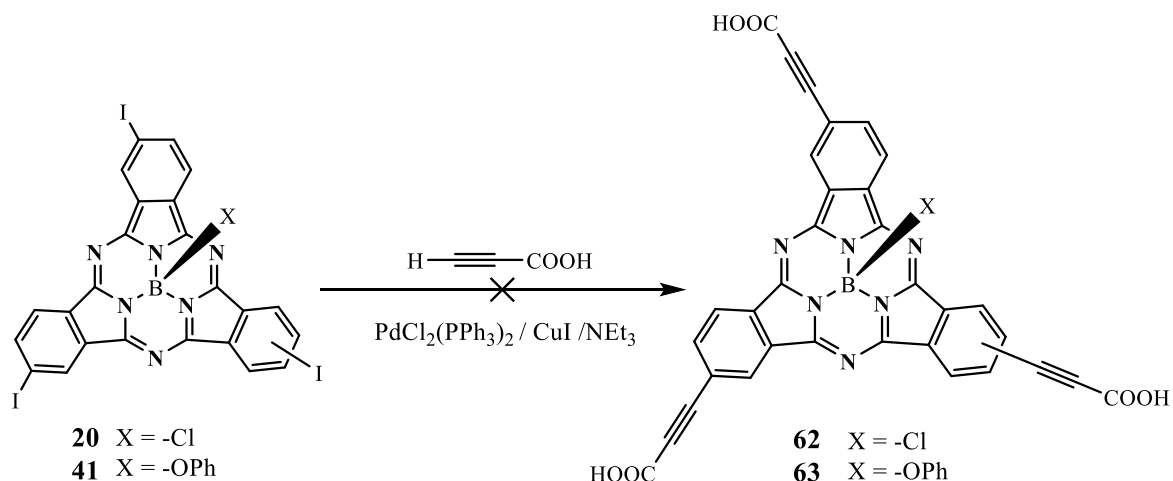
**Figure 48.** Different SubPc derivatives synthesised by Torres and colleagues.<sup>[125]</sup>

They studied the influence of the carboxylic acid groups on the dye-sensitized solar cell (DSSC) performance. They found a very low PCE with the axially substituted carboxy-SubPcs, owing to the absence of electronic transmission between the SubPc core and the anchoring group due to the presence of the boron atom. However, SubPc molecules bearing the carboxylic acid group at the periphery showed a PCE of 1.32% and 1.08%, respectively. These results are promising and encouraging considering that is the first SubPc-based DSSCs reported so far.

Subphthalocyanines bearing three carboxylic acids at the periphery are unknown.

### 2.3.3.3 Direct cross-coupling strategy

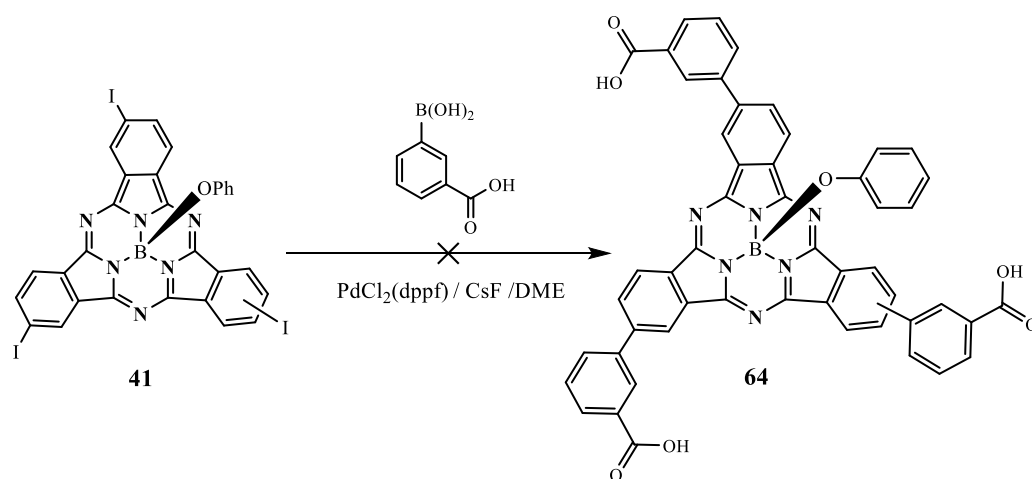
Considering the lack of published results in the literature and as proof of concept, the introduction of three readily available and simple carboxylic acid derivatives was attempted. A direct cross coupling reaction involving I-SubPc-Cl **20** and propiolic acid (Scheme 30) was first carried out. The reagents were sealed in a tube under nitrogen and stirred at room temperature. After 24 hours the reaction was checked by TLC and a pink spot could be observed on the baseline, the reaction was left to stir for further 4 days and after no more changes were noticeable on the TLC and most of the starting material was consumed the reaction was stopped. The usual aqueous work up was performed and after evaporation of the solvent under reduced pressure, the crude solid had changed colour to green implying decomposition of the macrocyclic core.



**Scheme 30.** Sonogashira reaction attempts with SubPc **20** and **41** and propiolic acid.

Perhaps the labile chlorine at the apical position facilitates the rapid decomposition of the resultant material. Consequently I-SubPc-OPh **41** was subjected to the same cross-coupling conditions represented in Scheme 30, obtaining essentially the same outcome. Different temperatures were subsequently tried, but all cases led to degraded material.

A Suzuki-Miyaura cross-coupling approach was also attempted in order to obtain SubPc **64** bearing three carboxylic acids. Accordingly, I-SubPc-OPh **41** was subjected to the optimised reaction conditions discussed earlier in this chapter. The coupling reaction with 3-carboxyphenylboronic acid (Scheme 31) was carried out in a sealed tube at 100 °C. After 6 hours only unreacted starting material was observed on the TLC. The reaction was left under those conditions for further 6 hours, after which only very faint pink spots were noticed and the majority of the mixture was recognised as decomposed material.

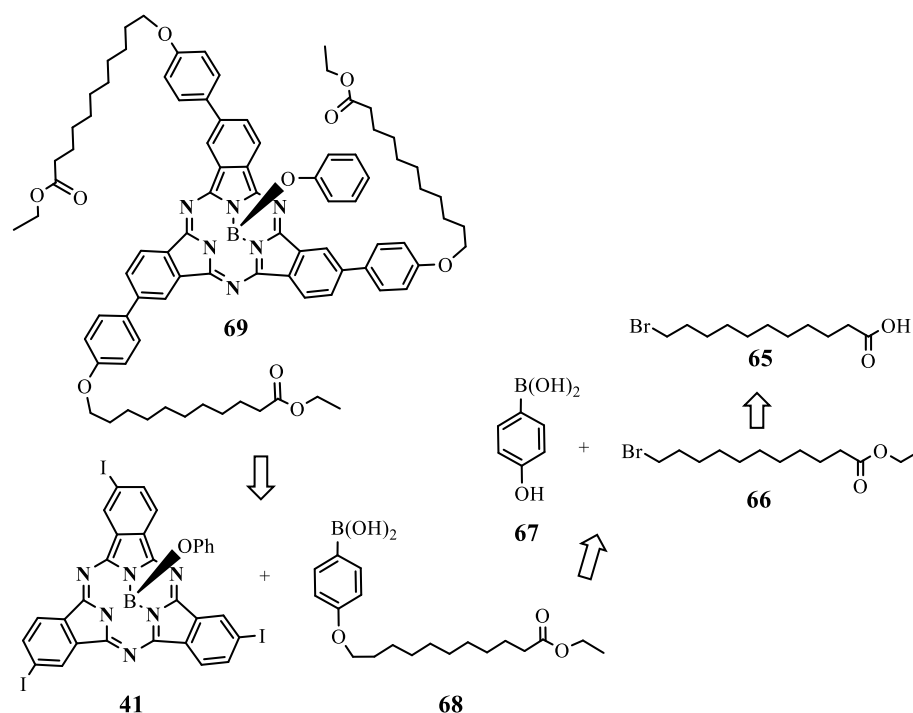


**Scheme 31.** Suzuki coupling attempted reaction.

### 2.3.3.4 Protected SubPc approach

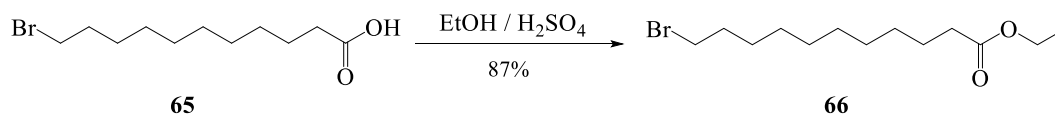
At this point it was decided to introduce protecting groups into the SubPc structure that could be easily deprotected in a mild way afterwards. Amongst all, esters seemed a good starting point due to the potentially easy alkaline hydrolysis that could regenerate the carboxylic acids.

The retrosynthetic strategy towards the target (alkylCOOH)<sub>3</sub>-SubPc-OPh **55** designed for this purpose was contemplated to involve building blocks which allow us to perform the minimum amount of steps involving the SubPc macrocycle (Scheme 32). Therefore a precursor **68** bearing the long chain was to be synthesised and the linkage to the SubPc core would be done in one single step by means of a Suzuki cross-coupling.



**Scheme 32.** Retrosynthetic path towards protected (alkylCOOEt)<sub>3</sub>-SubPc-OPh **69** formation.

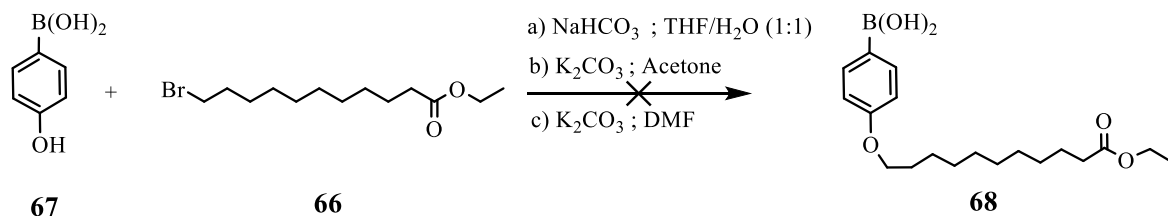
The synthesis began with an esterification reaction of 11-bromoundecanoic acid. A modified procedure from the literature was followed,<sup>[126]</sup> whereby the carboxylic acid **65** was refluxed overnight in ethanol, in the presence of sulphuric acid (Scheme 33). The solvent was then evaporated and an aqueous work up was carried out to obtain the desired ethyl ester **66** as a colourless oil in 87% yield.



**Scheme 33.** Esterification reaction of 11-bromoundecanoic acid.

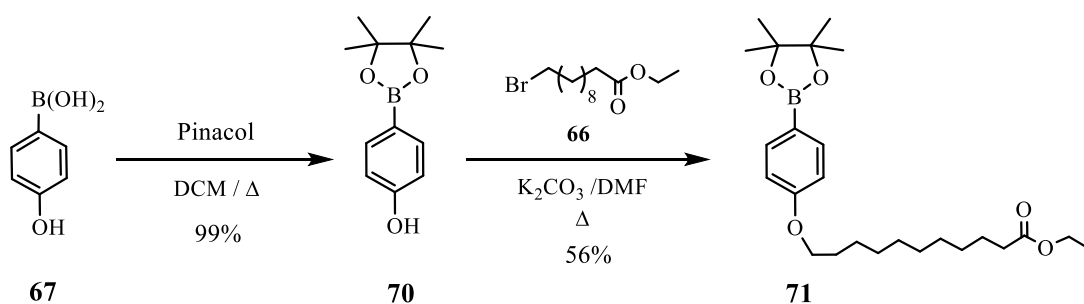
An alkylation reaction was then carried out with boronic acid **67** applying conditions a) outlined in Scheme 34. After 24 hours reacting only starting material was recovered so the base was

subsequently changed to  $K_2CO_3$  and the reaction mixture was then refluxed in acetone (Scheme 34. b). Unfortunately after 2 days starting materials were recovered and no product formation was observed. Poor solubility of *p*-hydroxyphenylboronic acid **67** in most organic solvents was noticed, therefore the solvent was changed to DMF (Scheme 34. c) to test if there was a solubility issue with this reaction. After one day refluxing under these conditions, there were more spots on the TLC but still there was a lot of unreacted starting material.



**Scheme 34.** Alkylation attempts to synthesise boronic acid **68**.

Although the performance of this reaction should be smooth and high yielding, perhaps the poor solubility of the derivative **67** together with the hydroxy-groups on the boronic acid are preventing the course of this reaction. Therefore boronic acid **67** was protected as a pinacol boronic ester **70** quantitatively under the conditions<sup>[127]</sup> represented in Scheme 35. Alkylation reaction was then carried out with this pinacol derivative in conjunction with alkyl ester **66**, refluxing in the presence of  $K_2CO_3$ . Although the reaction also worked using acetone as solvent, the best yield (56%) was obtained when DMF was employed. Column chromatography purification was necessary to obtain compound **71** pure as a colourless oil.



**Scheme 35.** Synthesis of pinacol derivative **71**.

Compound **71** was fully characterised by means of high resolution mass spectrometry, IR and NMR spectroscopy.  $^1H$ -NMR analysis shows a simple spectrum characteristic of a symmetrical molecule, with two doublets in the aromatic region (Figure 49). NOESY and COSY technique was necessary in order to assign all protons. Worth noting is the downfield shift of the protons in the aromatic ring closest to the boronic ester (b). A clear NOE signal between protons (b) and the methyl protons of the pinacol group (c) was observed, and a NOE signal between (a) and (d) was also obtained.

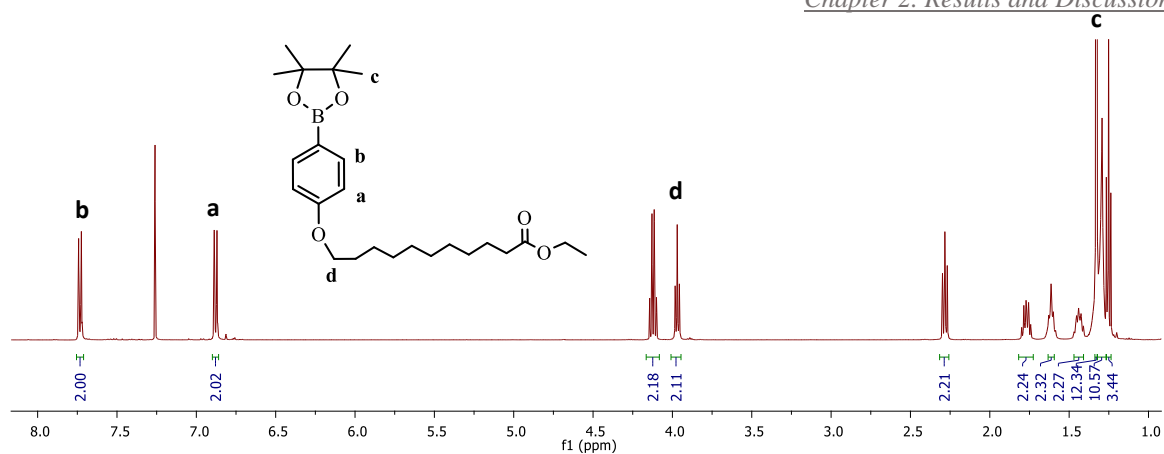
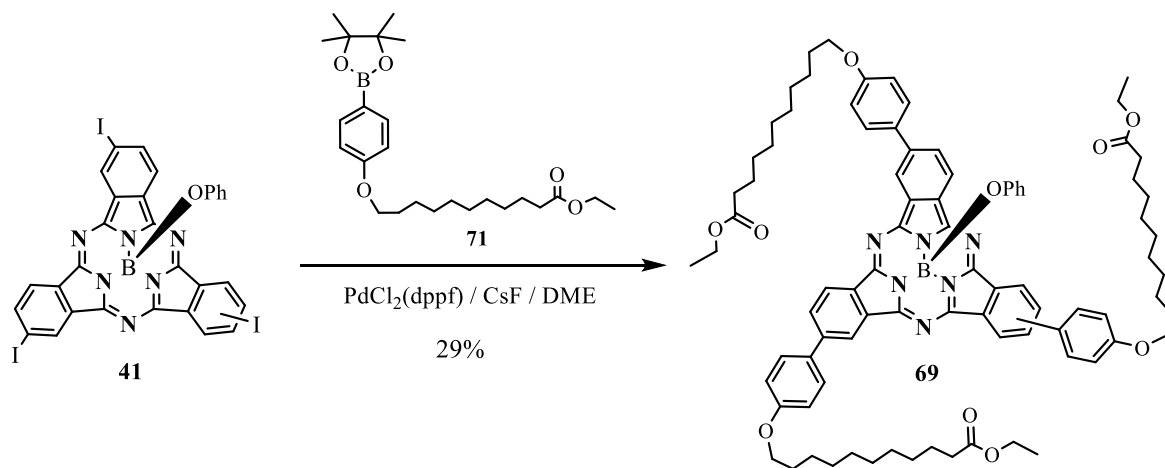


**Figure 49.**  $^1\text{H}$ -NMR of pinacol boronic ester derivative **71**.

$^{11}\text{B}$ -NMR spectroscopy also show the expected chemical shift at 31.32 ppm characteristic for boronic esters.<sup>[128]</sup> The last step implied a Suzuki coupling between the I-SubPc-OPh **41** and the building block **71** that was successfully synthesised. The best conditions found earlier in this chapter were applied for this reaction and are represented in Scheme 36. The reagents were placed in a sealed tube with catalytic amounts of palladium catalyst, CsF as base and distilled DME as reaction solvent. After heating the mixture up to 100 °C under argon for 6 hours the reaction was stopped due to the lack of starting material **41** remaining, and also because of the high amount of a green decomposed material observed on the baseline of the tlc. After extracting the product with ethyl acetate a column chromatography was necessary to separate it from the rest of side products.



**Scheme 36.** Suzuki-Miyaura cross-coupling between SubPc **41** and boronic ester **71**.

(AlkylCOOEt)<sub>3</sub>-SubPc-OPh **69** was obtained as a dark purple solid in 29% yield. It was fully characterised by NMR, IR, UV-Vis spectroscopies. MALDI-TOF spectra (Fig. 50) show the protonated molecular ion parent peak at 1402 m/z with the aid of DCTB as matrix. The corresponding loss of the phenyl group in the apical position gives rise to the hydroxylated SubPc peak with a mass of 1325 m/z, and the loss of the whole phenoxy-group at the apical position is observed with the peak corresponding to a mass of 1308 m/z.

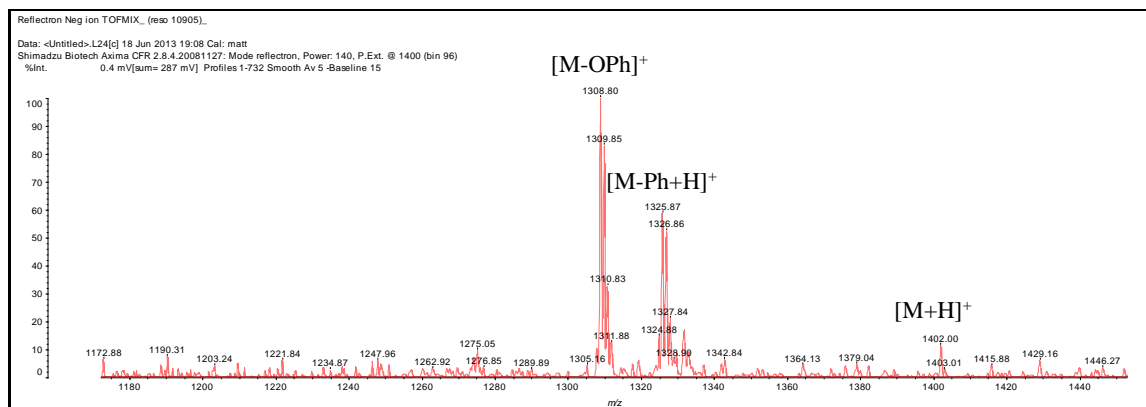
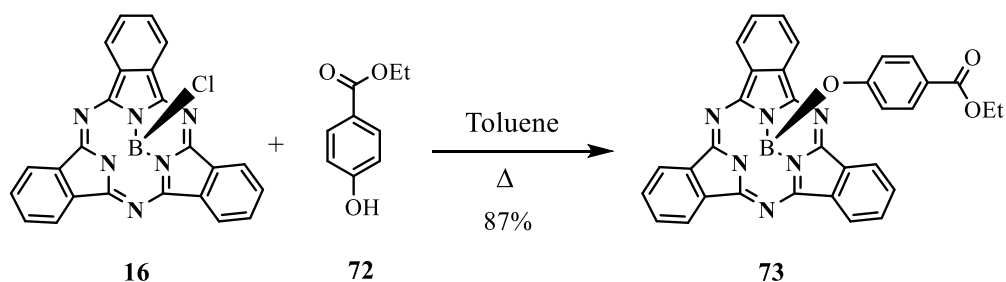


**Figure 50.** MALDI-TOF spectrum of SubPc **69**.

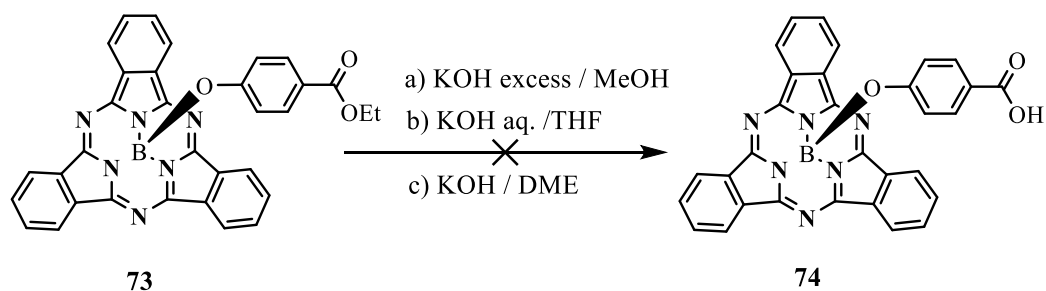
The next step towards the target carboxylic-SubPc **55** was the hydrolysis of the SubPc ester **69**. The synthesis of compound **69** proposed a challenging purification process that required a couple of column chromatographic separations to get high purity material. A notable amount of decomposed material was also obtained having an important impact on the modest yield of this reaction. Given the fact that compound **69** was a precious material, to find the appropriate and best hydrolysis conditions a simpler SubPc bearing just one ethyl ester on the apical site was consequently synthesised to use as model.

The synthesis required unsubstituted SubPc-Cl **16** to be refluxed in toluene in the presence of an excess of ethyl 4-hydroxybenzoate **72** for 21 hours, after which time the reaction was complete. The product was then precipitated with ethanol and thoroughly washed with ethanol and hexane. SubPc-(OPh-COOEt) **73** was obtained as a pure purple solid in 87% yield and fully characterised by mass spectrometry and NMR spectroscopy.



**Scheme 37.** Synthesis of SubPc-(OPh-COOEt) **73**.

Not long ago, Khurana et al.<sup>[129]</sup> reported the alkaline hydrolysis of esters without water involved in the reaction. This efficient, fast and high yielding procedure uses potassium hydroxide in methanol at room temperature. These mild conditions were subsequently applied for the hydrolysis of SubPc **73** to the respective carboxylic acid **74**. Subphthalocyanines are quite sensitive to strong bases but the core is strong enough to survive the treatment with potassium hydroxide. Hence SubPc **73** was stirred at room temperature in methanol in the presence of an excess of 2 equivalents of KOH (Scheme 38. a) but the macrocycle decomposed quite rapidly under those conditions.



**Scheme 38.** Hydrolysis test reactions performed with SubPc **74**.

The next trial reaction carried out involved stirring a solution of SubPc **73** in THF (Scheme 38 b) in the presence of aqueous KOH. In this case the solution remained pink and no signs of decomposition could be observed. The reaction was left under these conditions overnight but after checking the reaction by TLC only unreacted starting material was observed. The mixture was subsequently warmed up to 45 °C but after 4 hours no product formation was noticed. The reaction mixture was then refluxed and a colour change from pink to orange was then observed, the reaction was stopped and neutralised with HCl after which the solution turned back to pink. However the corresponding product peak could not be observed by MALDI-TOF MS.

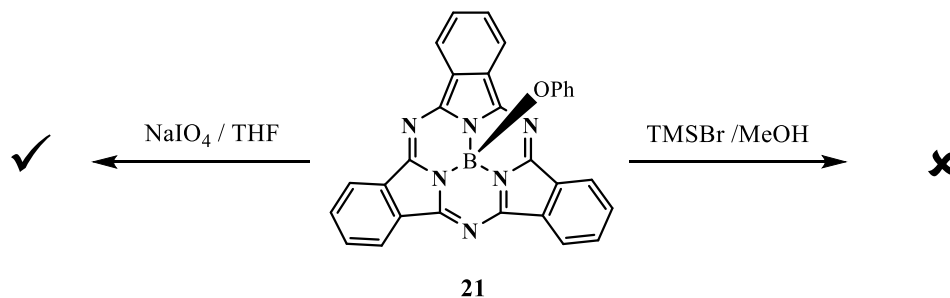
Conditions c) represented in Scheme 38 were then tested, whereby a solution of SubPc **73** and an excess of KOH were stirred in DME as solvent. The solution turned brown immediately, very slight changes were observed on the TLC so the reaction was stopped. The crude material was analysed by mass spectrometry where the product peak could not be found and <sup>1</sup>H-NMR spectroscopy revealed only unreacted SubPc **73** and decomposition product.

In essence, these conditions failed to produce the expected hydrolysed SubPc. In parallel work other protecting groups were also investigated, amongst all possible protecting groups in organic synthesis,<sup>[130]</sup> silicon derivatives are promising intermediates that could lead to SubPc functionalised with carboxylic acids after subsequent deprotection.

Amongst all silicon protecting groups –TIPS seemed a good choice due to readily availability of reagents and variety of deprotecting conditions that allows its selective removal.<sup>[131]</sup> Some of those conditions such as TBAF<sup>[132]</sup> or TFA<sup>[133]</sup> are unsuitable due to the sensitivity of the SubPc macrocycle towards these acids. However there are some interesting alternatives such as TMSBr or NaIO<sub>4</sub> worth investigating further.

Guiry et al.<sup>[134]</sup> reported an effective and high yielding cleavage of silyl esters by using catalytic amounts of TMSBr at room temperature. To test the compatibility of the SubPc core towards this reagent, an available SubPc-OPh **21** was stirred at room temperature with TMSBr in MeOH for 10 minutes (Scheme 39), but the outcome was the decomposition of the product, the molecular ion peak corresponding to the starting material SubPc was not found by mass spectrometry. It can be inferred from these results that these conditions degrade the SubPc core very rapidly.

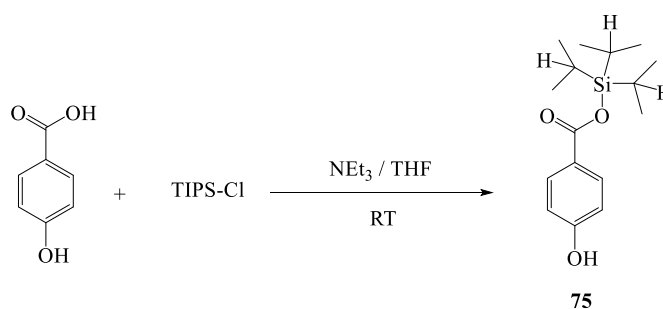




**Scheme 39.** Control experiments under deprotecting conditions.

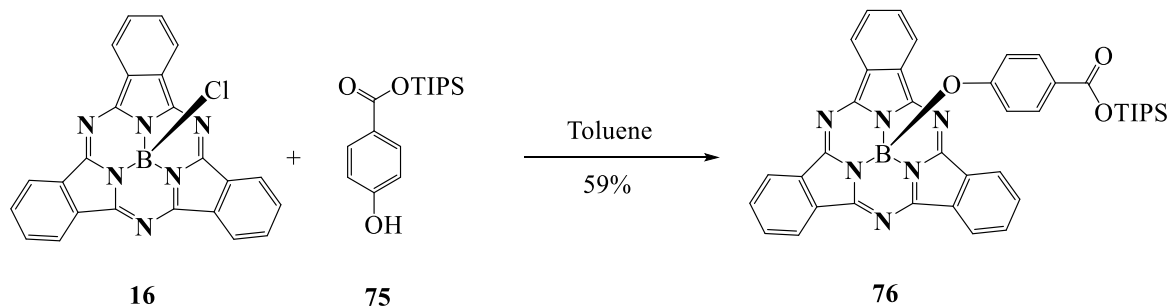
Sodium periodate has been used to cleave a wide range of silyl ethers by Yin et al.<sup>[135]</sup> in an effective and mild way, to recover the corresponding alcohols in a high yield. We investigated the possibility of applying this deprotection conditions for silyl ester. A control experiment was performed in order to study the survival of the macrocycle under those conditions. Consequently, SubPc **21** was treated with a saturated solution of NaIO<sub>4</sub> in THF, the solution was stirred for one hour after which time the mixture was heated up to 40 °C (Scheme 39). The product was subsequently subjected to the same work up, which involves the extraction of the resultant crude product with ethyl acetate, the organic layer was dried over MgSO<sub>4</sub> followed by evaporation of the solvent under vacuum. The sample was analysed by MALDI-TOF mass spectrometry. The results were very satisfactory, the molecular ion peak of SubPc **21** (488 m/z) was observed intact.

The next study for the applicability of this NaIO<sub>4</sub> as deprotecting agent, was the synthesis of a subphthalocyanine bearing just one -TIPS protected ester on the apical position. Following a literature procedure,<sup>[136]</sup> 4-hydroxybenzoic acid was treated with TIPS-Cl in the presence of triethylamine, in this manner the carboxylic acid was converted into the TIPS protected ester **75** in 29% yield (Scheme 40). It was found that this yield was considerably lower than the reported (78%) one, mainly due to the protection of the alcohol as TIPS ether. This reaction is not very selective and the fact that an excess of the silyl reagent was used triggered the formation of both products. However the amount of material was sufficient to carry on with the synthesis.



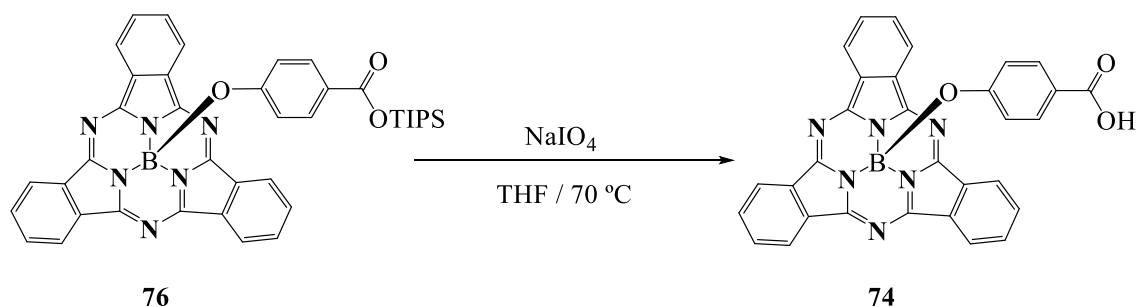
**Scheme 40.** Protection step of 4-hydroxybenzoic acid as TIPS derivative **75**.

TIPS-protected precursor **75** was subjected to conditions represented in scheme 41, whereby this compound and SubPc-Cl **16** were heated up to 110 °C in a sealed tube under inert atmosphere for 12 hours. The resultant crude material was purified by column chromatography in silica gel and washed with cold methanol to yield SubPc-(OPh-COOTIPS) **76** pink solid in a 59% yield.



**Scheme 41.** Synthesis of SubPc-(OPh-COOTIPS) **76**.

Product **76** was characterised by NMR and mass spectrometry and immediately used to perform the control experiment. SubPc **76** was dissolved in THF and an aqueous solution of NaIO<sub>4</sub> was then added, the mixture was heated up to 70 °C for 21 hours, time after which all starting material had been consumed. The formation of a new pink spot close to the baseline with an R<sub>f</sub> value of 0.07 (2:7 ethyl acetate/ petroleum ether), suggested the formation of the SubPc-(OPh-COOH) **74**. The appropriate aqueous work up was performed and a column chromatography was required.



**Scheme 42.** Deprotection step with sodium periodate.

A pink solid was isolated whose analysis by MALDI-TOF demonstrated the formation of SubPc-(OPh-COOH) **74** with the parent ion peak 532 m/z and the fragmentation corresponding to the loss of the apical position (395 m/z). Unfortunately, the product could not be further characterised due to the low quantity obtained.

These results show a promising way of deprotecting silyl esters to form SubPcs bearing carboxylic acids, the question remains on whether the macrocyclic core would be stable enough to withstand three of these functional groups. The lack of literature on this matter and the fact that Torres et al.<sup>[125]</sup> reported the synthesis of unsymmetrical SubPcs bearing just one of the acid groups, suggest that this is not a trivial question. However, satisfactory results with the TIPS-sodium periodate combination open an encouraging path that will be investigated further in our group.

## 2.4 Conclusions

Pyridyl- and hydroxy- SubPcs surfactants were designed towards the attachment of nanoparticles. Subphthalocyanines were synthesised by means of cross-coupling reactions, such as Sonogashira-Hagihara and Suzuki-Miyaura. Different peripherally functionalised SubPcs were also synthesised by the optimised methodologies. The apical position also allows group exchange in a high yielding manner. SubPcs synthesised in this work were fully characterised by means of mass spectrometry, where typical fragmentations are observed. Also by  $^1\text{H-NMR}$  spectroscopy where the effect of strong ring currents due to the cone-shaped structure of the macrocycle strongly affect the chemical shift obtained. Their unique optical properties were also investigated; peripheral substitution appears to have a more noticeable effect on both the absorption and emission bands than axial substitution.

CdSe QDs capped with oleic acid molecules were synthesised and characterised. Important parameters such as the average size of the quantum dots, the molar extinction coefficient, or the number of molecules of oleic acid capping each nanoparticle were also calculated. Ligand exchange experiments were performed with molecules with potentially high affinity towards QD's surface, such as 3-ethynylpyridine, benzyl alcohol or phenylacetic acid. The ligand exchange experiments were performed by titrating a solution of CdSe-OA with gradual amounts of the replacement ligand and the progress was monitored by  $^1\text{H-NMR}$  spectroscopy. The sharpening of the alkene resonance of oleic acid was indicative of desorption and replacement by the new ligand. It can be inferred from our results that pyridine and alcohols are poor binding ligands, whereas the high affinity of carboxylic acids by CdSe exchange very effectively removes the OA bound to the surface. Parallel results show that the pyridyl-SubPc does not effectively bind to the CdSe surface possibly owing to the absence of protons provided in the reaction mixture, along with the long aliphatic OA chains that could be acting to protect the surface towards ligand exchange.

The synthesis of a SubPc bearing three carboxylic acids at the periphery was unsuccessful. Direct approaches carried out reacting different carboxylic acid derivatives with the SubPc macrocycle yielded decomposed material. A protected SubPc bearing the ethyl esters at the periphery was successfully synthesised, in this case the functional groups were attached to the SubPc core by long aliphatic chains in order to facilitate its way through the hindered ligand shell. Unfortunately, tests carried out on a SubPc bearing just one ethyl ester at the apical position failed to yield the acid when subjected to basic conditions; decomposition of the macrocycle or unreacted material were the outcomes. Silyl protecting groups were also interrogated as possible candidates towards the target molecule and a SubPc functionalised with TIPS- protecting group at the axial position was successfully hydrolysed using sodium periodate, yielding the expected carboxylic acid. Satisfactory results with  $\text{NaIO}_4$  open an encouraging path towards deprotection of silyl ester to form SubPcs bearing carboxylic acids that will be further investigated in our group.

## CHAPTER 3. BORON SUBTRIBENZODIAZAPORPHYRINS (SubTBDAPs)

### 3.1 Introduction

#### *Phthalocyanine - Porphyrin hybrids: Tetrabenzozaporphyrins*

Perhaps the most challenging core-modification of the porphyrinoid macrocyclic core is the generation of hybrid structures.<sup>[137]</sup> Such variation leads to aromatic macrocycles whose framework lies between phthalocyanine and porphyrin parents, by means of the replacement of the bridging nitrogen atoms by methine moieties, preserving the 18- $\pi$  electron system that constitutes the core.

The terminology used to describe these compounds is as follows: **TBTAPs** (tetrabenzotriazaporphyrins), **TBDAPs** (*cis*- and *trans*- tetrabenzodiazaporphyrins) and **TBMAPs** (tetrabenzomonoazaporphyrins), Figure 51.

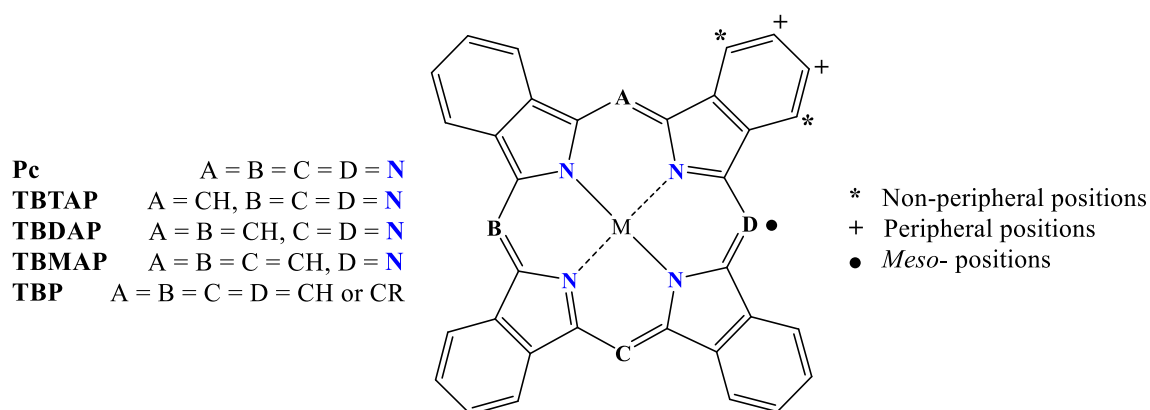


**Figure 51.** Structures of Pc, TBP and the hybrid macrocycles where M = H,H or a metal etc. as unsubstituted derivatives.

Their most important feature is that the structures lie between Pcs (already explored in chapter 1) and tetrabenzoporphyrins (TBPs) ring parents. The latter macrocycles are less readily accessible and less well studied than Pcs, but the interest in their research and exploration of their properties is increasing. In particular, there is interest in the investigation of new synthetic routes<sup>[138],[139]</sup> and their potential applicability in fields such as chemistry, catalysis, medical diagnostics, photodynamic therapy and materials science.<sup>[140]</sup>

The parent molecule TBPs **7** are porphyrins in which the macrocyclic core has been expanded by benzene rings fused at the  $\beta$ -pyrrolic positions (Fig. 52). The growing interest in this macrocyclic compound is originated from their synthetic versatility. Modifications in the structure have been made introducing different functional groups, at the periphery- and meso- positions, aside from complexation with a variety of metals.<sup>[138]</sup> These compounds exhibit UV-Vis absorption spectra similar to those of porphyrins. However, depending on the number of fused benzene rings the Q band will be red-shifted to 600-750 nm, becoming promising in applications for photodynamic therapy for cancer treatments.

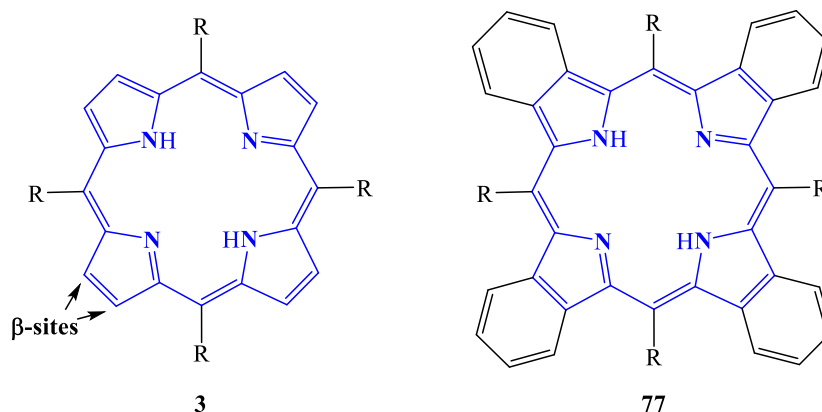
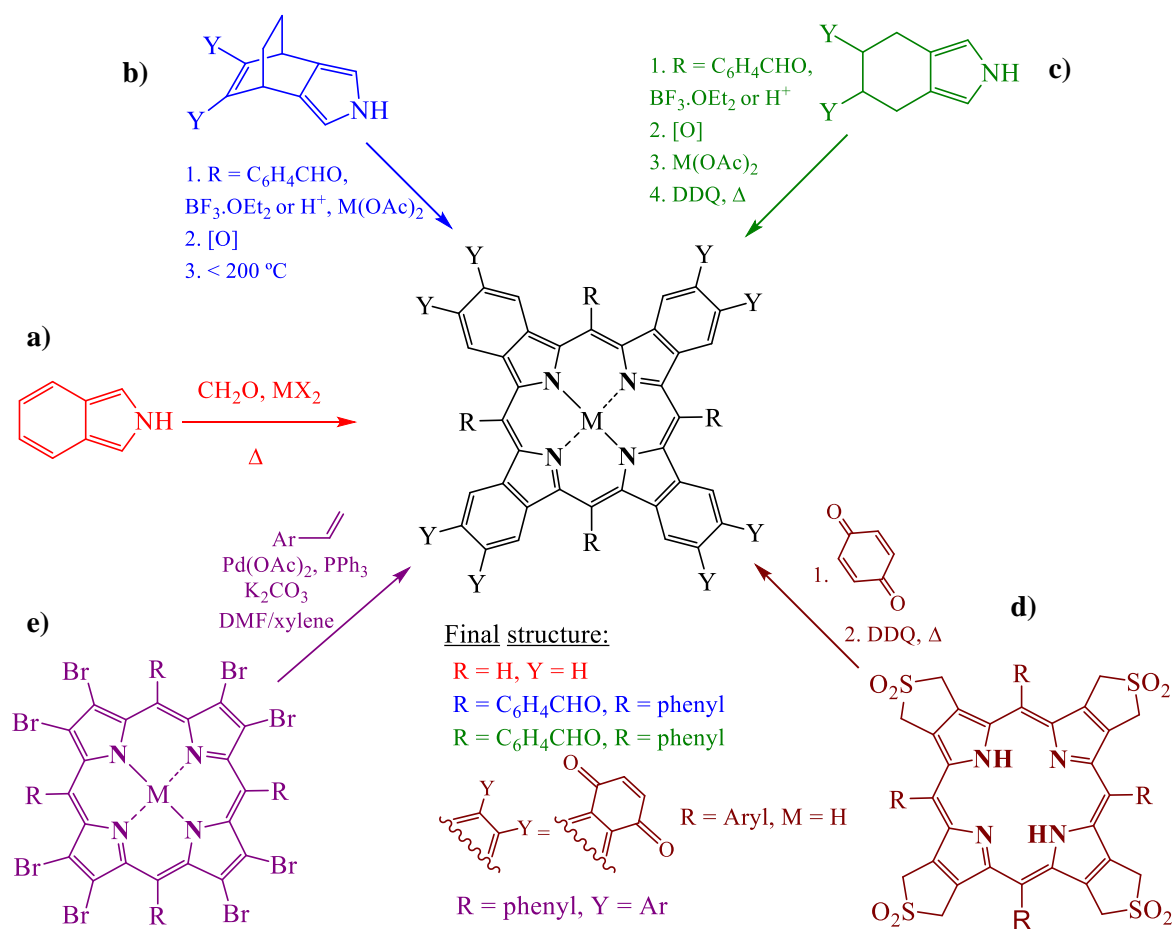


**Figure 52.** Porphyrin **3** and tetrabenzoporphyrin (TBP) **77** structures.

However, these compounds are not easily accessible. Researchers have been continuously developing novel pathways to give high yielding access to such macrocycles. Since their discovery in 1930s, five main routes for the synthesis of TBPs have been described in the literature (Scheme 43); **a)** condensation of isoindole precursors, **b)** retro-Diels–Alder, **c)** oxidative aromatisation, **d)** one-pot cycloaddition approach with aromatisation, and **e)** one-pot Heck approach with aromatisation.<sup>[140]</sup>



**Scheme 43.** Main synthetic routes for the synthesis of tetrabenzoporphyrins.<sup>[140]</sup>

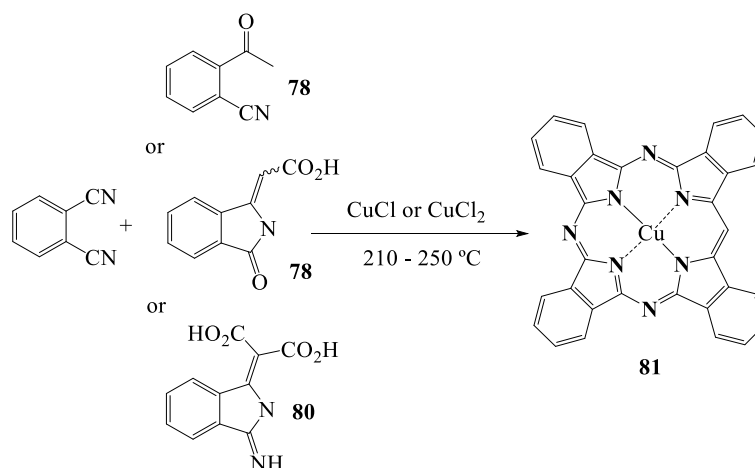
Despite the first identification of tetrabenzozaporphyrin hybrids being reported in the late 1930s by Dent<sup>[141]</sup> and Linstead,<sup>[142]</sup> these challenging hybrids have only generated a limited number of studies to date.<sup>[137]</sup> By far the greatest drawback to investigation toward these novel derivatives is the restricted synthetic availability. Nevertheless, interest in the hybrid structures has accelerated rapidly over the last decade even though syntheses, for the most part, have relied on the original protocols, albeit with some improvements.<sup>[137],[138]</sup> Remarkable synthetic research efforts from Cammidge, Cheprakov, Cook, Galanin, Leznoff and McKeown, amongst others,<sup>[143]</sup> have made available a wide range of tetraarenozaporphyrins substituted at the non-peripheral, peripheral and *meso*-positions, Figure 51.

### 3.1.1 TBTAPs: Tetrabenzotriazaporphyrins

The group's recent work is especially concerned with the TBTAP structure in which just one of the bridging aza groups is replaced by a  $sp^2$ -carbon atom, a system that represents the smallest structural difference to a phthalocyanine within the series of hybrid compounds.

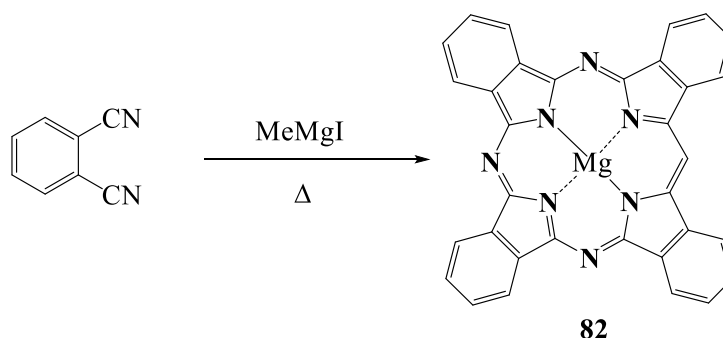
During the past decades, data on tetrabenzotriazaporphyrin derivatives was limited due to the small number of synthetic methods, the low selectivity of the reactions giving rise to mixtures up to five structurally similar macrocycles, and hence their difficult isolation.<sup>[144]</sup> Consequently, the chemistry of TBTAPs has advanced very modestly, with fewer than 50 papers of this member of the series reported to date.

The first synthesis of TBTAP was published in 1937 by Helberger and von Rebay.<sup>[145]</sup> The reaction was performed using phthalonitrile and *o*-cyanoacetophenone **78** in an equimolar ratio in the presence of copper (I) chloride. One year after, a patent<sup>[146]</sup> was granted to another protocol for the synthesis of CuTBTAP **81**, in which phthalimidineacetic acid **79** acts as a source of the methine bridge. Linstead et al.<sup>[147]</sup> also studied this reaction and suggested the use of compound **80** as the starting material. All methodologies (Scheme 44) involve the use of high boiling point solvent such as quinoline or 1-chloronaphthalene.



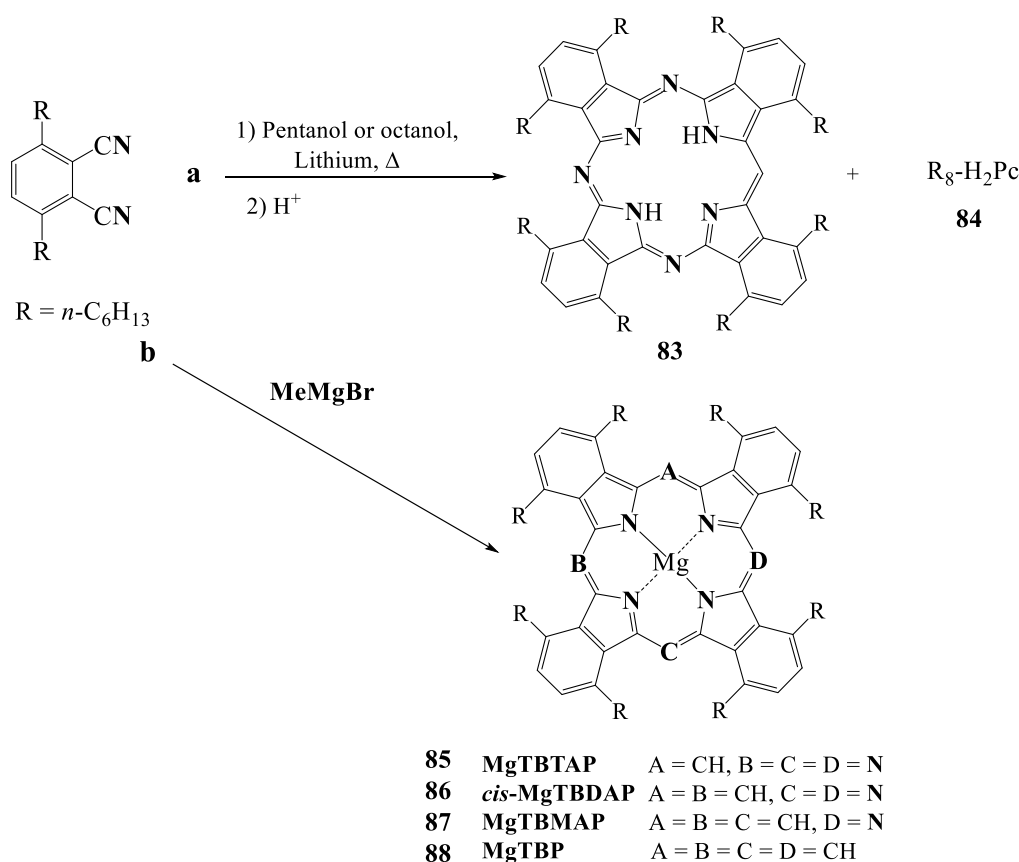
**Scheme 44.** First syntheses of CuTBTAP **81** using phthalonitrile and different precursors.

Barret and Linstead<sup>[142]</sup> developed a strategy whereby phthalonitriles are treated with an organometallic reagent such as methylmagnesium bromide at high temperature, resulting in the formation of MgTBTAP **82**, reportedly in around 40% yield. Subsequent acid treatment removed the magnesium, allowing further metals such as copper, zinc, lithium and iron to be incorporated.



**Scheme 45.** Linstead's synthesis of MgTBTAP **82**.

The reactivity of these hybrids is very extensive, particularly the functionalisation of the benzenoid ring has become target of various studies.<sup>[137]</sup> Cammidge, Cook and co-workers<sup>[148]</sup> reported the first example of a single-isomer TBTAP incorporating substituents on the benzenoid rings (Scheme 46. **a**). The serendipitous discovery occurred during the conversion of 3,6-dialkylphthalonitrile into the corresponding non-peripherally substituted octaalkyl phthalocyanine **84** when they observed the formation of octaalkyl-TBTAP **83**.



**Scheme 46.** **a**) Cammidge, Cook et al.'s octaalkyl-TBTAP **83** synthesis,<sup>[148]</sup> and **b**) optimised synthesis of a series of tetraporphyrin hybrids using varying equivalents of MeMgBr.<sup>[149]</sup>

The group subsequently extended its investigations towards the development of an efficient and controllable synthesis of non-peripherally octaalkyl-substituted derivatives using the Grignard reagent MeMgBr, but mixtures were still formed.<sup>[149]</sup> The protocol was based on McKeown and Leznoff's methodology for the preparation of tetrasubstituted TBTAP derivatives from 4-substituted phthalonitriles.<sup>[150]</sup> The reaction involved refluxing 3,6-dihexylphthalonitrile with various equivalents of MeMgBr in dry THF (Scheme 46. b). The solvent was subsequently exchanged to dry quinoline and the reaction mixture heated at 200 °C overnight. This methodology gave facile access to non-peripherally substituted octaalkyl-substituted tetrabenzoazaporphyrin hybrids, which could be subsequently demetallated with acetic acid. Re-metallation with copper was straightforward using copper (II) acetate. Some peripherally substituted derivatives were also obtained with this protocol.

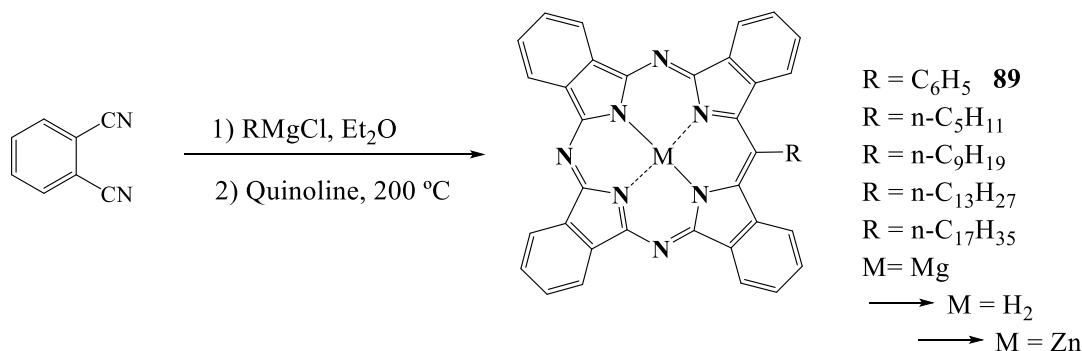
### 3.1.1.1 *meso*- Substituted TBTAPs

TBTAPs bearing a phenyl group on the *meso*-carbon bridge are very attractive materials, not only because their properties can be tuned by further functionalisation, but it opens a new direction of synthesis that was unfeasible in Pc, and that can serve, for example to attach the macrocycle to surfaces or allow the construction of more complex supramolecular systems. They are hybrid analogues of phthalocyanines and *meso*-phenyltetrabenzoporphyrin, and can be described as planar macrocycles, in which the phenyl group lies perpendicular to the porphyrinoid core with their  $\pi$ -systems decoupled.

The introduction of substituents on this position was investigated as well by Linstead,<sup>[142]</sup> they proposed the reaction between *n*-butyllithium and phthalonitrile. UV/Vis spectra indicated that a mixture of a TBTAP and magnesium phthalocyanine was produced, but due to poor solubility TBTAP could not be isolated. The preparation of the phenyl-MgTBTAP derivative **89** was also attempted, using benzylmagnesium chloride, but the reaction only yielded MgPc.

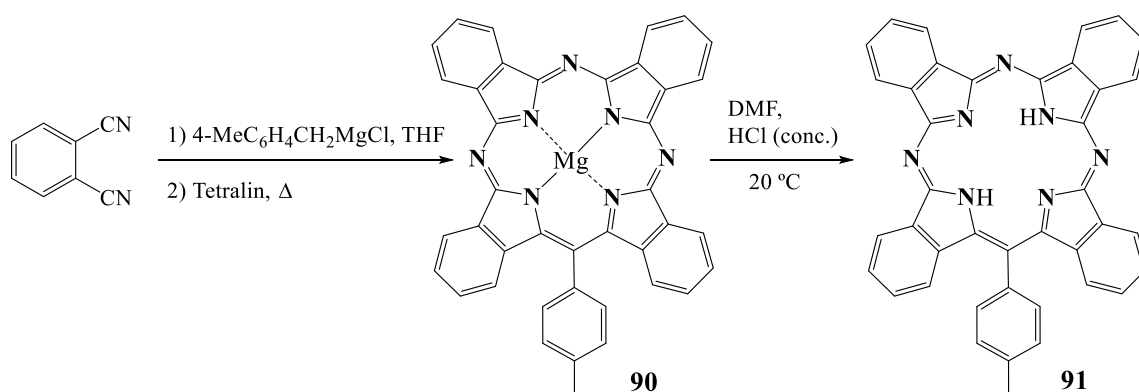
For some 50 years there was a lack of further investigation to expand the scope of TBTAPs' and other hybrids' syntheses. McKeown and Leznoff<sup>[150],[151]</sup> then reported an important breakthrough in the area, disclosing the successful synthesis of *meso*- aryl and alkyl substituted tetrabenzotriazaporphyrins as major products. The reaction of phthalonitrile with benzylmagnesium chloride at 200 °C resulted in the formation of Mg-phenyltetrabenzotriazaporphyrin **89** in 15% yield, Scheme 47.





**Scheme 47.** McKeown and Leznoff's synthesis of *meso*-aryl and alkyl-TBTAPs.

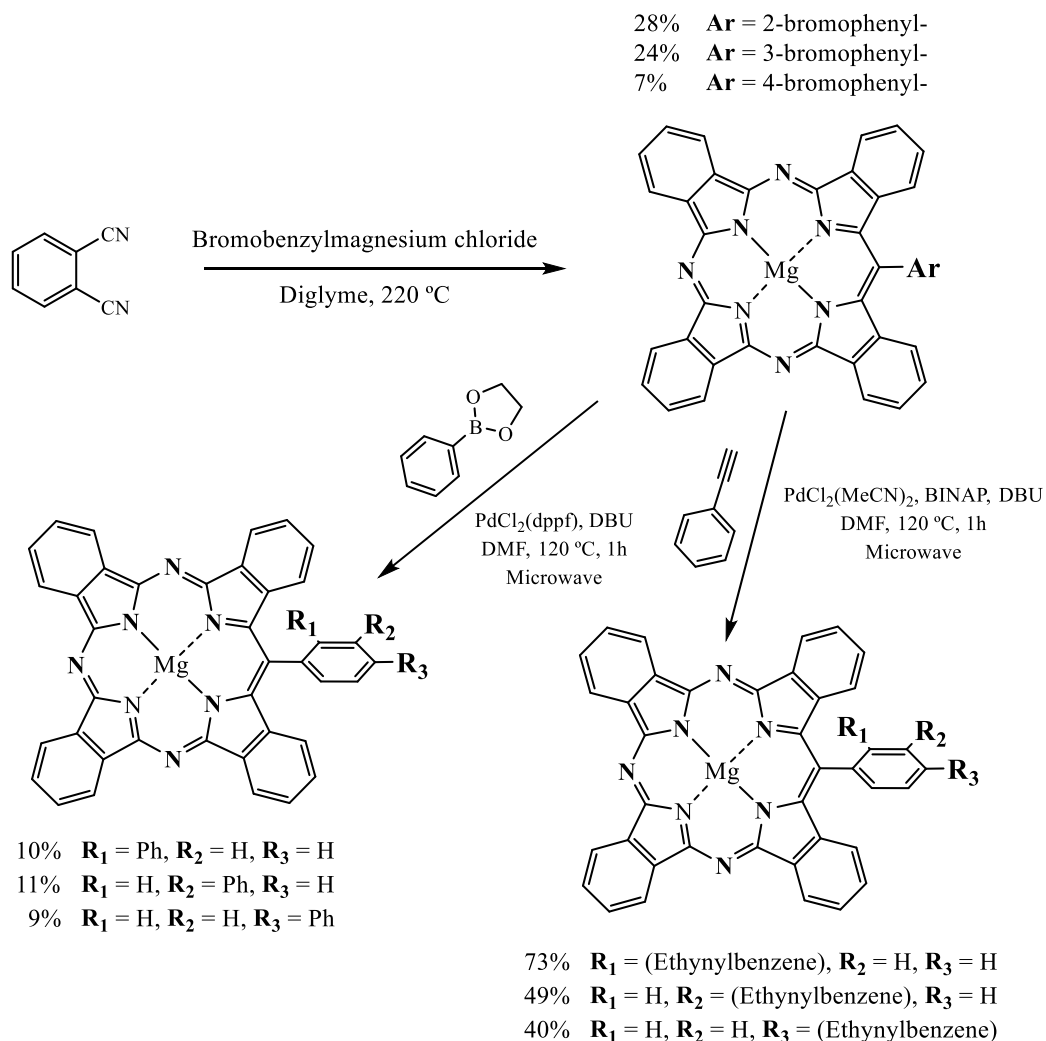
The formation of the (*p*-tolyl) MgTBTAP **90** and the subsequent demetallation to afford TBTAP **91** was subsequently covered with a patent.<sup>[152]</sup>



**Scheme 48.** Synthetic path for the formation of *meso*-substituted TBTAPs.<sup>[152]</sup>

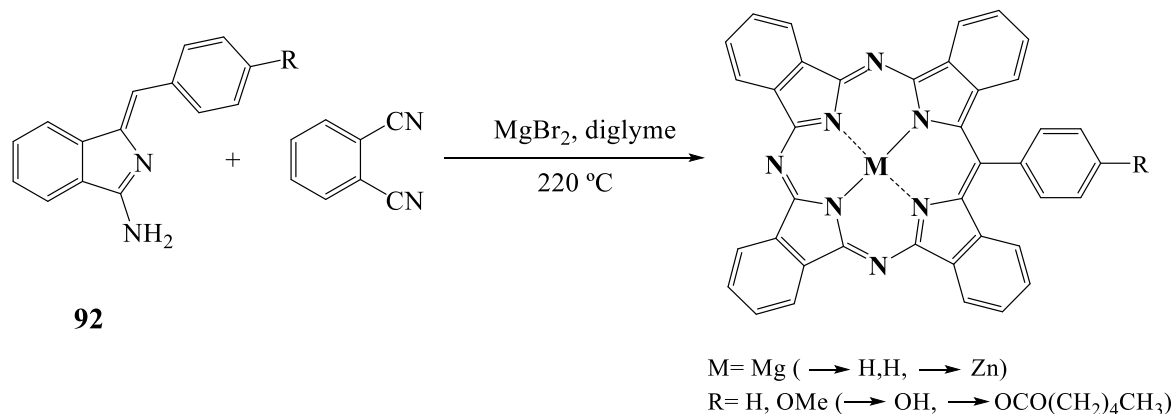
It is not possible to obtain non-peripherally functionalised derivatives, bearing a substituent on the *meso*-site due to the steric hindrance at the *meso*- position in the final, aromatic macrocycle. Hence, reactions of 3,6-didecyl phthalonitrile with benzyl and alkyl Grignard reagents yielded mainly TBTAP hybrids unsubstituted at the *meso*-position.<sup>[149]</sup>

Some *meso*-bromophenyl substituted TBTAPs were synthesised in our group<sup>[139]</sup> using an improved variation on the traditional reaction between phthalonitriles and Grignard reagents. The reaction involved heating a mixture of phthalonitrile with 2-, 3-, or 4-bromobenzylmagnesium chloride in diglyme at 200 °C. Subsequent purification gave rise to the TBTAP hybrids in modest yields, Scheme 49. In a following publication, the first examples of further functionalisation of the *meso*-sites were also disclosed by Cambridge's group this year.<sup>[153]</sup> The TBTAPs were functionalised by means of cross-coupling reactions carried out under microwave irradiation. Suzuki reaction proved to be challenging but anhydrous conditions gave rise to the TBTAP hybrids in low yields. However Sonogashira cross-coupling worked smoothly allowing high yields of the target TBTAP compounds to be isolated.



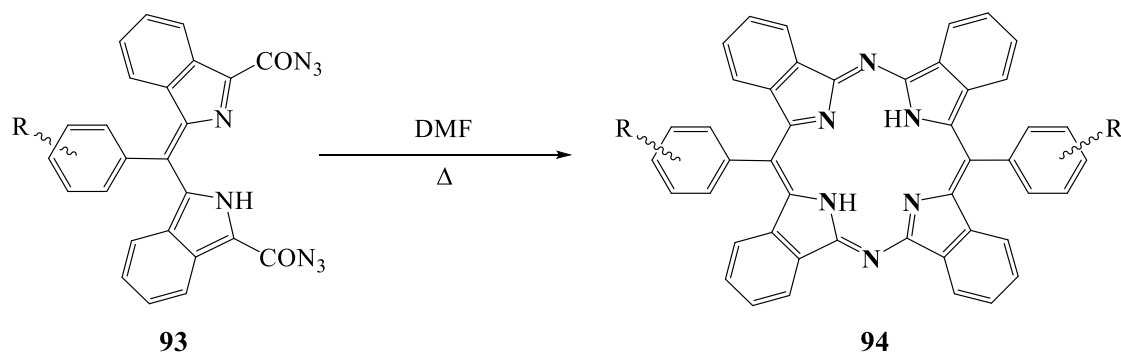
**Scheme 49.** Synthesis of *meso*-substituted TBTAPs via Grignard reagents,<sup>[139]</sup> and subsequent functionalisation.<sup>[153]</sup>

In an important recent breakthrough our group reported a novel and versatile protocol<sup>[154]</sup> that gives controlled access to functionalised TBTAPs (Scheme 50). Most importantly, the synthesis allows introduction of a variety of substituents at the *meso*-site.<sup>[139]</sup> The synthesis of TBTAP hybrids required a new approach, in order to give an easy access to these materials. Therefore aminoisindolene **92** intermediates were employed to initiate the macrocyclisation process around a magnesium template ion. The optimised reaction conditions involved heating phthalonitrile and MgBr<sub>2</sub> in diglyme at 220 °C. A mixture of phthalonitrile and aminoisindolene derivative **92** in diglyme was then added dropwise over a period of 1 hour. DABCO was subsequently used to complete the reaction thus giving impressive yields of 40% after chromatographic purification process. The straightforward and high yielding novel protocol is expected to expand TBTAPs chemistry and applicability.



**Scheme 50.** Synthetic path giving straightforward access to functionalised porphyrin-phthalocyanine hybrids.<sup>[154]</sup>

Cheprakov and co-workers<sup>[155]</sup> have subsequently reported a complementary approach to a second member of the hybrid series (Scheme 51), the *trans*-TBDAP **31**. The reaction proceeds via Curtius rearrangement involving azidocarbonyl derivatives of *meso*-aryldibenzodipyrromethenes **30**.



**Scheme 51.** Synthesis of *trans*-TBDAP.<sup>[155]</sup>

### 3.1.1.2 Properties and applications of tetrabenzoazaporphyrin hybrids

TBTAPs have lower symmetry ( $C_{2v}$ ) than Pcs ( $D_{4h}$ ), due to the presence of the methine bridge in the *meso*- position, this is manifested in the optical properties. The absorption spectrum of metallophthalocyanines shows one intense Q band (the lowest energy  $\pi-\pi^*$  absorption that occurs in the visible region of the spectra) around 700 nm, whereas the Q band of TBTAPs is split into two components (at 694 and 671 nm) due to the symmetry reduction. Furthermore, the Q band, shifts to shorter wavelength and lower intensity as the aza links are replaced by methine units (Fig. 53). The Soret band of MgTBTAP **33** is very broad with a maximum at 410 nm, similar to that of MgPc **32**. Overall the Q bands of TBTAP and Pc are more intense than the Soret band, being the opposite for TBP.

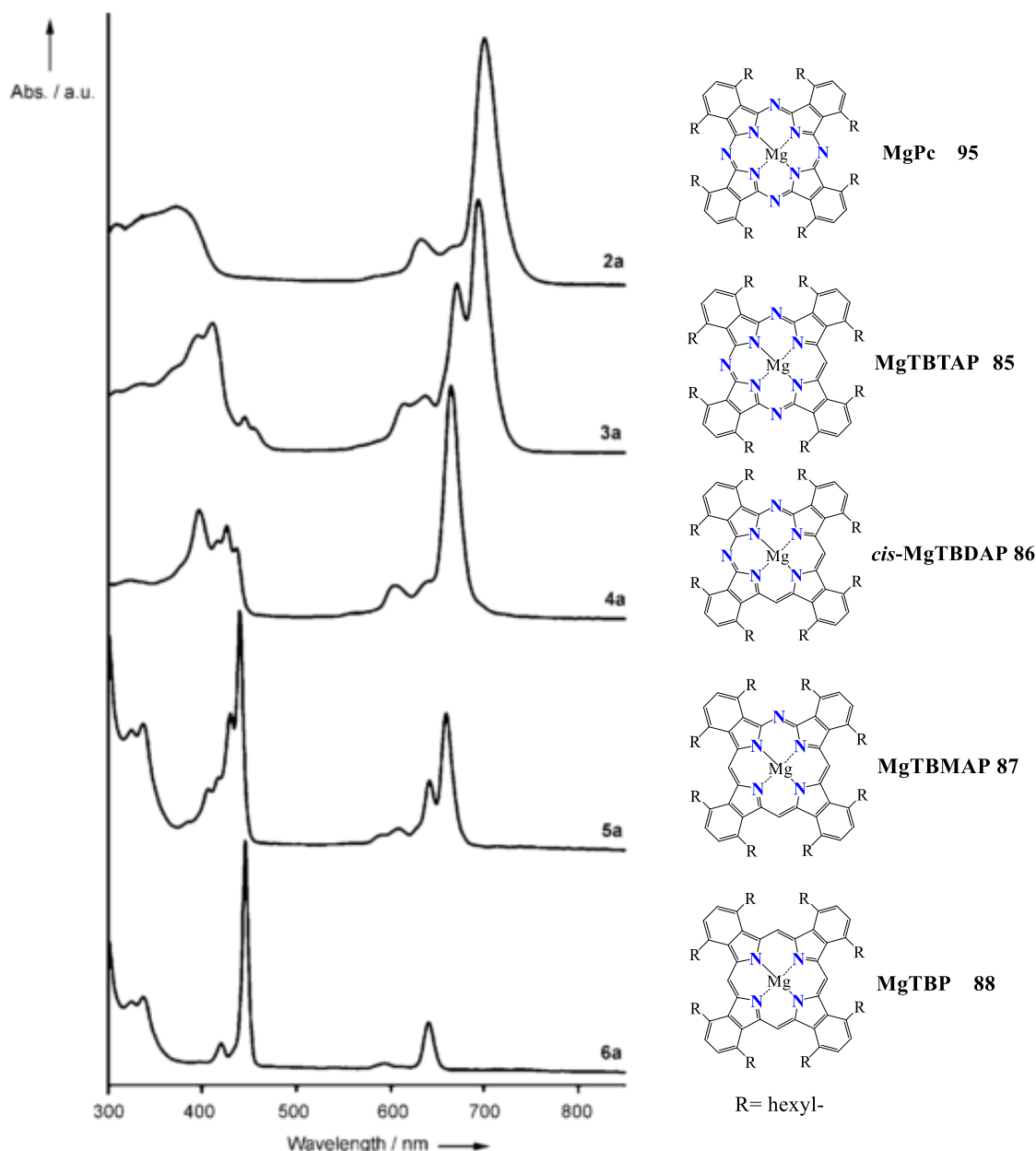


**Figure 53.** UV/Vis absorption spectra of the magnesium-metallated compounds Pc **95**, TBTAP **85**, *cis*-TBDAP **86**, TBMAP **87**, and TBP **88** in THF.<sup>[149]</sup>

The structural similarity between Pc and TBTAP is reflected in the similar physical properties, hence they have been applied in similar areas,<sup>[144]</sup> such as dyes, fluorescent markers in biological applications, catalysts, optical data carriers, OLEDs, etc. Latest advances in the field include their use as, for example, optical oxygen-sensing materials<sup>[156]</sup> and liquid crystals.<sup>[143]</sup>

In a very recent publication,<sup>[157]</sup> spin-coated films of nickel phthalocyanine **96** (NiPc) and non-peripherally substituted nickel tetrabenzotriazaporphyrin **97** (NiTBTAP) were employed as active semiconducting layers in the fabrication of organic thin film field-effect transistors (OTFTs) (Fig. 54). Comparative studies of the two devices revealed the superior performance of the TBTAP-Ni transistor in terms of high mobility, low threshold voltage, large on/off current ratio, and steeper sub-threshold slope. These improved properties of NiTBTAP over NiPc in OTFTs devices

are encouraging results which undoubtedly will persuade further investigation on their implementation in electronic devices.

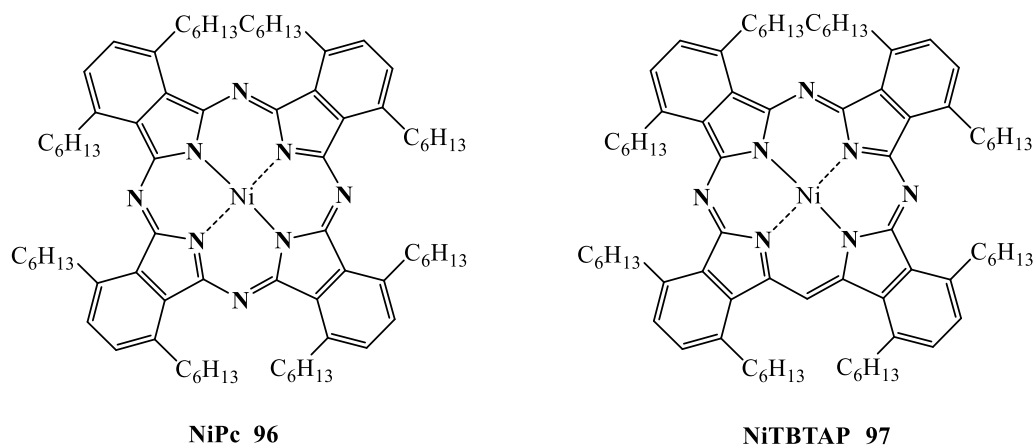
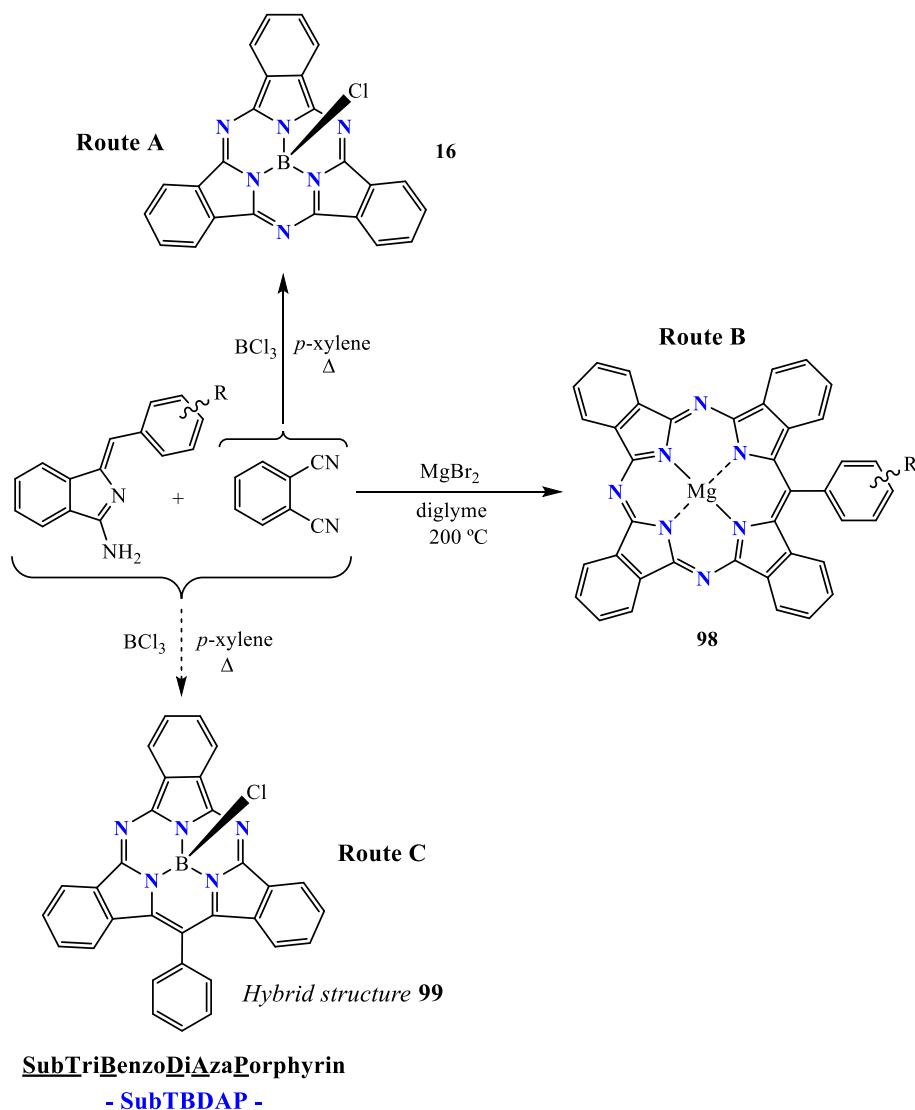


**Figure 54.** Structures of nickel Pc and nickel TBTDAP.

***Subphthalocyanine - benzoSubporphyrin hybrids: SubTriBenzoDiAzaPorphyrins (SubTBDAPs)***

**3.1.2 Aim of the project**

As previously mentioned, the optimised synthesis<sup>[93]</sup> of SubPc-Cl **16** (Scheme 52. A) typically involves the cyclotrimerisation reaction of phthalonitrile precursor with BCl<sub>3</sub> in a high boiling solvent (*p*-xylene). In these reactions the boron reagent acts as Lewis acid and template. In the newly developed synthesis<sup>[154]</sup> of TBTDAP hybrids **98** our group employed aminoisoindolene precursors to initiate the macrocyclisation process around a magnesium template ion at high temperature (Scheme 52. B). We therefore reasoned that the same precursor could potentially initiate the macrocyclisation process triggered by a boron template, leading to a hybrid in which a (functionalised) *meso*- sp<sup>2</sup> carbon formally replaces one of the bridging nitrogen atoms present in the SubPc parent, see Scheme 52. C. The target product is a SubTriBenzoDiAzaPorphyrin – **SubTBDAP 99** which is intermediate between the benzosubporphyrin (BzSubP) and the Subphthalocyanine parents (Fig. 55.)



**Scheme 52.** (**Route A**) Optimised SubPc synthetic route. (**Route B**) Newly developed synthesis of TBTAPs in our group. (**Route C**) Synthetic strategy towards the target molecule: Hybrid Structure (SubTBDAP-Cl **99**).

SubTBDAPs could offer unique possibilities for synthetic variation and tuning of material properties, with no isomer issues and perhaps better reactivity. Functionalisation on the axial and peripheral positions is something already accomplished for SubPcs and SubPs,<sup>[30]</sup> it is then possible to think that those changes would also be feasible on the new hybrid.

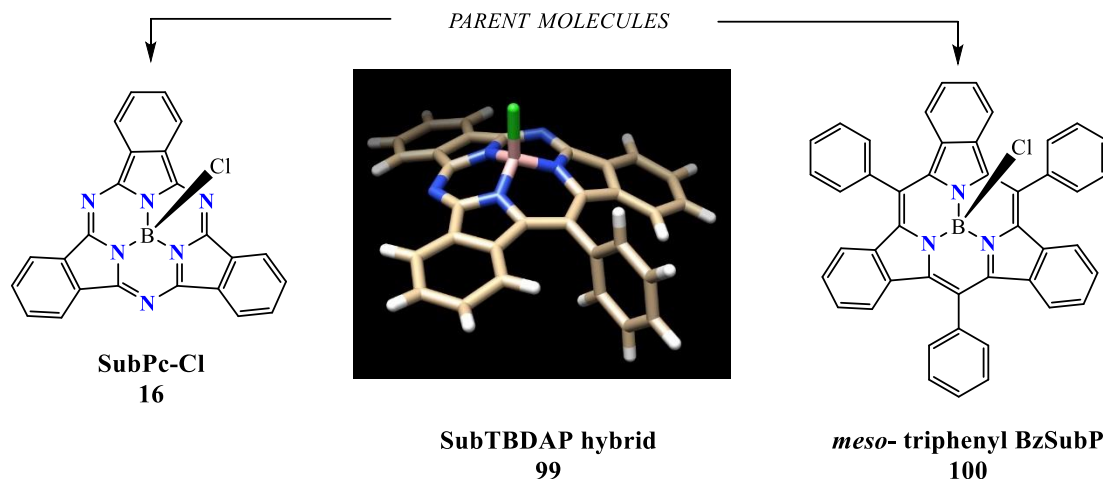


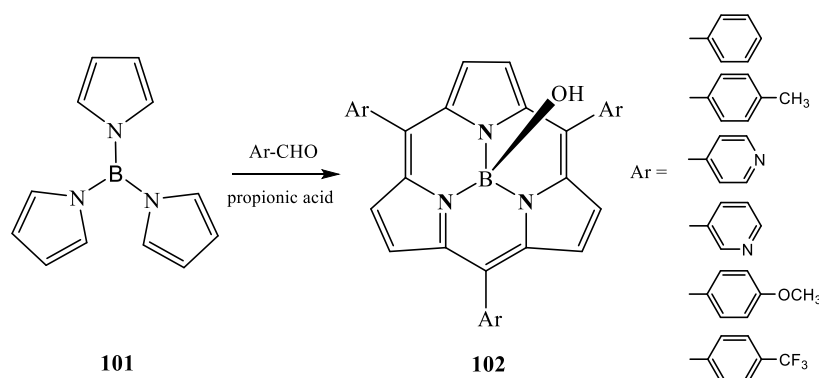
**Figure 55.** A representation of the desired hybrid compound's computational model, performed with Chimera 1.9 software, and parent macrocycles of the new hybrid.

What has certainly attracted our motivation is the new *meso*- position, a 3D representation (Fig. 55) of the hypothetical hybrid, shows similar curved shape and a central boron coordinated to three nitrogen and the axial chlorine as the parent structures. This intriguing new *meso*- site would deliver the possibility of monofunctionalisation and it would open a new direction on the reactivity and application of these new materials.

The new system represents the smallest structural difference to a subphthalocyanine, nevertheless it offers the potential to bridge the properties of the two systems, providing new chemistry to be investigated within the field of macrocyclic chemistry.

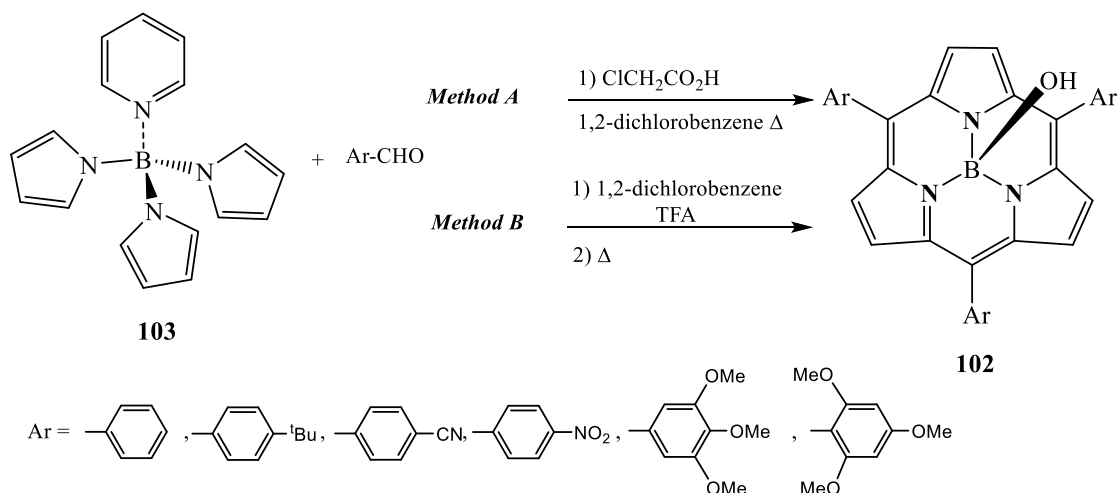
### 3.1.3 Subporphyrins (SubPs)

These non-planar contracted porphyrinoids are composed by three pyrrole units linked by methine bridges (aryl- substituted) hosting a tetrahedral boron in its core. *meso*-Triarylsubporphyrins **102** were reported for the first time in 2007 by Kobayashi et al.,<sup>[158]</sup> and most of the reported syntheses for symmetrical subporphyrins (SubPs) from then on have their origin in Adler methodology.<sup>[13]</sup> The reaction represented in Scheme 53, involves the treatment of tri-1-pyrrolylborane **101** with boron acting as a template, and a corresponding aryl aldehyde in refluxing propionic acid, obtaining modest yields that range 4-8%.



**Scheme 53.** Kobayashi methodology for the synthesis of Subporphyrin **102**.<sup>[158]</sup>

The same year Osuka et al.<sup>[159]</sup> reported the synthesis employing two different reaction conditions, both of them using *N*-pyridine-tri(1H-pyrrol-1-yl)borane **103** as template and also based on Adler conditions. One method (**A**, Scheme 54) is a condensation reaction with chloroacetic acid in refluxing 1,2-dichlorobenzene to afford subporphyrins in 1.1-3.2% yield. A two-step procedure was also described (method **B**, Scheme 54) consisting of the treatment of the two reagents with trifluoroacetic acid in 1,2-dichlorobenzene at 0 °C, followed by air-oxidation at reflux temperature to provide subporphyrins in up to 5.6% yield. These yields were further improved by oxidising the subchlorin formed as side product into the corresponding SubP using MnO<sub>2</sub>.<sup>[30]</sup>

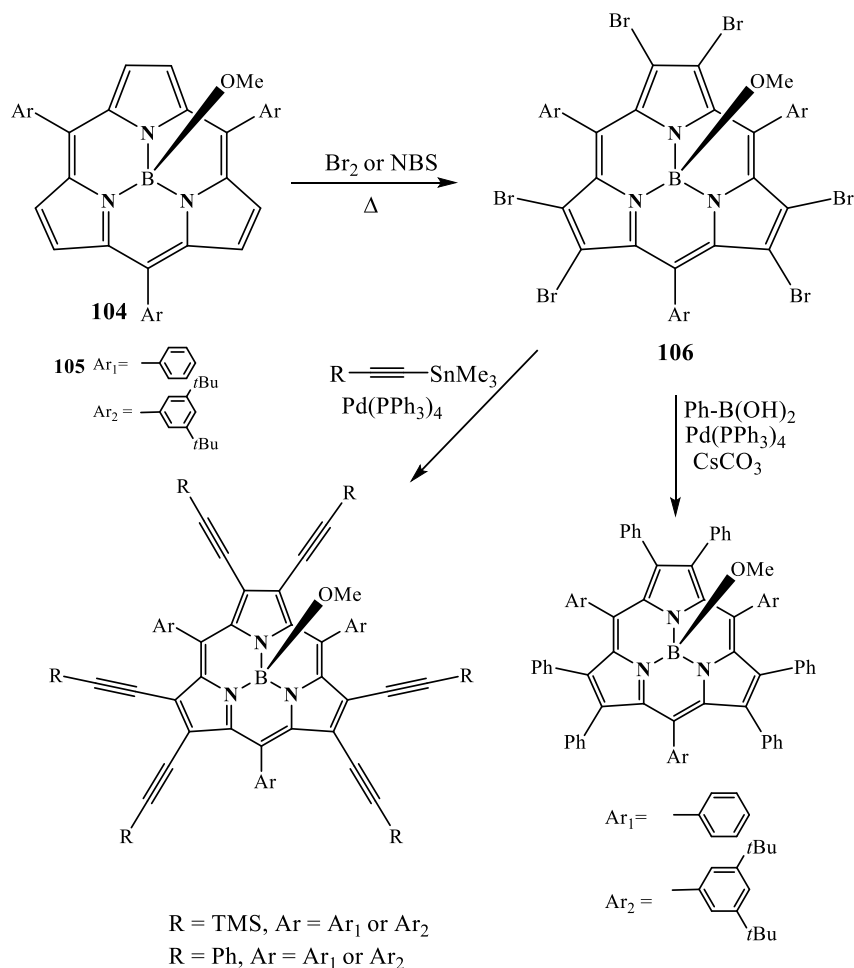


**Scheme 54.** Different methodologies for subporphyrin synthesis.

### 3.1.3.1 Reactivity and properties

There is a lack of literature on methodology to give straightforward access to compounds substituted at the periphery, mainly due to the fact that  $\beta$ -substituted tripyrrolylboranes are unreported. Nevertheless, the peripheral functionalisation has been successfully accomplished by reacting preformed SubPs. To date this is limited to hexabromo-SubP derivatives or compounds derivatised from them.<sup>[160]</sup> Bromination of **104** with *N*-bromosuccinimide (NBS) led to the  $\beta$ -perbrominated subporphyrin **106** in 90% yield in a very slow reaction. Bromine was a much more effective reagent since in 2 hours the reaction gave the desired product quantitatively. The authors reported as well further functionalisation by means of Stille and Suzuki couplings obtaining good yields, 63-89% and 55-73%, respectively.





**Scheme 55.** Bromination of subporphyrin **104** and further functionalisation by means of cross-coupling reactions.<sup>[160]</sup>

*meso*-Functionalisation of SubPs has also been accomplished by reacting the preformed macrocycle. The versatile syntheses allowed the isolation of a wide variety of subporphyrins bearing bromo-, nitro-, amino-, phenyl- derivatives, thiophenyl-, amongst others.<sup>[161],[30]</sup> Since axial hydroxy- SubPs are difficult to isolate most SubPs are reported as methoxy- derivatives that are obtained by substitution of the hydroxyl group using methanol. However, examples of subporphyrins substituted at the apical position with other alkoxy-, carbonyloxy-, or fluorine- groups are known.<sup>[30]</sup>

Their absorption spectra show a porphyrin-like intense Soret band at around 370 nm and very weak Q bands from 400 to 540 nm, the number depends on the symmetry, hence on the substitution of the molecule. Figure 56 represents a comparison spectra between SubP-OMe **105** (red) and zinc-tetraphenylporphyrin **107** (ZnTPP) (black). Subporphyrins show a blue-shift in the bands, presumably due to the reduction on the number of  $\pi$ -electrons (from  $18\pi e^-$  in TPP to  $14\pi e^-$  in SubPs).<sup>[159]</sup> Subporphyrins exhibit green fluorescence emission, normally observed as a mirror image of the Soret band in the 470 to 670 nm region, with the main peak in the 508-543 nm region.<sup>[30],[159]</sup>

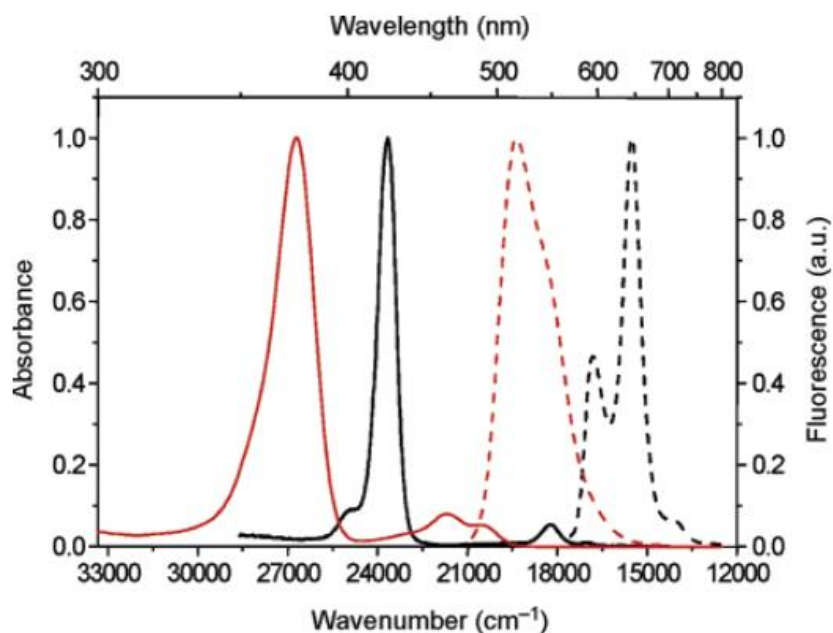
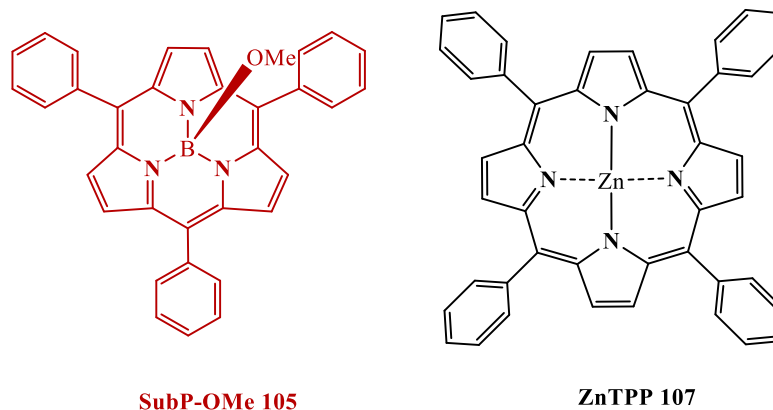
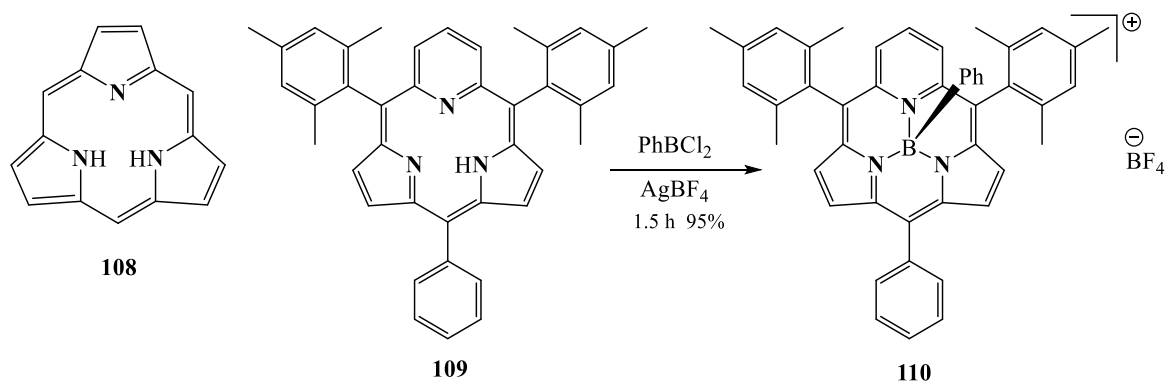


**Figure 56.** UV-Vis (solid lines) and emission (dashed lines) spectra of SubP-OMe **105** (red) and ZnTPP **107** (black).<sup>[159]</sup>

### 3.1.3.2 Triphyrins: *The exception*

Triphyrins (1.1.1) **108** (Scheme 56) constitute a new class of subporphyrinoids; they are formed by three pyrrole units, linked through *meso*-sp<sup>2</sup> carbon atoms (as in SubPs). In fact, they are the only class of cyclotrimerisation products that have been reported to date without the boron atom in the central core.<sup>[162],[30]</sup> Subpyriporphyrin **109** was reported by Latos-Grażyński in 2006 in a 6% yield.<sup>[163]</sup> It is the result of the replacement of one of the pyrrole rings by a pyridine; this change is believed to help the stabilisation of the free base form, owing to mitigation of possible steric repulsion between the inner -NH hydrogen atoms.<sup>[164]</sup> Interestingly, Subpyriporphyrin **109** reacts with dichlorophenyl borane (PhBCl<sub>2</sub>) at room temperature in the presence of silver tetrafluoroborate (AgBF<sub>4</sub>) to obtain the macrocyclic boron subpyriporphyrin **110** as a monoanionic ligand in 95% yield, Scheme 56.

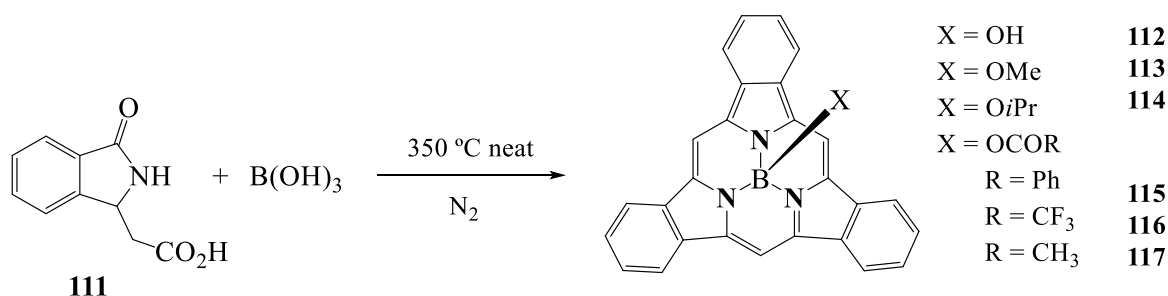


**Scheme 56.** Hypothetical [14] triphyrin (1.1.1) **108**. Reported subpyrriphyrin **109** and reaction to give subporphyrin **110**.<sup>[163]</sup>

There are few reports concerning this kind of macrocycles, but there is an increased interest in developing a protocol to produce derivatives due to their potential applications in optical data storage.<sup>[165]</sup>

### 3.1.4 BenzoSubPorphyrins (BzSubPs)

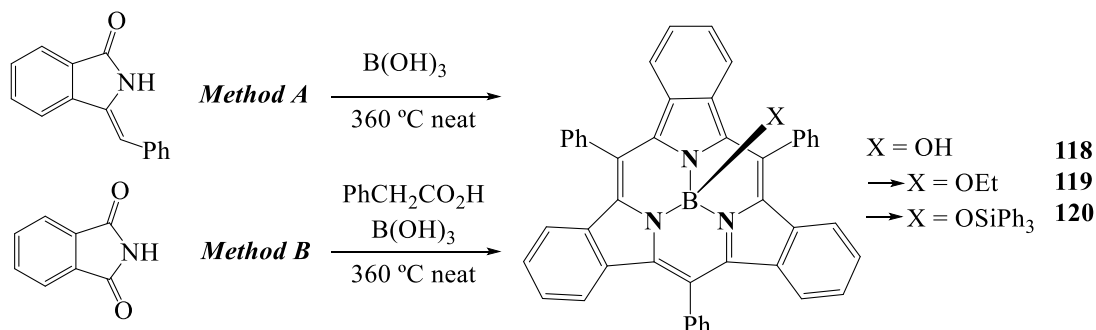
In 2006, 34 years after the discovery of SubPcs, Osuka et al.<sup>[166]</sup> reported the first example of the subporphyrinoid family, hydroxy-BenzoSubPorphyrin **112** (BzSubP-OH) was synthesised under harsh conditions. Applying a modified protocol developed by Gouterman et al.<sup>[167]</sup> 2-(3-oxo-2,3-dihydro-1H-isoindol-1-yl) acetic acid **111** was reacted with boric acid (used instead of the zinc salt as a template to construct the macrocycle). The reaction was carried out neat at 350 °C to give the product in a 1.4% yield. It could also be prepared under microwave irradiation yielding 1.2% of the desired compound.



**Scheme 57.** First synthesis of BzSubPs by Osuka.<sup>[166]</sup>

Facile replacement of the axial hydroxy- group could be achieved refluxing BzSubP **112** with the appropriate alcohol, such as methanol and propan-2-ol, obtaining a stable derivative **113** quantitatively, and **114** (unreported yield) which could be hydrolysed back to **112** with silica gel or adventitious water present in solution. The axial hydroxyl substituent could also be exchanged in an equilibrium reaction by a carboxy- group, stirring the mixture with an excess of a carboxylic acid provided quantitatively compounds **115**, **116** and **117**.

Two years later, Kobayashi, Luk'yanets and co-workers<sup>[168]</sup> disclosed the synthesis of *meso*-phenyl tribenzosubporphyrin **118** by condensation reaction of phthalimide with phenylacetic acid, as well as a self-condensation reaction of 3-benzalphthalimidine, using boric acid as boron template in both cases. This reaction also requires harsh conditions, heating the reagents neat at 360 °C, they obtained moderate yields up to 7.8%.



**Scheme 58.** Synthesis of *meso*-phenyl BzSubPs by Kobayashi.<sup>[168]</sup>

In this case, the hydroxyl- axial ligand could be replaced by an ethoxy- group giving BzSubP **119** using ethanol during the purification process.

### 3.1.4.1 Properties

The macrocyclic core of BzSubPs seems very robust,<sup>[165]</sup> however the possibility of performing chemical modifications on the periphery remains unexplored. As expected, the optical properties are similar to those of *meso*-aryl Subporphyrins.<sup>[30]</sup> The absorption spectrum of **113** (Fig. 57) exhibits a sharp Soret band at 353 nm, and a Q band at 514 nm with a shoulder at 480 nm, which are blue-shifted regarding metalloporphyrins, due to the reduced  $\pi$ -conjugation pathway. Interestingly, it exhibits green fluorescence at 514 nm and a very small Stokes Shift of 3 nm.

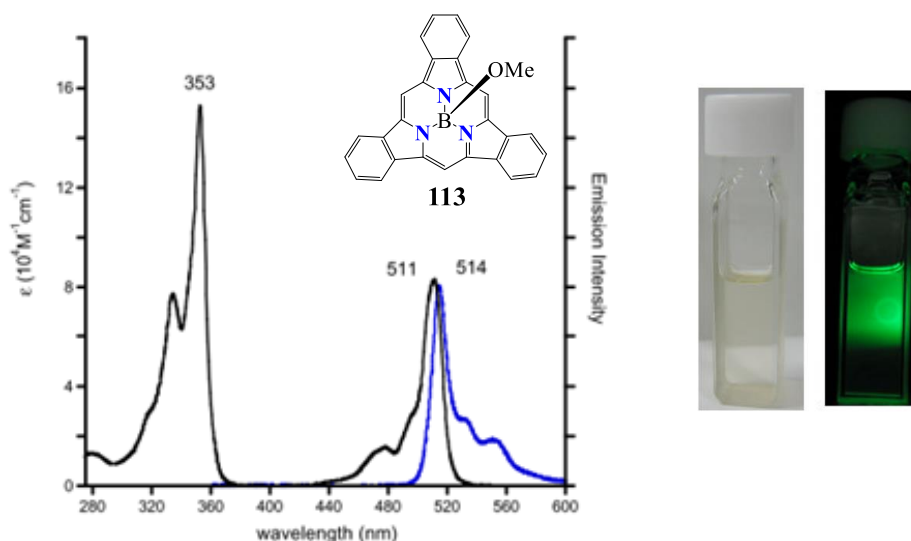


**Figure 57.** (Left) UV-Vis (black line) and emission (blue) spectra of OMe **113** in MeOH.

(Right) picture of the green fluorescence of **113** irradiated at 355 nm.<sup>[166]</sup>

The optical properties of *meso*-phenyl tribenzosubporphyrins (Fig. 58) are logically very similar to those of tribenzosubporphines. The UV/Vis absorption spectrum of phenyl-BzSubPs **118**, shows a very strong Soret band at 372 nm (almost identical in shape to the B band of **113** (Fig. 57)), and a Q band at 517 nm with a shoulder peak at 485 nm. It also exhibits green fluorescence at 524 nm upon excitation at 480 nm. The Stokes shift of 7 nm is smaller than the ones observed for *meso*-aryl subporphyrins and subphthalocyanines, but higher than for tribenzosubporphyrin **113**. In general, the small Stokes Shift values for subporphyrinoids reflects the rigid structure of the macrocyclic core.

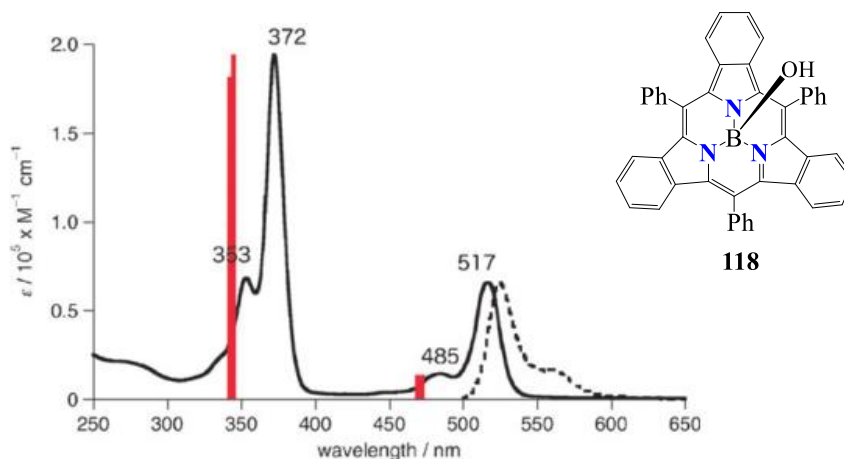


**Figure 58.** Absorption (solid line) and emission spectra (dashed line, upon excitation at 480 nm) of **118** in dichloromethane.<sup>[168]</sup>

X-Ray analysis demonstrated the bowl-shaped structure of BzSubPs (Fig. 59), with a variable curvature that depends on the axial group. The cone-like structure is very similar to that of the subphthalocyanines. The *meso*-phenyl groups lie almost perpendicular to the subporphyrin core and, although Kobayashi et al.<sup>[168]</sup> postulated that the free rotation of the phenyl groups is inhibited by the benzo- moieties, since the peaks arising from the *ortho*- and *meta*- protons still appear as broad signals at different chemical shifts even at room temperature, the steric hindrance certainly slows down the rotation to actually display four distinguished signals.

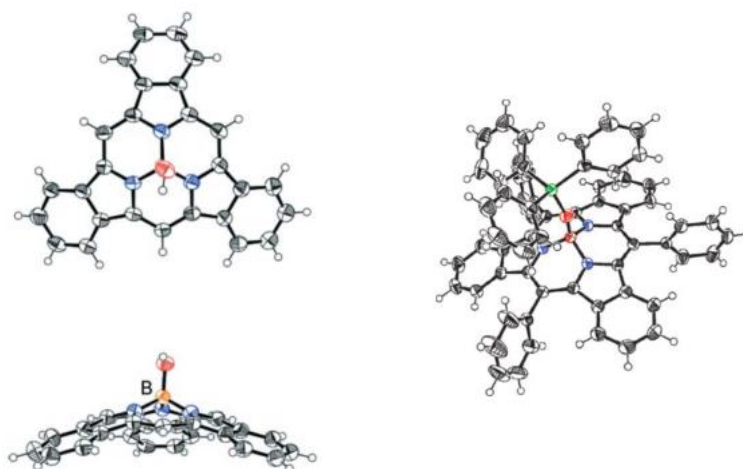


**Figure 59.** Crystal structure of BzSubP-OH **112** (left) and BzSubP-SiPh<sub>3</sub> **120** (right).<sup>[166],[168]</sup>

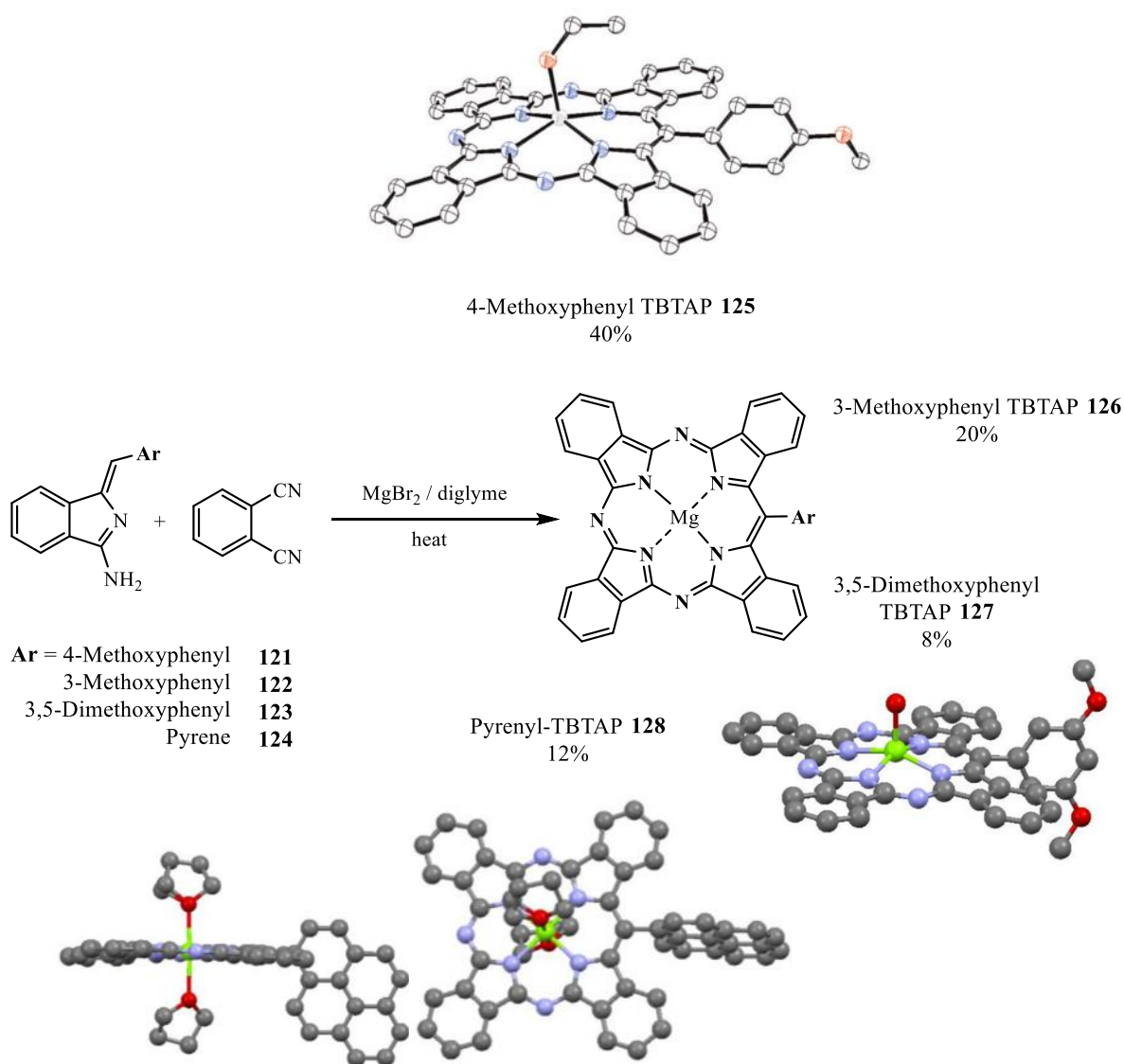
The curvature of subporphyrinoids makes them promising building blocks in supramolecular systems, as the concave and convex  $\pi$  surfaces can interact in different ways with other electroactive moieties. Deeper understanding of subporphyrinoids is required, doing so could lead to their application as dyes, in the field of nanotechnology and molecular materials.

This difference in investigation effort triggered by subporphyrins and subphthalocyanines is principally due to synthetic availability. As previously mentioned, subphthalocyanines can be prepared in good yields from a variety of phthalonitriles, whereas it has been illustrated that synthetic yields to date for benzosubporphyrins are generally low. Accordingly, there is a driving force for developing new synthetic routes to give easy access to related promising macrocycles. The potential of tuning the properties of *meso*-aryl SubPs by functionalising the aryl substituent is an important target for future applications.

## 3.2 Results and Discussion

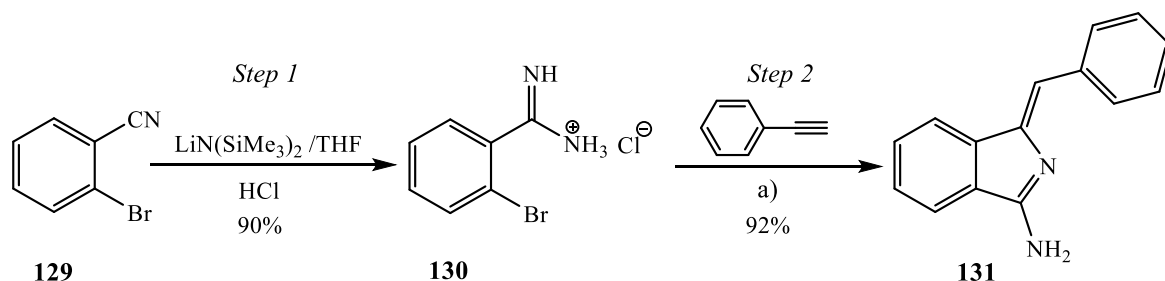
### 3.2.1 First Steps

At the heart of the strategy to obtain a SubTriBenzoDiAzaPorphyrin lies aminoisoindolene precursors as key intermediates for the macrocyclisation process leading to hybrids. As illustrated in the introductory section, aminoisoindolenes have already played an important role in the development and improvement of the reaction performance in the synthesis of tetrabenzotriazaporphyrins (TBTAPs).<sup>[154]</sup> This derivative presumably initiates the macrocyclisation process, providing the hybrid with the new *meso*-carbon site and the phenyl ring for further functionalisation.<sup>[154], [139]</sup> Scheme 59 represents some published TBTAP molecules by our group synthesised from pre-functionalised precursors **121-124**. The crystal structures illustrate the planar nature of the macrocyclic ring; the *meso*-phenyl derivative lies essentially perpendicular to the main framework, presumably due to the high steric effect between these two aromatic units.



**Scheme 59.** Published TBTAPs from our group following this protocol, and crystal structures of compounds **125**, **127** and **128**.<sup>[154], [139]</sup>

The first step in the investigation of the synthesis of our SubTBDAP hybrids was the preparation of aminoisoindolene **131**. The synthetic route is illustrated in Scheme 60. It begins following reported methodology for the formation of amidine **130**,<sup>[169]</sup> whereby treatment of 2-bromobenzonitrile with a solution of lithium bis(trimethylsilyl)amide in THF, followed by quenching with a solution of isopropanol and HCl, gave *o*-bromobenzamidine hydrochloride **130** as a white solid in 90% yield.



a) PdCl<sub>2</sub>(MeCN)<sub>2</sub> (0.05 eq), BINAP (0.055 eq), DBU (2.5 eq), DMF

**Scheme 60.** Two step synthesis of aminoisoindolene **131**.

The next step involves a palladium catalysed copper-free Sonogashira cross-coupling and a cycloisomerisation reaction following a microwave assisted protocol developed by Hellal and Cuny,<sup>[170]</sup> giving easy access to derivative **131**. The one-pot synthesis was carried out by placing in a microwave vial amidine **130**, phenyl acetylene, catalytic amounts of palladium catalyst and BINAP as ligand, in the presence of DBU as base and employing DMF as solvent for the reaction. The mixture was irradiated under microwave heating at 120 °C for 1 hour, after which an aqueous work up was performed and column chromatography gave the pure isoindolene **131** as a yellow powder in 92% yield. Compound **131** was characterised by mass spectrometry where the molecular ion peak (220.99 m/z) was observed. This one-pot reaction is stereoselective giving the (*Z*) –isomer as main product, (confirmed by <sup>1</sup>H-NMR spectroscopy showing the characteristic alkene proton at ~6.7 ppm), Figure 60.

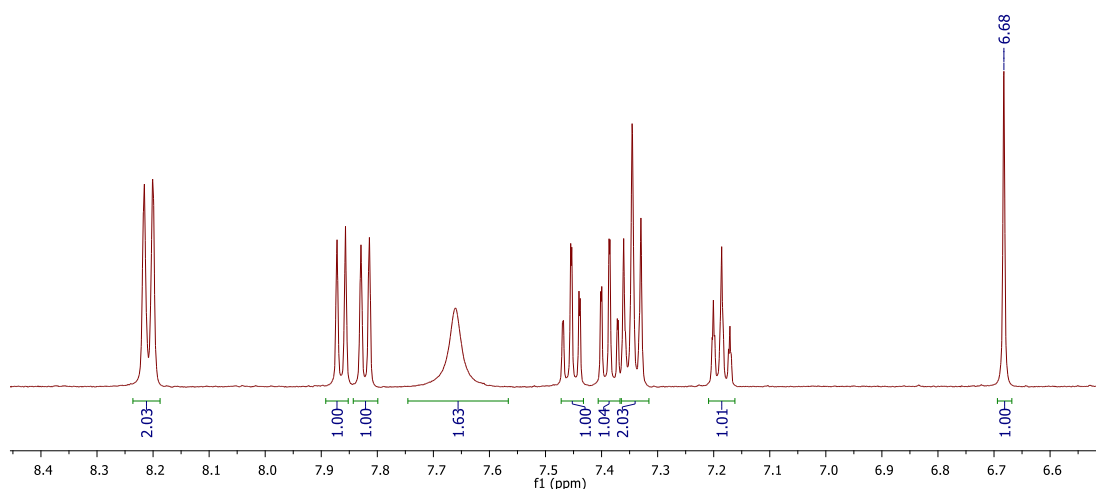
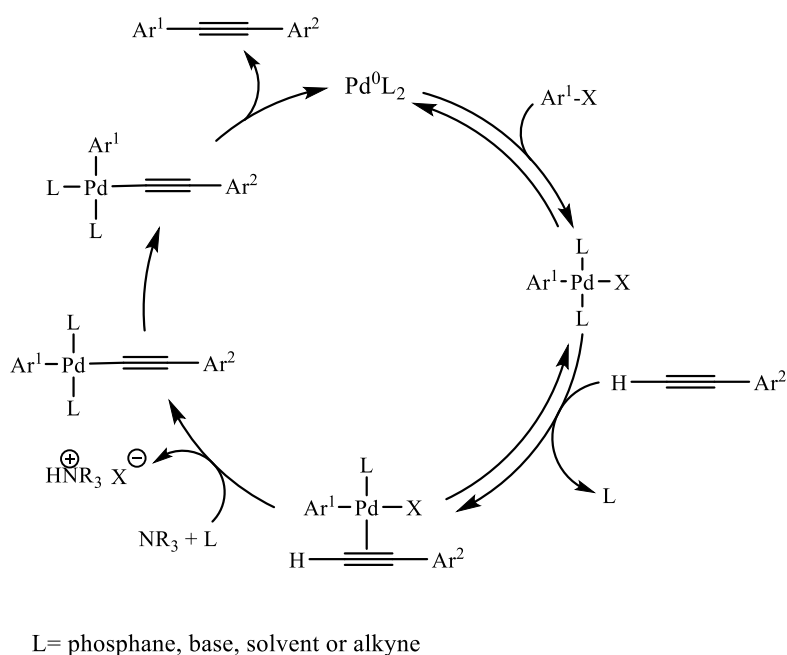


**Figure 60.** <sup>1</sup>H-NMR spectrum of phenyl isoindolene **131** in d<sub>6</sub>-DMSO.

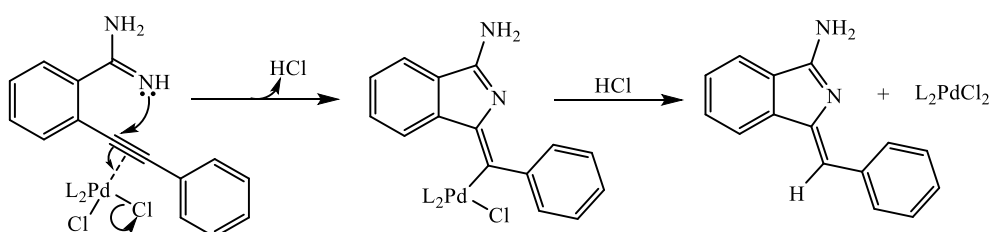


The mechanism for the copper-free Sonogashira cross-coupling has been explained<sup>[171]</sup> proposing the mechanism illustrated in Scheme 61. This catalytic cycle is initiated by the oxidative addition of the aryl halide to the active catalyst  $[\text{Pd}(0)\text{L}_2]$ . The following step involves a reversible  $\pi$ -coordination of the alkyne, this produces an alkyne–Pd(II) complex where the removal of the acetylenic proton by the base is facilitated by its now more acidic character. The acetylene ligand consequently coordinates to palladium metal, generating a complex that, after isomerisation, releases the cross-coupled product by reductive elimination, reforming the catalytic species  $[\text{Pd}(0)\text{L}_2]$  ready to start a new cycle.



**Scheme 61.** Proposed copper-free Sonogashira cross-coupling reaction.<sup>[171]</sup>

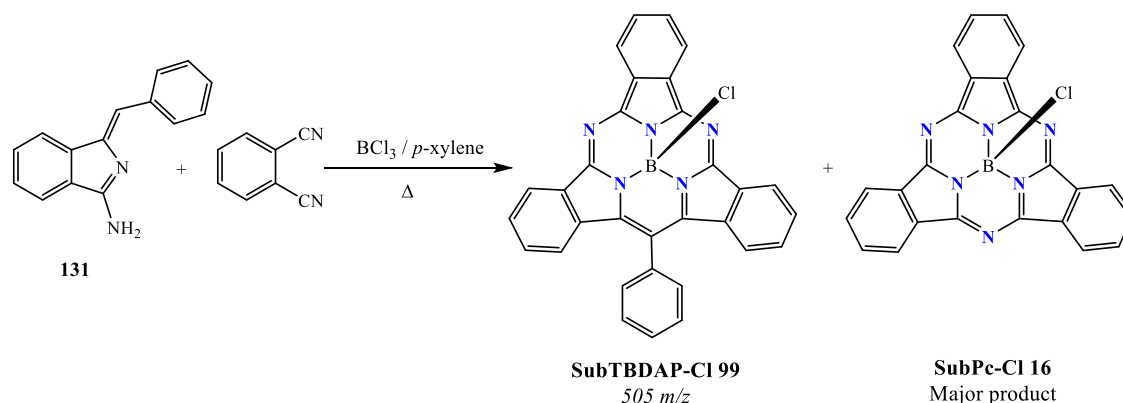
The above depicted mechanism has been commonly accepted if the amine is a poorer ligand for the palladium (II) metal than the alkyne. The contrary leads to a more sophisticated catalytic cycle involving the multiple role of the amine in the mechanism.<sup>[171]</sup> However, the role of the amine is not yet fully known, and the use of different acetylene derivatives or bases could affect the catalytic cycle that takes place. Hence this reaction still needs to be clearly understood. In the case of our reaction, coupling is immediately followed by a regioselective 5-exo-dig cycloisomerisation domino reaction to give the final product. The proposed mechanism is represented in Scheme 62. The first step is the coordination of the palladium catalyst to the alkyne, followed by the loss of HCl. The last step involves the reductive elimination and the recovery of the catalyst.



**Scheme 62.** Proposed mechanism for the 5-exo-dig cycloisomerisation.

In our first synthesis attempts towards SubTBDAP hybrids, intermediate **131** was combined with phthalonitrile and reacted with boron trichloride, acting as the boron template for the macrocyclisation process, and xylene as solvent. These are the optimal conditions for SubPc formation<sup>[30]</sup> and have been already discussed.

The synthesis is illustrated in Scheme 63. After refluxing the mixture for 3 hours a new pink spot was observed by TLC. It was identified as the expected homo-macrocyclisation product of phthalonitrile, SubPc-Cl **16**. The appearance of a second pink spot on the TLC with a distinctive intense yellow fluorescence when irradiated with a 365 nm UV lamp was promising, especially considering that SubPcs are pink fluorescent materials.



**Scheme 63.** Synthesis of SubTBDAP-Cl **99**.

MALDI-TOF MS performed on the crude product confirmed the formation of both species, with the chloro-SubPc **16** molecular ion peak (430 m/z) observed alongside a peak due to fragmentation of the apical position, the hydroxy-SubPc, and the borenium ion. As discussed in previous sections these are common species found by mass spectrometry for subphthalocyanines, Figure 61.

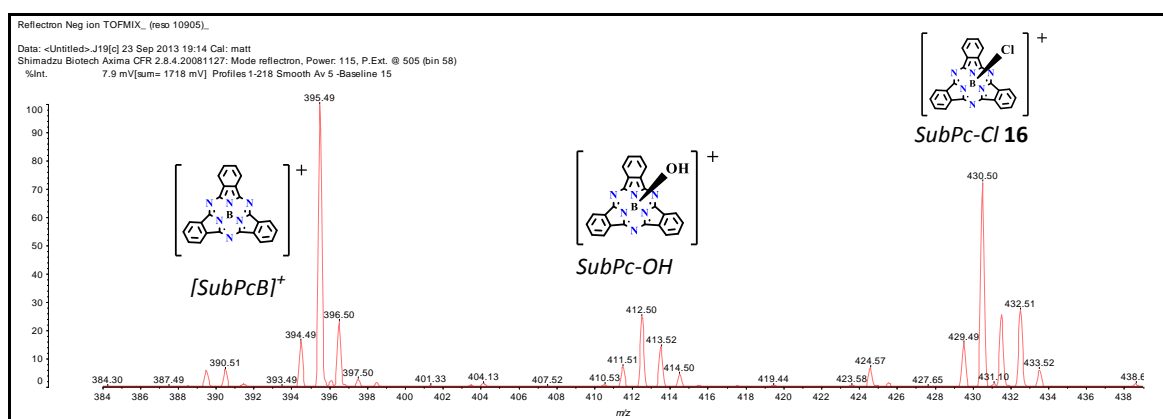


**Figure 61.** MALDI-TOF spectrum of the isolated SubPc-Cl **16** during the SubTBDAP formation and corresponding fragmentations.

MALDI-TOF mass spectrometry of the other observed compound is represented in Figure 62. The molecular ion peak corresponding to the target compound SubTBDAP **99** was observed at

505 m/z. Further confirmation of the successful formation of SubTBDAP hybrid was the isotopic pattern matching the theoretical one (Fig. 62 bottom).

As observed for SubPcs, the new hybrid macrocycle undergoes the same fragmentation processes, such as the loss of the chlorine at the apical position (470 m/z). A mass of 487 m/z corresponding to the hydroxy-SubTBDAP **132** species is also observed (Fig. 62), but at this stage there was uncertainty on whether the peak was obtained due to a process that occurred during the MALDI-TOF analysis or if the compound was formed during the reaction or workup.

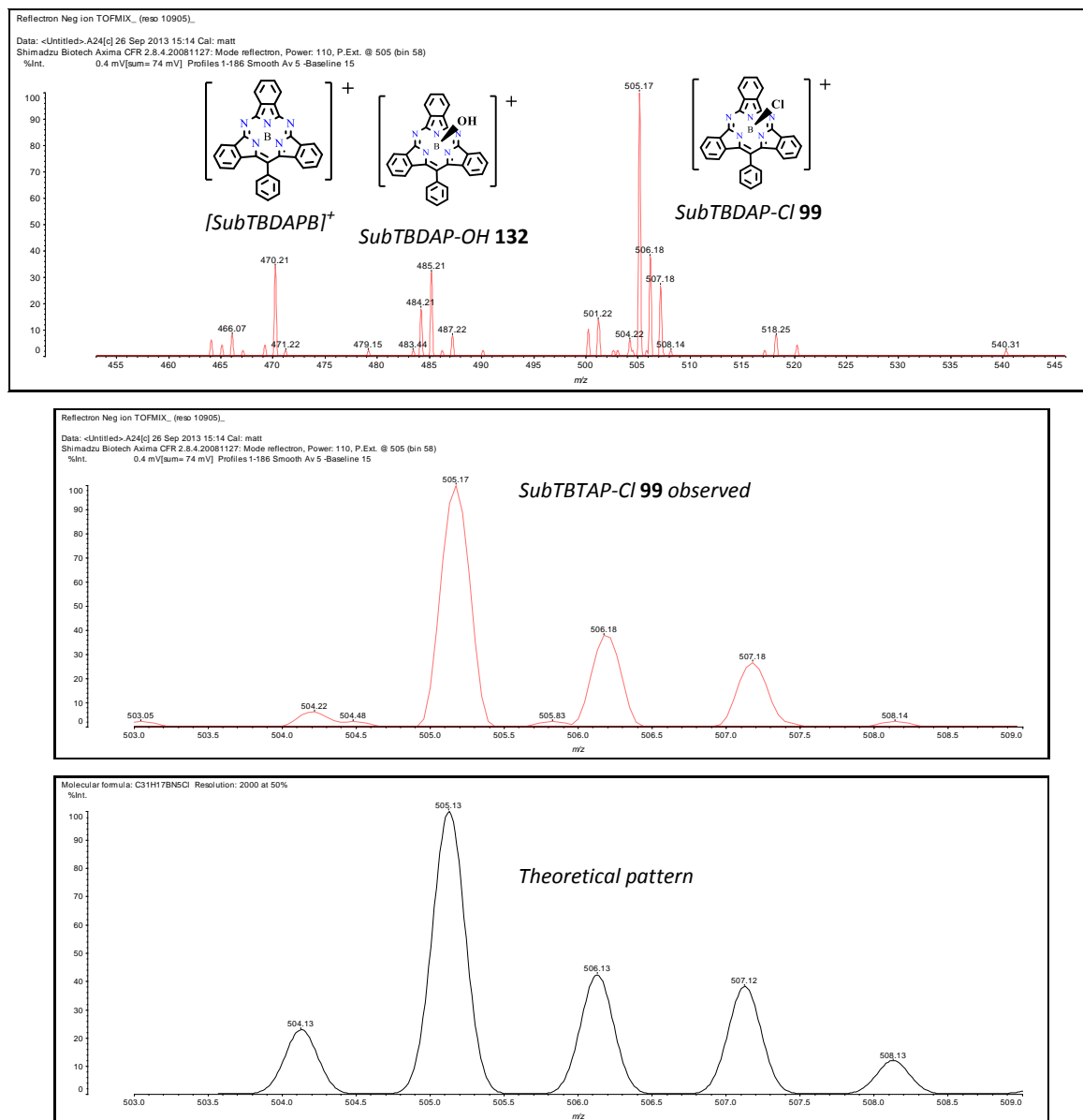
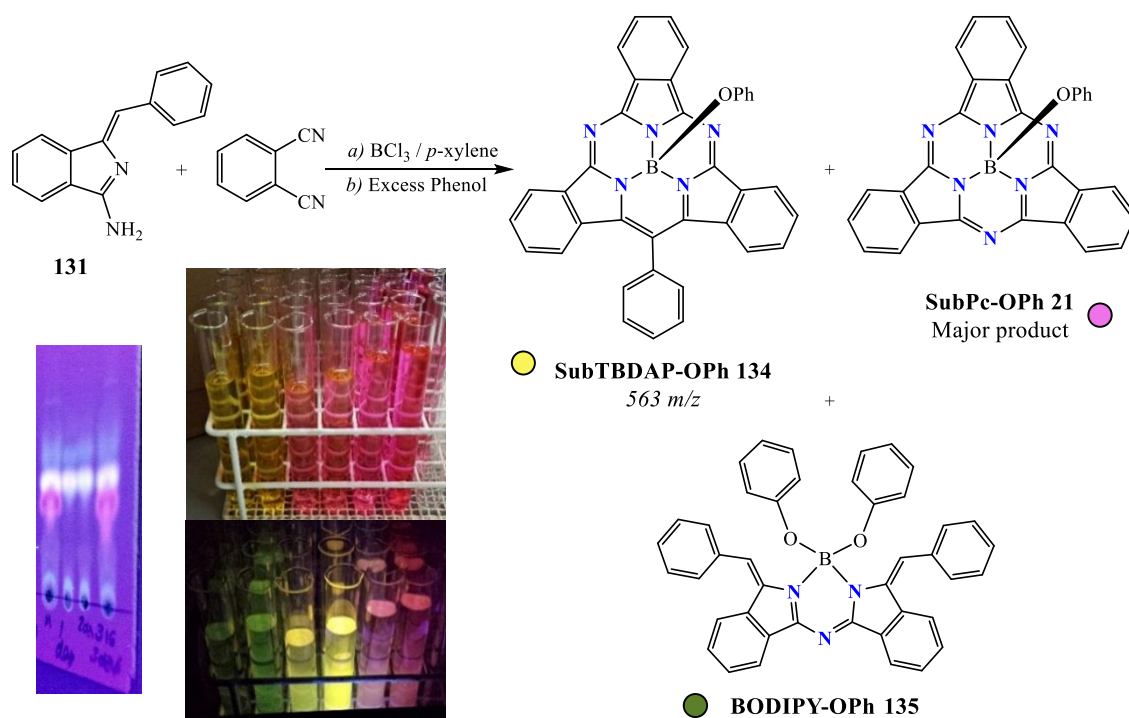


**Figure 62.** (Top) MALDI-TOF spectrum of the crude mixture depicting SubTBDAP-Cl **99** mass and its corresponding fragmentations. (Bottom) Theoretical and experimental isotopic pattern.

Although many reactions were subsequently performed, due to the reactivity of the labile B-Cl bond, every effort to isolate and fully characterise the new macrocycle was unsatisfactory. For instance, aqueous work up led to the hydrolysis of the apical site, or when methanol was involved at any stage of the purification process, then SubTBDAP-OMe **133** was immediately produced in the mixture as evidenced by its mass spectrum (501 m/z).

Consequently, the apical position was converted to a more stable B-OPh moiety in the one-pot reaction represented in Scheme 64. This synthesis was undertaken under inert atmosphere and in the dark, due to known light-driven instability of subphthalocyanines.<sup>[35]</sup> The synthesis involves two steps; the first one is the macrocyclisation process with BCl<sub>3</sub> in refluxing *p*-xylene (Scheme 64. a) for 3 hours, the time normally required for the complete consumption of starting material **131**. The next step (Scheme 64. b) is the substitution of the chlorine by adding an excess of phenol to the reaction vessel. The mixture was left under reflux conditions for 3 days, the reaction was then stopped and the solvent was evaporated.

Thin layer chromatography (Scheme 64, inset) revealed three highly coloured fluorescent products. Separation of the components was achieved by column chromatography followed by size exclusion chromatography (SEC). Subsequent reactions were purified without the slow SEC chromatography, but due to the spots being so close on the TLC a small second column chromatography was generally required. Pictures of the isolated fractions after column chromatography are illustrated in Scheme 64 under normal laboratory light (top) and under irradiation with a UV lamp at 365 nm (bottom). SubPc-OPh **21** is a pink compound that exhibits a pink fluorescence and it constituted the main product of the reaction. Formation of SubPc is of course expected because these initial conditions are known to lead to macrocyclisation of phthalonitrile alone. Finally, isolation of the first pure SubTBDAP-OPh **134** hybrid compound was achieved as a bright pink material with intense yellow fluorescence. Further confirmation was accomplished by MALDI-TOF MS with the observation of the molecular ion peak (563 m/z).



**Scheme 64.** Two step, one-pot reaction for the formation of hybrid SubTBDAP **134**. Inset, highly coloured products under normal light (top) and the same compounds under irradiation with a 365 nm light (bottom).

Apart from the two expected phenoxy-subporphyrinoids, SubPc **21** and SubTBDAP **134**, MALDI-TOF MS evidence implied the formation of an interesting third component, the azaBODIPY-type compound **135** as a yellow compound with green fluorescence (Scheme 64).

The BODIPY parent structure, represented in figure 63, consists of a boron dipyrromethene substituted commonly with two fluorine atoms. It has been subjected to modifications at its different positions<sup>[172],[173]</sup> and derivatives have found applications<sup>[174]</sup> as biolabels, artificial light harvesters, sensitisers for solar cells, ink compositions, fluorescent sensors, etc. The common feature for the BODIPY family is their intense fluorescence (520-650 nm), excellent chemical and photochemical stability, and their interesting photophysical properties.<sup>[175],[173]</sup> It has been referred to as “porphyrin’s little sister” due to their similarities within the structure.<sup>[173]</sup>

Very recently our group disclosed a new type of boron aza-(dibenzo)dipyrromethene derivative,<sup>[172]</sup> constituted by a BODIPY-type core. This azaBODIPY derivative incorporates all modifications simultaneously *via* a straightforward synthetic pathway. Examples **136** and **137** have been functionalised through derivatisation with benzyl rings at the  $\alpha$  positions, fused benzene rings at the  $\beta$  sites and replacement of the *meso*-carbon by a nitrogen atom, Figure 63. The optical properties of the new molecule differ significantly from typical BODIPY derivatives, presumably as a result of the local aromaticity that is preserved in the benzene rings giving a different electronic structure to that found in BODIPYs.<sup>[172]</sup>

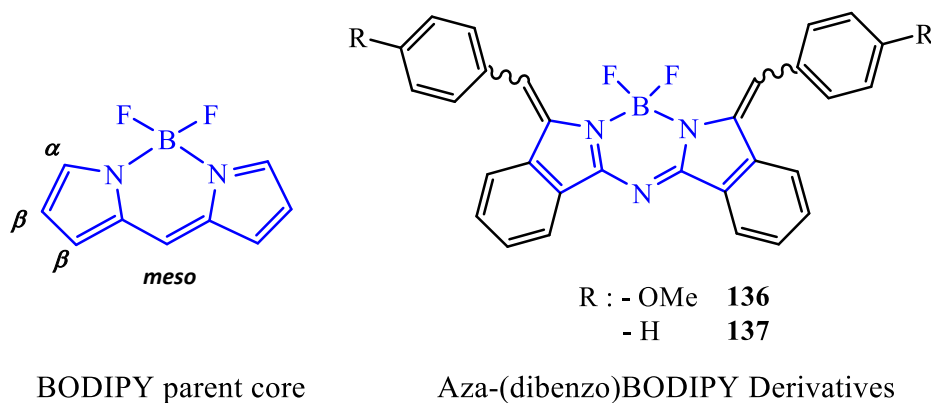


**Figure 63.** (Left) Boron dipyrromethene (BODIPY) parent structure, with positions for further modification indicated, and aza-(dibenzo)BODIPY derivatives synthesised in our group (right).<sup>[172]</sup>

Aza-BODIPY-OPh **135** was isolated during the synthesis of SubTBDAP hybrids as a side product. The <sup>1</sup>H-NMR spectrum strongly supported the *E,E* configuration with a singlet corresponding to the alkene protons at 8.36 ppm. The presence of a single isomer was suggested by the observation of one singlet in the <sup>11</sup>B-NMR spectrum at 2.34 ppm, and just one set of signals detected in the <sup>1</sup>H-NMR spectrum. However, it has been observed that azaBODIPYs **136** and **137** are prone to isomerisation at room temperature resulting in a *E/Z* mixture of isomers at equilibrium.<sup>[172]</sup>

Figure 64 illustrates the absorption and emission spectra of azaBODIPY **135**. This molecule exhibits two absorption bands at 451 and 319 nm with a very similar pattern to those for compounds **136** and **137**. It displays a molar extinction coefficient of  $2 \times 10^4 \text{ M}^{-1} \text{ cm}^{-1}$ , higher than the previous derivatives (ca.  $1.2 \times 10^4 \text{ M}^{-1} \text{ cm}^{-1}$ ), and its absorption maximum is the higher energy band at 319 nm presumably owing to the contributions of the phenoxy- rings attached to the boron atom. BODIPY **135** shows emission at 548 nm upon excitation at 450 nm, and Stokes Shift of 97 nm.

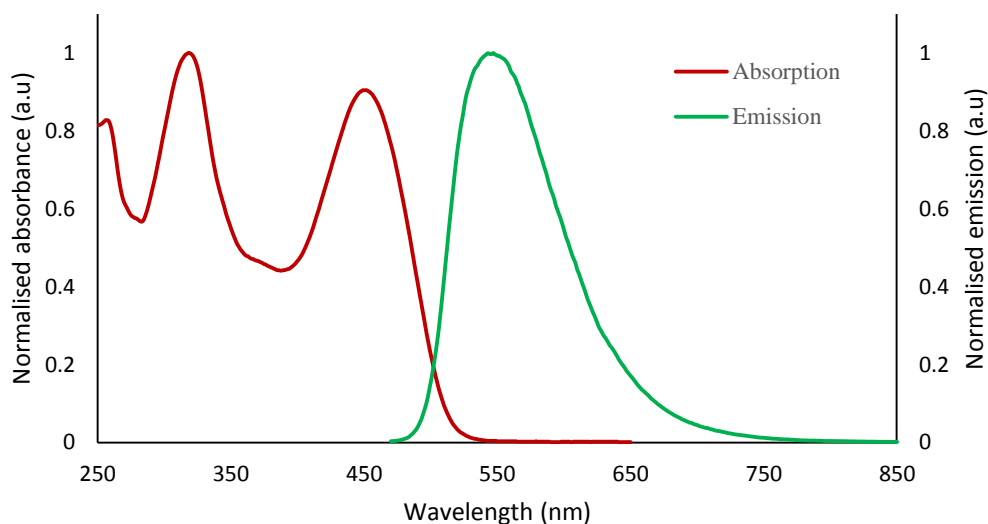


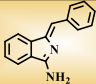
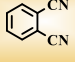
**Figure 64.** Absorption (red) and emission (green) spectra of the new BODIPY **135** formed as side product.

### 3.2.2 Optimisation of the conditions for SubTBDAP formation

To achieve the best reaction performance, different conditions were tested beginning with a screening of the reagent ratios. Table 3 summarises the results obtained during this process. When using a 1:1 ratio of the isoindolene **131** and phthalonitrile (PCN), mostly SubPc was formed (entries **A** and **E**), suggesting that boron trichloride was preferentially used to form the former macrocycle. However, an excess of the isoindolene **131** over PCN resulted in either higher quantity of BODIPY-type material being formed (entry **D**), or no macrocyclisation reaction observed at all (entry **F**). The increase in the equivalents of  $\text{BCl}_3$  impacted on higher decomposition (polar/ oligomeric) material obtained and the presence of another product with a mass of 544 m/z that could not be identified (entry **C**). All these attempts yielded less than 5% of the desired SubTBDAP product.

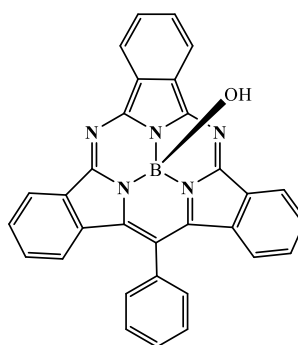
The best ratio experimentally found was the stoichiometric relationship between starting materials and macrocyclic core, hence 1 isoindoline **131** to 2 eq of PCN. 2 equivalents of  $\text{BCl}_3$  were necessary, less than 2 were not enough for the cyclisation reaction to occur, and more than 2 yielded mainly decomposed material.

In essence, application of 1:2:2 ratio (Scheme 64) gave rise to the isolation for the first time of pure phenoxy-SubTBDAP **134** in 15% yield as a pink solid.

Entry	Equivalents			Notes
			BCl <sub>3</sub>	
A	1	1	1	Mostly SubPc formed
B	1	2	2	15% yield
C	1	2	3	More decomposition + unknown material
D	2	1	2	Higher quantity of BODIPY formed
E	2	2	1.5	Mostly SubPc formed
F	3	1	1 → 2	No macrocyclisation observed

**Table 3.** Optimisation of the equivalents used in the reaction; optimal conditions are highlighted.

An element worth noting is the formation of another side product common in some of the reactions carried out when screening the conditions. SubTBDAP-OH **132** was formed as a consequence of the hydrolysis of the apical position possibly due to adventitious water in the reaction mixture. This product was initially observed as a pink spot characterised by the same intense yellow fluorescence under irradiation with the UV lamp. In accordance with its higher polarity, the spot was found very close to the baseline with a low  $R_f$  (0.06 in 2:7 ethyl acetate /cyclohexane). SubTBDAP-OH **132** was initially identified by MALDI-TOF MS with its corresponding molecular ion peak (487.32 m/z). Isotopic pattern obtained by high resolution nanospray ionisation (NSI) mass spectrometry confirmed formation of this product, which could subsequently be fully characterised by means of NMR, UV-Vis and fluorescence spectroscopy.



**SubTBDAP-OH 132**  
(side product)

During the optimisation process the heating procedure was also tested, from heating the reaction mixture instantly to 140 °C, to increasing the temperature gently over a period of 30 minutes. However, this parameter seemed not to affect dramatically the final outcome.

After years of research effort from worldwide groups, and due to many advantages that have been already illustrated, *p*-xylene is the most commonly used high boiling solvent for SubPc synthesis,<sup>[30]</sup> therefore it has been the solvent choice for this reaction. The amount of solvent indeed seems to affect the formation of the desired product. When the reaction was carried out with a very small amount solvent, i.e. very concentrated solution, decomposed material was predominant. A



more dilute solution (3 mL of solvent for 0.82 mmol of isoindolene **131** + PCN used), gave better results without compromising reaction times.

The yield for this reaction (15%) is impressive, especially taking into account the modest yields typically obtained for unsymmetrical Pcs and SubPcs.

### 3.2.3 Preliminary characterisation of SubTBDAP-OPh **134**

#### 3.2.3.1 X-Ray Diffraction

Crystals suitable for X-Ray diffraction were eventually grown from a mixture of acetone and hexane allowing determination of the solid-state structure.

In the crystal, the boron atom is bonded, with a tetrahedral geometry to the three pyrrolic nitrogen atoms and the phenoxy- oxygen atom, or this bonding arrangement can be viewed as trigonal pyramidal in which the phenoxy- group occupies the apical site, Figure 65. The boron atom is displaced 0.614(5) Å from the plane of the three N atoms, and the SubTBDAP ring framework is wrapped around the base; each benzo- ring plane is tilted ca. 20° from the plane of the three pyrrole ring N atoms, away from the phenoxy- group. The *meso*-phenyl ring is confirmed to be lying essentially perpendicular to the SubTBDAP core.

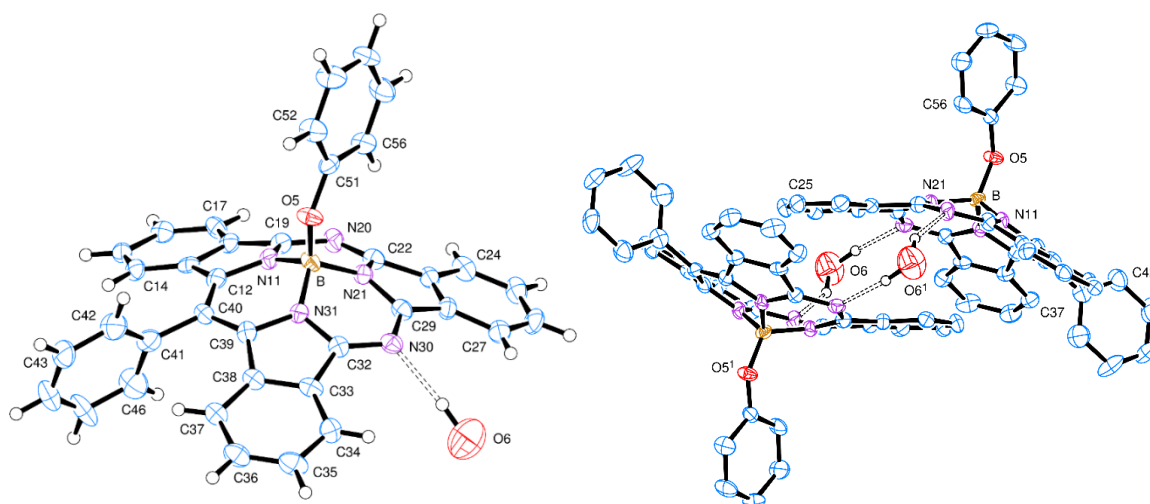


**Figure 65.** Crystal structure of SubTBDAP-OPh **134** with a hydrogen-bonded water molecule. Thermal ellipsoids are drawn at the 50% probability level (left). View of the dimer unit (right), optimised structure by Dr David Hughes at UEA.

Figure 65 depicts a representation of the dimer unit; interestingly the SubTBDAP molecules are arranged in pairs with the isoindole rings of N(21)-C(29) overlapping a centrosymmetrically related group, at ca 3.62 Å; these groups are linked by a pair of solvent water molecules which form hydrogen bonds to the nitrogen atoms N(20) and N(30).



### 3.2.3.2 $^1\text{H-NMR}$ Spectroscopy

Boron SubTriBenzoDiAzaPorphyrin **134** shows a clear  $^1\text{H-NMR}$  spectrum, with several very sharp and defined peaks at 298K. The coned-shape structure is very similar to that of SubPcs and therefore the macrocycle shielding cone,<sup>[30]</sup> observed for the former macrocycle, plays also an important role on the chemical shifts of the different substituents in the SubTBDAP framework.

The effect of strong ring current<sup>[32]</sup> is evidenced in the downfield chemical shift of the protons attached to the main macrocyclic core (observed from 6.9 to 9.0 ppm), and the apical phenoxy-group has shielded signals that appear upfield shifted (from 5.2 to 6.8 ppm), Figure 66.

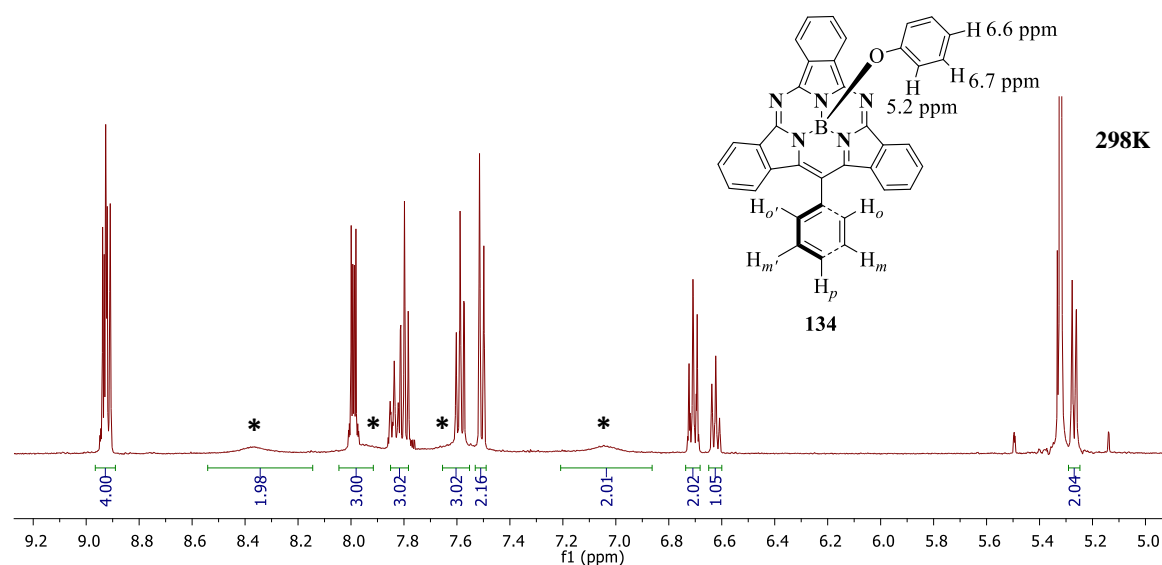


**Figure 66.**  $^1\text{H-NMR}$  spectrum of SubTBDAP **134** in  $\text{CD}_2\text{Cl}_2$  at 298K.

SubTBDAPs have a  $\text{C}_s$  symmetry point group, owing to a mirror plane of symmetry ( $\sigma$ ) that divides the framework in two. Figure 67 depicts a 3D-representation of the molecule with the corresponding  $\sigma$ , both the phenoxy- group on the apical position and the *meso*-phenyl group would be aligned in the solid-state to form the energetically most favourable conformation. However, in solution both rings are rotating through their B-O and C-C bonds, respectively. Such rotation is very fast in case of the apical group and the NMR spectrum depicts three distinctive signals (5.2, 6.6 and 6.7 ppm), the closest to the oxygen being the most shielded one, Figure 66.

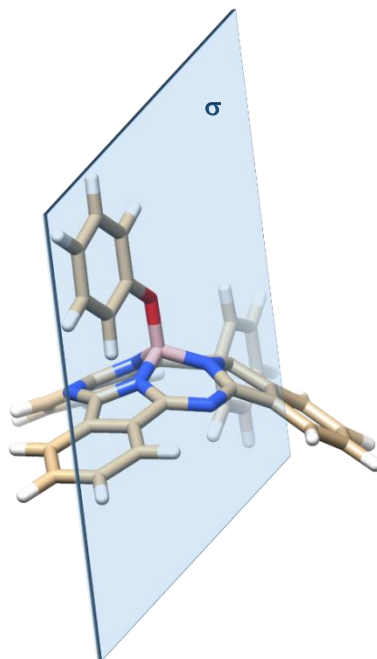


**Figure 67.** Plane of symmetry in SubTBDAP macrocycle.

However, the signals for the *o*- and *m*- hydrogens of the *meso*-phenyl substituent are very broad and featureless (Fig. 66 \*), indicating slow rotation of the group on the NMR timescale. Steric impediment owing to the proximity of the benzenoid rings that form the core and the *meso*-substituent slows down the rotation. Therefore, four broad signals can be distinguished on the NMR spectrum owing to their unique different environments (two on the top side of the molecule and the other two on the concave face); two of the signals at around 7.0 and 8.4 ppm appear clearly but the other two at 7.6 and 8.0 are overlapped with two other signals, but the integration reveals two extra protons in those regions.

### ***Variable temperature experiments***

The rotational dynamics of the *meso*-phenyl group were further investigated by means of variable temperature (VT) <sup>1</sup>H-NMR spectroscopy. It takes about 10<sup>-4</sup> seconds to examine a nucleus by NMR spectroscopy, which is a relatively long time-scale. Many dynamical processes occur much faster than this NMR timescale and the signals for protons that are rotating or exchanging are averaged into a single peak. VT NMR is a technique that allows us to cool the sample to a point at which the dynamic process slows down below the sampling rate.<sup>[176]</sup>

In the NMR spectrum (Fig. 66) at 298K, the *ortho*- and *meta*- protons of the *meso*-phenyl group consist of four peaks, integrating for one proton each. As expected, the proton in *para*- position (H<sub>p</sub>) is not influenced by the rotation because it remains unchanged through the process, therefore the signal appears sharp and resolved as a triplet even at room temperature. Lowering the temperature leads to sharpening and resolution of the signals. As a result, at 263K the spectrum changes dramatically; two of the proton resonances become triplets corresponding to the *meta*- protons (H<sub>m</sub> and H<sub>m'</sub> in Figure 68), and the other two protons in *ortho*- position appear now as doublets (H<sub>o</sub> and H<sub>o'</sub> in Figure 68). The coupling constant that they all experience is 7.6 Hz.

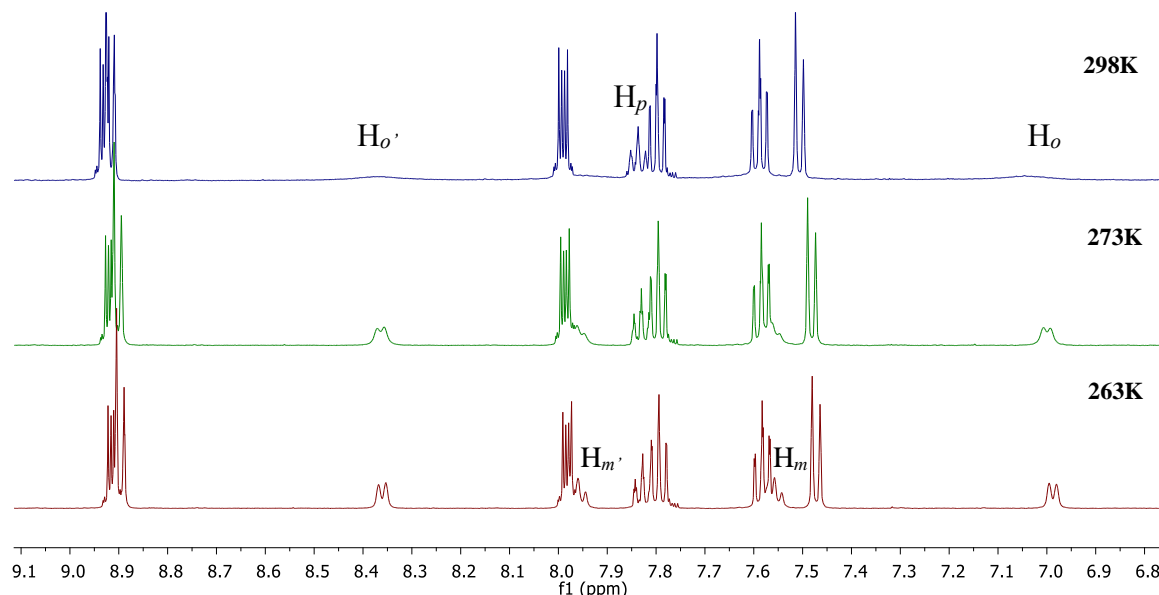


**Figure 68.** Variable temperature  $^1\text{H}$ -NMR spectra of hybrid **134** in  $\text{CD}_2\text{Cl}_2$ .

Assignment of all signals was assisted by VT COSY. Homonuclear COSY is a two dimensional NMR spectrum that shows chemical shifts from the nuclei on the f1 and f2 axes. The diagonal of this spectrum show signals where the chemical shift are the same in both axes ( $\delta_1 = \delta_2$ ), it is the analogue of a 1D  $^1\text{H}$ -NMR spectrum. Signals off the diagonal are cross peaks where  $\delta_1 \neq \delta_2$ , the cross peaks appear when the spins with chemical shifts of  $\delta_1$  and  $\delta_2$  are coupled to each other. The intensity of this signal is directly proportional to the  $J$ -value between such resonances.<sup>[177]</sup> Figure 69 depicts variable temperature COSY performed at 263K in  $\text{CD}_2\text{Cl}_2$ , alongside the respective assignment. As previously illustrated these spectra show “through bonds” interactions and it helped to build a clearer picture of the protons that had couplings between them, such as the cross peaks seen between the multiplets  $\text{H}_5$  and  $\text{H}_6$  that reveal an AA’BB’ pattern like those observed in SubPcs (Fig. 69. Blue rectangle), or the cross peaks that helped us to understand the protons that lie on the same face of the *meso*- phenyl group (Fig. 69. Grey and green rectangles). However, as this is a low symmetry molecule with a rather complicated spectrum, there were still some uncertainties regarding assignments.

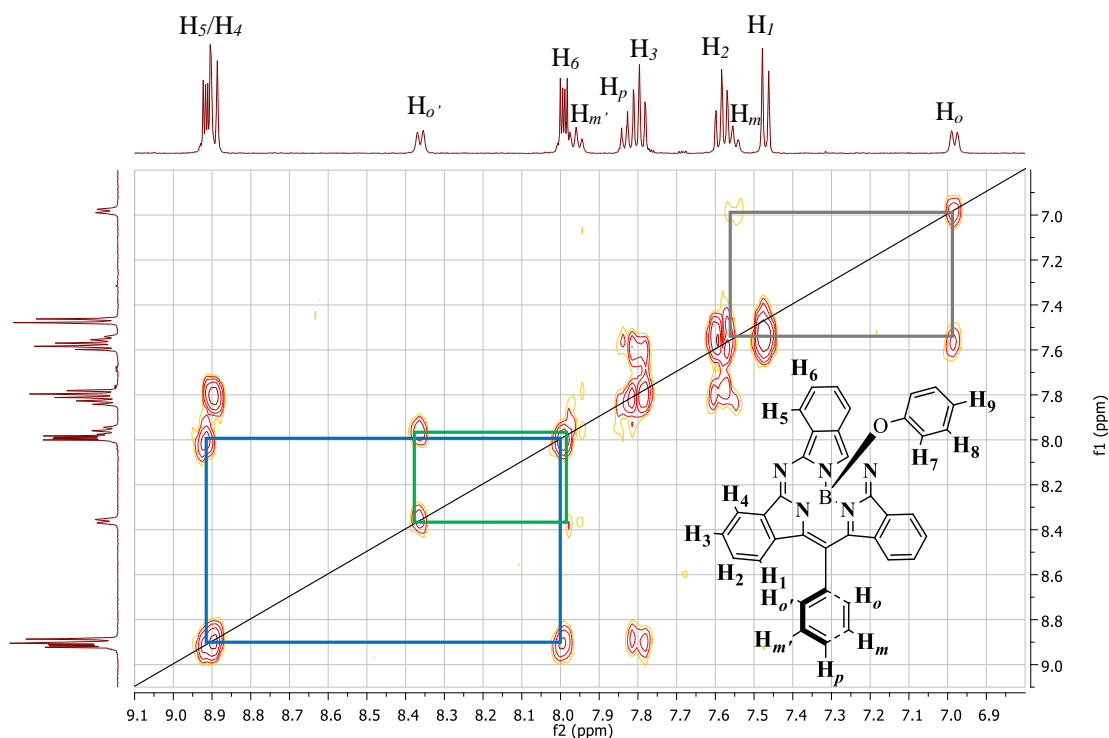


**Figure 69.** Variable temperature COSY of hybrid **134** at 263K in  $\text{CD}_2\text{Cl}_2$ .

Another technique that assisted the assignment of this molecule, was VT Nuclear Overhauser Effect Spectroscopy (NOESY), in which interactions between protons “through space” are observed. In the 2D NOESY spectrum (Fig. 70), cross peaks that have the same phase as the diagonal signal (red coloured) arise from chemical exchange, NOE cross peaks are negative (blue colour). This is a really useful technique that allows differentiation between the two different effects.

Interestingly, for the new hybrid there are some intense positive cross peaks in the NOESY spectra revealing chemical exchange due to rotation between protons  $\text{H}_o / \text{H}_o'$  and  $\text{H}_m / \text{H}_m'$ . These interactions can be observed in Figure 70 by the symbols  $\star$  and  $\blacklozenge$ , respectively.

Site- and conformational- exchange are processes that involve the exchange on an atom between molecules or between conformations of the same molecule. In SubTBDAP molecules it is a matter of conformational exchange that occurs because these two sites are chemically and magnetically distinguishable, the outcome is that these two protons are exchanging between conformations. As a result of this rotation the proton is sometimes in the convex face and then it changes to the concave face. Although all four signals appear at different ppm, the rate of exchange can be considered slow regarding the NMR time-scale due to the broadness<sup>[178]</sup> of the peaks at 298K. It is very typical for exchange processes to show extreme broadening of the resonances involved.<sup>[177]</sup>

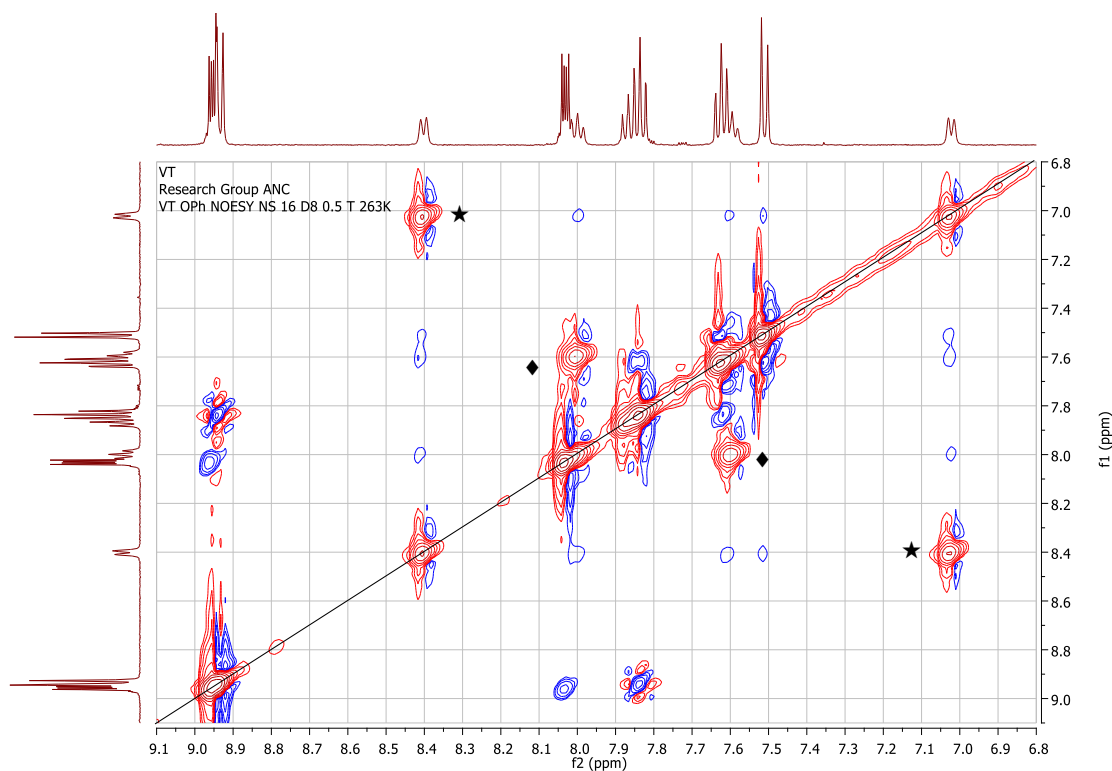


**Figure 70.** Variable temperature NOESY of hybrid **134** at 263K in  $\text{CD}_2\text{Cl}_2$ .

The rate of exchange is subjected to changes in temperature,<sup>[177]</sup> therefore variable temperature is often the ideal technique for its study. The room temperature spectrum of SubTBDAP **134** (Fig. 66) clearly shows broad signals for the *ortho*- and *meta*- protons with no coupling to other neighbouring protons (confirmed by COSY). Hence the chemical exchange under those conditions is faster than the NMR time-scale, the spectrometer records the averaged environment that detects for the exchanging protons,<sup>[179]</sup> resulting in broad signals and the suppression of the coupling between  $\text{H}_o$  and  $\text{H}_m$ .

Lowering the temperature to 263K slows the rotation of the *meso*-phenyl ring, and hence the rate of exchange to a point which is similar to the time-scale of the NMR experiment, and now all the signals sharpened and the coupling to vicinal hydrogens is observed (Figure 68).

The  $^1\text{H}$ -NMR spectrum had now been almost fully assigned, apart from the *ortho*- and *meta*-signals that are above and below the macrocyclic core that remained unknown. The large chemical shift difference observed for the two doublets corresponding to the *ortho*- hydrogens (7.0 and 8.4 ppm), is presumably due to the macrocycle shielding cone causing this effect.

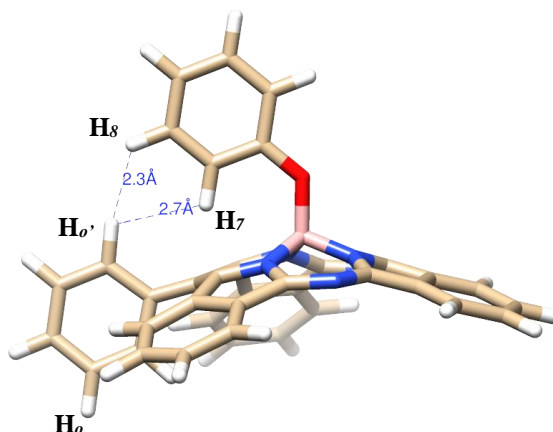


**Figure 71.** Estimated distances between *meso*- and apical rings with the phenoxy-ring lying completely perpendicular to the core.

We hoped the NOESY spectra would solve this assignment by looking for NOE signals between  $H_{6'}$  and either protons  $H_7$  or  $H_8$ , Figure 71. Unfortunately very weak NOE signals were observed and although many trials changing the experiment parameters were performed, the results were inconclusive. The questions arise in whether the rotation of the groups and the chemical exchange would allow any NOE signal to be observed, and if that signal would only be selective for one of the nuclei.

NOESY allows determination of interactions through space, the efficiency of the NOE signal detected depends on the physical distance between the irradiated and the observed spins. Only very close spins (less than  $5 \text{ \AA}$ ) will exhibit a strong dipolar interaction that may, upon irradiation of the resonances from one of the spins, increase the integrated intensity of the receiving spin's resonance in the NOE difference spectrum.<sup>[177]</sup> Figure 71 depicts the important protons that were monitored in the NOESY experiment, these distances are small enough  $\sim 2.3$  and  $\sim 2.7 \text{ \AA}$  to be subjected to this effect, so why is it that they are not observed in our experiments?

The explanation might be that the dipolar interaction is suppressed (drowned out) by other competing relaxation mechanisms. The expected increase in the integral of the resonance from what we expect to be the receiving spin will not be observed, even if the two spins (irradiated and receiving) are near to each other.<sup>[177]</sup> For instance, methyl groups are poor receivers of NOE enhancements. This insensitivity is due to the fact that methyl groups relax very efficiently as a result of their rapid rotation around the bond that links the group to the rest of the molecule. It is been accepted that when looking for an NOE between a methyl group and another proton, the methyl group is the irradiated one and the effect is searched for on the other spin.<sup>[177]</sup>

Considering this, a notorious drawback in SubTBDAPs could be the fact that both groups that are being monitored towards NOE signals are freely rotating at 263K, perhaps that makes both rings poor receivers of NOE enhancements. Final assignments for those protons was made after subsequent syntheses (see later).

### 3.2.3.3 Optical properties

SubTBDAP is a colourful chromophore expected to have unique optical properties. It shows a pink colour under normal light and a very intense yellow fluorescence when irradiated at 365 nm, the product can be easily monitored through the chromatographic process with an UV lamp, Figure 72. This intense yellow emission has been a real aid distinguishing between possible SubTBDAP-type products from SubPcs (i.e. pink fluorescence), and has certainly eased the very challenging purification processes required to obtain highly pure materials.

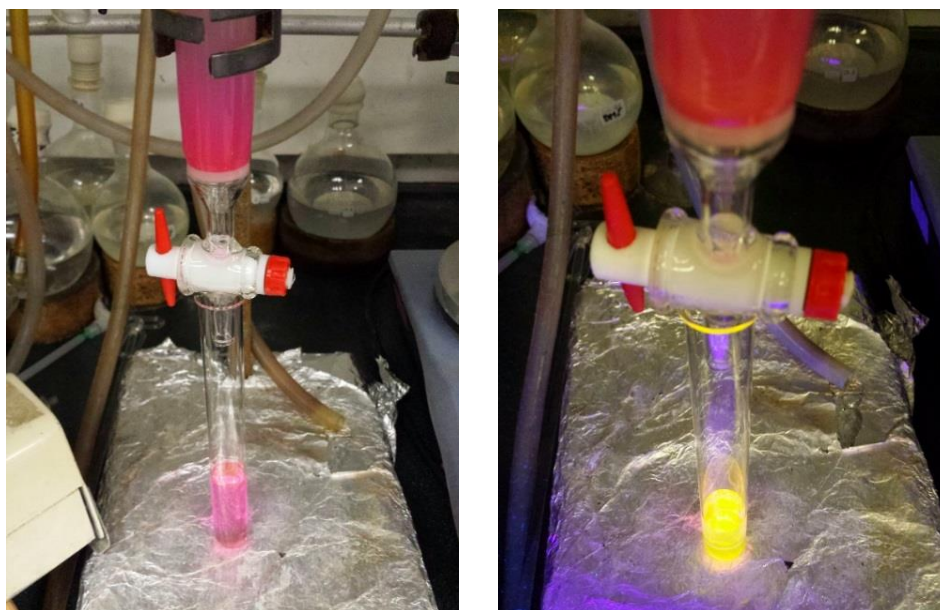


**Figure 72.** Picture of same fraction of a column chromatography under normal and UV light.

What certainly makes these hybrid molecules unique is their distinctive absorption and emission properties. Figure 73 depicts a comparison spectra of absorptions and emissions compared to those of the parent molecule SubPc. Like SubPcs, the absorption spectrum of SubTBDAP **134** also shows two main transitions, a Soret band at 324 nm and a Q band at 548 nm, the former band appears split as a consequence of its reduced symmetry. Fluorescence emission occurs from the lowest singlet excited state and appears as a single band at 559 nm upon excitation at 500 nm.



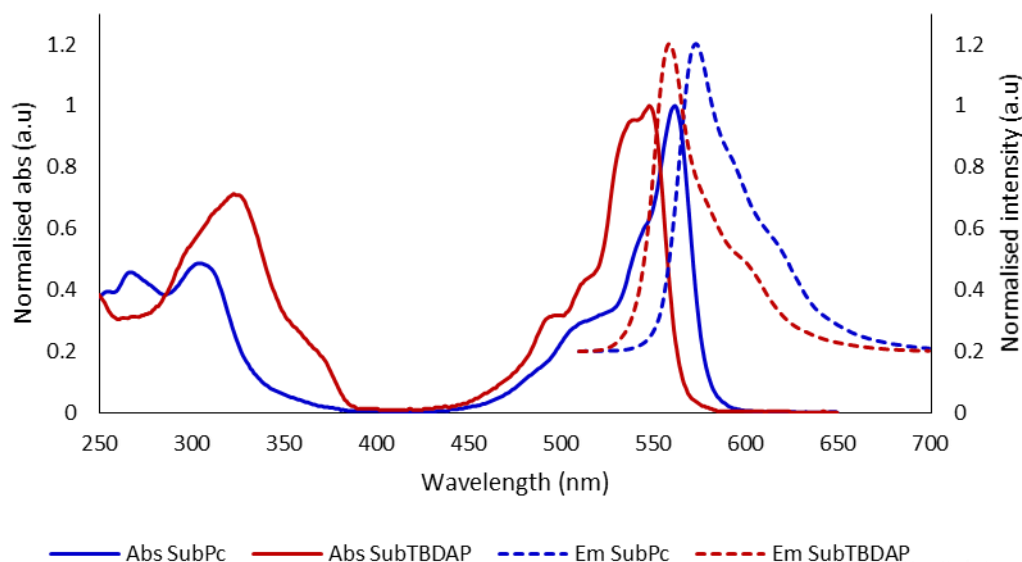


**Figure 73.** Absorption and emission spectra of hybrid SubTBDAP-OPh **134** and SubPc-OPh **21** in dichloromethane.

Both absorbance and emission maxima are blue-shifted by 14 and 16 nm respectively compared to SubPc-OPh **21**. This reflects the change towards more porphyrin-like character in the hybrid **134**; this higher porphyrinoid nature is also noticed in the increment of the intensity of the Soret band which for SubPc-OPh is around half as intense as the Q band, and for SubTBDAP **134** is more than 2/3 of the Q band.

The blue shift also demonstrates that the *meso*-phenyl substituent that lies perpendicularly to the core does not contribute to the main  $\pi$ -system. This parallels the arrangement in both the well-known *meso*-phenyl porphyrins<sup>[6b]</sup> and the *meso*-arylTBTAPs.<sup>[154]</sup>

SubTBDAP **134** reveals a very small Stokes-Shift (11 nm) as observed in the parent molecule SubPc-OPh **21** (13 nm), as expected for rigid molecules. This feature suggests a very small geometrically distorted excited state compared to the ground state.<sup>[30]</sup>

### 3.2.4 Towards a more efficient SubTBDAP synthesis

#### 3.2.4.1 Boron source - BORATES

The synthesis described in previous sections allowed the isolation of the first SubTBDAP hybrid. However, a serious drawback in the versatility of the synthesis is the simultaneous formation of symmetrical SubPc. Formation of SubPc is of course expected because these are the optimal conditions that lead to macrocyclisation of phthalonitrile alone. We therefore turned our attention and effort to developing reaction conditions that would lead to the formation of the desired hybrid structures without competing formation of SubPc.



If the existing approaches for the synthesis of subporphyrinoids are surveyed, then an idea of what boron templates could be successfully applied to the synthesis of hybrid SubTBDAPs can be formed. The most common approach to achieve B-O subphthalocyanines is the replacement of the chlorine atom by phenol, carboxylic acids, water or alkyl alcohols<sup>[30]</sup> in a second step. The boron reagents that have been reported so far for subphthalocyanine formation are  $BX_3$  and  $BX_2Y$  types, in which X and Y are bromine, chlorine, fluorine, phenyl or butyl.<sup>[32]</sup> The reactivity of these Lewis acids follows the trend,  $BBr_3 > BCl_3 > BF_3 > BPh_3 > B(\text{Alkyl})_3$ .<sup>[32]</sup> To the best of our knowledge there are no reports on the employment of other boron source reagents such as boronic esters or borates.

Regarding tribenzosubporphyrins introduced earlier, the existing reports only conceive the use of  $B(OH)_3$  as the boron template for the macrocyclisation, other boron sources remain unexplored. Finally, for the direct macrocyclisation to yield subporphyrins, Kobayashi<sup>[158a]</sup> and Osuka<sup>[159]</sup> illustrated the use of pyrrolylborane derivatives **101** and **103** (Fig. 74), and the use of boron sources similar to those employed for SubPcs or BzSubPs remain futile.

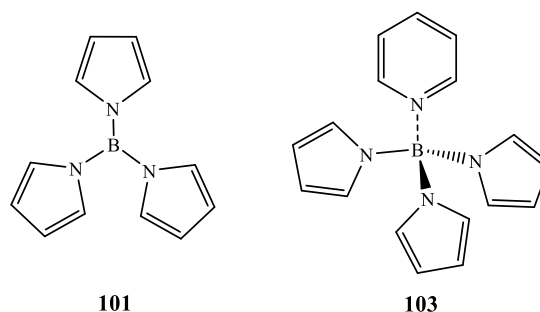
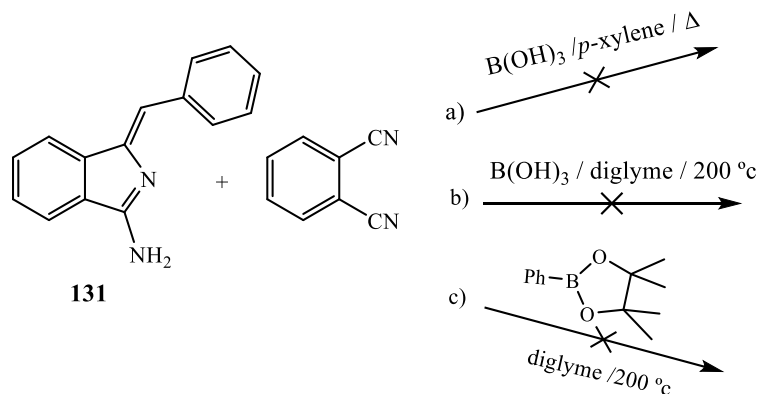


**Figure 74.** Borane derivatives employed in subporphyrin syntheses.

Boric acid and pinacol boronic esters were tested for the synthesis of SubTBDAPs. Both reagents gave rise to just traces of the corresponding SubTBDAP-OH **132** when heated at 200 °C with aminoisoidolene **131** and phthalonitrile in *p*-xylene (Scheme 65. a), giving the same result when the reaction was carried out in diglyme (Scheme 65. b), and suggesting that  $B(OH)_3$  is not a suitable Lewis acid for the macrocyclisation to efficiently occur.

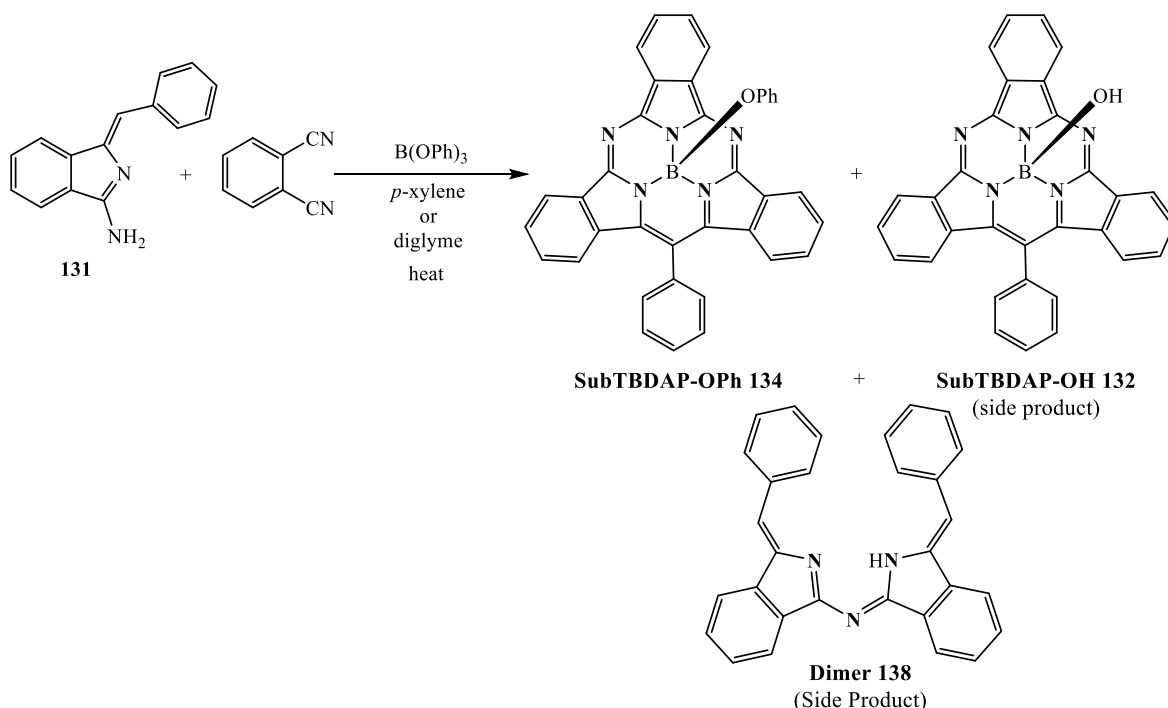


**Scheme 65.** Unsuccessful attempts with boric acid and pinacol boronic ester.

On the other hand, the use of phenyl pinacol boronic ester gave rise to mostly decomposition material after heating the mixture up to 200 °C in diglyme and no product was observed (Scheme 65. c).

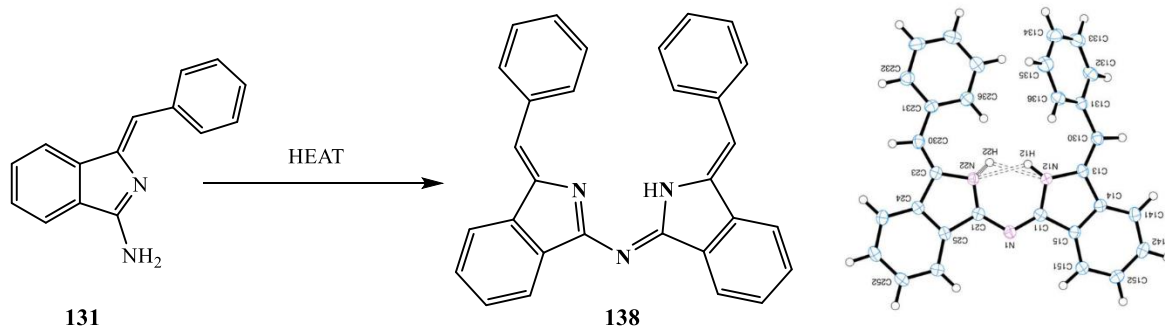
The best results were achieved employing a less reactive phenyl borate  $B(OPh)_3$ , as Lewis acid and template. It was recognised that phthalonitrile itself requires a more reactive boron source for SubPc formation such as  $BBr_3$  or  $BCl_3$ . The use of this boric ester has also the potential advantage of leading to the stable SubTBDAP-OPh **134** directly in one single step.

The first set of reactions were carried out heating the aminoisoindolene **131**, phthalonitrile and triphenyl borate in a sealed tube at various temperatures under argon using *p*-xylene as solvent. SubTBDAP-OPh **134** could immediately be recognised as one of the products in the reaction. Some attempts using diglyme as solvent were also carried out and, judging from the TLC, the results seemed much better than when xylene was employed.



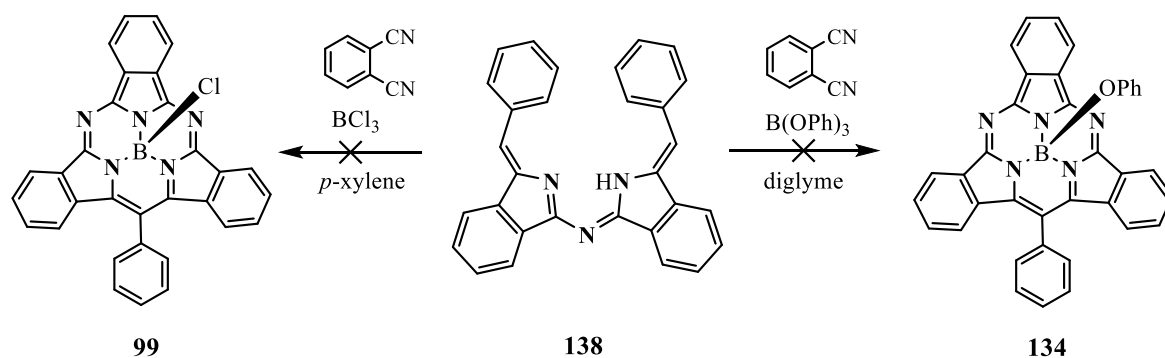
**Scheme 66.** Synthesis of SubTBDAP-OPh **134** using triphenyl borate, and side products.

During the course of these test reactions, two main side products could be identified. The first one was SubTBDAP-OH **132** (Scheme 66) already observed and isolated from the reaction performed with  $BCl_3$ . The second side-product was characterised as the expected azadipyrromethene **138**. It has been recently demonstrated by our group,<sup>[172]</sup> that this self-condensation reaction occurs very smoothly when refluxing precursor **131** in toluene to form dimer **138** in a high yield. They also reported the X-Ray structure of dimer **138** showing the same *Z, Z* configuration present in the starting material, Scheme 67.



**Scheme 67.** Self-condensation reaction of aminoisoindolene **131** and crystal structure of dimer **138**.<sup>[172]</sup>

This dimer could in theory act as precursor in the synthesis of TBDAP. However, experiments carried out in our group re-subjecting it to the reaction conditions in the presence of diimisoindoline, does not lead to the formation of hybrid macrocycles.<sup>[154]</sup>



**Scheme 68.** Reaction attempts with dimer **138** towards the formation of SubTBDAP-type molecule.

As control experiments dimer **138** was also re-subjected to the conditions that lead to the formation of SubTBDAP (Scheme 68). First of all precursor **138** was refluxed in *p*-xylene in the presence of phthalonitrile and BCl<sub>3</sub> but the reaction lead to the expected SubPc, unreacted dimer and mostly decomposed material. In a second attempt, dimer **138** was heated in the presence of phthalonitrile and triphenyl borate in diglyme, conditions that led eventually to decomposition of the dimer. In essence, SubTBDAP was not observed when using dimer **138** as precursor for the macrocyclisation.

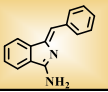
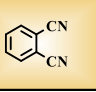
### 3.2.4.2 Screening the conditions

It had already been demonstrated that the use of triphenyl borate leads to the stable SubTBDAP-OPh **134** directly in one step, which is already a huge advantage. But most importantly it takes place without competing formation of SubPc, showing that phthalonitrile requires a more reactive boron source for macrocyclisation to form SubPc.

In order to find the best conditions for the synthesis of SubTBDAP *via* borates, some reaction parameters were tested, Table 4. From all the solvents that were tested, diglyme was found to be the most convenient one for this reaction; for instance the use of *p*-xylene in some cases led to the formation of traces of SubPc material, or the use of DMF and DME yielded mostly degraded residues. The use of a solvent with higher boiling point such as triglyme (216 °C) under reflux or heating in a sealed tube at 200 °C, led in all cases to brown polymeric baseline material. This reaction can indeed be performed in the absence of solvent but gives lower yield (4%), possibly due to faster decomposition of the materials in a solvent-free environment.

Temperatures ranging from 140 to 250 °C were also tested, finding that 200 °C offers a good compromise between reaction times, SubTBDAP product formed and degradation of materials. 1 Equivalent of aminoisoindolene **131** was used in order to diminish the amount of dimer formed during the reaction. On the other hand, the employment of increasing amounts of borate boosted the formation of azaBODIPY-OPh **135**. However, the utilisation of only 1 equivalent resulted in decomposed material. As expected the use of 1 or 2 equivalents of phthalonitrile produced higher amounts of dimer **138** and azaBODIPY **135**. From all these results it was concluded that 1:3:2 (isoindolene **131**/ phthalonitrile/ borate) was an appropriate and convenient ratio of reagents for this reaction.

This synthesis can also be performed under microwave irradiation at 220 °C for 1 hour in *p*-xylene. This fast reaction results in the formation of the hybrid compound in around 5% yield. BODIPY-OPh **135** is a side product in this reaction, together with other coloured compounds that could not be identified, and a considerable amount of black decomposed material. Consequently, it is not the preferable methodology but an interesting alternative to investigate further.

Equivalents			Solvents	Method	Temperature (°C)
		B(OPh) <sub>3</sub>			
1	1	1	<i>p</i> -xylene	<i>Sealed tube</i>	140
1	1	1	diglyme	<i>Round bottomed flask</i>	160
1	1	1	triglyme	<i>Microwave reaction</i>	180
1	2	2	DMF		200
1	2	3	DME		220
1	3	1	neat		250
1	3	2			
1	3	4			
1	9	2			

**Table 4.** Different reaction conditions modified during the screening of the reaction; optimal conditions are highlighted.

The best conditions experimentally found are highlighted on Table 4, and resulted in the formation of the hybrid SubTBDAP-OPh **134** in a 10% yield after 3 hours. When the reaction was completed, it was cooled and ethyl acetate was then added to the reaction mixture, the organic phase extracted three times with a saturated solution of NaHCO<sub>3</sub>, dried over MgSO<sub>4</sub> and the solvent

evaporated. Purification involved silica gel column chromatography using a mixture of ethyl acetate/ hexane (2:7) as solvent system. In most cases, a second column chromatography was also necessary in order to remove the excess of phthalonitrile in the reaction alongside hydrolysis products (phthalimide). This second column was carried out flushing first with pure dichloromethane and then changing to a mixture of diethyl ether/ hexane/ dichloromethane (1:3:2) as solvent system to achieve the pure material.

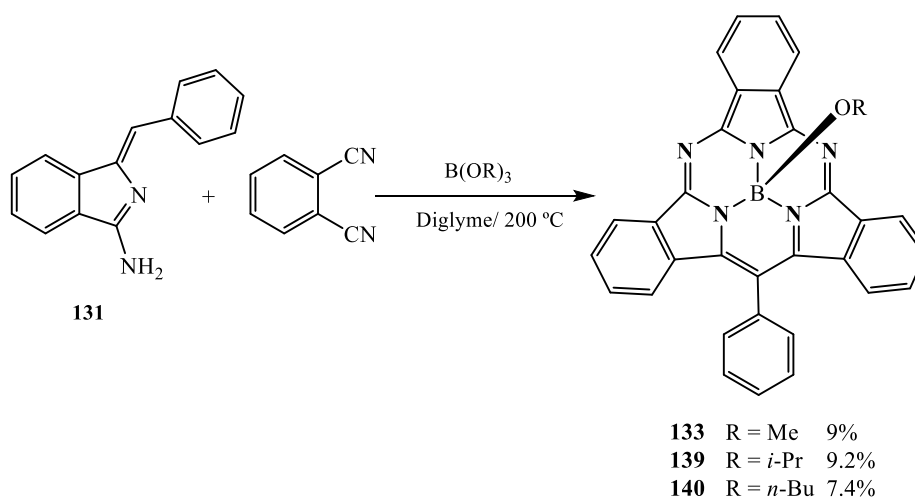
The other main side-products are the expected azadipyrromethene **138** and polar/oligomeric baseline material. This yield (10%) is slightly lower than the stepwise procedure (15%) but is compensated by synthetic convenience and versatility.

### 3.2.4.3 Scope of the protocol

#### *Apical Functionalisation*

The scope of the protocol was first interrogated by changing the borate template, leading to SubTBDAP structures with different functionalities on the apical position. Hybrid SubTBDAPs are intrinsically interesting because of their distinctive properties, but having the control over the substituents that are introduced would give us the power to tune such properties in order to engineer more complex structures.

An aryl- group has been already introduced in the apical position by this method, so we turned our attention to some simple alkyl substituents that were available as boric esters. Scheme 69 illustrates the selective synthesis of SubTBDAP hybrids using different borates.



**Scheme 69.** Selective syntheses of SubTBDAP hybrids selectively functionalised at the apical position.

The optimised conditions were employed using trimethyl borate B(OMe)<sub>3</sub> as a boron source and Lewis acid. The reagents were heated up to 200 °C in diglyme under inert atmosphere for 4 hours. TLC then revealed complete consumption of aminoisoidolene **131** and formation of a pink

spot subsequently confirmed to be the expected SubTBDAP-OMe **133** by MALDI TOF and high resolution mass spectrometry. The purification method involved the above mentioned aqueous work up followed by a column chromatography using diethyl ether/ hexane/ dichloromethane (1:4:2) as solvent system, which resulted in the isolation of hybrid **133** as a pink solid in 9% yield.

SubTBDAP-OMe **133** was characterised by  $^1\text{H-NMR}$  spectroscopy which gave sharp peaks apart from those subjected to the rotation of the *meso*-phenyl ring in accordance with the previously characterised SubPTBDAP-OPh **134**. Consequently, a VT  $^1\text{H-NMR}$  spectrum was necessary in order to analyse and assign all signals. Figure 75 depicts the proton NMR spectrum of hybrid **133** in  $\text{CD}_2\text{Cl}_2$  at 263K, where the expected pattern in the aromatic region can be observed (similar to the one obtained for SubTBDAP-OPh **134**), with all signals for the phenyl group in the *meso*- site resolved at low temperature into two doublets and two triplets for the *ortho*- and the *meta*- protons, respectively.

Interestingly, the influence of the core ring current is visible on the signal corresponding to the methoxy- proton at the apical position that appears shielded at high field in the spectrum (1.28 ppm).

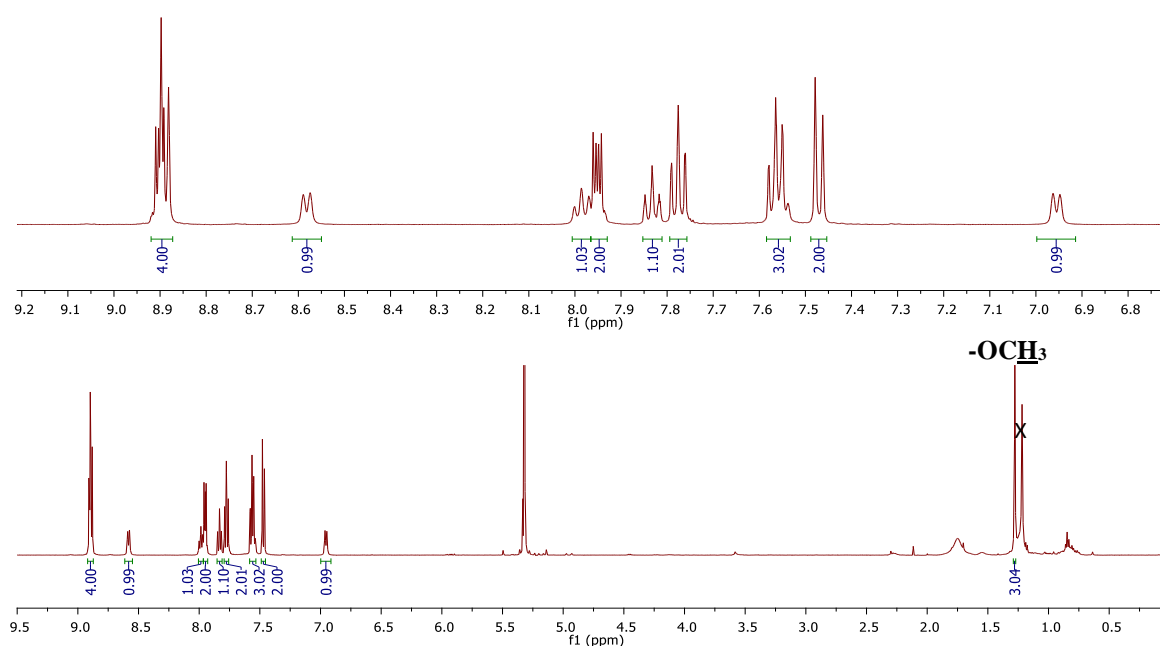


**Figure 75.**  $^1\text{H-NMR}$  of SubTBDAP-OMe **133** in  $\text{CD}_2\text{Cl}_2$  at 263K.

Crystals suitable for X-Ray diffraction were eventually grown dissolving SubTBDAP **133** in a mixture of dichloromethane/hexane and allowing slow diffusion with acetone. Figure 76 represents the fully elucidated crystal structure of hybrid compound **133**.

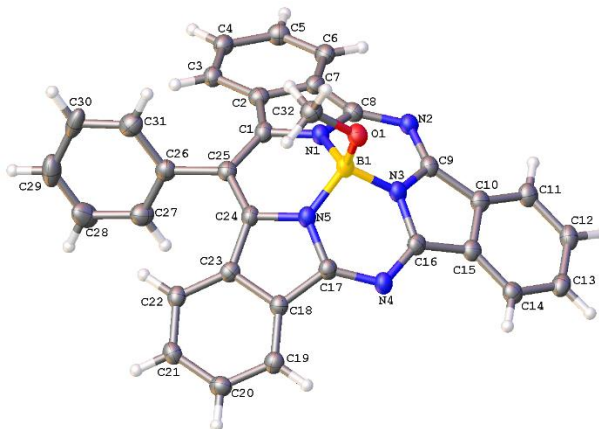
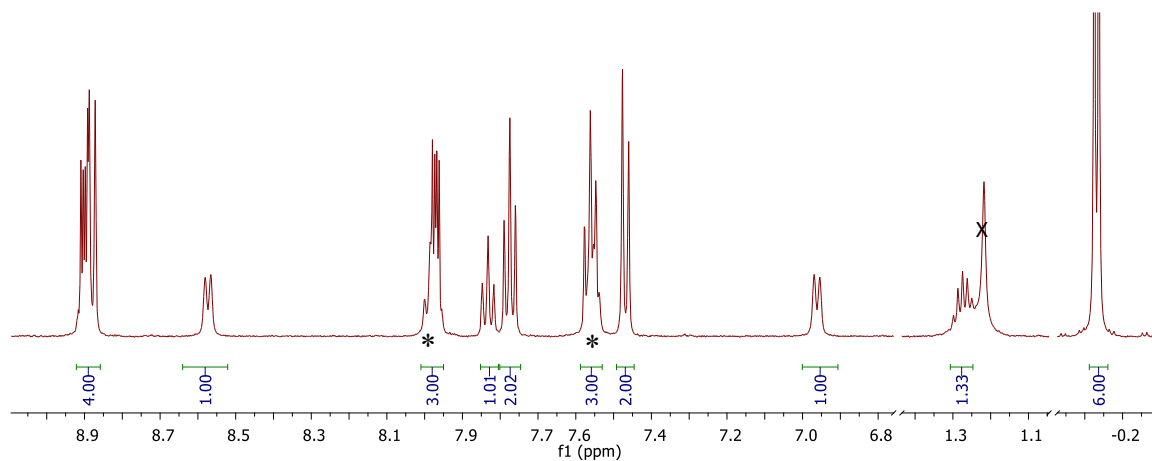


**Figure 76.** Crystal structure of SubTBDAP-OMe **133**.

The crystal reveals the same curved structure as the phenoxy-SubTBDAP **134**, where the tetrahedral boron is bonded to the three nitrogens forming the basal plane and a methoxy-group at the apical position. The *meso*-phenyl group lies almost perpendicular to the macrocyclic core and interestingly, the methoxy-group is accommodated facing the phenyl ring.

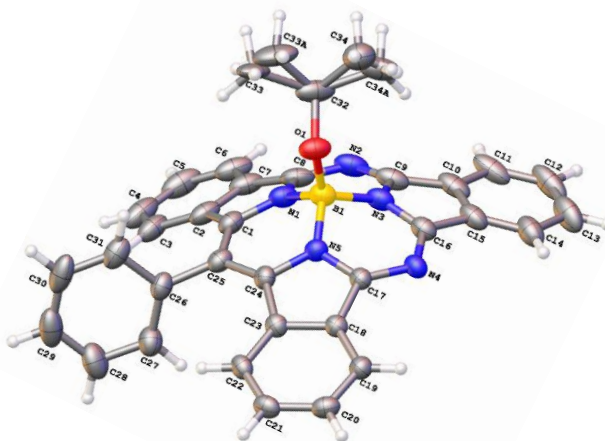
The next target to be accomplished was the SubTBDAP-*OiPr* hybrid **139** bearing an isopropoxy- group at the apical position. To do so aminoisindolene **131**, phthalonitrile and triisopropylborate were placed in a sealed tube under inert atmosphere. Diglyme was used as solvent according to the above described optimised protocol. The mixture was heated up to 200 °C for 6 hours and TLC revealed complete consumption of isoindolene **131** and phthalonitrile. The mixture was then cooled down and subjected to an aqueous work up, after which a column chromatography on silica gel using diethyl ether/ hexane/ dichloromethane (1:4:2), was necessary in order to separate the desired hybrid from the mixture of phthalonitrile, dimer, decomposed material and traces of SubTBDAP-OH **132** that had been formed in the course of the reaction. Recrystallisation from distilled DCM/distilled petroleum ether yielded the pure hybrid SubTBDAP-*OiPr* **139** as pink-red solid in 9.2% yield.

Figure 77 shows an expansion of the areas of interest in the  $^1\text{H-NMR}$  spectrum of SubTBDAP-*OiPr* **139** at low temperature (-10 °C) in deuterated dichloromethane. The aromatic region is quite similar to the previous hybrid derivatives, and shows two doublets at 8.6 and 7.0 ppm corresponding to the ortho-protons in the *meso*-ring. The *meta*-protons appear overlapped by two other signals but integration of those peaks confirmed their presence (\*). Regarding the apical group, as already discussed the effect of the ring current shifts the *iPr* protons to high fields; in essence, the two  $-\text{CH}_3$  appear as a doublet with a  $^3J$  value of 6.1 Hz at ca. -0.2 ppm, and the  $-\text{CH}$  proton is located at around 1.3 ppm as a multiplet overlapped with the signal of water.



**Figure 77.** Variable temperature  $^1\text{H-NMR}$  of SubTBDAP-OiPr **139** at 263K in  $\text{CD}_2\text{Cl}_2$ .

The structure was elucidated by X-Ray diffraction analysis, after a single crystal was slowly grown from a mixture of cyclohexane/acetone. In this case the isopropoxide- substituent is disordered over two positions (60:40) as illustrated in Figure 78.



**Figure 78.** X-Ray structure of SubTBDAP-OiPr **139** showing two conformations of the isopropoxide-substituent.

The attachment of a straight aliphatic chain was successfully achieved applying optimised conditions illustrated above. Aminoisoindolene **131**, phthalonitrile and tributyl borate were heated in a sealed tube at 200 °C. After two hours TLC showed the formation of the expected product confirmed by the corresponding parent ion peak with a  $m/z$  of 543.24 by MALDI-TOF MS, and also the presence of dimer **138** and few other colourful spots that could not be further identified. Consequently, the reaction was stopped and subjected to the usual work up and a purification process that involved the performance of two column chromatography separations to obtain high purity material. The product was then isolated after recrystallisation from a mixture of distilled dichloromethane and distilled petroleum ether as a pink solid in 7.4% yield.

The  $^1\text{H-NMR}$  spectrum was obtained and its assignment was in full accordance to previous analogues. Crystals suitable for X-Ray diffraction were grown dissolving SubTBDAP-OBu **140** in a mixture of dichloromethane/acetone allowing slow diffusion of cyclohexane. Figure 79 illustrates



the crystal structure of the hybrid **140**. As already observed for previous examples, the *meso*-phenyl group lies almost perpendicularly to the core.

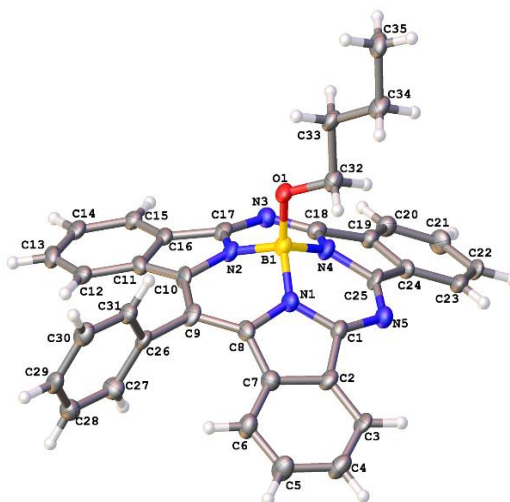


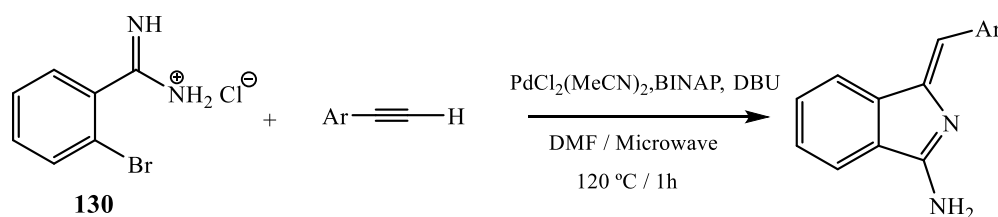
**Figure 79.** Crystal structure of SubTBDAP-OBu **140**.

An element worth noting is the butyl chain accommodated in its most stable conformation in the solid-state structure, which is pointing out from the macrocyclic core. However, this chain will freely rotate in solution.

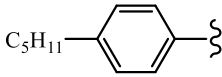
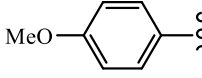
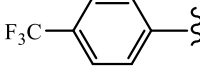
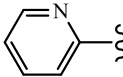
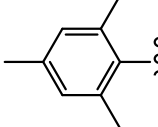
### *Functionalisation at the new meso-site*

The scope of this protocol has been successfully demonstrated by the incorporation of different substituents at the apical position. Selection of borate templates leads to control over the apex site, allowing us to synthesise and fully characterise the novel hybrids (SubTBDAPs **133**, **134**, **139** and **140**) discussed in previous sections. What undoubtedly could make these hybrids uniquely attractive, would be the synthetic control to engineer the new *meso*-site at will.

For such purpose we turned our attention to producing some aminoisoindolene precursors, as they are the key compounds to introduce the desired functionalities in the SubTBDAP macrocycle. Scheme 70 illustrates the reaction conditions followed for the synthesis of aminoisoindolenes listed in Table 5.



**Scheme 70.** Reaction scheme for the formation of substituted aminoisoindolenes illustrated below.

Entry	Ar =	Product	Yield (%)
1		<b>141</b>	76
2		<b>142</b>	76
3		<b>143</b>	73
4		<b>144</b>	58
5		<b>145</b>	32

**Table 5.** Reaction of amidine **130** in conjunction with acetylenic precursors to form the products listed above and the corresponding yields obtained.

As already mentioned these general reaction conditions were published by Hellal and Cuny<sup>[170]</sup> and are illustrated in Scheme 70. The reaction is easy to perform and fast; the reagents are heated up to 120 °C under microwave irradiation for one hour, after which an aqueous work up was performed. A column chromatography on silica gel was carried out using 100% DCM to EA/DCM (1:1) to 100% EA as solvent gradient in all cases. The products were recrystallised from a mixture of dichloromethane/ hexane to yield the aminoisoindolenes illustrated in Table 5.

This one-pot reaction allowed the introduction of different substituents on the phenyl ring, with high selectivity giving the *Z* isomer as major product. This was confirmed by <sup>1</sup>H-NMR spectroscopy with the characteristic alkene proton at around 6.7 ppm in all cases, and by NOESY technique where the NOE signal between the alkene proton and the closest proton in the benzenoid ring was also observed.

Particularly interesting from a spectroscopic viewpoint is the <sup>13</sup>C-NMR spectrum of aminoisoindolene-CF<sub>3</sub> **143**. An expansion of the region of interest is represented in Figure 80. The <sup>13</sup>C experiment is proton decoupled but the couplings between <sup>13</sup>C and <sup>19</sup>F are clearly observed. All signals are split into quartets; C1 gives a signal at 124.5 ppm with a <sup>1</sup>J<sub>CF</sub> of 272 Hz (represented as \* in Figure 80), C2 is located at 128.6 ppm with a <sup>2</sup>J<sub>CF</sub> value of 32 Hz (●) and the smallest coupling (<sup>3</sup>J<sub>CF</sub> = 3.8 Hz) is observed for the furthest C3 at 125.4 ppm (◇).

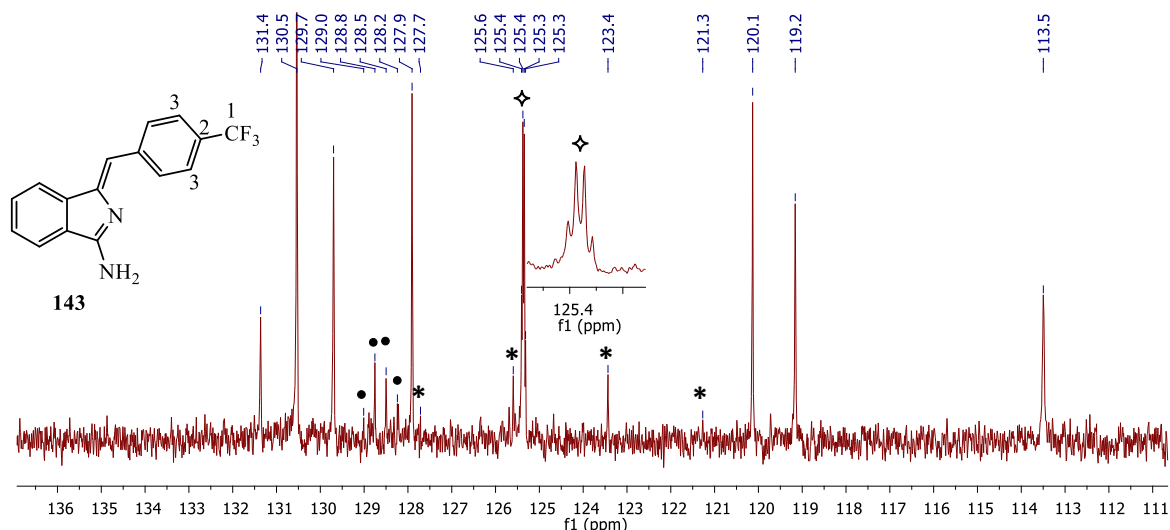


**Figure 80.** Expansion of  $^{13}\text{C}$ -NMR spectrum of aminoisoindolene- $\text{CF}_3$  **143**.

A particular case is aminoisoindolene **145** bearing three methyl groups on the phenyl ring. Due to steric repulsion between such methyl groups and the pyrrolic nitrogen, the *Z* isomer was isolated as minor product in 32% yield. The  $^1\text{H}$ -NMR spectrum showed, as expected, two singlets in the aromatic region, one corresponding to the alkene proton at 6.62 ppm, and the other corresponding to the two protons in the phenyl substituent at 6.94 ppm. The product was fully characterised by UV-Vis, MS and NMR spectroscopies, and full elucidation of the structure was possible after suitable crystals were grown slowly from pure methanol.

Figure 81 illustrates the crystal structure of aminoisoindolene **145**, the solid-state structure is stabilised by rotation of the phenyl group lying approximately perpendicular to the isoindolene framework.

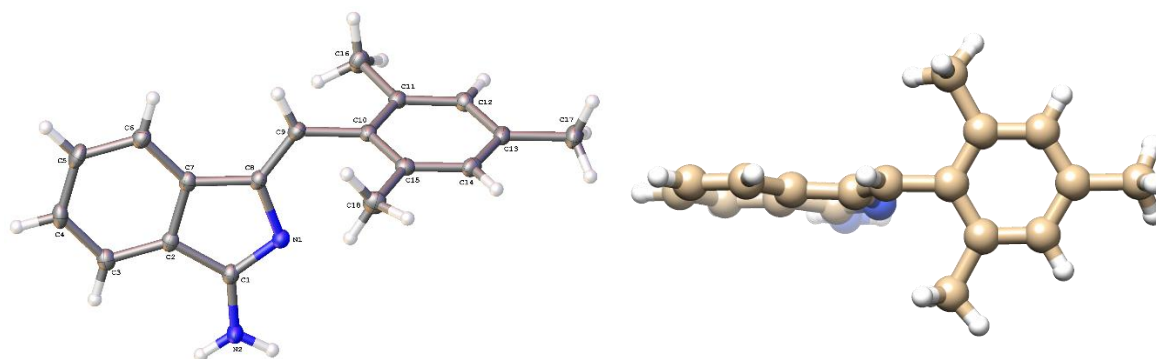
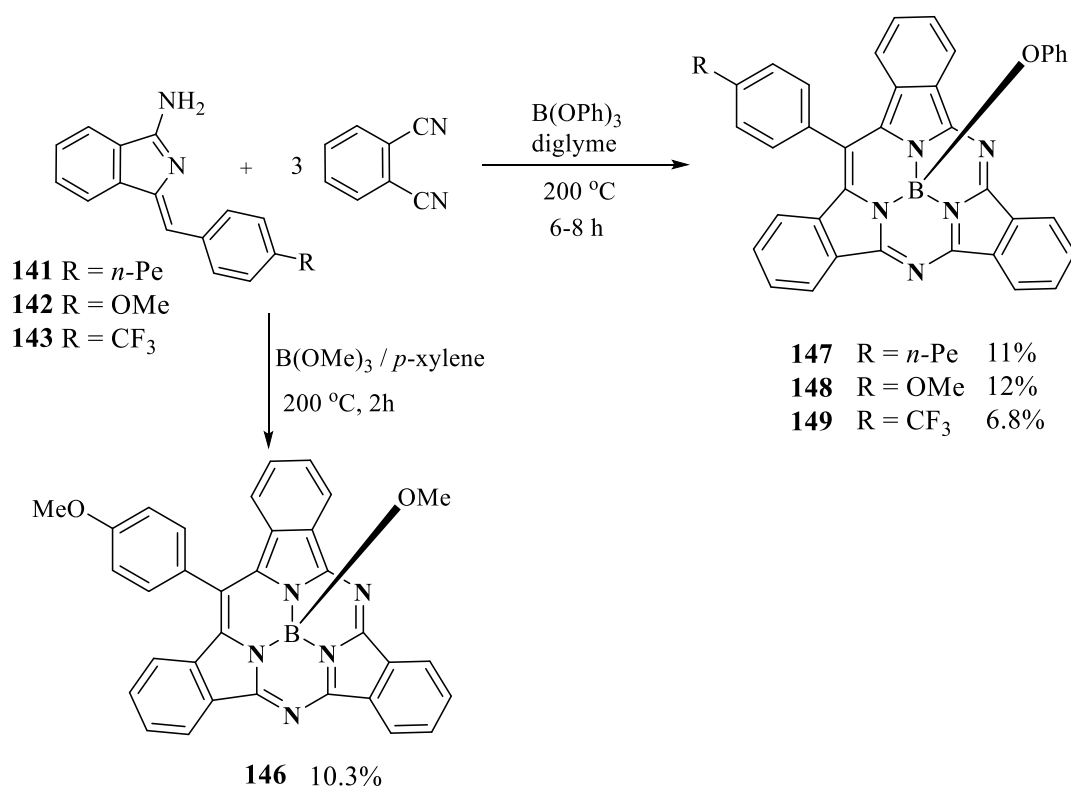


**Figure 81.** Crystal structure of aminoisoindolene **145**.

Scheme 71 represents the scope of the procedure whereby a variety of SubTBDAP hybrids are synthesised bearing different substituents at the apical position and most importantly at the *meso*-phenyl substituent. The introduction of the functionality in the boron atom can be designed choosing the desired trisubstituted borate, whereas the substitution at the alkene moiety is achieved by the aminoisoindolene precursors that have just been described.

As proof of concept, a homo-functionalised OMe-SubTBDAP-OMe **146** was synthesised bearing methoxy- groups in both positions. To achieve it aminoisoindolene **142** was treated with an excess of phthalonitrile and trimethyl borate under an argon atmosphere, and the mixture was heated up to 200 °C. Although the reaction also works using diglyme as solvent, the performance of this particular reaction was considerably better when using *p*-xylene. Hence after 2 hours TLC showed complete consumption of aminoisoindolene **142**. The main products were the expected dimer **138**, the desired hybrid compound **146**, decomposed material and some colourful material that could not be identified. After cooling the reaction, the solvent was evaporated under reduced pressure. Two subsequent column chromatography separations on silica gel were performed in order to obtain the pure SubTBDAP **146** as pink solid in 10.3% yield.



**Scheme 71.** Versatile syntheses of SubTBDAP hybrid demonstrating selective functionalisation at the *meso*- and apical sites.

The VT <sup>1</sup>H-NMR of this hybrid showed the expected pattern for the benzenoid protons that form the core, Figure 82. The *meso*phenyl- methoxy- protons appear at the expected chemical shift for ethers (4.05 ppm). This is a nice example on how the strong ring current of the SubTBDAP core affects the chemical shift, since the signal for the methoxy- protons at the apical position is shown upfield at 1.27 ppm, Figure 82.

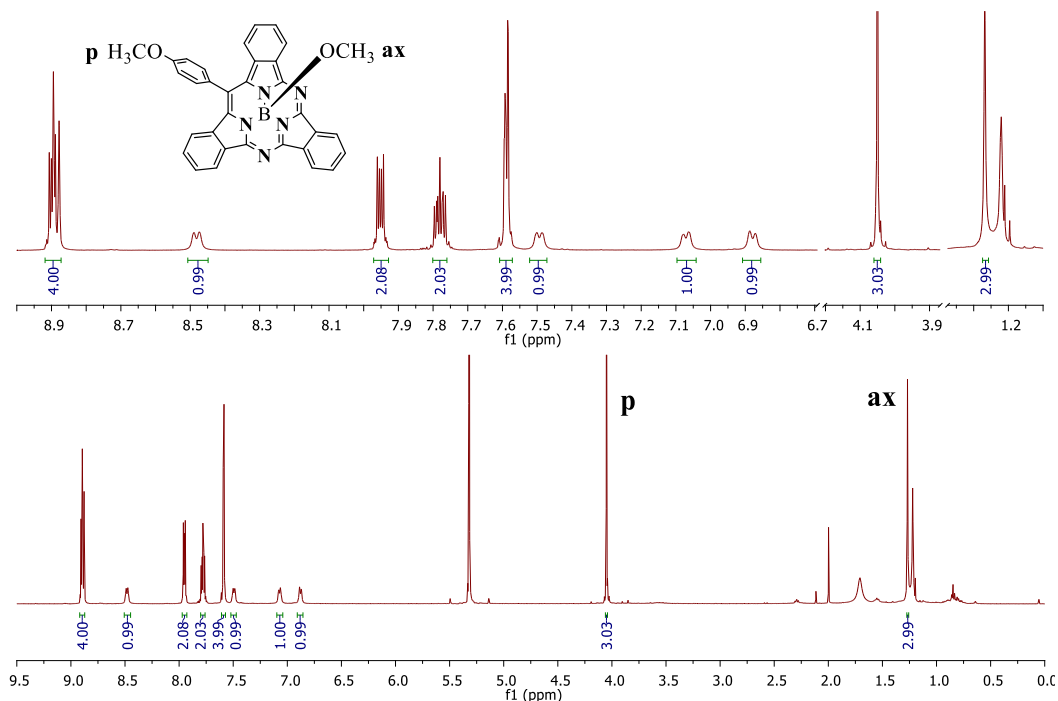


**Figure 82.** Full VT  $^1\text{H}$ -NMR spectrum of OMe-SubTBDAP-OMe **146** in  $\text{CD}_2\text{Cl}_2$  at 263 K (bottom) and expansion of the selected regions (top).

Now all signals corresponding to the *ortho*- and *meta*- protons appear as doublets with very different chemical shifts and coupling constants of 7.6 Hz. A VT COSY experiment was performed in order to assign the protons that are on the same face, i. e. either on the top side of the macrocycle or the concave side. Figure 83 shows the cross peaks between the doublets that are coupled. In essence, the protons that appear at lowest field (blue lines) are on the same side of the ring, and the same for the ones marked with green lines.

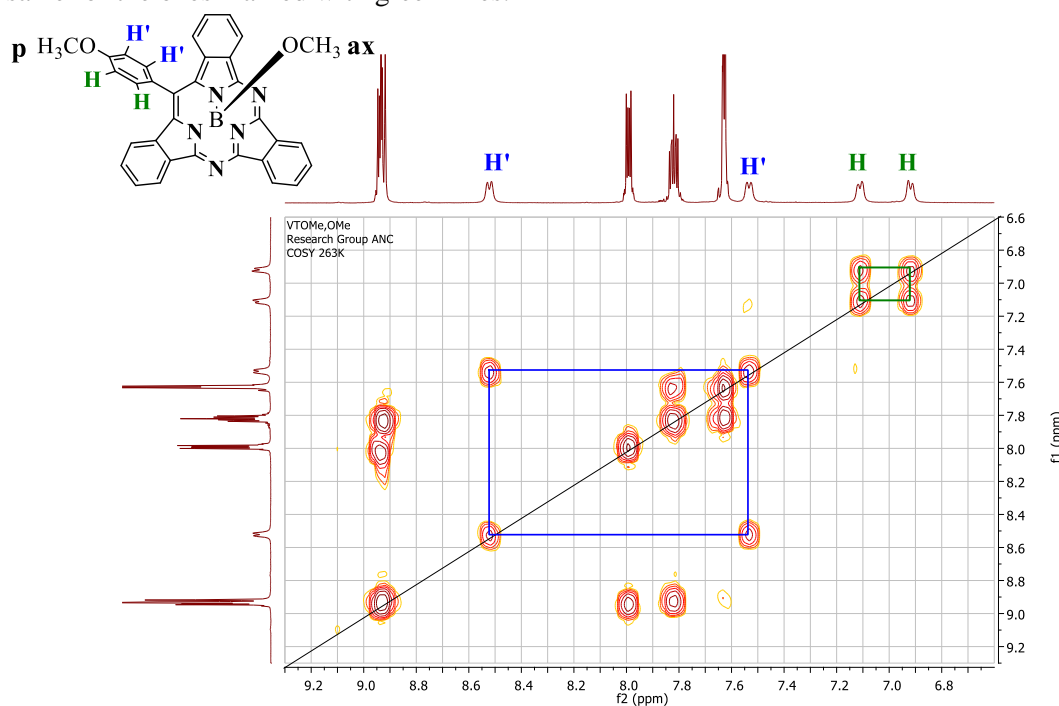


**Figure 83.** VT COSY experiment showing cross peaks between *meso*-phenyl protons in hybrid **146**.

The structure of OMe-SubTBDAP-OMe **146** was fully elucidated by X-Ray diffraction, after crystals were grown from a mixture of dichloromethane/acetone and allowing slow diffusion of methanol. Figure 84 illustrates the crystal structure of hybrid **146**; in the crystal the *meso*-phenyl ring is distorted into two positions. The methoxy- group at the apical position is pointing towards the *meso*-substituent as already seen in the crystal of the SubTBDAP-OMe **133**. The methoxy-group in the *meso*-site is also facing the convex side of the macrocycle.

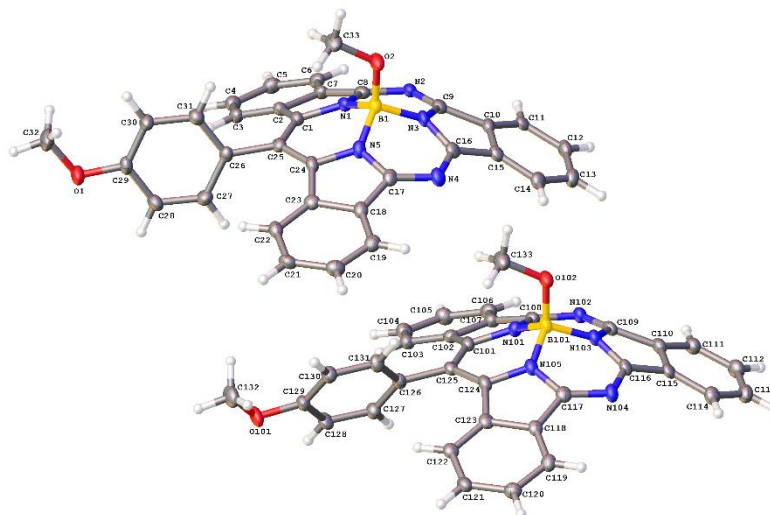


**Figure 84.** Crystal structure of OMe -SubTBDAP-OMe **146**, where the phenyl group is tilted into two different conformations.

The synthetic procedure allows introduction of an alternative substituent at the aryl group. Some other examples bearing different substituents at both sites were subsequently synthesised having a phenyl group at the apical position in all cases, and the *meso*-phenyl group was functionalised with substituents with different electronic effects. Scheme 71 represents the reaction conditions followed as well as the yields obtained for each derivative.

In this manner, aminoisoindolenes **141**, **142** and **143**, were heated up to 200 °C in a sealed tube, with 3 equivalents of phthalonitrile and triphenyl borate in diglyme. The reactions proceeded smoothly and in 6 hours both *n*Pe-SubTBDAP-OPh **147** and CF<sub>3</sub>-SubTBDAP-OPh **149** had been formed; 8 hours were required for OMe-SubTBDAP-OPh **148**. The reactions were stopped and the crude materials were subjected to the optimised purification protocol to achieve SubTBDAP **147**, **148** and **149** as pink solids in 11%, 12% and 6.8%, respectively.

Unfortunately, the same reaction carried out with pyridyl-aminoisoindolene **144** was unfruitful, the reaction mixture suffered a change in colour to green-brownish and the TLC revealed mostly polar/oligomer baseline material. Due to a lack of time aminoisoindolene **145** could not be subjected to the reaction conditions for the synthesis of the corresponding SubTBDAP hybrid. Nevertheless, the availability of this new compound will definitely urge its subsequent utilisation in our group.

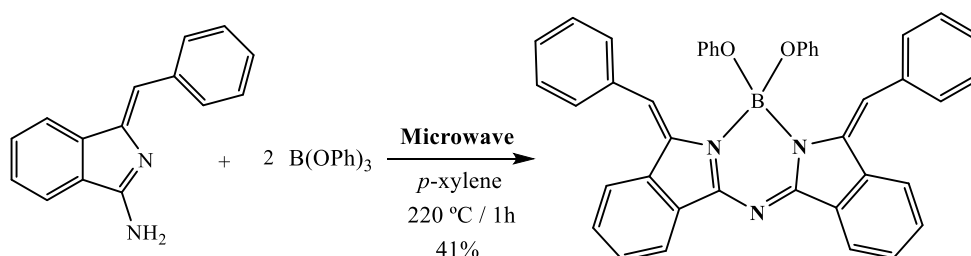
The scope of the protocol has been demonstrated by the derivatives herein described. This versatile synthetic protocol is easy to set up, reliable and the products can be isolated as pure, freely soluble, crystalline solids. The control over the substitution of both positions opens endless possibilities towards the discovery of novel architectures.

### Controlled synthesis of azaBODIPY derivatives

As already discussed, azaBODIPY analogue **135** belongs to an important class of materials that had been obtained as a side product during the formation of SubTBDAP-OPh **134**. However, it is possible to synthesise azaBODIPY compounds in a controlled manner. The aim is to build architectures with the desired functionalities both at the boron atom and in the alkene moiety, in one single reaction step.

It was recognised that the utilisation of aminoisindolene precursors and an excess of borate could lead straightaway to the formation of the target BODIPY molecules. Hence as a control experiment, aminoisindolene **131** and triphenyl borate were heated up to 200 °C in *p*-xylene. After 3 hours both dimer **138** and azaBODIPY-OPh **135** were observed in the TLC together with some other unrecognised spots. The reaction performance was very poor and non-selective towards the target compound. We turned our attention to alternative methods such as microwave irradiation, a powerful and fast technique that allows formation of aminoisindolenes in an effective and high yielding way.

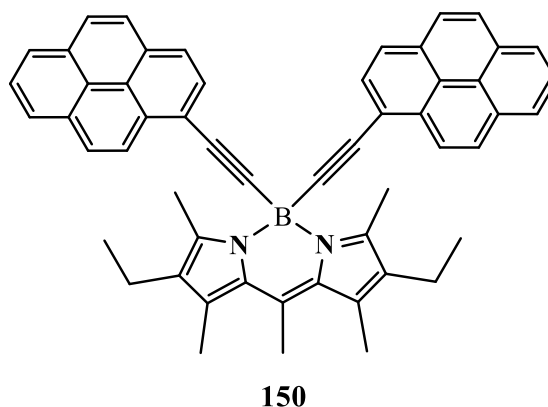
Hence both reagents were placed in a microwave vessel under inert atmosphere, *p*-xylene was selected as solvent for this reaction (Scheme 72). The mixture was then irradiated under microwaves at 220 °C for 1 hour, after which time TLC revealed complete consumption of aminoisindolene **131**. No dimer formation was observed and the main spot was the desired azaBODIPY **135**. After an aqueous work up and a column chromatography on silica gel using ethyl acetate/ petroleum ether (2:7) as solvent eluent, azaBODIPY-OPh **135** was isolated as yellow solid in 41% yield with the same spectroscopic properties already illustrated in the previous section.



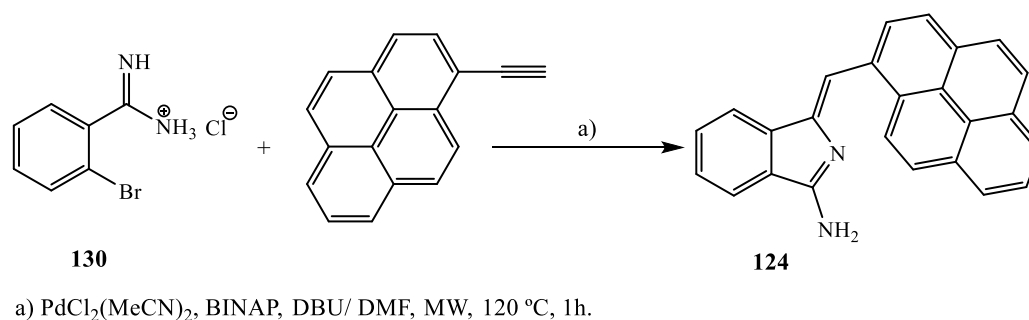
**Scheme 72.** Controlled synthesis of azaBODIPY-OPh **135** under microwave irradiation.

Once the concept had been demonstrated, this protocol was followed to synthesise an azaBODIPY derivative that allowed us to expand the light absorption region. The strategy relies on the incorporation of a chromophore that absorbs in the region from 360 to 390 where the azaBODIPY core does not absorb, such as pyrene molecules.

Ulrich and Ziesel<sup>[180]</sup> reported the synthesis of a BODIPY core functionalised at the boron center with two ethynylpyrene units, for protein labelling and energy transfer studies. They successfully demonstrated the efficient intramolecular energy transfer from the pyrene to the BODIPY moiety, so that the ethynylpyrene-BODIPY **150** acts as a small cascade device. Their new molecule showed high quantum yield and a very large Stokes Shift of around 156 nm.



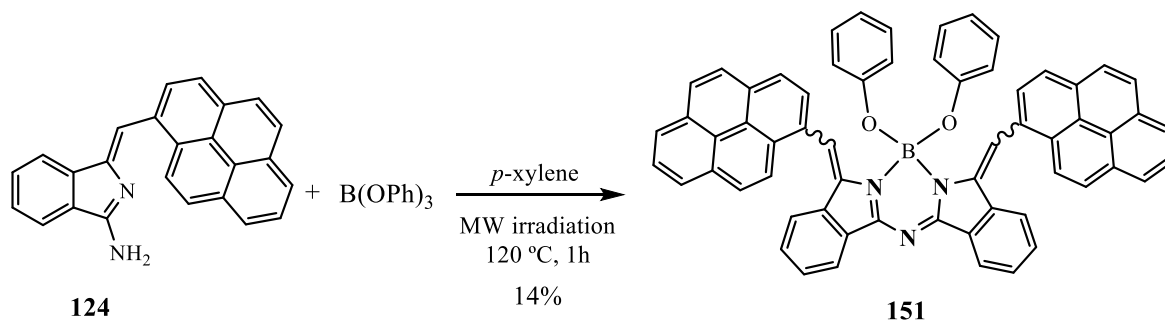
The synthesis towards an azaBODIPY derivative bearing pyrene molecules started from the synthesis of pyrenyl-aminoisindolene **124**, a precursor successfully reported by our group.<sup>[139]</sup> The synthetic protocol has been discussed in earlier sections (Scheme 73). This synthesis proved to be challenging; not only were there some issues regarding the solubility of the final material, but the product stuck to MgSO<sub>4</sub> and presumably to silica gel during the purification process. The product was eventually isolated as yellow solid as its *Z*-isomer in 25% yield.



**Scheme 73.** Synthesis of pyrenyl-BODIPY **124** as *Z*-isomer.

The above mentioned controlled synthesis for BODIPY formation was then undertaken. Pyrenyl-aminoisindolene **124** and triphenyl borate were placed in a microwave vial under inert atmosphere and *p*-xylene was used as solvent. The mixture was subjected to microwave irradiation at 120 °C for 1 hour. After that, TLC revealed the formation of two spots, later confirmed by mass spectrometry to be the self-condensation product and the desired BODIPY **151**. The purification process required two column chromatography separations on silica gel, which resulted in the pure pyrenyl-BODIPY-OPh **151** as a red solid in 14% yield, Scheme 74.





**Scheme 74.** Synthesis of pyrenyl-azaBODIPY-OPh **151**.

Although MALDI-TOF MS produced an ion peak with a mass for the fragmentation corresponding to the loss of one phenoxy-group (774  $m/z$ ), the high resolution nanospray ionisation (NSI) mass spectrum supports the structure with a signal at  $m/z$  868.3135 (calculated for  $[\text{C}_{62}\text{H}_{38}\text{BN}_3\text{O}_2]^+$ : 868.3140  $m/z$ ).  $^{11}\text{B}$ -NMR showed two singlets at 2.76 and 1.80 ppm confirming the presence of two isomers in a ratio (4:1); due to steric hindrance with the phenoxy-rings it is therefore reasonable to think that the ratio favours the *E,E* configuration, matching previous results for other azaBODIPY analogues reported by our group.<sup>[172]</sup> As expected two different sets of signals are shown in the  $^1\text{H}$ -NMR spectrum. The structure was fully elucidated by X-Ray diffraction after suitable crystals were grown from a mixture of dichloromethane/ methanol.

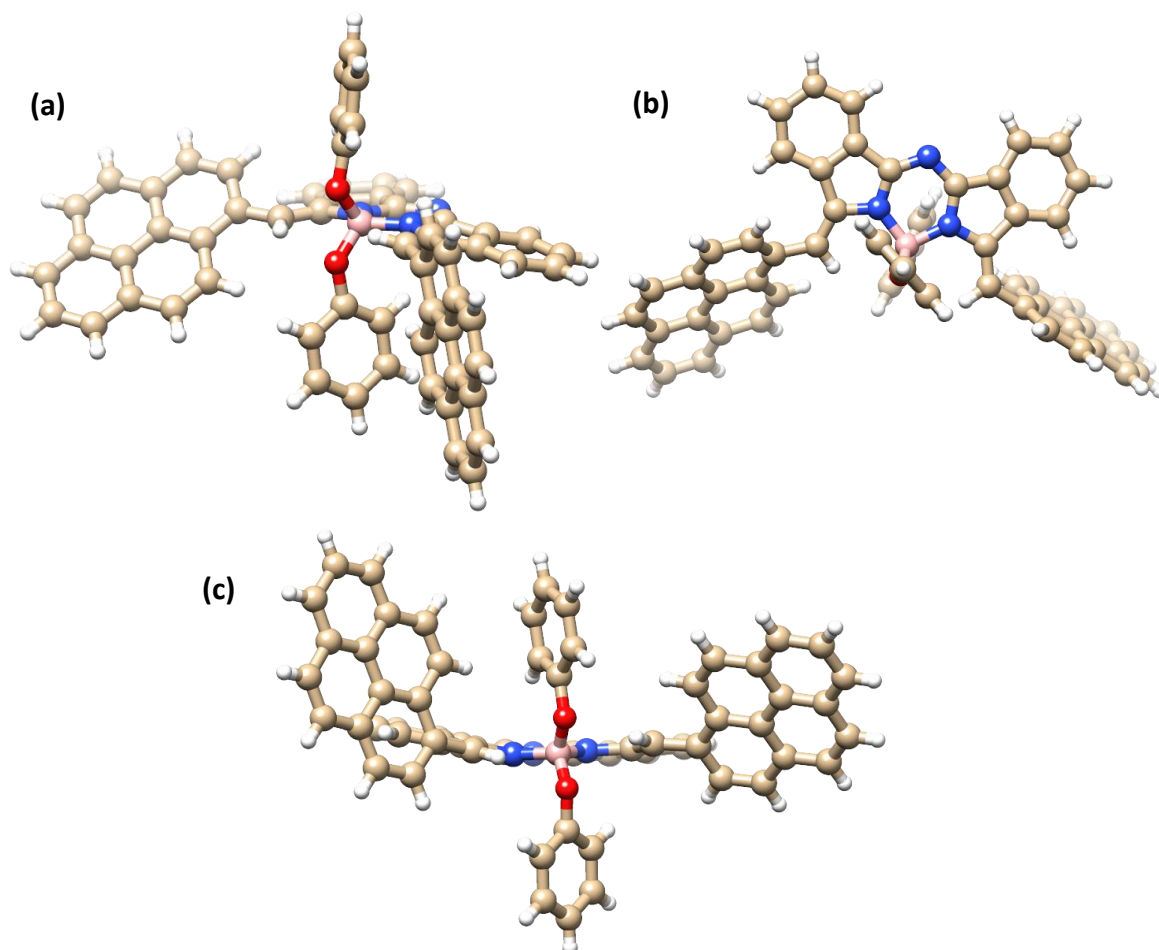


**Figure 85.** Crystal structure of pyrenyl-azaBODIPY-OPh **151**. Three different views: (a) side, (b) top, and (c) front.

The crystal structure (Fig. 85) shows a tetrahedral geometry for the boron atom. With the two pyrene systems lying tilted almost perpendicularly to the BODIPY framework (**a**). As expected the phenoxy-groups are accommodated at the top and bottom sides of the molecule (**c**), interestingly they are found lying perpendicular to each other in the solid-state (**b**), although it is expected that all groups attached to the main BODIPY core will be freely rotating in solution. What makes this structure uniquely fascinating, is the successful implementation of five individual light absorbing units lying at intrinsically different directions of space in one molecule.

As a result, azaBODIPY **151** exhibits an extremely broad absorption spectrum, with four distinctive bands that absorb all the way across the UV-Vis spectrum from 250 to 600 nm, Figure 86. The spectrum features a maximum at 489 nm which corresponding to the azaBODIPY part, and three other maxima at 346, 277 and 267 nm attributed to the pyrene substituents. The emission band is a mirror image of the lowest energy band in the absorption spectrum, and it is shown at 629 nm after excitation at 489 nm. These features give rise to a large Stokes Shift of 140 nm, see Figure 86. This remarkable molecule will be one focus of study in our group to fully elucidate its properties.

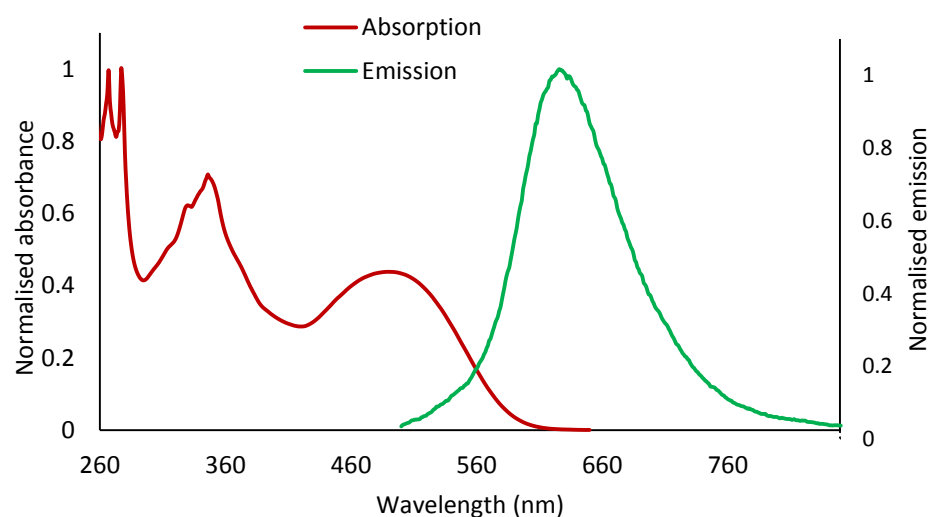
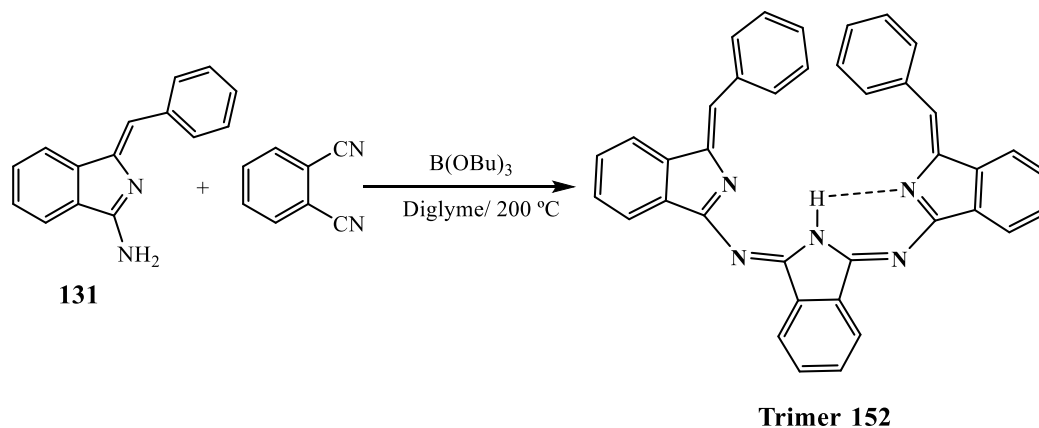


**Figure 86.** UV-Vis and Emission spectra (exc. 490 nm) of pyrenyl-BODIPY-OPh **151**.

#### 3.2.4.4 Preliminary mechanism study for SubTBDAP formation, and an interesting intermediate

In a preliminary mechanistic investigation, aliquots were removed from a typical SubTBDAP reaction at regular intervals (Scheme 75). After 30 minutes heating aminoisoindolene **131**, phthalonitrile and tributyl borate at 200 °C in diglyme, a brown spot on the TLC attracted our attention. The disappearance of the spot through the reaction progress was even more intriguing.

After a challenging isolation which involved the performance of a preparative TLC, the intermediate was isolated and characterised by mass spectrometry and NMR spectroscopy.



**Scheme 75.** Reaction conditions and formation of intermediate **152**.

MALDI-TOF MS revealed a mass of 551 m/z with a simple isotopic pattern similar to the one observed for the dimer **138** (Fig. 87). Trimer **152** depicted a rather complicated  $^1\text{H-NMR}$ , but assistance obtained from COSY and NOESY experiments made possible the elucidation of the structure. It consisted on the arrangement of two of the isoindolene **131** precursors with one unit of phthalonitrile giving rise to this trimer-like structure (Scheme 75). However, at this point the structure was uncertain due to other possibilities that could have occurred in the reaction.

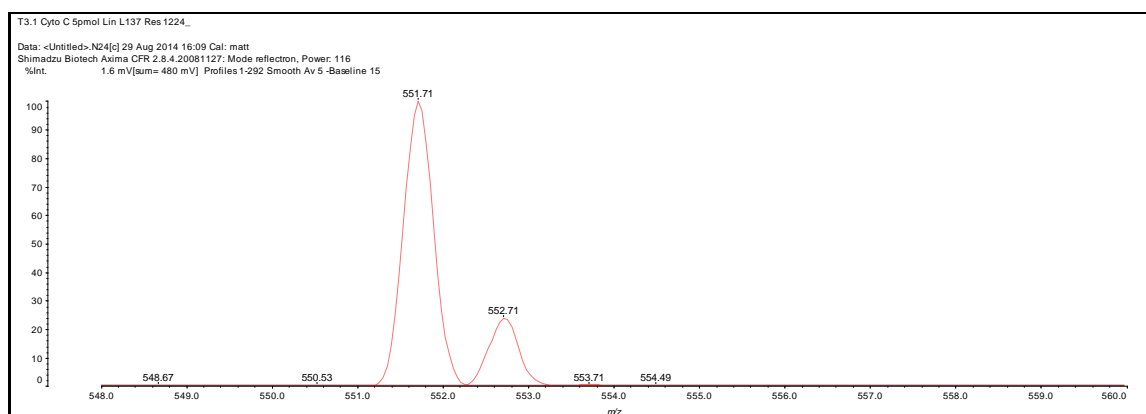


**Figure 87.** MALDI-TOF spectrum showing the parent ion peak of trimer **152**.

After many recrystallisation attempts, crystals suitable for X-Ray diffraction were grown from a mixture of distilled dichloromethane / distilled petroleum ether, enabling the confirmation and complete elucidation of the structure. In the crystal (Figure 88) the structure shows a helical-like conformation stabilised with a hydrogen bond between  $\text{N1-H1}\cdots\text{N3}$ .

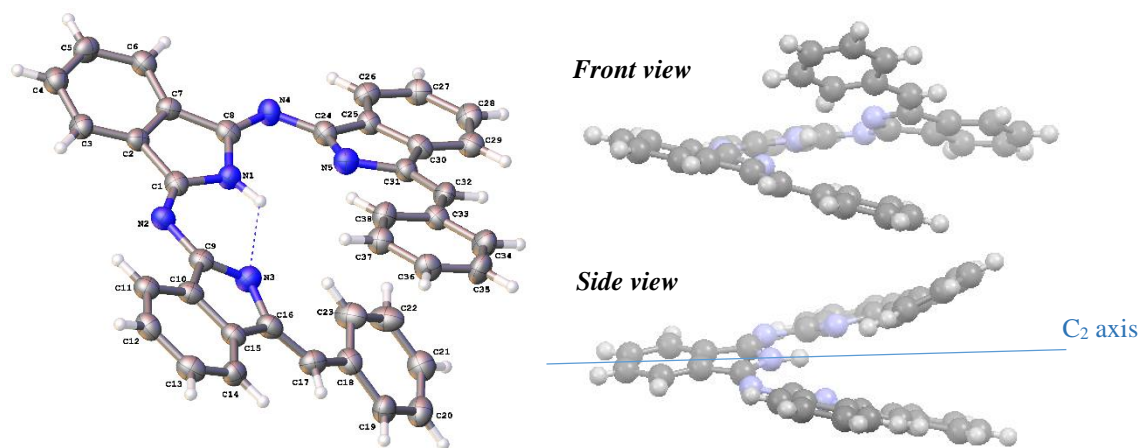


**Figure 88.** Crystal structure of trimer **152** showing hydrogen bond between N1–H1...N3.

Interestingly, the structure is very similar to those of helicenes. The hexahelicene **153** was first synthesised and resolved by Newman et al.<sup>[181]</sup> in 1956, and since then they have become a subject of interest in the investigation and development of novel drugs and materials.<sup>[182]</sup> Helicenes are *ortho*-condensed polycyclic aromatic compounds, due to the steric repulsion between the terminal benzene rings these aromatic systems adopt a nonplanar distorted structure, possessing a chiral helical  $\pi$ -electron system. The helix winds around a central axis either with right-handed (P-configuration) or left-handed (M-configuration) helicity, Figure 89.<sup>[183]</sup>

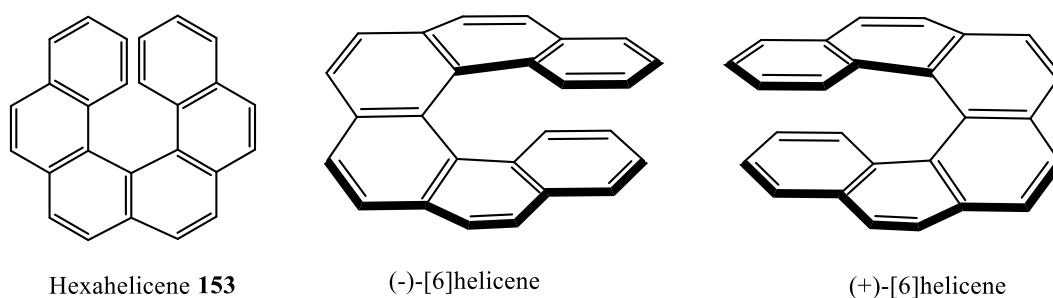


**Figure 89.** Structure of [6]helicene **153** and enantiomers.

Like hexahelicene **153**, trimer **152** also possess a C<sub>2</sub> axis implying the unchanged character of the molecule upon rotation of 180 ° around such axis, Figure 88. The chirality of the new trimer **152** in the crystal analysed is left-handed as can be observed in the front and side views in Figure 88.

Trimer **152** is a brown compound, which shows only weak fluorescence emission and a broad UV-Vis spectrum with a maximum at 334 nm and molar extinction coefficient of  $1.28 \times 10^4 \text{ M}^{-1} \text{ cm}^{-1}$ . Figure 90 depicts a comparison spectra between the UV-Vis absorption of trimer **152** and dimer **138**. Surprisingly, dimer **138** show a longer wavelength absorption band, absorption maxima at 465 nm and 343 nm are observed.

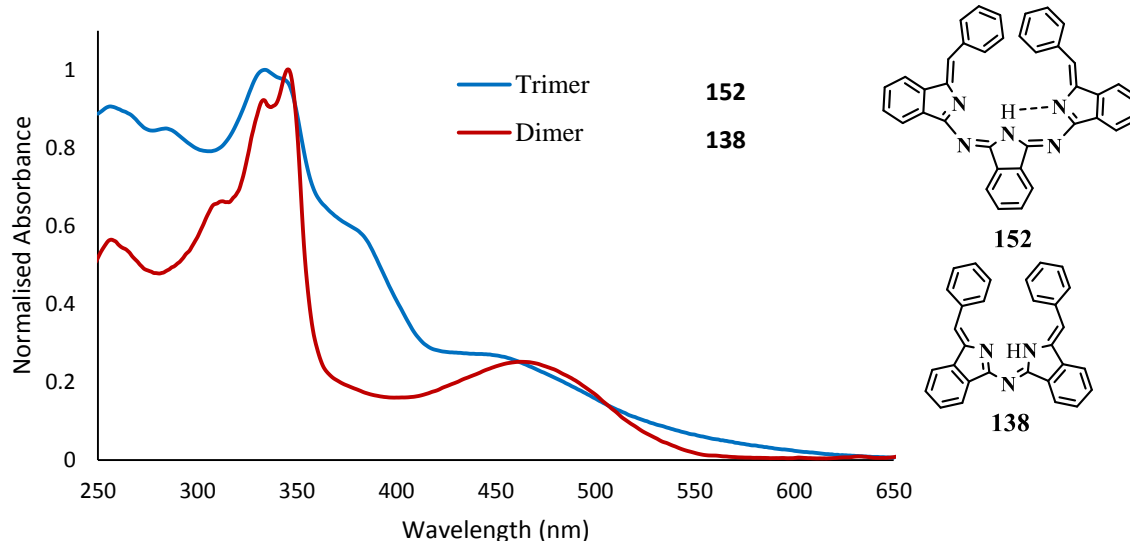


**Figure 90.** Comparison UV-Vis spectra of trimer **152** and dimer **138** in dichloromethane.

The mechanism of formation of the hybrid materials (TBTAPs and SubTBDAPs) remains unclear, but the isolation of this intermediate could provide a clue. The isolated “trimer” comes from reaction between the aminoisoindolenes and phthalonitrile. Cyclisation of this intermediate around a boron template, with loss of a benzyl unit could conceivably lead to the observed SubTBDAPs. A related process could occur in the presence of  $Mg^{2+}$  template to give TBTAPs, but at this stage both suggestions are speculative.

### 3.2.4.5 Properties of SubTriBenzoDiAzaPorphyrins

#### *Photophysical properties*

Absorption spectra of SubTBDAPs exhibit a Soret band at ca. 320 nm, and a split Q band at ca. 547 nm with two small shoulders at 496 nm and 511 nm due to the symmetry reduction. This feature is exemplified in Figure 91 with the absorption and emission spectra of SubTBDAP-OMe **133**. The novel hybrid compounds exhibit yellow fluorescence at ca. 558 nm, and a very small Stokes Shift of 11 nm that might be attributed to the rigidity of the macrocyclic core. The structural similarity between hybrids and the parent molecules is reflected in the similar optical properties. However, some significant differences can still be found.

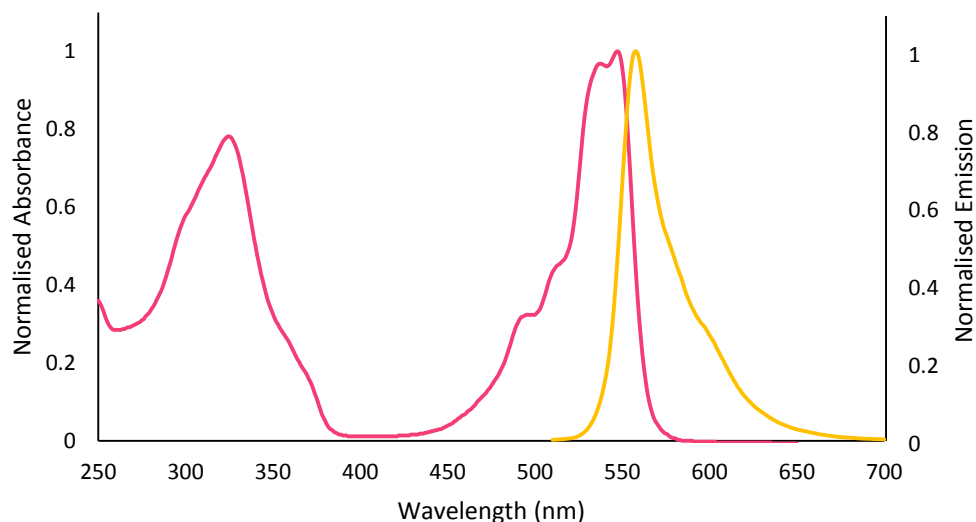


**Figure 91.** Absorption and Emission spectrum of SubTBDAP-OMe **133**.

A summary of some properties of SubTBDAP such as absorption maxima of Q and B bands, molar extinction coefficients and Stokes Shifts is illustrated in Table 6. SubTBDAP hybrids represent the smallest structural difference to a subphthalocyanine, which is reflected in their very similar absorption and emission maxima. However, both bands are blue-shifted around 10-20 nm compared to SubPc indicating the change towards more subporphyrin-like character in the hybrids, this blue-shift is also indicative that the *meso*-phenyl ring does not contribute to the main  $\pi$ -system, lying as demonstrated with the crystal structures perpendicular to the core.

SubTBDAP hybrids show a Soret band with extinction coefficients of  $\sim 3.9 \times 10^4 \text{ M}^{-1} \text{ cm}^{-1}$ , this value is more similar to the ones obtained for SubPcs ( $\sim 2.5 \times 10^4 \text{ M}^{-1} \text{ cm}^{-1}$ ) than the extinction coefficients of *meso*-aryl tribenzosubporphyrins  $\sim 16 \times 10^4 \text{ M}^{-1} \text{ cm}^{-1}$  that are similar to the intense Soret bands of porphyrins. The  $\epsilon$  values of the Q bands of SubTBDAP hybrids range from 5.19 to  $6.72 \times 10^4 \text{ M}^{-1} \text{ cm}^{-1}$  similar to those of SubPcs that are generally  $5\text{-}6 \times 10^4 \text{ M}^{-1} \text{ cm}^{-1}$ .

SubTBDAP	Apical, <i>meso</i> - aryl	Abs Q $\lambda_{\text{max}}$	$\epsilon$ (Q) ( $10^4$ )	Abs B $\lambda_{\text{max}}$	$\epsilon$ (B) ( $10^4$ )	Em $\lambda_{\text{max}}$	Stokes Shift (nm)
<b>134</b>	OPh, –	548	5.57	324	3.96	559	11
<b>133</b>	OMe, –	547	5.97	324	4.61	558	11
<b>139</b>	O <i>i</i> Pr, –	547	5.19	325	3.98	558	11
<b>140</b>	OBu, –	547	4.85	325	3.74	558	11
<b>146</b>	OMe, OMe	548	5.48	322	3.49	558	10
<b>147</b>	OPh, <i>n</i> pentyl	549	5.86	327	3.89	559	10
<b>148</b>	OPh, OMe	549	5.25	315	3.41	559	10
<b>149</b>	OPh, CF <sub>3</sub>	547	6.72	323	4.64	559	12

**Table 6.** Summary of optical properties of SubTBDAPs where the units for  $\lambda_{\text{max}}$  are nm, and for  $\epsilon$  are ( $\text{M}^{-1} \text{ cm}^{-1}$ ).

The fluorescence quantum yield ( $\Phi_F$ ) of a fluorophore is the ratio of fluorescence photons emitted to photons absorbed per time unit, and it is an important physical characteristic of molecules that might be used in diverse fields such as chemistry, physics, biology or medicine. One of the most common ways to determine this parameter is measuring the efficiency of the fluorescence process relative to that of a standard solution. Rhodamine B was chosen as fluorescence standard because it presents similar UV-Vis absorption and fluorescence maxima to the new compounds (see Fig. 92), and its quantum yield is well known (0.69 in MeOH)<sup>[184]</sup>.

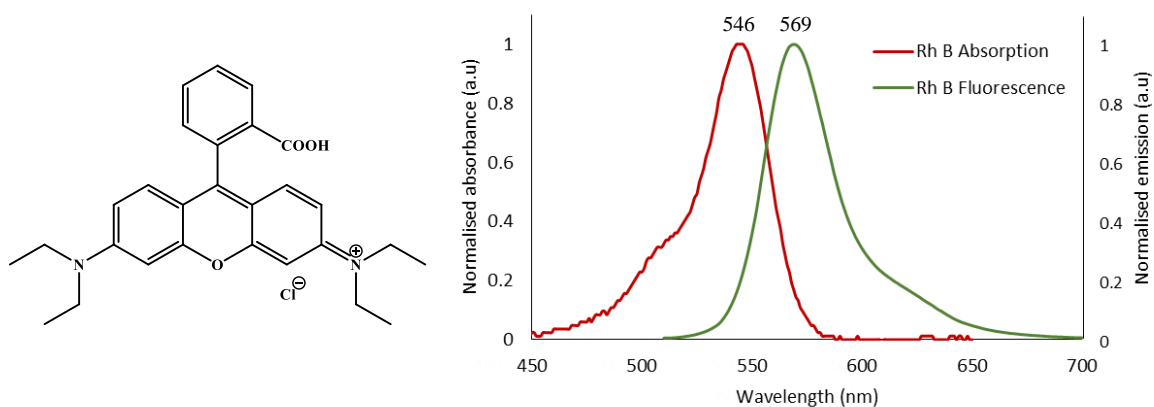


**Figure 92.** Structure Rhodamine B and absorption and emission spectrum in MeOH.

The fluorescence quantum yield values of SubTBDAPs were measured in DCM, due to good solubility of the compounds in this solvent. An excitation wavelength of 500 nm was chosen to obtain the emission spectra of each compound, since both standard and unknown samples show almost identical absorbance at this wavelength. Spectra were recorded under aerobic conditions. The  $\Phi_F$  values were calculated using equation:

$$\Phi_u = \Phi_s \left( \frac{IA_u}{IA_s} \right) \left( \frac{\eta_u^2}{\eta_s^2} \right)$$

Where  $\Phi$  is the quantum yield, IA the integrated area under the emission curve,  $\eta$  the refractive index of the solvents, and  $u$  and  $s$  are the subscripts used to refer to the unknown and the standard, respectively.

This technique allowed determination of the relative quantum yields of all SubTBDAP hybrids synthesised as ca. **0.45** (Table 7). This is a relative high value considering that  $\Phi_F$  of SubPc range from 0.1 to 0.5,<sup>[30]</sup> and 0.13-0.35 for subporphyrins.<sup>[161]</sup> The only reported value for benzosubporphyrins is 0.41 for BzSubP-OH **112**,<sup>[166]</sup> which is lower but very close to the ones obtained for the new hybrids.

Name	SubTBDAP n.	$\Phi_F$
SubTBDAP-OPh	<b>134</b>	0.44
SubTBDAP-OMe	<b>133</b>	0.43
SubTBDAP-O <i>i</i> Pr	<b>139</b>	0.43
SubTBDAP-OBu	<b>140</b>	0.45
OMe-SubTBDAP-OMe	<b>146</b>	0.44
<i>n</i> pe-SubTBDAP-OPh	<b>147</b>	0.44
OMe-SubTBDAP-OPh	<b>148</b>	0.45
CF <sub>3</sub> -SubTBDAP-OPh	<b>149</b>	0.37

**Table 7.** Fluorescence quantum yields obtained for SubTBDAP hybrids.

### Nuclear magnetic resonance

Boron NMR spectra of hybrids exhibit a singlet around -14.7 ppm. This value is very similar to the ones reported for benzosubporphyrins and subporphyrins (-14.6 to -16.2 ppm),<sup>[30]</sup> but less shielded than those generally obtained for subphthalocyanines that appear in the range of -17.7 to -19.6 ppm.<sup>[32]</sup>

Table 8 illustrates the values obtained in <sup>11</sup>B-NMR spectroscopy for SubTBDAP hybrids. All SubTBDAPs with a phenoxy-group at the apical position and a different substitution in the *meso*-site (**134**, **147**, **148** and **149**) show the signal at ca. -14.6 ppm, therefore such *meso*-functionalisation seems not to have a noticeable influence on the chemical shifts. However, the effect of the axial substituent is more perceptible; for instance, SubTBDAP-OMe **133** exhibit a chemical shift of -14.45 ppm or  $\delta = -14.85$  ppm in case of SubTBDAP-O*i*Pr **139**. Identical chemical shift (-14.66 ppm) is observed when aliphatic chains are either at the apical or in the *meso*-position for SubTBDAP-OBu **140** and *n*pe-SubTBDAP-OPh **147**.

SubTBDAP	Apical, <i>meso</i>	<sup>11</sup> B-NMR (ppm)
<b>134</b>	OPh, –	-14.67
<b>133</b>	OMe, –	-14.45
<b>139</b>	O <i>i</i> Pr, –	-14.85
<b>140</b>	OBu, –	-14.66
<b>146</b>	OMe, OMe	-14.44
<b>147</b>	OPh, <i>n</i> pentyl	-14.66
<b>148</b>	OPh, OMe	-14.65
<b>149</b>	OPh, CF <sub>3</sub>	-14.67

**Table 8.** <sup>11</sup>B-NMR chemical shifts of some SubTBDAP hybrids.

As already discussed in section 3.2.3.2, <sup>1</sup>H-NMR spectroscopy of SubTBDAPs shows sharp signals except for the *ortho*- and *meta*- protons of the *meso*-phenyl ring which are very broad and



featureless, indicating slow rotation of the group. It has been demonstrated that lowering the temperature leads to sharpening and resolution of the signals (see page 102). Thanks to VT NOESY and COSY, protons facing the same side of the macrocycle could be assigned. However, the identification of the protons facing either the concave or the convex face had failed by means of VT NOESY due to the lack of NOE effect between the phenoxy-group on top and the meso-ring, as previously discussed. More VT experiments were subsequently carried out with the functionalised SubTBDAP hybrids herein synthesised, but no significant spatial interaction effects were noticed and the results remained inconclusive. However, the availability of a range of hybrids allowed comparisons of their spectra.

Significant chemical shift difference is observed for the two doublets corresponding to the *ortho*-hydrogen atoms ( $\Delta\delta \sim 1.4$  ppm) reflecting the different influence of the core ring current; a  $\Delta\delta \sim 0.4$  ppm is observed for the *meta*- protons. Figure 94 illustrates a comparison VT  $^1\text{H-NMR}$  spectra of some SubTBDAP hybrids based on their axial and *meso*-substitution at 263K.

It was recognised that the Ho protons lying on the same side as the apical alkoxide- would be more likely to suffer changes in chemical shift. Experimentally Ho' appear to be more sensitive to interchange of the apical alkoxide- substituent, since the proton shifts quite dramatically in the range of 8.2–8.6 ppm (see Fig. 94). However, the resonance for Ho exhibit approximately the same chemical shift (6.9 ppm) in all cases. Based on this evidence, we have assigned Ho' and Hm' to be the protons lying on the same side as the alkoxide-, and Ho and Hm the protons lying under the conical macrocycle. See Figure 93 for assignment of all *meso*- protons regarding the curvature of the hybrid.

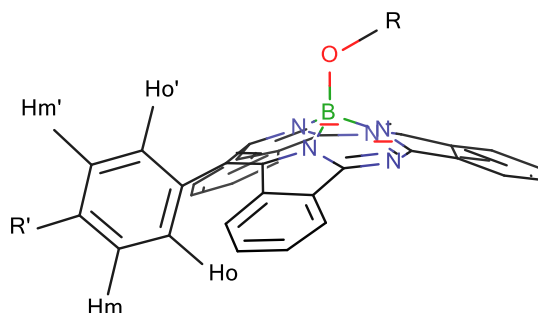


**Figure 93.** General R'-SubTBDAP-OR showing the assignment of the *meso*-protons regarding the shape of the hybrid.

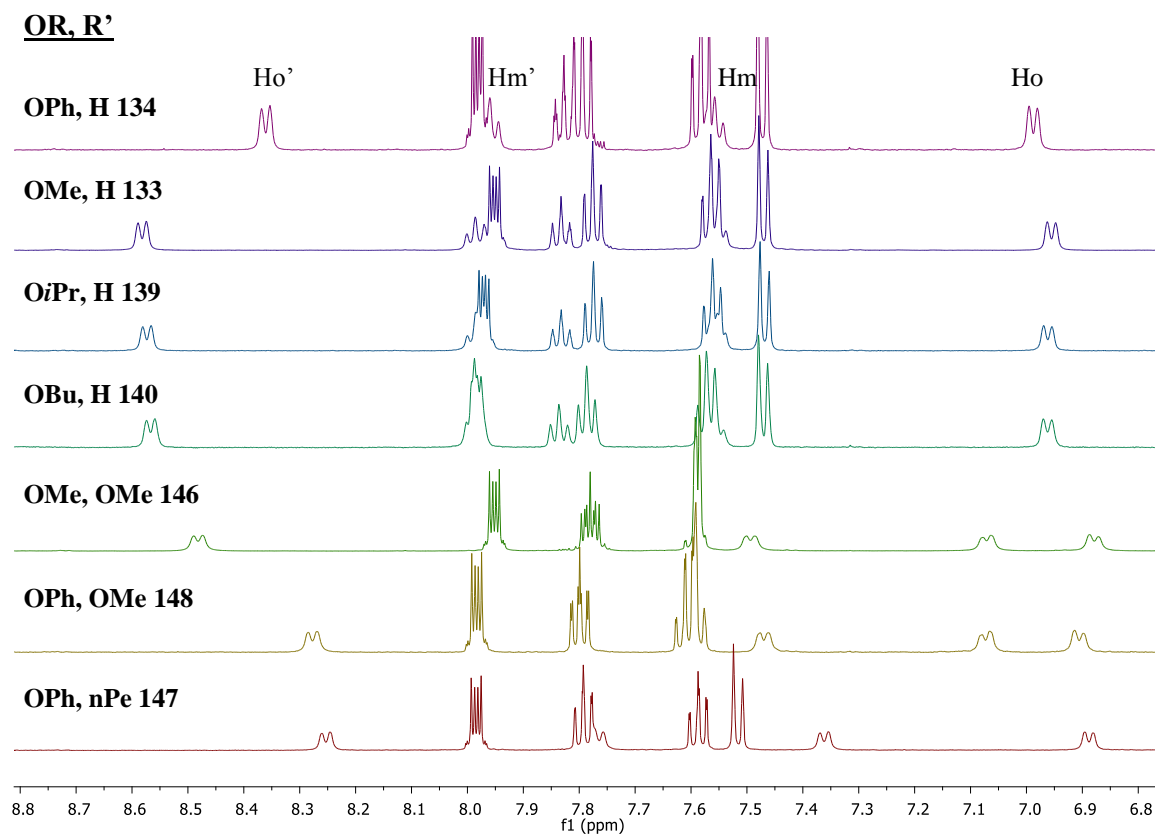


**Figure 94.** VT  $^1\text{H}$ -NMR comparison of SubTBDAP hybrids in  $\text{CD}_2\text{Cl}_2$  at 263K. The legend describes the substitution of the molecule (axial, *meso*) and the number of compound.

These results are in agreement with the experiments reported by Osuka and Inokuma.<sup>[185]</sup> They prepared a series of capped subporphyrins to study the encapsulation of solvent molecules. Subporphyrin **154** depicts a curved shape structure similar to the one obtained for SubTBDAP hybrids as it can be observed from its crystal structure (Fig. 95). They successfully assigned the protons at the *meso*-sites by means of NOESY experiments, whereby  $\text{H}^a$  and  $\text{H}^e$  featured very strong through-space proton correlations. Thereby they postulated that  $\text{H}^e$  is the proton located in the concave side of the subporphyrin macrocycle; this proton is the one located at lower chemical shift.

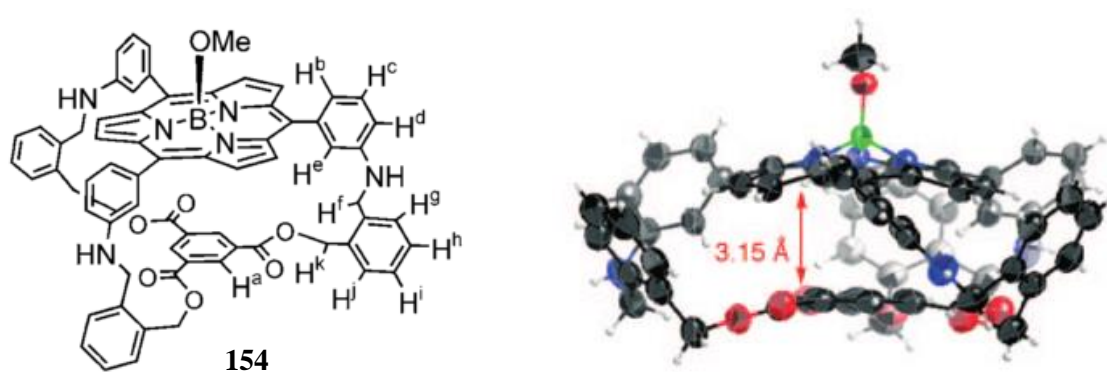


**Figure 95.** Structure of capped subporphyrin **154** and its crystal structure.<sup>[185]</sup>

### DFT Calculations

The assignment was further supported by density functional theory (DFT) calculations, the chemical shifts of protons in compound SubTBDAP-OMe **133** were computed at the BP86-D3/def2-SVP level of theory. Calculated ppm values for the *meso*-phenyl substituent protons are 6.78 for *ortho*-proton facing the concave side of the macrocycle; 7.97 for the *ortho*-proton facing the axial substituent side of the macrocycle; 7.07 for the *meta*-proton facing the cavity side of the macrocycle; 7.44 for the *meta*-proton facing the axial substituent side of the macrocycle; and 7.26 for the *para*-proton, the values are represented in red in Figure 96.

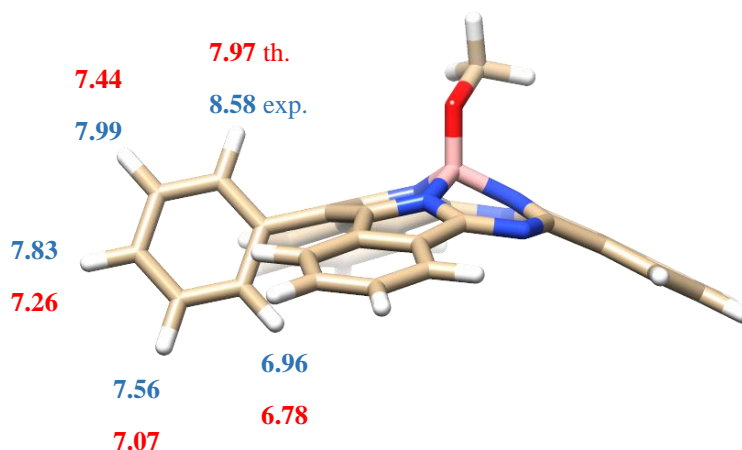


**Figure 96.** Theoretical chemical shift values calculated by DFT performed on SubTBDAP-OMe **133** (red), and experimental values (blue).

It is important to notice that this calculation does not take into account the solvent effect, therefore the exact values will be somehow displaced, but it is assumed that would affect all signals almost equally. The experimentally observed NMR values for the *ortho*-protons are 6.96 and 8.58 ppm, 7.56 and 7.99 ppm for *meta*-protons and 7.83 ppm for the *para*-proton (Figure 96, blue values), supporting our assignments based on sensitivity to apical substituent.

### 3.2.5 Conclusions

The first examples of a new class of hybrid system, SubTriBenzoDiAzaPorphyrin (SubTBDAP) are reported. The framework lies between the parent structures subphthalocyanine and benzosubporphyrins. The first tests yielded SubTBDAP-Cl in a macrocyclisation reaction with boron trichloride as template, attempts to isolate and characterise the new product were unsuccessful due to the labile B-Cl bond. This drawback was overcome converting the apical position into a stable B-O moiety treating the crude mixture with an excess of phenol in a two step, one pot reaction. The SubTBDAP-OPh product could be isolated as a bright pink material with yellow fluorescence, in an impressive 15% yield.

The symmetry reduction compared to SubPcs and benzoSubPs is noticeable in the split of the Q band in the UV-Vis spectrum. Both absorbance and emission maxima are blue-shifted by

approximately 10-20 nm compared to those of subphthalocyanine indicating the change towards more subporphyrin-like character in the hybrids. Extinction coefficients are similar to those obtained for SubPcs. The new hybrids exhibit high fluorescence quantum yields of ca. 0.5.

$^1\text{H-NMR}$  spectroscopy of SubTBDAPs show sharp signals for all protons in the molecule, except for the *ortho*- and *meta*- protons located on the *meso*-phenyl ring due to the slow rotation of the group. The rotation dynamics of the *meso*-group were investigated by variable temperature  $^1\text{H-NMR}$  spectroscopy experiments. It has been demonstrated that lowering the temperature leads to sharpening and resolution of all signals.

X-Ray analysis allowed full elucidation of the macrocyclic structure. The curvature of the molecule was confirmed to be very similar to those observed for subporphyrinoids, the *meso*-phenyl ring is essentially lying almost perpendicular to the core in the solid-state.

The synthesis involving  $\text{BCl}_3$  has a competing process where the symmetric SubPc is obtained as major product. The reaction conditions were optimised by changing the boron source to less reactive borate ( $\text{B(OR)}_3$ ) templates. The new optimised protocol is straightforward and reproducible. The synthetic versatility and scope allows introduction of different functionalities at the apical position, but most importantly, at the new-*meso* site at will. Although purification processes are challenging highly pure materials are always obtained, allowing full characterisation of this new family of macrocycles. Yields are marginally lower (7-12%) than for the stepwise procedure but compensated by synthetic convenience and versatility.

Full assignment of protons in the macrocyclic core was achieved by careful analysis of VT experiments. However, the protons located in the *meso*-phenyl substituent are seen as four distinctive signals subjected to the strong SubTBDAP shielding cone. As a result, a large chemical shift difference was observed for the *ortho*-protons that were assigned based on sensitivity to apical substituent. In essence, protons lying on the convex face of the macrocycle appear less shielded than those accommodated at the concave face. The assignment was further supported by DFT calculations.

These results open endless possibilities towards the controlled synthesis of novel SubTBDAP hybrid structures. The versatility of the protocol allows tailoring of the properties at will for the design of unique materials.

## CHAPTER 4. EXPERIMENTAL

### 4.1 General Methods

Reagents and solvents were purchased from commercial sources and used without further purification, with the following exceptions: phthalonitrile was recrystallized from hot xylene, recrystallisations were performed using distilled solvents. IR spectra were recorded using a Perkin-Elmer Spectrum BX FT-IR spectrometer.  $^1\text{H}$ ,  $^{13}\text{C}$ ,  $^{11}\text{B}$ ,  $^{19}\text{F}$ -NMR spectra were recorded at 500.1 or 400.1 (as indicated), 125.7 (or 100.6), 160.5 and 470.4 MHz, respectively, using a Bruker Ascend<sup>TM</sup> 500 or an Ultrashield Plus<sup>TM</sup> 400 spectrometer. The residual solvent peaks were used as references in the case of  $^1\text{H}$  and  $^{13}\text{C}$ , and the instrument calibrated with external references such as  $\text{BF}_3\cdot\text{OEt}_2$  for  $^{11}\text{B}$ -NMR and  $\text{CFCl}_3$  for  $^{19}\text{F}$ -NMR.

Spectra of SubTBDAPs are of recrystallised samples (distilled dichloromethane/distilled petroleum ether). 2D COSY, NOESY and ROESY experiments were used to assist with the NMR spectroscopy assignments. Microwave reactions used a Biotage Initiator 2.5 reactor (400W) equipped with an external temperature sensor. Thin layer chromatography (TLC) was carried out on aluminium sheets coated with silica gel 60 F252 (Merck), with visualization by UV light and by charring with 0.1% ninhydrin in EtOH when necessary. Column chromatography was carried out on silica gel Davisil<sup>®</sup> LC60A 40-63 micron (Grace GmbH & Co). MALDI-TOF mass spectra were obtained using a Shimadzu Biotech Axima instrument. High resolution mass spectrometry was performed by the ESPRC UK National Mass Spectrometry Service Centre at Swansea. UV-Vis and emission spectra were recorded at room temperature on a Hitachi U-3000 spectrophotometer and on a Hitachi F-4500 fluorescence spectrophotometer, respectively. Melting points were measured using a Reichert ThermoVar microscope with a thermopar based temperature control. X-Ray crystallography data was collected and analysed by Dr Simon J. Coles and Dr Graham J. Tizzard at the UK National Crystallography Service at Southampton and by Dr David Hughes at UEA.

### 4.2 Fluorescence Quantum Yield

The fluorescence quantum yield ( $\Phi_F$ ) values of SubTBDAPs were measured in DCM, due to good solubility of the compounds in this solvent. The measurements were performed under air conditions. The QY were determined using as fluorescence standard Rhodamine B in MeOH,<sup>[184]</sup> it presents a similar UV-Vis absorption and fluorescence maxima to the new compounds.  $\lambda_{\text{exc}} = 500 \text{ nm}$  was chosen to obtain the emission spectra of each compound, since both standard and unknown compounds show the same absorbance at this wavelength. The  $\Phi_F$  values were calculated using equation 1:

$$\Phi_u = \Phi_s \left( \frac{IA_u}{IA_s} \right) \left( \frac{\eta_u^2}{\eta_s^2} \right)$$

Where  $\Phi$  is the quantum yield, IA the integrated area under the emission curve,  $\eta$  the refractive index of the solvents, and  $u$  and  $s$  are the subscripts used to refer to the unknown and the standard, respectively.

### 4.3 General Procedures for the Synthesis of Subphthalocyanines

#### General procedure A for the synthesis of chloro-subphthalocyanines

Phthalonitrile (1.5 eq) was placed in a 2-necked round bottomed flask, 30 mL (per 8.2 mmol used of phthalonitrile) of anhydrous *p*-xylene were added and the mixture was stirred under inert atmosphere until everything dissolved. BCl<sub>3</sub> (5.5mL, 1M in *p*-xylene, 1eq) was then added dropwise and the reaction mixture was heated up to 140 °C gently over a period of 30 minutes, and subsequently heated for further 3.5 hours or until completion. The reaction mixture was cooled down and subjected to the purification process specified for each compound.

#### General procedure B for the synthesis of axially-substituted subphthalocyanines

SubPc-Cl **16** (1 eq) and an excess of phenol (or derivative) (5 eq) were placed in a round bottomed flask and were dissolved in toluene (3 mL). The mixture was refluxed under inert atmosphere until completion (27-48 hours). The reaction mixture was then cooled down to room temperature, and the resultant solid was dissolved in dichloromethane (75 mL) and extracted with water (3x100 mL). The organic layer was dried over MgSO<sub>4</sub>, filtered and the solvent evaporated.). Sometimes the resultant product required to be washed with cold methanol, followed by cold hexane and filtered.

#### General procedure C for the Sonogashira-Hagihara cross-coupling reactions for the synthesis of subphthalocyanines

The haloaryl (1 eq) was mixed with the alkyne (3 eq or 6 eq as indicated), Pd catalyst (0.03 eq per coupling reaction) and CuI (0.03 eq per coupling reaction) in freshly distilled NEt<sub>3</sub> (5 mL, unless specified). The suspension was stirred at room temperature (unless heating is specified) under inert atmosphere, the reaction was monitored by TLC until completion. After that time the reaction mixture was cooled to room temperature (if applicable) and the solvent evaporated under reduced pressure. The crude material was dissolved in ethyl acetate (50 mL) and extracted with water (3x75 mL). The organic layer was dried over Mg<sub>2</sub>SO<sub>4</sub>, filtered and the solvent evaporated. The resultant product was purified as specified in each compound.

\* In some cases pyridyl-substituted subphthalocyanines required a further extraction with a solution of EDTA in water to remove copper coordination with the nitrogen ligands, thereby obtaining sharp and clearer peaks in the <sup>1</sup>H-NMR spectrum.

### General procedure D for alkynol group deprotection

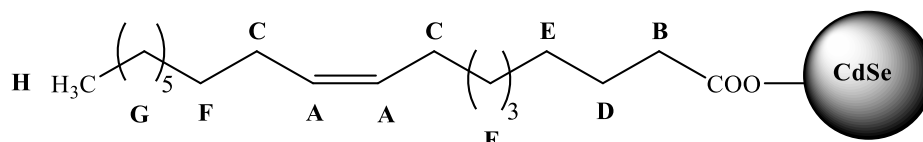
A mixture of the alkynol-derivative (1 eq) and sodium hydroxide (3 eq, unless otherwise specified) in dry toluene were stirred at room temperature (unless otherwise specified), and the reaction was monitored by TLC. When completed, the solvent was evaporated and the resultant residue was dissolved in dichloromethane (50 mL) and extracted with water (3x75 mL). The organic layer was dried over MgSO<sub>4</sub>, filtered and the solvent evaporated. The residue was purified as specified for each compound.

### General procedure E for the Suzuki-Miyaura cross-coupling reactions

CsF (6 or 9 eq) was placed in a sealable tube connected to vacuum, the solid was heated up with a heat gun to remove any possible water present due to the hygroscopic nature of the reagent. The haloSubPc (1 eq), the boronic acid derivative (6 or 9 eq), PdCl<sub>2</sub>(dppf) (0.09 eq) and were then introduced. The system was purged and refilled with N<sub>2</sub> or Ar three times and dry DME was added. The mixture was sonicated and degased before heating it in an oil bath for (4-23 h). The reaction was monitored by TLC. After completion, the mixture was cooled, diluted with ethyl acetate (50 mL), and was extracted with water (3x75 mL). The organic layer was dried over Mg<sub>2</sub>SO<sub>4</sub>, filtered and the solvent evaporated. The resultant product was further purified as specified for each compound.

## 4.4 Experimental Details and Characterisation: SubPcs-CdSe conjugation project

### Oleic acid capped CdSe QDs



A mixture of cadmium oxide (301 mg, 2.34 mmol) and oleic acid (2 mL) in octadecene (20 mL) was stirred under vacuum for 10 minutes. Nitrogen was then added and the solution was heated to 250 °C. The mixture was heated at this temperature until a clear solution was obtained. The mixture was left to cool down below 100 °C. Selenium powder (100.1 mg) was subsequently added, and the mixture was re-heated to 240 °C monitoring the temperature with a thermometer introduced in the solution. At first the solution was grey, but it changes colour progressively from yellow to orange. The progress and size of the nanoparticles were monitored by taking aliquots from the reaction mixture and checking the colour under the UV lamp (irradiated at 365 nm). When the required size of nanoparticles was obtained, the reaction was immediately cooled down, first using a water bath and then an ice-bath. Toluene (10 mL) was then added. The solution was transferred to two large centrifuge tubes with filtration (syringe filter – 0.20 μL). The volume of both tubes was adjusted to 30 mL with toluene and 20 mL of acetone were added. The formation of a white precipitate of unreacted material instantly crashed out, the tubes were placed into an ice bath to aid



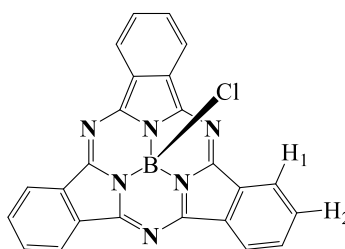
the complete precipitation. The tubes were after that centrifuged (4000 rpm, 4 min), the orange solutions were collected and the white precipitates discarded. The solutions were placed in another two centrifuged tubes (containing approximately 25 mL each). The same amount of methanol was added to it followed by centrifugation. An orange oil was formed at the bottom which was collected and combined in a single tube. After which methanol (25 mL) and toluene (25 mL) were added and the mixture centrifuged. The clear solution at the top was discarded and the oil was transferred into a small tube, and hexane (7 mL) and isopropanol (7 mL) were subsequently added followed by centrifugation. The top solution was once again discarded and isopropanol (14 mL) was added now, the solution sonicated for 30 minutes and then centrifuged. This step was repeated several times until a free flowing powder was obtained.

**<sup>1</sup>H-NMR** (500 MHz, CDCl<sub>3</sub>, 298 K):  $\delta$  (ppm) = 5.33 (br s, 2H, H<sub>A</sub>), 2.01 (br s, 4H, H<sub>C</sub>), 1.72 (br s, 2H, H<sub>D</sub>), 1.26 (br s, 20H, H<sub>E</sub>, H<sub>F</sub>, H<sub>G</sub>), 0.88 (br s, 6H, H<sub>B</sub>, H<sub>H</sub>).

**UV-Vis** (CH<sub>2</sub>Cl<sub>2</sub>):  $\lambda$  max (nm) = 512 nm.

**Fluorescence** (dist. CH<sub>2</sub>Cl<sub>2</sub>, Excitation at 350 nm): 526 nm.

### Subphthalocyanine-Cl<sup>[186]</sup> (16)



Synthesised following general procedure A from phthalonitrile (1.05 g, 8.21 mmol, 1.5 eq), BCl<sub>3</sub> (5.5 mL, 1 eq) in p-xylene (30 mL). Reaction time: 3.5 hours. The reaction mixture was cooled down and transferred to a bigger flask with the aid of toluene, the solvent was then evaporated under reduced pressure. The resultant crude product was placed in the vacuum overnight to ensure complete dryness of the sample, after which it was introduced in the thimble of a Soxhlet extractor and washed with cold methanol. The remaining solid was extracted into chloroform using the Soxhlet apparatus for 7 hours or until almost colourless washings were observed. Chloroform was subsequently evaporated allowing the isolation of the pure *title compound* as a brown-golden solid (0.483 g, 41%).

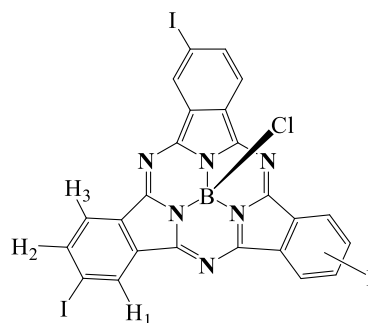
**<sup>1</sup>H-NMR** (500 MHz, CDCl<sub>3</sub>, 298 K):  $\delta$  (ppm) = 8.93 – 8.88 (m, 6H, H<sub>1</sub>), 7.98 – 7.94 (m, 6H, H<sub>2</sub>).

**MS** (MALDI-TOF):  $m/z$  = 430.30 [M]<sup>+</sup>

**UV-Vis** (dist. CH<sub>2</sub>Cl<sub>2</sub>):  $\lambda$  max (nm) = 564, 304.

**Fluorescence** (dist. CH<sub>2</sub>Cl<sub>2</sub>, Excitation at 500 nm): 577 nm.



**I-Subphthalocyanine-Cl<sup>[187]</sup> (20)**

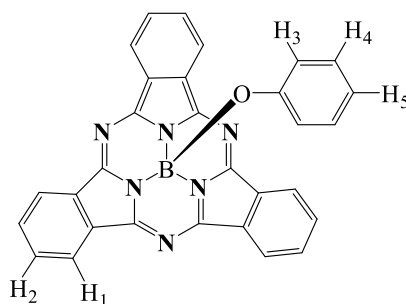
Synthesised following general procedure A from 4-iodophthalonitrile (1.50 g, 5.91 mmol, 1.5 eq), BCl<sub>3</sub> (3.9 mL, 1eq) in *p*-xylene (21.5 mL). Reaction time: 4 hours. The mixture was cooled down to room temperature and the solvent evaporated under reduce pressure, the resultant crude was left to dry under vacuum. The resultant solid was washed first with cold methanol and then with cold hexane, followed by filtration. The *title compound* was isolated as dark purple solid (1.43 g, 90%).

**<sup>1</sup>H-NMR** (500 MHz, CDCl<sub>3</sub>, 298 K): δ (ppm) = 9.25 (d, 3H, *J* = 0.6 Hz, H<sub>1</sub>), 8.61 – 8.57 (m, 3H, H<sub>3</sub>), 8.27 – 8.24 (m, 3H, H<sub>2</sub>).

**MS** (MALDI-TOF): *m/z* = 808.01 [M]<sup>+</sup>

**UV-Vis** (dist. CH<sub>2</sub>Cl<sub>2</sub>): λ max (nm) = 572, 271.

**Fluorescence** (dist. CH<sub>2</sub>Cl<sub>2</sub>, Excitation at 500 nm): 583 nm.

**Subphthalocyanine-OPh<sup>[188]</sup> (21)**

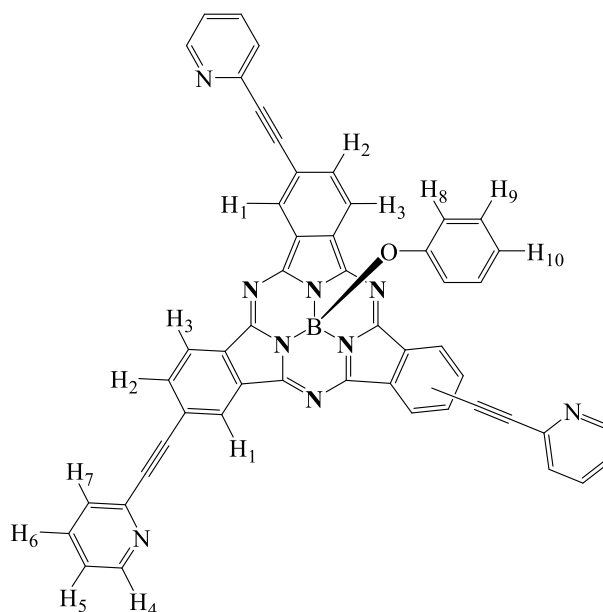
Product formed during the synthesis of SubTBDAP derivatives and characterised as follows:

**<sup>1</sup>H-NMR** (500 MHz, CDCl<sub>3</sub>, 298 K): δ (ppm) = 8.95 – 8.77 (m, 6H, H<sub>1</sub>), 8.03 – 7.82 (m, 6H, H<sub>2</sub>), 6.75 (t, 2H, *J* = 7.5 Hz, H<sub>4</sub>), 6.62 (t, 1H, *J* = 7.5 Hz, H<sub>5</sub>), 5.39 (d, 2H, *J* = 7.5, H<sub>3</sub>).

**MS** (MALDI-TOF): *m/z* = 488.31 [M]<sup>+</sup>

**UV-Vis** (dist. CH<sub>2</sub>Cl<sub>2</sub>): λ max (nm) = 562, 305, 267.

**Fluorescence** (dist. CH<sub>2</sub>Cl<sub>2</sub>, Excitation at 500 nm): 575 nm.

**(2-Pyridyl)<sub>3</sub>-SubPc-OPh<sup>[103]</sup> (34)**

Synthesised following general procedure C for Sonogashira cross-coupling reaction from I-SubPc-OPh **41** (73.7 mg, 0.0857 mmol, 1eq), 2-ethynylpyridine **45** (50  $\mu$ L, 0.511 mmol, 6 eq), PdCl<sub>2</sub>(dppf) (6.7 mg, 7.7x10<sup>-3</sup> mmol, 0.09 eq) and CuI (1.5 mg, 7.7x10<sup>-3</sup> mmol, 0.09 eq) in NEt<sub>3</sub>, the reaction mixture was heated at 70 °C for 7 hours. After work up, the residue was purified by column chromatography in silica gel using EtOAc /PE (1:1) then 100% EtOAc as solvent gradient. Recrystallisation from dichloromethane / hexane gave pure *title compound* as a dark purple solid (33.8mg, 50%).

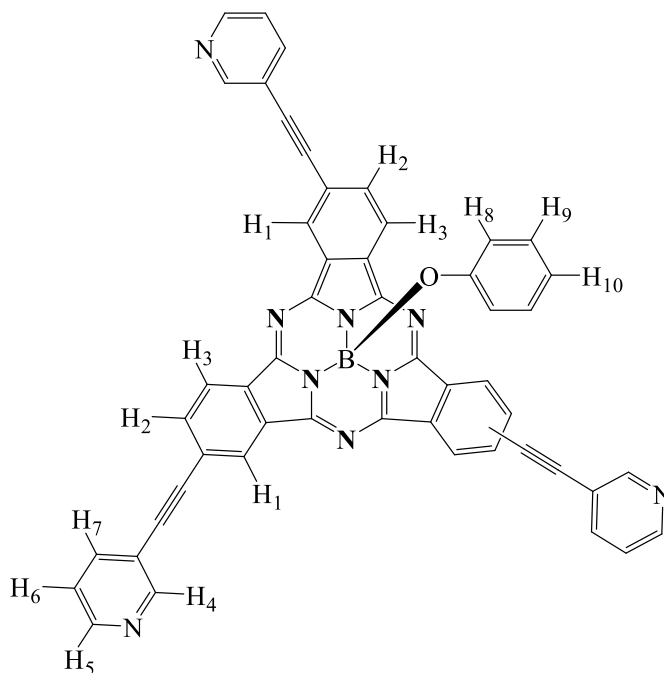
<sup>1</sup>H-NMR (500 MHz, CDCl<sub>3</sub>, 298 K):  $\delta$  (ppm) = 9.07 (s, 3H, H<sub>1</sub>), 8.81 (d, 3H,  $J$  = 8.1 Hz, H<sub>3</sub>), 8.68 (d, 3H,  $J$  = 4.4 Hz, H<sub>4</sub>), 8.10 (d, 3H,  $J$  = 8.1 Hz, H<sub>2</sub>), 7.75 (t, 3H,  $J$  = 7.6 Hz, H<sub>6</sub>), 7.64 (dd, 3H,  $J$  = 7.6, 4.4 Hz, H<sub>7</sub>), 7.33 – 7.28 (m, 3H, H<sub>5</sub>), 6.78 (t, 2H,  $J$  = 7.6 Hz, H<sub>9</sub>), 6.65 (t, 1H,  $J$  = 7.6 Hz, H<sub>10</sub>), 5.42 (d, 2H,  $J$  = 7.6 Hz, H<sub>8</sub>).

<sup>11</sup>B-NMR (160.5 MHz, CDCl<sub>3</sub>, 298 K):  $\delta$  (ppm) = -14.60 (s, 1B).

MS (MALDI-TOF):  $m/z$  = 792.79 [M+H]<sup>+</sup>

UV-Vis (dist. CH<sub>2</sub>Cl<sub>2</sub>):  $\lambda$  max (nm) = 586, 261.

Fluorescence (dist. CH<sub>2</sub>Cl<sub>2</sub>, Excitation at 500 nm): 598 nm.

**(3-Pyridyl)<sub>3</sub>-SubPc-OPh<sup>[103]</sup> (35)**

Synthesised following general procedure C for Sonogashira cross-coupling reaction from I-SubPc-OPh **41** (106 mg, 0.122 mmol, 1eq), 3-ethynylpyridine **46** (77.1 mg, 0.733 mmol, 6 eq), PdCl<sub>2</sub>(PPh<sub>3</sub>)<sub>2</sub> (7.7 mg, 0.011 mmol, 0.09 eq) and CuI (2.1 mg, 0.01 mmol, 0.09 eq) in NEt<sub>3</sub>. The reaction mixture was heated at 50 °C for 9 hours. After work up, the residue was purified by column chromatography in silica gel using 100% EtOAc as solvent eluent. Recrystallisation from dichloromethane / hexane gave pure *title compound* as a dark purple solid (62.8 mg, 65%).

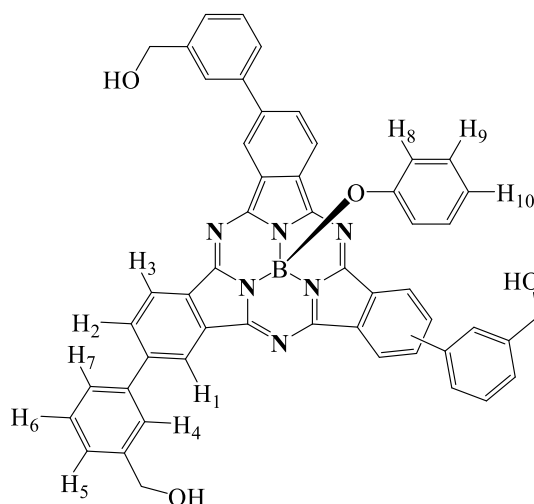
**<sup>1</sup>H-NMR** (500 MHz, CDCl<sub>3</sub>, 298 K): δ (ppm) = 9.03 (d, 3H, *J* = 4.9, H<sub>1</sub>), 8.87 (br s, 3H, H<sub>4</sub>), 8.84 – 8.79 (m, 3H, H<sub>3</sub>), 8.61 (d, 3H, *J* = 4.7 Hz, H<sub>5</sub>), 8.05 (d, 3H, *J* = 8.2 Hz, H<sub>2</sub>), 7.91 (d, 3H, *J* = 7.8 Hz, H<sub>7</sub>), 7.35 (dd, 3H, *J* = 7.8, 4.7 Hz, H<sub>6</sub>), 6.79 (t, 2H, *J* = 7.8 Hz, H<sub>9</sub>), 6.66 (t, 1H, *J* = 7.8 Hz, H<sub>10</sub>), 5.43 (d, 2H, *J* = 7.8 Hz, H<sub>8</sub>).

**<sup>11</sup>B-NMR** (160.5 MHz, CDCl<sub>3</sub>, 298 K): δ (ppm) = -14.63 (s, 1B).

**MS** (MALDI-TOF): *m/z* = 792.79 [M]<sup>+</sup>

**UV-Vis** (distilled CH<sub>2</sub>Cl<sub>2</sub>): λ max (nm) (ε (dm<sup>3</sup>·mol<sup>-1</sup>·cm<sup>-1</sup>)) = 586, 297.

**Fluorescence** (distilled CH<sub>2</sub>Cl<sub>2</sub>, Excitation at 500 nm): 599 nm.

**(Ph-CH<sub>2</sub>OH)<sub>3</sub>-SubPc-OPh (36)**

Synthesised following general procedure E for Suzuki cross-coupling reaction from I-SubPc-(OPh) **41** (48.3 mg, 0.0558 mmol, 1eq), 3-(hydroxymethyl)phenylboronic acid **51** (77.8 mg, 0.502 mmol, 9eq), PdCl<sub>2</sub>(dppf) (4.1 mg, 0.005 mmol, 0.09 eq), and CsF (76.3 mg, 0.502 mmol, 9 eq) in dry DME. The reaction was heated at 100 °C for 9.5 hours. The residue was purified by column chromatography in (10:1) toluene/THF to (2:1) EtOAc/PE. Recrystallisation of the product from DCM/hexane gave the pure *title compound* as dark purple solid (32.7 mg, 72%).

**Mp** 204 °C

**<sup>1</sup>H-NMR** (500 MHz, C<sub>3</sub>D<sub>6</sub>O, 298 K): δ (ppm) = 9.06 (s, 3H, H<sub>1</sub>), 8.87 (dd, 3H, *J* = 8.2, 3.9 Hz, H<sub>3</sub>), 8.32 – 8.24 (m, 3H, H<sub>2</sub>), 7.97 (s, 3H, H<sub>4</sub>), 7.82 (d, 3H, *J* = 7.4 Hz, H<sub>7</sub>), 7.56 – 7.50 (m, 3H, H<sub>6</sub>), 7.48 – 7.44 (m, 3H, H<sub>5</sub>), 6.80 (t, 2H, *J* = 7.6 Hz, H<sub>9</sub>), 6.63 (t, 1H, *J* = 7.6 Hz, H<sub>10</sub>), 5.51 (d, 2H, *J* = 7.6 Hz, H<sub>8</sub>), 4.81 (d, 6H, *J* = 5.3 Hz, -CH<sub>2</sub>), 4.74 (s, 1H, -OH), 4.69 (s, 1H, -OH), 4.42 (s, 1H, -OH).

**<sup>13</sup>C-NMR** (125.7 MHz, C<sub>3</sub>D<sub>6</sub>O, 298 K): δ (ppm) = 154.0, 152.7, 152.6, 144.6, 141.1, 141.0, 129.9, 129.8, 129.7, 127.3, 126.9, 126.6, 126.5, 123.3, 122.2, 120.7, 120.2, 118.3, 64.6, 64.5.

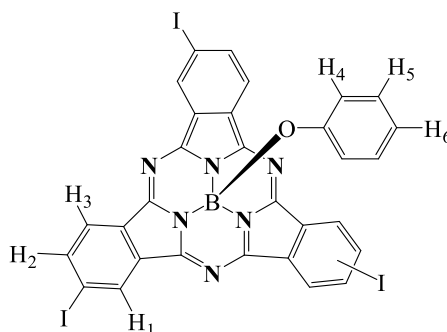
**<sup>11</sup>B-NMR** (160.5 MHz, C<sub>3</sub>D<sub>6</sub>O, 298 K): δ (ppm) = -14.33 (s, 1B).

**MS** (MALDI-TOF): *m/z* = 806.87 [M]<sup>+</sup>

**HR-MS** (FTMS + p NSI) (C<sub>51</sub>H<sub>36</sub>B<sub>1</sub>N<sub>6</sub>O<sub>4</sub>) [M+H]<sup>+</sup>: Calc.: 807.2894; Found: 807.2890.

**UV-Vis** (distilled CH<sub>2</sub>Cl<sub>2</sub>): λ max (nm) (ε (dm<sup>3</sup>·mol<sup>-1</sup>·cm<sup>-1</sup>)) = 576 (6.35·10<sup>4</sup>), 338 (3.14·10<sup>4</sup>).

**Fluorescence** (distilled CH<sub>2</sub>Cl<sub>2</sub>, Excitation at 500 nm): 588 nm

**I-Subphthalocyanine-OPh<sup>[106]</sup> (41)**

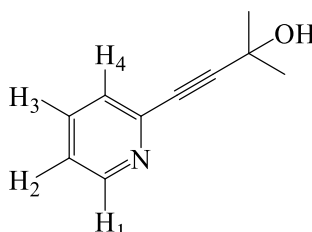
Synthesised following general procedure B from I-SubPc-Cl **20** (191.0 mg, 0.2364 mmol, 1 eq) and an excess of phenol (111.2 mg, 1.182 mmol, 5 eq). Reaction time: 27 hours. The purification process yielded the pure *title compound* as purple solid (187 mg, 91%).

<sup>1</sup>H-NMR (400 MHz, CDCl<sub>3</sub>, 298 K):  $\delta$  (ppm) = 9.19 (br s, 3H, H<sub>1</sub>), 8.57 – 8.51 (m, 3H, H<sub>3</sub>), 8.23 – 8.19 (m, 3H, H<sub>2</sub>), 6.76 (t, 2H,  $J = 7.5$  Hz, H<sub>5</sub>), 6.64 (t, 1H,  $J = 7.5$  Hz, H<sub>6</sub>), 5.35 (d, 2H,  $J = 7.5$  Hz, H<sub>4</sub>).

MS (MALDI-TOF):  $m/z = 865.91$  [M]<sup>+</sup>

UV-Vis (dist. CH<sub>2</sub>Cl<sub>2</sub>):  $\lambda$  max (nm) = 569.

Fluorescence (dist. CH<sub>2</sub>Cl<sub>2</sub>, Excitation at 500 nm): 580 nm.

**2-Methyl-4-(2-pyridyl)but-3-yn-2-ol<sup>[111]</sup> (44)**

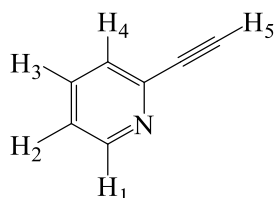
2-Bromopyridine **42** (0.6 mL, 6.26 mmol, 1 eq) was mixed with 2-methyl-3-butyn-2-ol **43** (1.58 g, 18.8 mmol, 3 eq), PdCl<sub>2</sub>(PPh<sub>3</sub>)<sub>2</sub> (0.132 g, 0.188 mmol, 0.03 eq) and CuI (0.0404 g, 0.188 mmol, 0.03 eq) in freshly distilled NEt<sub>3</sub> (10 mL). The suspension was stirred at room temperature for 6 hours under argon atmosphere. The mixture was subsequently diluted with a 1:1 mixture of DCM/H<sub>2</sub>O (20mL) and the organic layer separated, the aqueous layer was extracted with DCM (20mL) twice. The combined organic extracts were dried over MgSO<sub>4</sub>, filtered and evaporated. The resultant crude product was purified by column chromatography in 100% EtOAc giving the *title compound* as an off-white liquid (0.630 g, 62%).

<sup>1</sup>H-NMR (400 MHz, CDCl<sub>3</sub>, 298 K):  $\delta$  (ppm) = 8.62 – 8.51 (br s, 1H, H<sub>1</sub>), 7.67 – 7.60 (m, 1H, H<sub>3</sub>), 7.46 – 7.39 (m, 1H, H<sub>4</sub>), 7.25 – 7.21 (m, 1H, H<sub>2</sub>), 3.38 (br s, 1H, -OH), 1.63 (s, 6H, -CH<sub>3</sub>).

MS (MALDI-TOF):  $m/z = 162.04$  [M+H]<sup>+</sup>

**FT-IR**  $\nu_{\max}$  (NaCl)/  $\text{cm}^{-1}$ : 3289 (br O-H), 3061 (arC-H st), 2981 (C-H st), 2932 (C-H st), 2237 (C $\equiv$ C st), 1585 and 1563 (arC-C), 1465 (CH<sub>3</sub>  $\delta$  asym), 1429, 1376 and 1364 (CH<sub>3</sub>  $\delta$  sym), 1278, 1169 (C-O st), 967 (py), 912, 779 (py C-H, 2-mono-substituted).

### 2-Ethynylpyridine<sup>[111]</sup> (45)



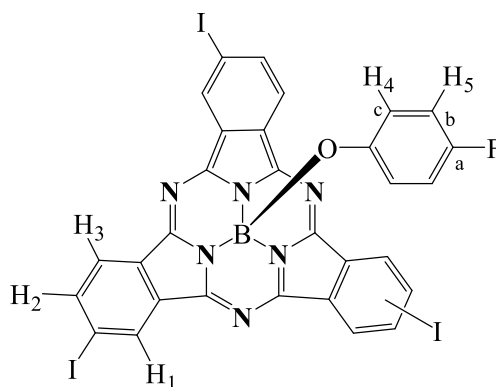
According to general procedure D 2-Methyl-4-(2-pyridyl)but-3-yn-2-ol **44** (0.617 g, 3.83 mmol, 1 eq) and sodium hydroxide (0.11 g, 2.3 mmol, 0.6 eq) were heated under reflux in toluene (15 mL) for two hours. Work up afforded pure *title compound* as a colourless liquid (0.294 g, 75%).

**<sup>1</sup>H-NMR** (400 MHz, CDCl<sub>3</sub>, 298 K):  $\delta$  (ppm) = 8.59 (br d, 1H,  $J$  = 5 Hz, H<sub>1</sub>), 7.66 (td, 1H,  $J$  = 7.7, 1.8 Hz, H<sub>3</sub>), 7.48 (dt, 1H,  $J$  = 7.7, 1.0 Hz, H<sub>4</sub>), 7.29 – 7.26 (m, 1H, H<sub>2</sub>), 3.16 (s, 1H, H<sub>5</sub>).

**MS** (MALDI-TOF):  $m/z$  = 103.99 [M+H]<sup>+</sup>

**FT-IR**  $\nu_{\max}$  (NaCl)/  $\text{cm}^{-1}$ : 3293 ( $\equiv$ C-H st), 3053 (arC-H st), 3005 (arC-H st), 2110 (C $\equiv$ C st), 1583 and 1561 (arC-C), 1462, 1428, 991 (py), 780 (py C-H, 2-mono-substituted), 740, 658 ( $\equiv$ C-H  $\delta$ ).

### I-SubPc-(4-F-OPh) (47)



Synthesised following general procedure B using I-SubPc-Cl **20** (152.1 mg, 0.1882 mmol, 1 eq) and an excess of 4-fluorophenol (105.5 mg, 0.9411 mmol, 5 eq) in toluene. The mixture was refluxed for 48 hours. The purification process yielded the pure *title compound* as purple solid (117 mg, 70%).

**Mp** 228 °C

**<sup>1</sup>H-NMR** (400 MHz, CDCl<sub>3</sub>, 298 K):  $\delta$  (ppm) = 9.20 (s, 3H, H<sub>1</sub>), 8.54 (br d, 3H,  $J$  = 8.3 Hz, H<sub>3</sub>), 8.22 (br d, 3H,  $J$  = 8.3 Hz, H<sub>2</sub>), 6.44 (t, 2H,  $J$  = 8.8 Hz, H<sub>5</sub>), 5.30 (dd, 2H,  $J$  = 8.8, 4.6 Hz, H<sub>4</sub>).

**<sup>11</sup>B-NMR** (160.5 MHz, CDCl<sub>3</sub>, 298 K):  $\delta$  (ppm) = -14.88 (s, 1B).

**<sup>19</sup>F-NMR** (470.6 MHz, CDCl<sub>3</sub>, 298 K):  $\delta$  (ppm) = -121.73 (s, 1F).

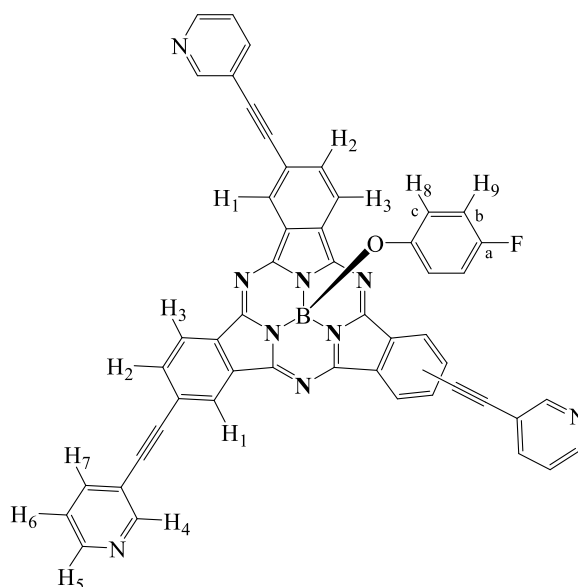
**MS** (MALDI-TOF):  $m/z$  = 884.52 [M+H]<sup>+</sup>

**HR-MS** (FTMS + p NSI) (C<sub>30</sub>H<sub>14</sub>B<sub>1</sub>F<sub>1</sub>I<sub>3</sub>N<sub>6</sub>O<sub>1</sub>) [M+H]<sup>+</sup>: Calc.: 884.8440; Found: 884.8445.

**UV-Vis** (distilled CH<sub>2</sub>Cl<sub>2</sub>):  $\lambda$  max (nm) ( $\epsilon$  (dm<sup>3</sup>·mol<sup>-1</sup>·cm<sup>-1</sup>)) = 570 (9.05·10<sup>4</sup>), 318 (3.25·10<sup>4</sup>), 271 (5.85·10<sup>4</sup>).

**Fluorescence** (distilled CH<sub>2</sub>Cl<sub>2</sub>, Excitation at 500 nm): 581 nm

### (3-Pyridyl)<sub>3</sub>-SubPc-(4-F-OPh) (48)



Synthesised following general procedure C for Sonogashira cross-coupling reaction from I-SubPc-(4-F-OPh) **47** (50.2 mg, 0.122 mmol, 1 eq), 3-ethynylpyridine **46** (77.1 mg, 0.733 mmol, 6 eq), PdCl<sub>2</sub>(PPh<sub>3</sub>)<sub>2</sub> (7.7 mg, 0.011 mmol, 0.09 eq) and CuI (2.1 mg, 0.01 mmol, 0.09 eq) in NEt<sub>3</sub>. The reaction mixture was heated at 50 °C for 7 hours. The residue was purified by column chromatography in silica gel using 100% EtOAc as solvent eluent. Recrystallisation from dichloromethane / hexane gave pure *title compound* as a dark purple solid (62.8 mg, 65%).

**Mp** 145 – 146 °C

**<sup>1</sup>H-NMR** (400 MHz, CDCl<sub>3</sub>, 298 K):  $\delta$  (ppm) = 9.01 (d, 3H,  $J$  = 5.6 Hz, H<sub>1</sub>), 8.85 (s, 3H, H<sub>4</sub>), 8.79 (t, 3H,  $J$  = 7.9 Hz, H<sub>3</sub>), 8.59 (d, 3H,  $J$  = 4 Hz, H<sub>5</sub>), 8.03 (d, 3H,  $J$  = 7.9 Hz, H<sub>2</sub>), 7.89 (d, 3H,  $J$  = 7.8 Hz, H<sub>7</sub>), 7.40 – 7.37 (m, 3H, H<sub>6</sub>), 6.51 (t, 2H,  $J$  = 8.7 Hz, H<sub>9</sub>), 5.42 (dd, 2H,  $J$  = 8.7, 4.6 Hz, H<sub>8</sub>).

**<sup>11</sup>B-NMR** (160.5 MHz, CDCl<sub>3</sub>, 298 K):  $\delta$  (ppm) = -14.58 (s, 1B).

**$^{19}\text{F}$ -NMR** (470.6 MHz,  $\text{CDCl}_3$ , 298 K):  $\delta$  (ppm) = -121.81 (s, 1F).

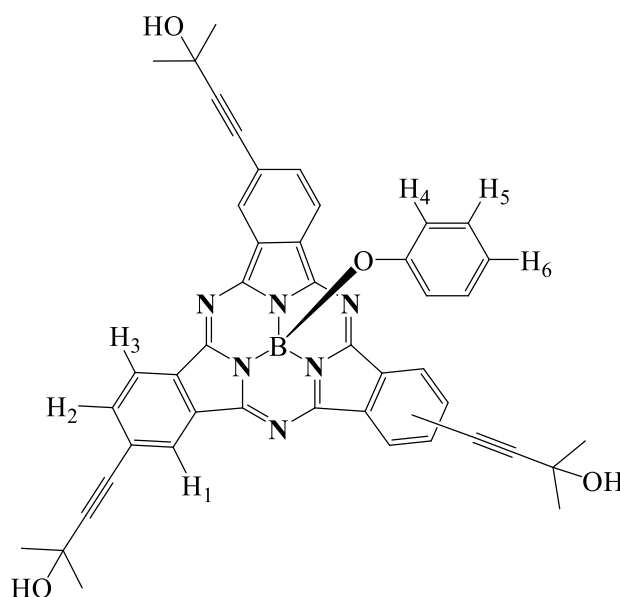
**MS** (MALDI-TOF):  $m/z$  = 810.82  $[\text{M}+\text{H}]^+$

**HR-MS** (FTMS + p NSI) ( $\text{C}_{51}\text{H}_{26}\text{B}_1\text{F}_1\text{N}_9\text{O}_1$ )  $[\text{M}+\text{H}]^+$ : Calc.: 810.2340; Found: 810.2338.

**UV-Vis** (distilled  $\text{CH}_2\text{Cl}_2$ ):  $\lambda$  max (nm) ( $\epsilon$  ( $\text{dm}^3 \cdot \text{mol}^{-1} \cdot \text{cm}^{-1}$ )) = 586 ( $6.03 \cdot 10^4$ ), 285 ( $\cdot 10^4$ ).

**Fluorescence** (distilled  $\text{CH}_2\text{Cl}_2$ , Excitation at 500 nm): 598 nm.

**(Alkynol) $_3$ -SubPc-(OPh) (49)**



Sonogashira cross-coupling reaction of I-SubPc-OPh **41** (185.8 mg, 0.2145 mmol, 1 eq) with 2-methylbut-3-yn-2-ol **43** (0.13 mL, 1.287 mmol, 6 eq), using  $\text{PdCl}_2(\text{PPh}_3)_2$  (13.5 mg, 0.0193 mmol, 0.09 eq) and  $\text{CuI}$  (3.8 mg, 0.0193 mmol, 0.09 eq) in  $\text{NEt}_3$  following to general procedure C. The mixture was stirred at room temperature for 25 hours. The residue was purified by column chromatography in silica gel using 100% EtOAc as solvent eluent. Recrystallisation from dichloromethane / hexane gave pure *title compound* as a dark purple solid (107.9 mg, 69%).

**Mp** 149 – 150 °C

**$^1\text{H}$ -NMR** (400 MHz,  $\text{CDCl}_3$ , 298 K):  $\delta$  (ppm) = 8.89 – 8.85 (m, 3H, H<sub>1</sub>), 8.74 – 8.68 (m, 3H, H<sub>3</sub>), 7.91 – 7.87 (m, 3H, H<sub>2</sub>), 6.75 (br t, 2H,  $J$  = 7.5 Hz, H<sub>5</sub>), 6.63 (tt, 1H,  $J$  = 7.5, 1.0 Hz, H<sub>6</sub>), 5.38 (br d, 2H,  $J$  = 7.5 Hz, H<sub>4</sub>), 2.16 (br s, 3H, -OH), 1.70 (s, 18H, -CH<sub>3</sub>).

**$^{13}\text{C}$ -NMR** (101 MHz,  $\text{CDCl}_3$ , 298 K):  $\delta$  (ppm) = 152.4, 151.1, 132.9, 130.9, 129.8, 129.1, 125.9, 124.8, 122.2, 122.1, 121.8, 119.2, 97.0, 82.2, 65.8, 31.6.

**$^{11}\text{B}$ -NMR** (160.5 MHz,  $\text{CDCl}_3$ , 298 K):  $\delta$  (ppm) = -14.72 (s, 1B).

**MS** (MALDI-TOF):  $m/z$  = 734.34  $[\text{M}]^+$

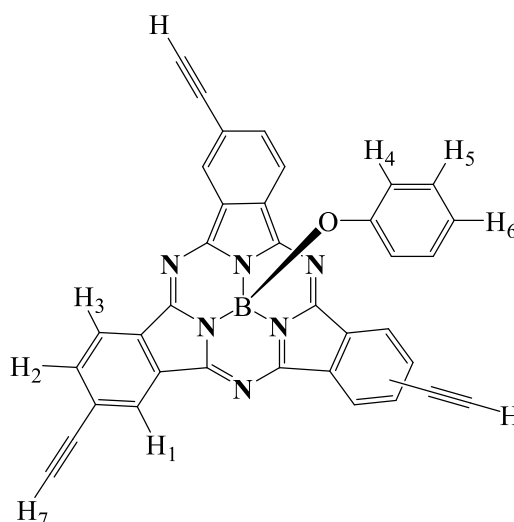


**HR-MS** (FTMS + p NSI) ( $C_{45}H_{36}B_1N_6O_4$ )  $[M+H]^+$ : Calc.: 735.2893; Found: 735.2885.

**UV-Vis** (distilled  $CH_2Cl_2$ ):  $\lambda$  max (nm) ( $\epsilon$  ( $dm^3 \cdot mol^{-1} \cdot cm^{-1}$ )) = 579 ( $4.93 \cdot 10^4$ ), 271 ( $4.61 \cdot 10^4$ ).

**Fluorescence** (distilled  $CH_2Cl_2$ , Excitation at 500 nm): 590 nm.

**(Ethynyl)<sub>3</sub>-SubPc-(OPh)<sup>[117]</sup> (50)**



Synthesised following general procedure D using (Alkynol)<sub>3</sub>-SubPc-(OPh) **49** (43 mg, 0.059 mmol, 1eq) and sodium hydroxide (7.2 mg, 0.18 mmol, 3 eq) in toluene (3 mL). The mixture was refluxed for 5 hours. After work up, a column chromatography in silica gel was performed using (1:1) EtOAc/PE as solvent eluent. The product was recrystallised from DCM/hexane to afford the pure *title compound* as a purple solid (20.9 mg, 64%).

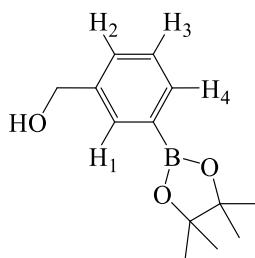
**<sup>1</sup>H-NMR** (400 MHz,  $CDCl_3$ , 298 K):  $\delta$  (ppm) = 8.96 (d, 3H,  $J = 0.9$  Hz, H<sub>1</sub>), 8.76 – 8.75 (m, 3H, H<sub>3</sub>), 8.00 – 7.98 (m, 3H, H<sub>2</sub>), 6.76 (br t, 2H,  $J = 7.5$  Hz, H<sub>5</sub>), 6.64 (tt, 1H,  $J = 7.5, 1.0$  Hz, H<sub>6</sub>), 5.38 (d, 2H,  $J = 7.5$  Hz, H<sub>4</sub>), 3.35 (s, 3H, H<sub>7</sub>).

**MS** (MALDI-TOF):  $m/z = 560.29$   $[M]^+$

**<sup>11</sup>B-NMR** (160.5 MHz,  $CDCl_3$ , 298 K):  $\delta$  (ppm) = -14.70 (s, 1B).

**UV-Vis** (distilled  $CH_2Cl_2$ ):  $\lambda$  max (nm) = 576.

**Fluorescence** (distilled  $CH_2Cl_2$ , Excitation at 500 nm): 587 nm

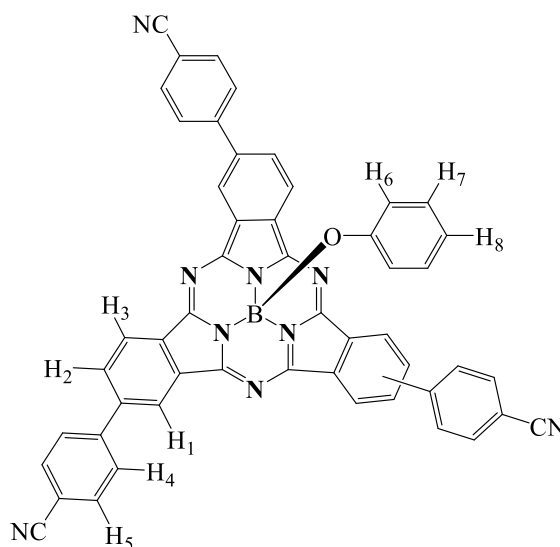
**3-(4,4,5,5-tetramethyl-1,3,2-dioxaborolan-2-yl)-benzenemethanol<sup>[189]</sup> (52)**

A mixture of 3-(hydroxymethyl)benzene boronic acid **51** (0.1606 g, 1.057 mmol, 1 eq) and pinacol (0.1236 g, 1.036 mmol, 0.98 eq) were refluxed in dichloromethane for 5 hours. After evaporation of the solvent under reduced pressure, the resulting crude was filtered through a silica pad using (4:1) PE/EtOAc as solvent system to give the *title compound* as a white solid (0.200 g, 71%).

**<sup>1</sup>H-NMR** (500 MHz, CDCl<sub>3</sub>, 298 K):  $\delta$  (ppm) = 7.80 (s, 1H, H<sub>1</sub>), 7.74 (br d, 1H,  $J = 7.5$  Hz, H<sub>4</sub>), 7.49 (br d, 1H,  $J = 7.5$  Hz, H<sub>2</sub>), 7.38 (t, 1H,  $J = 7.5$  Hz, H<sub>3</sub>), 4.71 (s, 2H, -CH<sub>2</sub>), 1.35 (s, 12H, -CH<sub>3</sub>).

**<sup>13</sup>C-NMR** (125.7 MHz, CDCl<sub>3</sub>, 298 K):  $\delta$  (ppm) = 140.3, 134.2(C<sub>4</sub>), 133.5(C<sub>1</sub>), 130.2(C<sub>2</sub>), 128.2(C<sub>3</sub>), 84.0(quat.), 65.5(-CH<sub>2</sub>), 25.0(-CH<sub>3</sub>).

**FT-IR**  $\nu_{\max}$  (NaCl)/ cm<sup>-1</sup>: 3419 (br O-H), 3061 (arC-H st), 2979 (C-H st), 2869 (C-H st), 1608, 1488 (CH<sub>2</sub>  $\delta$  and CH<sub>3</sub>  $\delta$  asym), 1431 (O-H  $\delta$  ip), 1360 (B-O st), 1316, 1144 (B-C st), 1020 (C-O st), 852, 709.

**(Ph-CN)<sub>3</sub>-SubPc-OPh (53)**

Synthesised following general procedure E for Suzuki cross-coupling reaction from I-SubPc-(OPh) **41** (100.3 mg, 0.1158 mmol, 1 eq), 4-cyanophenyl boronic acid (104.2 mg, 0.6949 mmol, 6 eq), PdCl<sub>2</sub>(dppf) (8.5 mg, 0.010 mmol, 0.09 eq), and CsF (105.6 mg, 0.6949 mmol, 6 eq) in dry DME. The mixture was heated up to 85 °C for 23 hours. The residue was purified by

column chromatography in (20:1) toluene/THF to 100% THF as solvent gradient. Recrystallisation of the product from DCM/hexane gave the pure *title compound* as dark purple solid (13.8 mg, 15%).

**Mp** 231 – 232 °C

**<sup>1</sup>H-NMR** (500 MHz, CDCl<sub>3</sub>, 298 K): δ (ppm) = 9.09 (m, 3H, H<sub>1</sub>), 8.94 (br t, *J* = 8.3 Hz, 3H, H<sub>3</sub>), 8.17 – 8.14 (m, 3H, H<sub>2</sub>), 7.97 – 7.94 (m, 6H, H<sub>4</sub>), 7.86 – 7.84 (m, 6H, H<sub>5</sub>), 6.79 (t, 2H, *J* = 7.4 Hz, H<sub>7</sub>), 6.67 (tt, 1H, *J* = 7.4, 1.0 Hz, H<sub>8</sub>), 5.44 (d, 2H, *J* = 7.4 Hz, H<sub>6</sub>).

**<sup>13</sup>C-NMR** (125.7 MHz, CDCl<sub>3</sub>, 298 K): δ (ppm) = 152.4, 151.8, 151.5, 151.3, 144.9, 141.3, 133.1, 131.9, 130.7, 129.2, 128.5, 123.2, 121.9, 121.2, 119.2, 118.8, 112.1.

**<sup>11</sup>B-NMR** (160.5 MHz, CDCl<sub>3</sub>, 298 K): δ (ppm) = -14.65 (s, 1B).

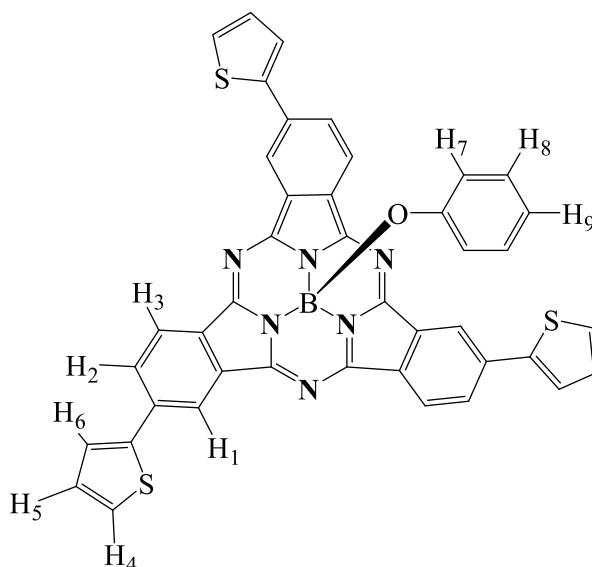
**MS** (MALDI-TOF): *m/z* = 792.57 [M+H]<sup>+</sup>

**HR-MS** (FTMS + p NSI) (C<sub>51</sub>H<sub>27</sub>B<sub>1</sub>N<sub>9</sub>O<sub>1</sub>) [M+H]<sup>+</sup>: Calc.: 792.2435; Found: 792.2428.

**UV-Vis** (dist. CH<sub>2</sub>Cl<sub>2</sub>): λ max (nm) (ε (dm<sup>3</sup>·mol<sup>-1</sup>·cm<sup>-1</sup>)) = 578 (8.23·10<sup>4</sup>), 278 (8.27·10<sup>4</sup>).

**Fluorescence** (dist. CH<sub>2</sub>Cl<sub>2</sub>, Excitation at 500 nm): 594 nm

#### (Thiophenyl)<sub>3</sub>-SubPc-OPh (54)



Synthesised following general procedure E for Suzuki cross-coupling reaction from I-SubPc-(OPh) **41** (51.5 mg, 0.0595 mmol, 1 eq), 2-thienylboronic acid (69.9mg, 0.535 mmol, 9 eq), PdCl<sub>2</sub>(dppf) (4.4 mg, 0.0054 mmol, 0.09 eq), and CsF (81.3 mg, 0.535 mmol, 9 eq) in dry DME. The reaction mixture was heated at 100 °C for 4 hours. The residue was purified by column chromatography in (3:1) PE/EtOAc. The product was washed with hexane to give the *title compound* as dark purple solid (18.4 mg, 42%).

**Mp** 173 – 175 °C

**<sup>1</sup>H-NMR** (500 MHz, CDCl<sub>3</sub>, 298 K): δ (ppm) = 9.10 – 9.08 (m, 3H, H<sub>1</sub>), 8.84 – 8.81 (m, 3H, H<sub>3</sub>), 8.18 – 8.15 (m, 3H, H<sub>2</sub>), 7.67 – 7.65 (m, 3H, H<sub>6</sub>), 7.44 (dd, 3H, *J* = 5.0, 0.6 Hz, H<sub>4</sub>), 7.21 (dd, 3H, *J* = 5.0, 3.6 Hz, H<sub>5</sub>), 6.78 (t, 2H, *J* = 7.5 Hz, H<sub>8</sub>), 6.65 (tt, 1H, *J* = 7.5, 1.1 Hz, H<sub>9</sub>), 5.43 (d, 2H, *J* = 7.5 Hz, H<sub>7</sub>).

**<sup>13</sup>C-NMR** (125.7 MHz, CDCl<sub>3</sub>, 298 K): δ (ppm) = 143.9, 136.6, 136.5, 136.4, 131.2, 129.1, 128.7, 127.8, 127.7, 126.6, 125.8, 124.9, 124.5, 122.9, 119.3, 119.1.

**<sup>11</sup>B-NMR** (160.5 MHz, CDCl<sub>3</sub>, 298 K): δ (ppm) = -14.62 (s, 1B).

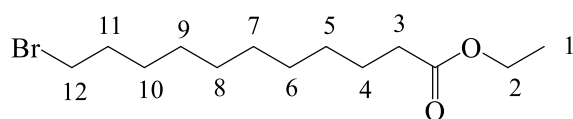
**MS** (MALDI-TOF): *m/z* = 735.86 [M+H]<sup>+</sup>

**HR-MS** (FTMS + p NSI) (C<sub>42</sub>H<sub>24</sub>B<sub>1</sub>N<sub>6</sub>O<sub>1</sub>S<sub>3</sub>) [M+H]<sup>+</sup>: Calc.: 735.1269; Found: 735.1267.

**UV-Vis** (dist. CH<sub>2</sub>Cl<sub>2</sub>): λ max (nm) (ε (dm<sup>3</sup>·mol<sup>-1</sup>·cm<sup>-1</sup>)) = 590 (5.02·10<sup>4</sup>), 361 (2.44·10<sup>4</sup>), 289 (4.65·10<sup>4</sup>).

**Fluorescence** (dist. CH<sub>2</sub>Cl<sub>2</sub>, Excitation at 500 nm): 604 nm

### Ethyl 11-bromoundecanoate<sup>[126]</sup> (**66**)

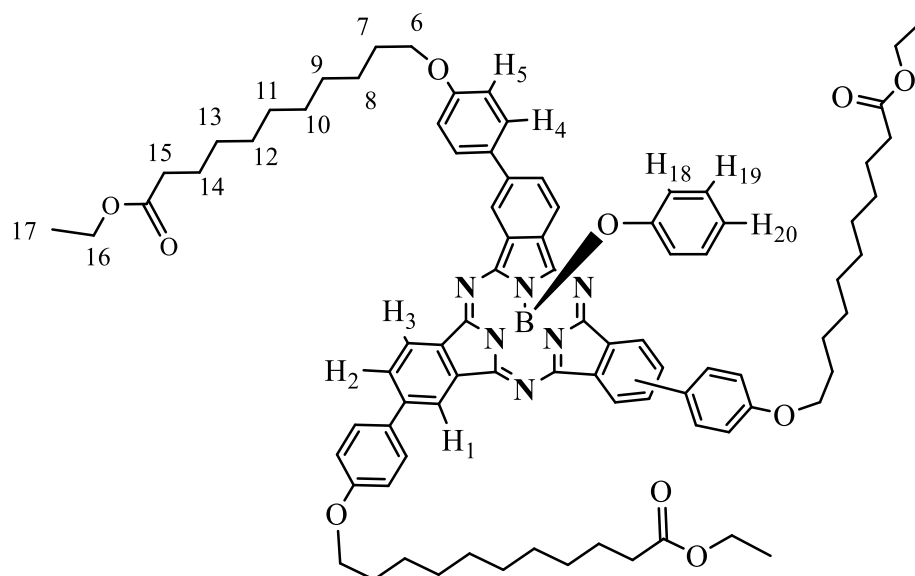


11-Bromoundecanoic acid **65** (1.0122 g, 3.82 mmol, 1eq) was dissolved in ethanol (50 mL) and 1 mL of H<sub>2</sub>SO<sub>4</sub> was added to the solution, and the mixture was heated under reflux for 25 hours. After cooling, the solvent was evaporated and the solid was dissolved in a mixture of hexane/EtOAc (1:1) and washed with water. The organic layer was dried over MgSO<sub>4</sub>, filtered and the solvent evaporated. The product was purified by column chromatography in silica gel using (2:1) DCM/PE to yield the pure *title compound* as colourless liquid (2.3262 g, 70%).

**<sup>1</sup>H-NMR** (500 MHz, CDCl<sub>3</sub>, 298 K): δ (ppm) = 4.12 (q, 2H, *J* = 7.1 Hz, H<sub>2</sub>), 3.40 (t, 2H, *J* = 6.9 Hz, H<sub>12</sub>), 2.28 (t, 2H, *J* = 7.5 Hz, H<sub>3</sub>), 1.85 (m, 2H, H<sub>11</sub>), 1.61 (quintet, 2H, *J* = 7.5 Hz, H<sub>4</sub>), 1.41 (quintet, H, *J* = 7.4 Hz, H<sub>10</sub>), 1.35 – 1.28 (m, 10H, H<sub>9</sub>, H<sub>8</sub>, H<sub>7</sub>, H<sub>6</sub>, H<sub>5</sub>), 1.25 (t, 3H, *J* = 7.1 Hz, CH<sub>3</sub>-1).

**<sup>13</sup>C-NMR** (125.7 MHz, CDCl<sub>3</sub>, 298 K): δ (ppm) = 174.0 (C=O), 60.3(C<sub>2</sub>), 34.5(C<sub>3</sub>), 34.2(C<sub>12</sub>), 33.0(C<sub>11</sub>), [(29.5, 29.4, 29.3, 29.2, 28.9) (C<sub>9</sub>, C<sub>8</sub>, C<sub>7</sub>, C<sub>6</sub>, C<sub>5</sub>)], 28.3(C<sub>10</sub>), 25.1(C<sub>4</sub>), 14.4(C<sub>1</sub>).

**FT-IR** ν<sub>max</sub> (NaCl)/ cm<sup>-1</sup>: 2929 (C-H st), 2856 (C-H st), 1733 (s C=O st), 1464 (CH<sub>2</sub> δ and CH<sub>3</sub> δ asym), 1373, 1246 (C-O st), 1179 (C-O st), 1036, 723 (CH<sub>2</sub> γ), 645.

**(AlkylCOOEt)<sub>3</sub>-SubPc-OPh (69)**

Synthesised following general procedure E for Suzuki cross-coupling reaction from I-SubPc-(OPh) **41** (46.1 mg, 0.0533 mmol, 1 eq), pinacol boronate ester **71** (138.2 mg, 0.3196 mmol, 6eq), PdCl<sub>2</sub>(dppf) (3.9 mg, 0.0048 mmol, 0.09 eq), and CsF (48.6 mg, 0.320 mmol, 6 eq) in DME. The reaction mixture was heated at 100 °C for 6 hours. The residue was purified by column chromatography in (9:1) PE/EtOAc. The product was washed with hexane to give the *title compound* as dark purple solid (21.8 mg, 29%).

**<sup>1</sup>H-NMR** (500 MHz, CDCl<sub>3</sub>, 298 K): δ (ppm) = 9.04 (br s, 3H, H<sub>1</sub>), 8.87 – 8.84 (m, 3H, H<sub>2</sub>), 8.13 – 8.10 (m, 3H, H<sub>3</sub>), 7.80 (dd, 6H, *J* = 8.7, 1.8, Hz, H<sub>5</sub> or H<sub>4</sub>), 7.08 (dd, 6H, *J* = 8.7, 1.8, Hz, H<sub>5</sub> or H<sub>4</sub>), 6.78 (t, 2H, *J* = 7.3 Hz, H<sub>19</sub>), 6.64 (t, 1H, *J* = 7.3 Hz, H<sub>20</sub>), 5.45 (d, 2H, *J* = 7.3 Hz, H<sub>18</sub>), 4.13 (q, 6H, *J* = 7.1 Hz, H<sub>16</sub>), 4.06 (t, 6H, *J* = 6.5 Hz, H<sub>6</sub>), 2.30 (t, 6H, *J* = 7.5 Hz, H<sub>15</sub>), 1.84 (m, 6H, H<sub>7</sub>), 1.65 – 1.47 (m, 12H, H<sub>14</sub>, H<sub>8</sub>), 1.32 (br s, 30H, H<sub>9</sub>, H<sub>10</sub>, H<sub>11</sub>, H<sub>12</sub>, H<sub>13</sub>), 1.25 (t, 9H, *J* = 7.1 Hz, -CH<sub>3</sub> 17).

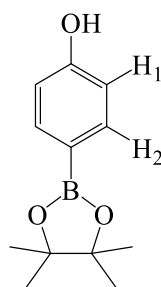
**<sup>13</sup>C-NMR** (125.7 MHz, CDCl<sub>3</sub>, 298 K): δ (ppm) = 174.1, 168.0, 167.9, 160.2, 147.7, 134.2, 133.7, 133.0, 132.3, 131.2, 130.3, 129.1, 128.9, 128.7, 124.2, 121.7, 115.4, 68.4, 60.3, 34.5, 29.8, 29.6, 29.5 (4), 29.5 (2), 29.4, 29.3, 26.2, 25.1, 14.4.

**<sup>11</sup>B-NMR** (160.5 MHz, CDCl<sub>3</sub>, 298 K): δ (ppm) = -14.58 (s, 1B).

**MS** (MALDI-TOF): *m/z* = 1402.00 [M+H]<sup>+</sup>

**UV-Vis** (dist. CH<sub>2</sub>Cl<sub>2</sub>): λ max (nm) (ε (dm<sup>3</sup>·mol<sup>-1</sup>·cm<sup>-1</sup>)) = 583 (5.03·10<sup>4</sup>), 269 (2.11·10<sup>4</sup>).

**Fluorescence** (dist. CH<sub>2</sub>Cl<sub>2</sub>, Excitation at 500 nm): 597 nm

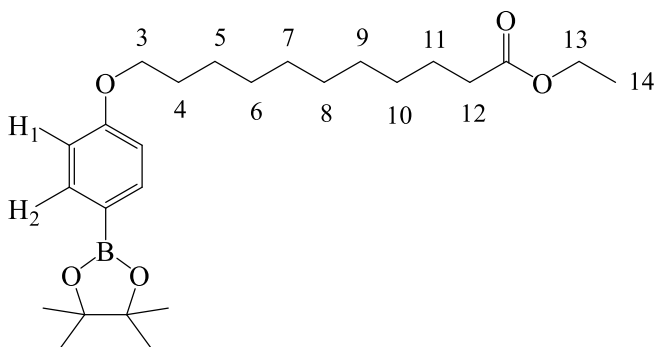
**4-(Hydroxyphenyl)boronate pinacol ester<sup>[127]</sup> (70)**

A mixture of 4-hydroxyphenyl boronic acid **67** (0.2406 g, 1.745 mmol, 1 eq) and pinacol (0.1236 g, 1.036 mmol, 1.1 eq) were refluxed in dichloromethane for 4 hours. After evaporation of the solvent under reduced pressure, the resulting crude was subjected to a column chromatography in silica gel using (5:1) PE/EtOAc as solvent system to give the *title compound* as a white solid (0.3802 g, 99%).

**<sup>1</sup>H-NMR** (500 MHz, CDCl<sub>3</sub>, 298 K):  $\delta$  (ppm) = 7.71 (d, 2H,  $J$  = 8.5 Hz, H<sub>1</sub>), 6.82 (d, 2H,  $J$  = 8.5 Hz, H<sub>2</sub>), 4.84 (s, 1H, -OH), 1.33 (s, 12H, -CH<sub>3</sub>).

**<sup>13</sup>C-NMR** (125.7 MHz, CDCl<sub>3</sub>, 298 K):  $\delta$  (ppm) = 158.6(quat.), 158.5(quat.), 136.9(C1), 115.0(C2), 83.8(quat.), 25.0(-CH<sub>3</sub>).

**FT-IR**  $\nu_{\max}$  (NaCl)/ cm<sup>-1</sup>: 3352 (br O-H), 3064 (arC-H st), 2980 (C-H st), 1609, 1587, 1470 (CH<sub>3</sub>  $\delta$  asym), 1429 (O-H  $\delta$  ip), 1360 (B-O st), 1268 (C-O st), 1142 (B-C st), 1088, 962.06, 838, 654.

**Boronate pinacol ester (71)**

4-(Hydroxyphenyl)boronate pinacol ester **70** (0.1113 g, 0.506 mmol, 1eq), ethyl-11-bromoundecanoate **66** (0.1421 g, 0.486 mmol, 0.96 eq), and K<sub>2</sub>CO<sub>3</sub> (0.3530 g, 2.528 mmol, 5 eq) were refluxed in DMF (8 mL) under inert atmosphere for 25 hours. After cooling, water was added (50 mL) and the solution extracted with EtOAc (3x75 mL), the combined organic layers were dried over MgSO<sub>4</sub>, filtered and the solvent evaporated. The resultant solid was purified by column chromatography in silica gel using (10:1) PE/EtOAc to give *title compound* as white solid (0.1172 g, 54%).

**$^1\text{H-NMR}$**  (500 MHz,  $\text{CDCl}_3$ , 298 K):  $\delta$  (ppm) = 7.73 (d, 2H,  $J = 8.7$  Hz,  $\text{H}_2$ ), 6.88 (d, 2H,  $J = 8.7$  Hz,  $\text{H}_1$ ), 4.12 (q, 2H,  $J = 7.1$  Hz,  $\text{H}_{13}$ ), 3.97 (t, 2H,  $J = 6.6$  Hz,  $\text{H}_3$ ), 2.28 (t, 2H,  $J = 7.5$  Hz,  $\text{H}_{12}$ ), 1.77 (quintet, 2H,  $J = 6.6$  Hz,  $\text{H}_4$ ), 1.63 – 1.58 (m, 2H,  $\text{H}_{11}$ ), 1.47 – 1.41 (m, 2H,  $\text{H}_5$ ), 1.33 (s, 12H,  $-\text{CH}_3$  pinacol), 1.25 (t, 3H,  $J = 7.1$  Hz,  $-\text{CH}_3$   $\text{H}_{14}$ ).

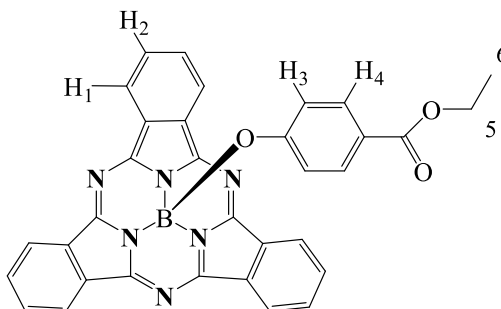
**$^{13}\text{C-NMR}$**  (125.7 MHz,  $\text{CDCl}_3$ , 298 K):  $\delta$  (ppm) = 174.1(COOR), 161.9( $\text{Csp}^2$   $\underline{\text{C}}-\text{O}$ ), 136.6( $\text{C}_2$ ), 120.8( $\text{Csp}^2$   $\underline{\text{C}}-\text{B}$ ), 114.0( $\text{C}_1$ ), 83.6( $\text{Csp}^2$  pinacol), 67.9( $\text{C}_3$ ), 60.3( $\text{C}_{13}$ ), 34.5( $\text{C}_{12}$ ), [(29.6, 29.5, 29.4, 29.4, 29.3, 29.2) ( $\text{C}_4$ ,  $\text{C}_6$ ,  $\text{C}_7$ ,  $\text{C}_8$ ,  $\text{C}_9$ ,  $\text{C}_{10}$ )], 26.1( $\text{C}_5$ ), 25.1( $-\text{CH}_3$  pinacol), 25.0( $\text{C}_{11}$ ), 14.4( $\text{C}_{14}$ ).

**$^{11}\text{B-NMR}$**  (160.5 MHz,  $\text{CDCl}_3$ , 298 K):  $\delta$  (ppm) = 31.32 (br s, 1B).

**HR-MS** (FTMS + p NSI) ( $\text{C}_{25}\text{H}_{45}\text{B}_1\text{O}_5\text{N}_1$ ) [ $\text{M}+\text{NH}_4$ ] $^+$ : Calc.: 450.3386; Found: 450.3376.

**FT-IR**  $\nu_{\text{max}}$  (NaCl)/  $\text{cm}^{-1}$ : 3041 (arC-H st), 2979 (C-H st), 2929 (C-H st), 2856 (C-H st), 1738 (s C=O st), 1606, 1469 ( $\text{CH}_2$   $\delta$  and  $\text{CH}_3$   $\delta$  asym), 1361 (B-O st), 1318, 1275 (C-O st), 1246 (C-O st), 1145 (B-C st), 1092, 1033, 861, 832, 655.

### SubPc-(OPh-COOEt) (**73**)



Synthesised following general procedure B from SubPc-Cl **16** (71.1 mg, 0.1651 mmol, 1 eq) and 4-hydroxybenzoate **72** (277.1 mg, 1.651 mmol, 10 eq) in toluene. Reaction time: 21 hours. After cooling the solvent was evaporated under reduce pressure, the product was precipitated with ethanol and filtered to give *title compound* as dark purple solid (80.5 mg, 87 %).

**Mp** 284 °C

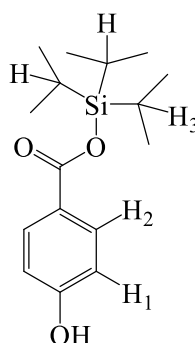
**$^1\text{H-NMR}$**  (500 MHz,  $\text{CDCl}_3$ , 298 K):  $\delta$  (ppm) = 9.07 – 8.77 (m, 6H,  $\text{H}_1$ ), 8.42 – 7.74 (m, 6H,  $\text{H}_2$ ), 7.74 (d, 2H,  $J = 8.7$  Hz,  $\text{H}_4$ ), 5.38 (d, 2H,  $J = 8.7$  Hz,  $\text{H}$ ), 4.20 (q, 2H,  $J = 7.1$  Hz,  $\text{H}_5$ ), 1.26 (t, 2H,  $J = 7.1$  Hz,  $-\text{CH}_3$ ).

**$^{13}\text{C-NMR}$**  (125.7 MHz,  $\text{CDCl}_3$ , 298 K):  $\delta$  (ppm) = 166.3, 157.1, 151.5, 131.1, 130.1, 123.6, 122.4, 118.6, 60.6, 14.4, 1.2.

**MS** (MALDI-TOF):  $m/z = 560.29$  [ $\text{M}$ ] $^+$

**UV-Vis** (distilled  $\text{CH}_2\text{Cl}_2$ ):  $\lambda$  max (nm) ( $\epsilon$  ( $\text{dm}^3 \cdot \text{mol}^{-1} \cdot \text{cm}^{-1}$ )) = 562 ( $6.81 \cdot 10^4$ ), 304 ( $3.56 \cdot 10^4$ ).

**Fluorescence** ( $\text{CH}_2\text{Cl}_2$ , Excitation at 500 nm): 575 nm.

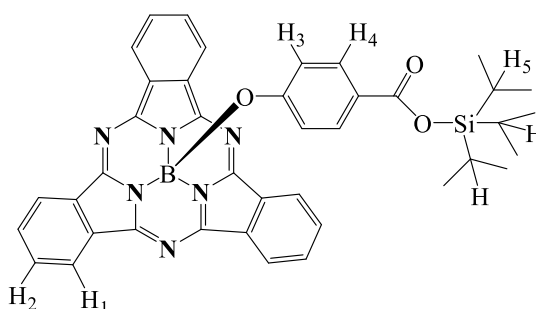
**4-Hydroxy-, tris(1-methylethyl)silyl benzoate ester<sup>[136]</sup> (75)**

A solution of 4-hydroxybenzoic acid (1.01 g, 7.34 mmol, 1 eq) in THF (240 mL) and  $\text{NEt}_3$  (4 mL), was treated with chloro-triisopropylsilane (2.3 mL, 10.8 mmol, 1.5 eq). The reaction was stirred for 30 minutes after which a column chromatography in silica gel was performed using (1:4) EtOAc/PE as solvent eluent, to give the pure *title compound* as colourless solid (0.618 g, 29%).

**$^1\text{H-NMR}$**  (500 MHz,  $\text{CDCl}_3$ , 298 K):  $\delta$  (ppm) = 7.98 (br d, 2H,  $J = 8.8$  Hz,  $\text{H}_2$ ), 6.86 (br d, 2H,  $J = 8.8$  Hz,  $\text{H}_1$ ), 5.36 (s, 1H,  $-\text{OH}$ ), 1.41 (septet, 3H,  $J = 7.4$  Hz,  $\text{H}_3$ ), 1.14 (d, 18H,  $J = 7.4$  Hz,  $-\text{CH}_3$ ).

**$^{13}\text{C-NMR}$**  (125.7 MHz,  $\text{CDCl}_3$ , 298 K):  $\delta$  (ppm) = 166.5(quat.), 160.0(quat.), 132.7( $\text{C}_2$ ), 124.2(quat.), 115.3( $\text{C}_1$ ), 18.0( $-\text{CH}_3$ ), 12.3( $-\text{CH}$ ).

**FT-IR**  $\nu_{\text{max}}$  (NaCl)/  $\text{cm}^{-1}$ : 3373 (br O-H), 3070 (arC-H st), 2947 (C-H st), 2869 (C-H st), 1661.34 (s C=O st), 1608, 1592, 1514, 1464 ( $\text{CH}_3$   $\delta$  asym), 1447, 1387 and 1369 ( $\text{CH}_3$   $\delta$  sym), 1319 and 1286 (C-O st), 1160 (Si-O st), 883, 779, 739, 686.

**SubPc-(OPh-TIPS) (76)**

Synthesised following general procedure B from SubPc-Cl **16** (31 mg, 0.072 mmol, 1 eq) and TIPS-derivative **75** (0.106 g, 0.361 mmol, 5 eq) in toluene (3 mL). Reaction time: 12 hours. The resultant solid was purified by column chromatography in (1:9) EtOAc/ PE to (2:7) EtOAc/PE as solvent gradient, the product was subsequently washed with cold methanol and filtered to give the pure *title compound* as pink solid (29.1 mg, 59%).



$^1\text{H-NMR}$  (400 MHz,  $\text{CDCl}_3$ , 298 K):  $\delta$  (ppm) = 8.89 – 8.84 (m, 6H,  $\text{H}_1$ ), 7.94 – 7.89 (m, 6H,  $\text{H}_2$ ), 7.48 (d, 2H,  $J = 8.8$  Hz,  $\text{H}_4$ ), 5.38 (d, 2H,  $J = 8.8$  Hz,  $\text{H}_3$ ), 1.29 (septet, 3H,  $J = 7.4$  Hz,  $\text{H}_5$ ), 1.04 (d, 18H,  $J = 7.4$  Hz,  $-\text{CH}_3$ ).

**MS** (MALDI-TOF):  $m/z = 688.34$   $[\text{M}]^+$

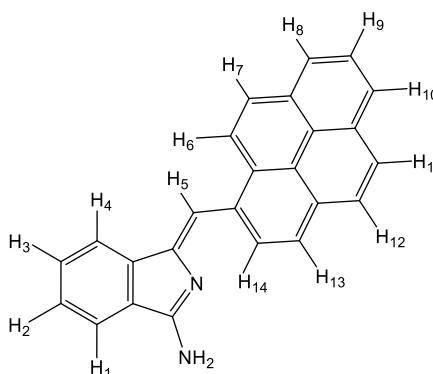
## 4.5 Experimental details and Characterisation for SubTBDAPs project

### 4.5.1 Aminoisoindolene precursors

#### General procedure F for (Z)-1-(phenylderivative-methylene)-1H-isoindol-3-amine<sup>[170]</sup>

A mixture of *o*-bromobenzamidine hydrochloride<sup>[169]</sup> (1eq), BINAP (0.055 eq) and  $\text{PdCl}_2(\text{MeCN})_2$  (0.05 eq) was sealed in a microwave vessel with a magnetic bar and then purged and refilled with  $\text{N}_2$  three times. Then, a solution of the acetylene-derivative (1.2 eq) and DBU (2.5 eq) in dry DMF (12 mL) was added. The mixture was stirred under  $\text{N}_2$  for 5 min. Finally, the mixture was irradiated in a microwave reactor at 120 °C for 1 h. After cooling, 50 mL of ethyl acetate were added and the mixture washed with a saturated solution of  $\text{NaHCO}_3$  (75 mL) three times. The organic layer was dried over  $\text{MgSO}_4$ , filtered and concentrated. The residue was finally purified by column chromatography using 100% dichloromethane to 1:1 ethyl acetate/petroleum ether to 100% ethyl acetate as solvent gradient. The resulting solid was recrystallised from a 1:1 mixture of dichloromethane/petroleum ether to yield the desired compounds.

#### (Z)-1(1-Pyrenylmethylene)-1H-isoindol-3-amine<sup>[139]</sup> (**124**)



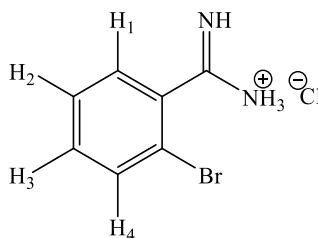
Synthesised following the general procedure F from *o*-bromobenzamidine hydrochloride **130** (523.8 mg, 2.222 mmol, 1 eq), BINAP (78.1 mg, 0.126 mmol, 0.055 eq),  $\text{PdCl}_2(\text{MeCN})_2$  (31.2 mg, 0.120 mmol, 0.05 eq), 1-ethynylpyrene (600.6 mg, 2.7 mmol, 1.2 eq), and DBU (0.84 mL, 5.53 mmol, 2.5 eq) in DMF. The work up and purification process yielded the *title compound* as orange/brown powder (188.2 mg, 25%).

**Mp** 280 – 282 °C

**<sup>1</sup>H-NMR** (500.1 MHz, CD<sub>3</sub>OD, 263 K)  $\delta$  (ppm) = 8.55 (d, 1H,  $J$  = 8.0 Hz, H<sub>14</sub>), 8.50 (d, 1H,  $J$  = 9.2 Hz, H<sub>6</sub>), 8.27-8.21 (m, 4H, H<sub>7</sub>, H<sub>8</sub>, H<sub>10</sub>, H<sub>13</sub>), 8.14 (d, 1H,  $J$  = 7.6 Hz, H<sub>4</sub>), 8.11 (q, 2H,  $J$  = 7.6 Hz, H<sub>11</sub>, H<sub>12</sub>), 8.04 (t, 1H,  $J$  = 7.6 Hz, H<sub>9</sub>), 7.93 (d, 1H,  $J$  = 7.6 Hz, H<sub>1</sub>), 7.91 (s, 1H, H<sub>5</sub>), 7.68 (t, 1H,  $J$  = 7.6 Hz, H<sub>3</sub>), 7.54 (1H, t,  $J$  = 7.6 Hz, H<sub>2</sub>).

**MS** (MALDI-TOF):  $m/z$  = 345.12 [M+H]<sup>+</sup> (100%).

### ***o*-Bromobenzamidine Hydrochloride<sup>[169]</sup> (130)**



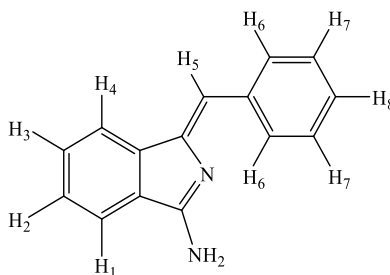
2-Bromobenzonitrile **129** (4.179 g, 22.7 mmol, 1 eq) was dissolved in tetrahydrofuran (3.4 ml). This mixture was added to lithium bis(trimethylsilyl)amide (1M in THF) (25 ml, 1.1 eq) and stirred for 4 hours at room temperature. The reaction was cooled down on an ice bath and 15 mL of a 1:1 mixture of HCl (5N) and isopropanol was added dropwise, and then it was left to stir overnight. The reaction mixture was filtered in cold and the resultant solid was washed with diethyl ether (10 mL x 2) and dried under vacuum to yield the *title compound* (4.7951 g, 90%) as a colourless solid.

**<sup>1</sup>H-NMR** (500 MHz, (CD<sub>3</sub>)<sub>2</sub>SO, 298 K):  $\delta$  (ppm) = 9.69 (br s, 1H, -NH), 9.63 (br s, 3H, -NH<sub>3</sub><sup>+</sup>), 7.82 (d,  $J$  = 5.0 Hz, 1H, H<sub>4</sub>), 7.62 (d,  $J$  = 5.0 Hz, 1H, H<sub>1</sub>), 7.60 – 7.53 (m, 2H, H<sub>2</sub>, H<sub>3</sub>).

**<sup>13</sup>C-NMR** (125.7 MHz, CDCl<sub>3</sub>, 298 K):  $\delta$  (ppm) = 165.7, 133.1, 133.0, 131.8, 129.8, 128.0, 119.5.

**FT-IR**  $\nu_{\max}$  (NaCl)/ cm<sup>-1</sup>: 3222 (NH st), 3062 (arC-H st), 1674, 1595, 1520, 1456 (NH<sub>3</sub><sup>+</sup>  $\delta$ ), 1425 (NH<sub>3</sub><sup>+</sup>  $\delta$ ), 1095, 1040, 1030.

### **(Z)-1-(Phenylmethylene)-1H-isoindol-3-amine<sup>[170]</sup> (131)**



Synthesised following the general procedure F from *o*-bromobenzamidine hydrochloride **130** (0.7073g, 3.003 mmol, 1eq), BINAP (0.1060 g, 0.1652 mmol, 0.055 eq), PdCl<sub>2</sub>(MeCN)<sub>2</sub>

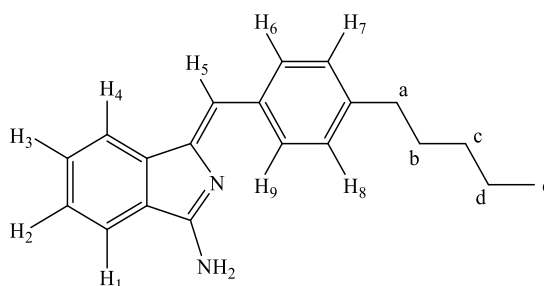
(39.3 mg, 0.150 mmol, 0.05 eq), phenyl acetylene (0.37 mL, 3.6 mmol, 1.2 eq) and DBU (1.14 mL, 2.5 eq) in DMF. Work up and purification process yielded the *title compound* as yellow solid (608 mg, 92%).

**<sup>1</sup>H-NMR** (500 MHz, DMSO, 298 K):  $\delta$ (ppm) = 8.21 (d, 2H,  $J = 7.5$  Hz, 2xH<sub>6</sub>), 7.86 (d, 1H,  $J = 7.5$  Hz, H<sub>4</sub>), 7.82 (d, 1H,  $J = 7.5$  Hz, H<sub>1</sub>), 7.66 (s, 2H, -NH<sub>2</sub>), 7.45 (td, 1H,  $J = 7.5, 1.0$  Hz, H<sub>3</sub>), 7.39 (td, 1H,  $J = 7.5, 1.0$  Hz, H<sub>2</sub>), 7.36-7.33 (m, 2H, 2xH<sub>7</sub>), 7.19 (tt, 1H,  $J = 7.5, 1.0$  Hz, H<sub>8</sub>), 6.68 (s, 1H, H<sub>5</sub>).

**<sup>13</sup>C-NMR** (125.7 MHz, CDCl<sub>3</sub>, 298 K):  $\delta$  (ppm) = 165.3, 146.4, 142.7, 136.6, 130.8, 130.5, 129.6, 128.6, 127.5, 127.4, 119.9, 119.4, 114.9.

**MS** (MALDI-TOF):  $m/z = 220.99$  [M]<sup>+</sup>

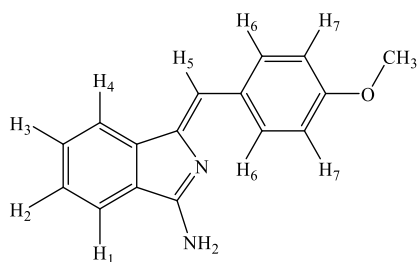
**(Z)-1-(4-Pentylphenylmethylene)-1H-isoindol-3-amine<sup>[172]</sup> (141)**



Synthesised following the general procedure F from *o*-bromobenzamidine hydrochloride **130** (0.7073g, 3.003 mmol, 1eq), BINAP (0.1060 g, 0.17 mmol, 0.055 eq), PdCl<sub>2</sub>(MeCN)<sub>2</sub> (39.3 mg, 0.151 mmol, 0.05 eq), 1-ethynyl-4-pentylbenzene (0.72 mL, 3.6 mmol, 1.2 eq) and DBU (1.14 mL, 2.5 eq) in DMF. The work up and purification process yielded the *title compound* as brown solid (660.2 mg, 76%).

**<sup>1</sup>H-NMR** (500 MHz, CDCl<sub>3</sub>, 298 K):  $\delta$ (ppm) = 8.00 (br d, 2H,  $J = 8.1$  Hz, H<sub>6</sub>), 7.82 – 7.78 (m, 1H, H<sub>4</sub>), 7.50 – 7.45 (m, 2H, H<sub>1</sub>, H<sub>3</sub>), 7.37 (td, 1H,  $J = 7.4, 1.0$ , H<sub>2</sub>), 7.21 (br d,  $J = 8.1$  Hz, 2H, H<sub>7</sub>), 6.76 (s, 1H, H<sub>5</sub>), 2.62 (t, 2H,  $J = 7.7$ , H<sub>a</sub>), 1.63 (quintet,  $J = 7.5$  Hz, 2H, H<sub>b</sub>), 1.37 – 1.30 (m, 4H, H<sub>c</sub>, H<sub>d</sub>), 0.89 (t, 3H,  $J = 7.0$  Hz, H<sub>e</sub>).

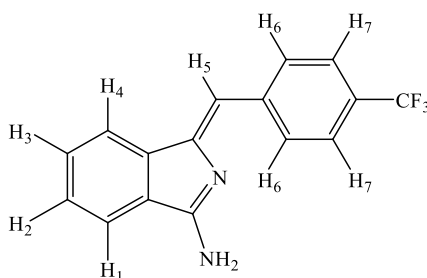
**MS** (MALDI-TOF):  $m/z = 290.1$  [M]<sup>+</sup> (100%)

**(Z)-1-(4-Methoxyphenylmethylene)-1H-isoindol-3-amine<sup>[154]</sup> (142)**

Synthesised following the general procedure F from *o*-bromobenzamidine hydrochloride **130** (0.7065 g, 3 mmol, 1eq), BINAP (0.1060 g, 0.1650 mmol, 0.055 eq), PdCl<sub>2</sub>(MeCN)<sub>2</sub> (39.3 mg, 0.150 mmol, 0.05 eq), 4-ethynylanisole (0.48 mL, 3.6 mmol, 1.2 eq), and DBU (1.14 mL, 2.5 eq) in DMF. Work up and purification process yielded the *title compound* as yellow solid (569.6 mg, 76%).

<sup>1</sup>H-NMR (500 MHz, CDCl<sub>3</sub>, 298 K): δ(ppm) = 8.09 (br d, 2H, *J* = 8.8 Hz, H<sub>6</sub>), 7.78 (br d, 1H, *J* = 7.5 Hz, H<sub>4</sub>), 7.48-7.43 (m, 2H, H<sub>1</sub>, H<sub>3</sub>), 7.36 (br td, 1H, *J* = 7.5, 0.6 Hz, H<sub>2</sub>), 6.94 (br d, 2H, *J* = 8.8 Hz, H<sub>7</sub>), 6.75 (s, 1H, H<sub>5</sub>), 5.30 (br s, 2H, -NH<sub>2</sub>), 3.85 (s, 3H, -OCH<sub>3</sub>).

MS (MALDI-TOF): *m/z* = 250.1 [M]<sup>+</sup> (100%)

**(Z)-1-(4-Trifluoromethylphenylmethylene)-1H-isoindol-3-amine (143)**

Synthesised following the general procedure F from *o*-bromobenzamidine hydrochloride **130** (707.3 mg, 3.003 mmol, 1eq), BINAP (106.1 mg, 0.165 mmol, 0.055 eq), PdCl<sub>2</sub>(MeCN)<sub>2</sub> (39.3 mg, 0.150 mmol, 0.05 eq), 1-ethynyl-4-(trifluoromethyl)benzene (0.6 mL, 3.6 mmol, 1.2 eq) and DBU (1.14 mL, 7.51 mmol, 2.5 eq) in DMF. The work up and purification process yielded the *title compound* as yellow crystals (635.5 mg, 73%).

Rf 0.32 Hexane/ THF/MeOH (10:3:1)

Mp 161 - 162 °C

<sup>1</sup>H-NMR (500.1 MHz, CDCl<sub>3</sub>, 298 K): δ (ppm) = 8.20 (d, 2H, *J* = 8.1 Hz, H<sub>6</sub>), 7.80 (d, 1H, *J* = 7.6 Hz, H<sub>4</sub>), 7.61 (d, 2H, *J* = 8.1 Hz, H<sub>7</sub>), 7.53 – 7.44 (m, 2H, H<sub>1</sub>, H<sub>3</sub>), 7.41 (t, 1H, *J* = 7.1 Hz, H<sub>2</sub>), 6.73 (s, 1H, H<sub>5</sub>).

**<sup>13</sup>C-NMR** (125.7 MHz, CDCl<sub>3</sub>, 298 K):  $\delta$  (ppm) = 166.0, 149.6, 142.9, 140.4, 131.4, 130.5, 129.7, 128.6 (q, 1C, <sup>2</sup>J = 32.3 Hz), 127.9, 125.4 (q, 2C, <sup>3</sup>J = 3.8 Hz), 124.5 (q, 1C, <sup>1</sup>J = 272 Hz), 120.1, 119.2, 113.5.

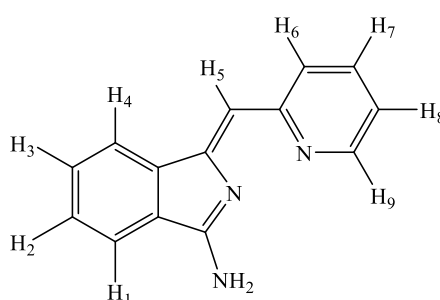
**<sup>19</sup>F-NMR** (470.6 MHz, CDCl<sub>3</sub>, 298 K):  $\delta$  (ppm) = -62.41 (s, 1F, -CF<sub>3</sub>).

**MS** (MALDI-TOF):  $m/z$  = 288.93 [M]<sup>+</sup> (100%)

**HR-MS** (FTMS + p NSI) (C<sub>16</sub>H<sub>12</sub>N<sub>3</sub>F<sub>2</sub>) [M+H]<sup>+</sup>: Calc.: 289.0947; Found: 289.0946

**UV-Vis** (CH<sub>2</sub>Cl<sub>2</sub>):  $\lambda$  max (nm) ( $\epsilon$  (dm<sup>3</sup>·mol<sup>-1</sup>·cm<sup>-1</sup>)) = 364 (2.45·10<sup>4</sup>), 284 (9.32·10<sup>3</sup>).

### (Z)-1-(2-Pyridylmethylene)-1H-isoindol-3-amine (144)



Synthesised following the general procedure F from *o*-bromobenzamidine hydrochloride **130** (0.7118 g, 3.022 mmol, 1eq), BINAP (0.1044 g, 0.166 mmol, 0.055 eq), PdCl<sub>2</sub>(MeCN)<sub>2</sub> (38.8 mg, 0.151 mmol, 0.05 eq), 2-ethynylpyridine (0.37 mL, 3.6 mmol, 1.2 eq), and DBU (1.15 mL, 2.5 eq) in DMF. Work up and purification process yielded the *title compound* as brown solid (387.5 mg, 58%).

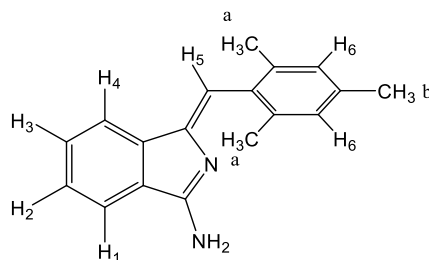
**Mp** 79 – 80 °C

**<sup>1</sup>H-NMR** (500 MHz, CDCl<sub>3</sub>, 298 K):  $\delta$ (ppm) = 8.58 (ddd, 1H,  $J$  = 4.9, 1.5, 0.6 Hz, H<sub>9</sub>), 7.79 (br d, 1H,  $J$  = 7.5 Hz, H<sub>1</sub>), 7.74 (br dt, 1H,  $J$  = 7.5 Hz, 1.0, H<sub>4</sub>), 7.63 (td, 1H,  $J$  = 7.7, 1.5 Hz, H<sub>7</sub>), 7.56 (td, 1H,  $J$  = 7.5, 1.0 Hz, H<sub>3</sub>), 7.51 (td, 1H,  $J$  = 7.5, 1.0 Hz, H<sub>2</sub>), 7.24 (br d, 1H,  $J$  = 7.7 Hz, H<sub>6</sub>), 7.04 (ddd, 1H,  $J$  = 7.7, 4.9, 1.5 Hz, H<sub>8</sub>), 6.18 (s, 1H, H<sub>5</sub>).

**<sup>13</sup>C-NMR** (125.7 MHz, CDCl<sub>3</sub>, 298 K):  $\delta$  (ppm) = 168.0 (quat.), 162.4, (quat.), 155.7 (quat.), 149.4 (C9), 139.9 (quat.), 137.2 (quat.), 136.7 (C7), 132.0 (C3), 129.8 (C2), 124.2 (C6), 123.5 (C1), 121.1 (C8), 120.4 (C4), 102.3 (C5).

**MS** (MALDI-TOF):  $m/z$  = 222.34 [M+H]<sup>+</sup> (100%)

**HR-MS** (FTMS + p NSI) (C<sub>14</sub>H<sub>45</sub>N<sub>3</sub>) [M+H]<sup>+</sup>: Calc.: 222.1026; Found: 222.1025.

**(Z)-1-(1,3,5-Trimethylphenylmethylene)-1H-isoindol-3-amine (145)**

Synthesised following the general procedure F from *o*-bromobenzamidine hydrochloride **130** (707.3 mg, 3.003 mmol, 1eq), BINAP (106.1 mg, 0.165 mmol, 0.055 eq), PdCl<sub>2</sub>(MeCN)<sub>2</sub> (39.3 mg, 0.150 mmol, 0.05 eq), 2-ethynyl-1,3,5-trimethylbenzene (0.59 mL, 3.6 mmol, 1.2 eq) and DBU (1.14 mL, 7.51 mmol, 2.5 eq) in DMF. The work up and purification process yielded the *title compound* as yellow crystals (250 mg, 32%).

**Mp** 136 – 137 °C

**<sup>1</sup>H-NMR** (500.1 MHz, CDCl<sub>3</sub>, 298 K): δ (ppm) = 7.90 (d, 1H, *J* = 7.5 Hz, H<sub>4</sub>), 7.77 (d, 1H, *J* = 7.5 Hz, H<sub>1</sub>), 7.46 (td, 1H, *J* = 7.5, 1.0 Hz, H<sub>3</sub>), 7.39 (td, 1H, *J* = 7.5, 1.0 Hz, H<sub>2</sub>), 6.84 (s, 2H, H<sub>6</sub>), 6.69 (s, 1H, H<sub>5</sub>), 2.24 (s, 3H, -CH<sub>3</sub> b), 2.19 (s, 6H, -CH<sub>3</sub> a).

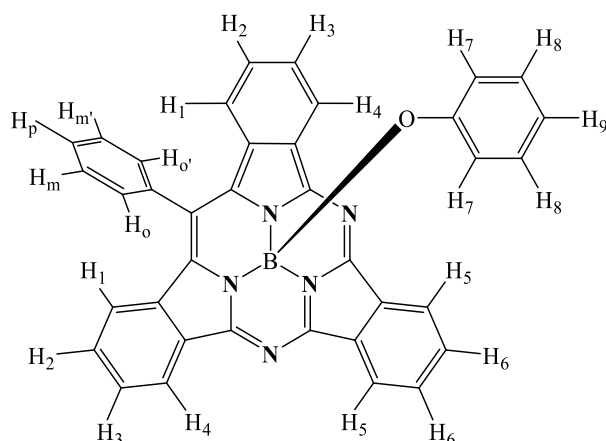
**<sup>13</sup>C-NMR** (125.7 MHz, CDCl<sub>3</sub>, 298 K): δ (ppm) = 164.8 (q), 149.0 (q), 141.7 (q), 136.1 (q), 135.1 (q), 133.3 (q), 132.8 (q), 128.6 (C3), 127.6 (C6), 127.1 (C2), 119.9 (C1), 119.7 (C4), 111.3 (C5), 20.9 (-CH<sub>3</sub> a), 20.7 (-CH<sub>3</sub> Cb).

**MS** (MALDI-TOF): *m/z* = 262.99 [M]<sup>+</sup> (100%)

**HR-MS** (FTMS + p NSI) (C<sub>18</sub>H<sub>19</sub>N<sub>2</sub>) [M+H]<sup>+</sup>: Calc.: 263.1543; Found: 263.1545.

## 4.5.2 SubTriBenzoDiAzaPorphyrins (SubTBDAPs)

### *meso*-PhenylSubTBDAP-OPh (134)



### General method G for the synthesis of SubTBDAPs

(*Z*)-1-(Phenylmethylene)-1H-isoindol-3-amine **131**<sup>[170]</sup> (51.3 mg, 0.233 mmol, 1 eq.) and phthalonitrile (59.7 mg, 0.466 mmol, 2 eq.) were dissolved in 3 mL of *p*-xylene under argon. BCl<sub>3</sub> (1M in *p*-xylene, 0.47 mL, 0.47 mmol, 2 eq.) was added dropwise. The mixture was refluxed under argon for 3 hours, after which an excess of phenol (219 mg, 2.33 mmol, 10 eq) was added and the reaction was refluxed for further 19 hours. The solvent was evaporated and the crude residue was subjected to silica gel column chromatography using 2:7 ethyl acetate/hexane as eluent. The intensely yellow fluorescent product was easily monitored on the column by irradiating with a 366 nm UV lamp. A second silica gel column chromatographic separation (eluent 1:3:2 diethyl ether/hexane/dichloromethane) and recrystallisation from distilled DCM/distilled petroleum ether yielded the pure *title compound* as pink-red solid (19.5 mg, 15%).

### General method H for the synthesis of SubTBDAPs

A mixture of (*Z*)-1-(phenylmethylene)-1H-isoindol-3-amine **131**<sup>[170]</sup> (99.0 mg, 0.449 mmol, 1 eq.), phthalonitrile (173 mg, 1.35 mmol, 3 eq.) and triphenyl borate (263 mg, 0.898 mmol, 2 eq.) were dissolved in diglyme (3.3 mL), degassed with argon and placed in a sealed tube. The reaction was heated to 200 °C for 3 hours, after which time tlc indicated complete consumption of **12**. After cooling, ethyl acetate (50 mL) was added and the mixture washed with a saturated solution of NaHCO<sub>3</sub> (75 mL x 3). The organic layer was dried over MgSO<sub>4</sub>, filtered and concentrated. The mixture was purified as above to yield the *title compound* as pink-red crystals (25.0 mg, 10%).

**Rf** 0.47 Ethyl Acetate/ Cyclohexane (2:7)

**Mp** 329 °C

**<sup>1</sup>H-NMR** (500.1 MHz, CD<sub>2</sub>Cl<sub>2</sub>, 263 K): δ (ppm) = 8.93 – 8.90 (m, 2H, H<sub>5</sub>), 8.89 (br d, *J* = 8.0 Hz, 2H, H<sub>4</sub>), 8.36 (d, *J* = 7.6 Hz, 1H, H<sub>o'</sub>), 8.00 – 7.96 (m, 2H, H<sub>6</sub>), 7.95 (t, *J* = 7.6 Hz, 1H, H<sub>m'</sub>), 7.83 (tt, *J* = 7.6, 1.2 Hz, 1H, H<sub>p</sub>), 7.79 (ddd, *J* = 8.0, 7.0, 1.0 Hz, 2H, H<sub>3</sub>), 7.58 (ddd, *J* = 8.0, 7.0, 1.0 Hz, 2H,

$^1\text{H-NMR}$  (500.1 MHz,  $\text{CD}_2\text{Cl}_2$ , 298 K):  $\delta$  (ppm) = 7.56 (t,  $J = 7.6$  Hz, 1H,  $\text{H}_m$ ), 7.47 (d,  $J = 8.0$  Hz, 2H,  $\text{H}_1$ ), 6.99 (d,  $J = 7.6$  Hz, 1H,  $\text{H}_o$ ), 6.70 (t,  $J = 7.4$  Hz, 2H,  $\text{H}_8$ ), 6.63 (t,  $J = 7.4$  Hz, 1H,  $\text{H}_9$ ), 5.25 (d,  $J = 7.4$  Hz, 2H,  $\text{H}_7$ ).

$^{13}\text{C-NMR}$  (125.7 MHz,  $\text{CD}_2\text{Cl}_2$ , 298 K):  $\delta$  (ppm) = 153.1, 150.3, 150.1, 135.4, 134.1, 132.6, 131.5, 130.0, 129.9, 129.6, 129.2, 128.8, 128.6, 127.9, 127.8, 124.4, 123.0, 122.7, 122.2, 121.5, 119.7.

$^{11}\text{B-NMR}$  (160.5 MHz,  $\text{CDCl}_3$ , 298 K):  $\delta$  (ppm) = -14.68 (s, 1B).

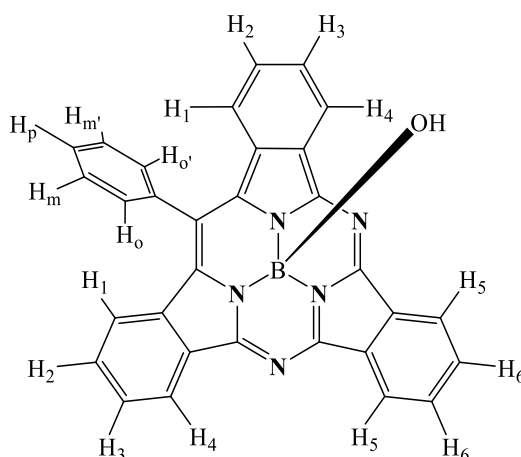
**MS** (MALDI-TOF):  $m/z = 563.41$  [ $\text{M}$ ] $^+$  (100%)

**HR-MS** (FTMS + p APCI) ( $\text{C}_{37}\text{H}_{23}\text{B}_1\text{N}_5\text{O}_1$ ) [ $\text{M}+\text{H}$ ] $^+$ : Calc.: 564.1997; Found: 564.1976

**UV-Vis** (distilled  $\text{CH}_2\text{Cl}_2$ ):  $\lambda$  max (nm) ( $\epsilon$  ( $\text{dm}^3 \cdot \text{mol}^{-1} \cdot \text{cm}^{-1}$ )) = 548 ( $5.57 \cdot 10^4$ ), 324 ( $3.96 \cdot 10^4$ ).

**Fluorescence** ( $\text{CH}_2\text{Cl}_2$ , Excitation at 500 nm): 559 nm,  $\Phi_F = 0.44$

### *meso*-PhenylSubTBDAP-OH (**132**)



SubTBDAP-OH **132** was isolated as side-product and characterised as follows:

**Rf** 0.35 Ethyl Acetate/ Cyclohexane (1:1)

**Mp** 139 °C

$^1\text{H-NMR}$  (500.1 MHz,  $\text{CD}_2\text{Cl}_2$ , 263 K):  $\delta$  (ppm) = 8.93 – 8.88 (m, 4H,  $\text{H}_4$ ,  $\text{H}_5$ ), 8.61 (br s, 1H,  $\text{H}_o$ ), 8.00 – 7.95 (m, 3H,  $\text{H}_m$ ,  $\text{H}_6$ ), 7.84 (t, 1H,  $J = 7.6$  Hz, 1H,  $\text{H}_p$ ), 7.78 (ddd, 2H,  $J = 8.0, 7.0, 1.0$  Hz,  $\text{H}_3$ ), 7.57 (ddd, 2H,  $J = 8.0, 7.0, 1.0$  Hz,  $\text{H}_2$ ,  $\text{H}_m$ ), 7.50 (dt, 2H,  $J = 8.0, 1.0$  Hz,  $\text{H}_1$ ), 7.05 (br s, 1H,  $\text{H}_o$ ).

**MS** (MALDI-TOF):  $m/z = 487.32$  [ $\text{M}$ ] $^+$  (100%)

**HR-MS** (FTMS + p NSI) ( $\text{C}_{31}\text{H}_{18}\text{B}_1\text{N}_5\text{O}_1$ ) [ $\text{M}+\text{H}$ ] $^+$ : Calc.: 488.1683; Found: 488.1671

**UV-Vis** (distilled  $\text{CH}_2\text{Cl}_2$ ):  $\lambda$  max (nm) = 536, 324.

**Fluorescence** ( $\text{CH}_2\text{Cl}_2$ , Excitation at 500 nm): 561 nm

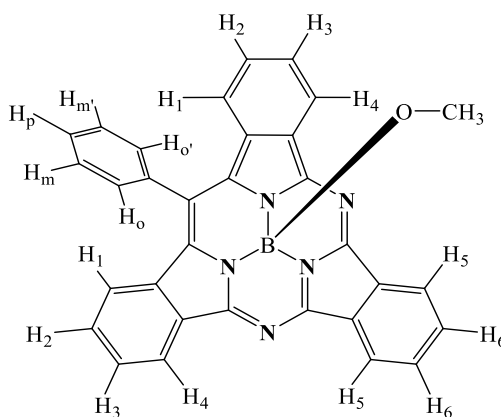


SubTBDAP Hybrids 133-149 were prepared following Procedure G using isoindolenes 131, 141-143 and the appropriate borate.

Compound	Reaction time	1 <sup>st</sup> column	2 <sup>nd</sup> column	Yield
133	4 h	1:4:2 Et <sub>2</sub> O / Hexane /DCM	none	13.7 mg, <b>9 %</b>
139	6 h	1:4:2 Et <sub>2</sub> O / Hexane /DCM	none	23.3 mg, <b>9.2 %</b>
140	2 h	100% DCM → 1:4:2 Et <sub>2</sub> O/Hex/DCM	2:7 EtOAc/ Hexane	11.8 mg, <b>7.4 %</b>
146	2 h*	1:4:2 Et <sub>2</sub> O / Hexane /DCM	2:7 EtOAc/ Hexane	16.6 mg, <b>10.3 %</b>
147	6 h	1:4:2 Et <sub>2</sub> O / Hexane /DCM	100% Hex → (1:1) Hex/DCM → 100% DCM	6.5 mg, <b>11 %</b>
148	8 h	1:3:2 Et <sub>2</sub> O / Hexane /DCM	2:7 EtOAc/ Hexane	13.2 mg, <b>12 %</b>
149	6 h	2:7 EtOAc /Hexane	1:1 Hex/ DCM → 100% DCM	17.5 mg, <b>6.8 %</b>

\*Reaction solvent: *p*-xylene

### *meso*-PhenylSubTBDAP-OMe (133)



**Rf** 0.32 Ethyl Acetate/ Cyclohexane (2:7)

**Mp** 319 °C

**<sup>1</sup>H-NMR** (500.1 MHz, CD<sub>2</sub>Cl<sub>2</sub>, 263 K): δ (ppm) = 8.92 – 8.88 (m, 4H, H<sub>4</sub>, H<sub>5</sub>), 8.58 (d, 1H, *J* = 7.6 Hz, H<sub>o'</sub>), 7.99 (t, 1H, *J* = 7.6 Hz, H<sub>m'</sub>), 7.97 – 7.93 (m, 2H, H<sub>6</sub>), 7.83 (tt, 1H, *J* = 7.6, 1.2 Hz, H<sub>p</sub>), 7.78 (ddd, 2H, *J* = 8.0, 7.1, 0.9, H<sub>3</sub>), 7.59 – 7.53 (m, 3H, H<sub>m</sub>, H<sub>2</sub>), 7.47 (br d, 2H, *J* = 8.0 Hz, H<sub>1</sub>), 6.96 (d, 1H, *J* = 7.6 Hz, H<sub>o</sub>), 1.28 (s, 3H, -CH<sub>3</sub>).

**<sup>13</sup>C-NMR** (125.7 MHz, CD<sub>2</sub>Cl<sub>2</sub>, 298 K): δ (ppm) = 151.2, 150.7, 136.0, 135.0, 134.8, 133.0, 131.9, 130.3, 130.3, 130.0, 129.6, 128.8, 128.1, 124.9, 123.4, 122.8, 122.2, 47.0.

$^{11}\text{B-NMR}$  (160.5 MHz,  $\text{CDCl}_3$ , 298 K):  $\delta$  (ppm) = -14.45 (s, 1B).

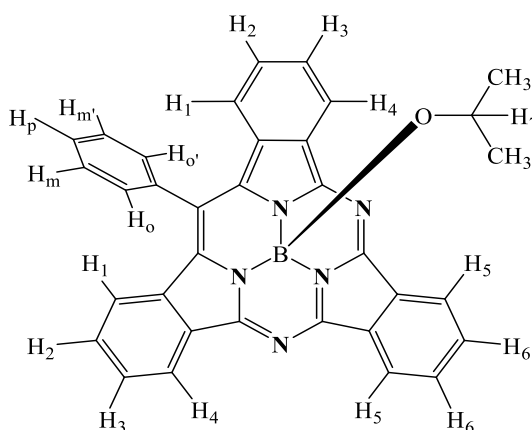
**MS** (MALDI-TOF):  $m/z$  = 501.27  $[\text{M}]^+$  (100%)

**HR-MS** (FTMS + p APCI) ( $\text{C}_{32}\text{H}_{21}\text{B}_1\text{N}_5\text{O}_1$ )  $[\text{M}+\text{H}]^+$ : Calc.: 502.1839; Found: 502.1820

**UV-Vis** (distilled  $\text{CH}_2\text{Cl}_2$ ):  $\lambda$  max (nm) ( $\epsilon$  ( $\text{dm}^3 \cdot \text{mol}^{-1} \cdot \text{cm}^{-1}$ )) = 547 ( $5.97 \cdot 10^4$ ), 324 ( $4.61 \cdot 10^4$ ).

**Fluorescence** ( $\text{CH}_2\text{Cl}_2$ , Excitation at 500 nm): 558 nm,  $\Phi_F$  = 0.43

**meso-PhenylSubTBDAP-O<sup>i</sup>Pr (139)**



**Rf** 0.44 Ethyl Acetate/ Cyclohexane (2:7)

**Mp** 322 °C

$^1\text{H-NMR}$  (500.1 MHz,  $\text{CD}_2\text{Cl}_2$ , 263 K):  $\delta$  (ppm) = 8.92 – 8.89 (m, 2H,  $\text{H}_5$ ), 8.88 (br d, 2H,  $J$  = 8.0 Hz,  $\text{H}_4$ ), 8.57 (d, 1H,  $J$  = 7.6 Hz,  $\text{H}_{o'}$ ), 8.01 – 7.95 (m, 3H,  $\text{H}_{m'}$ ,  $\text{H}_6$ ), 7.83 (t, 1H,  $J$  = 7.6 Hz,  $\text{H}_p$ ), 7.77 (br t, 2H,  $J$  = 7.4 Hz,  $\text{H}_3$ ), 7.59 – 7.53 (m, 3H,  $\text{H}_m$ ,  $\text{H}_2$ ), 7.47 (br d, 2H,  $J$  = 8.0 Hz,  $\text{H}_1$ ), 6.96 (d, 1H,  $J$  = 7.6 Hz,  $\text{H}_o$ ), 1.30 – 1.24 (m, 1H,  $\text{H}_7$ ), -0.13 (d,  $J$  = 6.1 Hz, 6H,  $-\text{CH}_3$ ).

$^{13}\text{C-NMR}$  (125.7 MHz,  $\text{CD}_2\text{Cl}_2$ , 298 K):  $\delta$  (ppm) = 151.0, 150.6, 136.0, 134.8, 134.2, 133.0, 131.9, 130.4, 130.2, 130.0, 129.6, 128.8, 128.0, 124.9, 123.4, 122.8, 122.2, 61.7, 24.4.

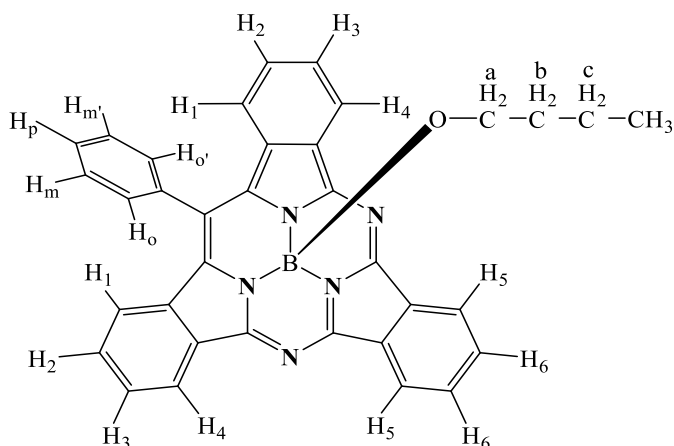
$^{11}\text{B-NMR}$  (160.5 MHz,  $\text{CDCl}_3$ , 298 K):  $\delta$  (ppm) = -14.85 (s, 1B).

**MS** (MALDI-TOF):  $m/z$  = 529.39  $[\text{M}]^+$  (100%)

**HR-MS** (FTMS + p APCI) ( $\text{C}_{34}\text{H}_{25}\text{B}_1\text{N}_5\text{O}_1$ )  $[\text{M}+\text{H}]^+$ : Calc.: 530.2153; Found: 530.2143

**UV-Vis** (distilled  $\text{CH}_2\text{Cl}_2$ ):  $\lambda$  max (nm) ( $\epsilon$  ( $\text{dm}^3 \cdot \text{mol}^{-1} \cdot \text{cm}^{-1}$ )) = 547 ( $5.19 \cdot 10^4$ ), 325 ( $3.98 \cdot 10^4$ ).

**Fluorescence** ( $\text{CH}_2\text{Cl}_2$ , Excitation at 500 nm): 558 nm,  $\Phi_F$  = 0.43.

**meso-PhenylSubTBDAP-OBu (140)**

**Rf** 0.47 Ethyl Acetate/ Cyclohexane (2:7)

**Mp** 295 °C

**<sup>1</sup>H-NMR** (500.1 MHz, CD<sub>2</sub>Cl<sub>2</sub>, 298 K): δ (ppm) = 8.96 – 8.91 (m, 4H, H<sub>4</sub>, H<sub>5</sub>), 8.57 (d, 1H, *J* = 7.6 Hz, H<sub>0'</sub>), 8.01 – 7.99 (m, 3H, H<sub>m'</sub>, H<sub>6</sub>), 7.84 (t, 1H, *J* = 7.6 Hz, H<sub>p</sub>), 7.79 (ddd, 2H, *J* = 8.0, 7.0, 1.0 Hz, H<sub>3</sub>), 7.59 – 7.54 (m, 3H, H<sub>m</sub>, H<sub>2</sub>), 7.47 (br d, 2H, *J* = 8.0 Hz, H<sub>1</sub>), 6.96 (d, 1H, *J* = 7.6 Hz, H<sub>0</sub>), 1.28 (t, 2H, *J* = 6.6 Hz, -CH<sub>2</sub> a), 0.49 – 0.39 (m, 2H, CH<sub>2</sub> c), 0.37 – 0.30 (m, 5H, -CH<sub>2</sub> b, -CH<sub>3</sub>).

**<sup>13</sup>C-NMR** (125.7 MHz, CD<sub>2</sub>Cl<sub>2</sub>, 298 K): δ (ppm) = 151.1, 150.6, 136.0, 134.9, 133.0, 131.9, 130.3, 130.2, 130.0, 129.6, 128.8, 128.1, 124.8, 123.4, 122.8, 122.2, 59.2, 33.4, 18.9, 13.7.

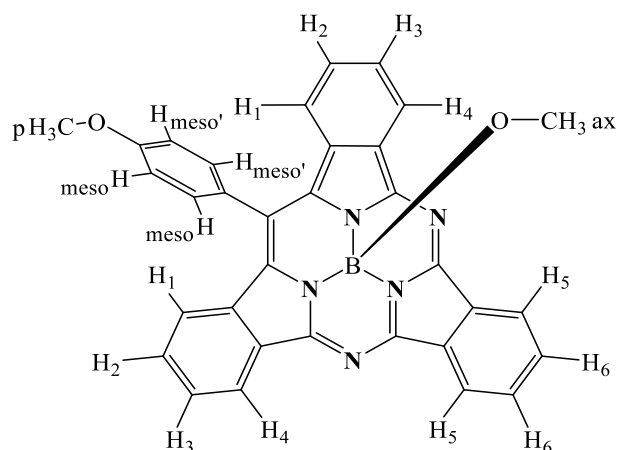
**<sup>11</sup>B-NMR** (160.5 MHz, CD<sub>2</sub>Cl<sub>2</sub>, 298 K): δ (ppm) = -14.66 (s, 1B).

**MS** (MALDI-TOF): *m/z* = 543.24 [M]<sup>+</sup> (100%)

**HR-MS** (FTMS + p NSI) (C<sub>35</sub>H<sub>27</sub>B<sub>1</sub>N<sub>5</sub>O<sub>1</sub>) [M+H]<sup>+</sup>: Calc.: 544.2309; Found: 544.2297

**UV-Vis** (distilled CH<sub>2</sub>Cl<sub>2</sub>): λ max (nm) (ε (dm<sup>3</sup>·mol<sup>-1</sup>·cm<sup>-1</sup>)) = 547 (4.85·10<sup>4</sup>), 325 (3.74·10<sup>4</sup>).

**Fluorescence** (CH<sub>2</sub>Cl<sub>2</sub>, Excitation at 500 nm): 558 nm, Φ<sub>F</sub> = 0.45

**meso-(4-Methoxyphenyl)SubTBDAP-OMe (146)**

**Rf** 0.26 Ethyl Acetate/ Cyclohexane (2:7)

**Mp** 310 °C

**<sup>1</sup>H-NMR** (500.1 MHz, CD<sub>2</sub>Cl<sub>2</sub>, 263 K):  $\delta$  (ppm) = 8.92 – 8.87 (m, 4H, H<sub>4</sub>, H<sub>5</sub>), 8.48 (d, 1H,  $J$  = 7.6 Hz, H<sub>meso'</sub>), 7.98 – 7.93 (m, 2H, H<sub>6</sub>), 7.80 – 7.76 (m, 2H, H<sub>3</sub>), 7.62 – 7.57 (m, 4H, H<sub>1</sub>, H<sub>2</sub>), 7.49 (d, 1H,  $J$  = 7.6 Hz, H<sub>meso'</sub>), 7.07 (d, 1H,  $J$  = 7.6 Hz, H<sub>meso</sub>), 6.88 (d, 1H,  $J$  = 7.6 Hz, H<sub>meso</sub>), 4.05 (s, 3H, -CH<sub>3</sub> p), 1.27 (s, 3H, -CH<sub>3</sub> ax).

**<sup>13</sup>C-NMR** (125.7 MHz, CD<sub>2</sub>Cl<sub>2</sub>, 298 K):  $\delta$  (ppm) = 161.3, 151.1, 150.6, 135.2, 133.1, 131.9, 130.3, 130.2, 128.8, 128.1, 127.8, 124.8, 123.5, 122.8, 122.2, 120.4, 115.0, 56.1, 47.0.

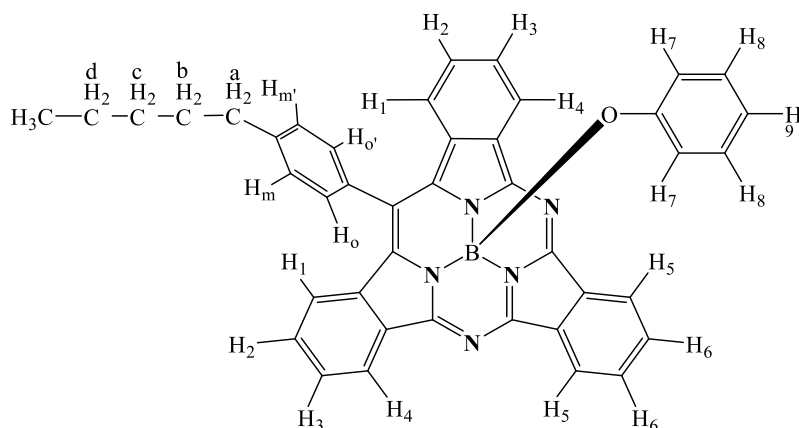
**<sup>11</sup>B-NMR** (160.5 MHz, CDCl<sub>3</sub>, 298 K):  $\delta$  (ppm) = -14.44 (s, 1B).

**MS** (MALDI-TOF):  $m/z$  = 531.26 [M]<sup>+</sup> (100%)

**HR-MS** (FTMS + p NSI) (C<sub>33</sub>H<sub>23</sub>B<sub>1</sub>N<sub>5</sub>O<sub>2</sub>) [M+H]<sup>+</sup>: Calc.: 532.1945; Found: 532.1935

**UV-Vis** (distilled CH<sub>2</sub>Cl<sub>2</sub>):  $\lambda$  max (nm) ( $\epsilon$  (dm<sup>3</sup>·mol<sup>-1</sup>·cm<sup>-1</sup>)) = 548 (5.48·10<sup>4</sup>), 322 (3.49·10<sup>4</sup>).

**Fluorescence** (CH<sub>2</sub>Cl<sub>2</sub>, Excitation at 500 nm): 558 nm,  $\Phi_F$  = 0.44.

**meso-(4-*n*-Pentylphenyl)SubTBDAP-OPh (147)**

**Rf** 0.53 Ethyl Acetate/ Cyclohexane (2:7)

**Mp** 274 °C

**<sup>1</sup>H-NMR** (500.1 MHz, CD<sub>2</sub>Cl<sub>2</sub>, 263 K): δ (ppm) = 8.93 – 8.89 (m, 2H, H<sub>5</sub>), 8.89 (d, 2H, *J* = 8.0 Hz, H<sub>4</sub>), 8.25 (d, 1H, *J* = 7.6 Hz, H<sub>0'</sub>), 8.01 – 7.95 (m, 2H, H<sub>6</sub>), 7.81 – 7.75 (m, 3H, H<sub>m'</sub>, H<sub>3</sub>), 7.59 (ddd, 2H, *J* = 8.0, 7.0, 1.0 Hz, H<sub>2</sub>), 7.52 (br d, 2H, *J* = 8.0 Hz, H<sub>1</sub>), 7.36 (d, 1H, *J* = 7.6 Hz, H<sub>m</sub>), 6.89 (d, 1H, *J* = 7.6 Hz, H<sub>0</sub>), 6.70 (t, 2H, *J* = 7.4 Hz, H<sub>8</sub>), 6.62 (t, 1H, *J* = 7.4 Hz, H<sub>9</sub>), 5.24 (d, 2H, *J* = 7.4 Hz, H<sub>7</sub>), 2.91 (t, 2H, *J* = 7.7 Hz, -CH<sub>2</sub> a), 1.89 – 1.82 (m, 2H, -CH<sub>2</sub> b), 1.51 – 1.41 (m, 4H, -CH<sub>2</sub> c, d), 0.99 (t, 3H, *J* = 7.0 Hz, -CH<sub>3</sub>).

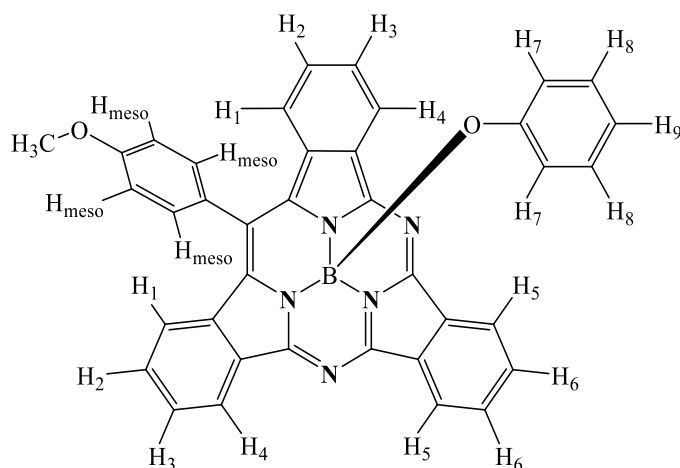
**<sup>13</sup>C-NMR** (125.7 MHz, CD<sub>2</sub>Cl<sub>2</sub>, 298 K): δ (ppm) = 153.7, 150.7, 150.3, 146.7, 145.2, 134.8, 133.1, 132.8, 131.9, 130.4, 129.7, 129.1, 128.9, 128.2, 127.9, 125.3, 123.6, 122.9, 122.3, 121.8, 120.1, 36.5, 32.2, 31.8, 23.2, 14.5.

**<sup>11</sup>B-NMR** (160.5 MHz, CD<sub>2</sub>Cl<sub>2</sub>, 298 K): δ (ppm) = -14.66 (s, 1B).

**MS** (MALDI-TOF): *m/z* = 634.34 [M+H]<sup>+</sup>

**UV-Vis** (distilled CH<sub>2</sub>Cl<sub>2</sub>): λ max (nm) (ε (dm<sup>3</sup>·mol<sup>-1</sup>·cm<sup>-1</sup>)) = 549 (5.86·10<sup>4</sup>), 327 (3.89·10<sup>4</sup>).

**Fluorescence** (CH<sub>2</sub>Cl<sub>2</sub>, Excitation at 500 nm): 559 nm, Φ<sub>F</sub> = 0.44

**meso-(4-Methoxyphenyl)SubTBDAP -OPh (148)**

**Rf** 0.44 Ethyl Acetate/ Cyclohexane (2:7)

**Mp** 300 °C

**<sup>1</sup>H-NMR** (500.1 MHz, CD<sub>2</sub>Cl<sub>2</sub>, 263 K): δ (ppm) = 8.93 – 8.89 (m, 2H, H<sub>5</sub>), 8.89 (br d, 2H, J = 8.1 Hz, H<sub>4</sub>), 8.28 (d, 1H, J = 7.6 Hz, H<sub>meso</sub>), 8.01 – 7.96 (m, 2H, H<sub>6</sub>), 7.80 (ddd, 2H, J = 7.9, 6.5, 1.5 Hz, H<sub>3</sub>), 7.63 – 7.57 (m, 4H, H<sub>2</sub>, H<sub>1</sub>), 7.47 (d, 1H, J = 7.6 Hz, H<sub>meso</sub>), 7.07 (d, 1H, J = 7.6 Hz, H<sub>meso</sub>), 6.91 (d, 1H, J = 7.6 Hz, H<sub>meso</sub>), 6.70 (t, 2H, J = 7.5 Hz, H<sub>8</sub>), 6.62 (t, 2H, J = 7.5 Hz, H<sub>9</sub>), 5.24 (t, 2H, J = 7.5 Hz, H<sub>7</sub>), 4.05 (s, 3H, -CH<sub>3</sub>).

**<sup>13</sup>C-NMR** (125.7 MHz, CD<sub>2</sub>Cl<sub>2</sub>, 298 K): δ (ppm) = 161.3, 150.7, 150.3, 134.9, 134.5, 134.0, 131.9, 130.4, 129.1, 129.0, 128.2, 127.6, 125.0, 123.6, 122.9, 122.3, 121.8, 121.3, 121.2, 120.1, 115.0, 56.1.

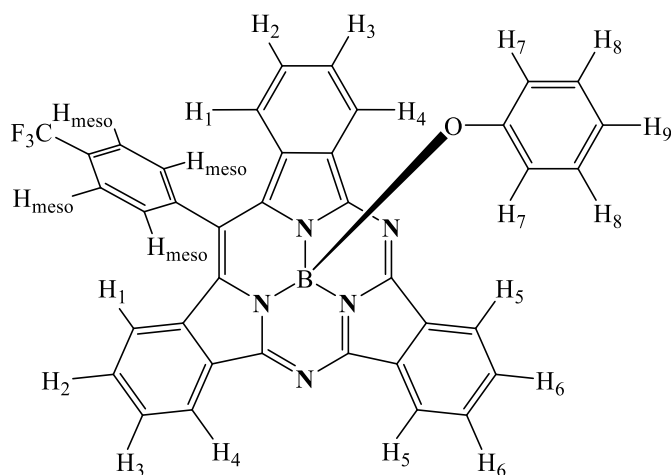
**<sup>11</sup>B-NMR** (160.5 MHz, CD<sub>2</sub>Cl<sub>2</sub>, 298 K): δ (ppm) = -14.65 (s, 1B).

**MS** (MALDI-TOF): *m/z* = 593.39 [M]<sup>+</sup>

**HR-MS** (FTMS + p NSI) (C<sub>38</sub>H<sub>25</sub>B<sub>1</sub>N<sub>5</sub>O<sub>2</sub>) [M+H]<sup>+</sup>: Calc.: 594.2102; Found: 594.2091.

**UV-Vis** (distilled CH<sub>2</sub>Cl<sub>2</sub>): λ max (nm) (ε (dm<sup>3</sup>·mol<sup>-1</sup>·cm<sup>-1</sup>)) = 549 (5.25·10<sup>4</sup>), 315 (3.41·10<sup>4</sup>).

**Fluorescence** (CH<sub>2</sub>Cl<sub>2</sub>, Excitation at 500 nm): 559 nm, Φ<sub>F</sub> = 0.45

**meso-(4-(Trifluoromethyl)phenyl)SubTBDAP-OPh (149)**

**Rf** 0.53 Ethyl Acetate/ Cyclohexane (2:7)

**Mp** 270 °C

**<sup>1</sup>H-NMR** (500.1 MHz, CD<sub>2</sub>Cl<sub>2</sub>, 263 K): δ (ppm) = 8.96 – 8.93 (m, 4H, H<sub>4</sub>, H<sub>5</sub>), 8.50 (s, 1H, *J* = 7.8 Hz, H<sub>meso</sub>), 8.24 (d, 1H, *J* = 7.8 Hz, H<sub>meso</sub>), 8.03 – 8.00 (m, 2H, H<sub>6</sub>), 7.85 – 7.81 (m, 3H, H<sub>meso</sub>, H<sub>3</sub>), 7.62 (ddd, 2H, *J* = 8.1, 7.1, 1.0 Hz, H<sub>2</sub>), 7.42 (br d, 2H, *J* = 8.1 Hz, H<sub>1</sub>), 7.18 (d, 1H, *J* = 7.8 Hz, H<sub>meso</sub>), 6.71 (t, 2H, *J* = 7.5 Hz, H<sub>8</sub>), 6.64 (t, 1H, *J* = 7.5, H<sub>9</sub>), 5.25 (d, 2H, *J* = 7.5 Hz H<sub>7</sub>).

**<sup>13</sup>C-NMR** (125.7 MHz, CD<sub>2</sub>Cl<sub>2</sub>, 298 K): δ (ppm) = 153.6, 150.8, 150.7, 139.9, 137.8, 134.2, 133.1, 132.8, 132.1 (q, 1C, <sup>2</sup>*J* = 32 Hz), 131.9, 130.6, 130.4, 129.3, 129.2, 128.4, 126.6 (q, 2C, <sup>3</sup>*J* = 4 Hz), 124.9 (q, 1C, <sup>1</sup>*J* = 272 Hz), 123.2, 123.0, 122.5, 121.9, 120.1.

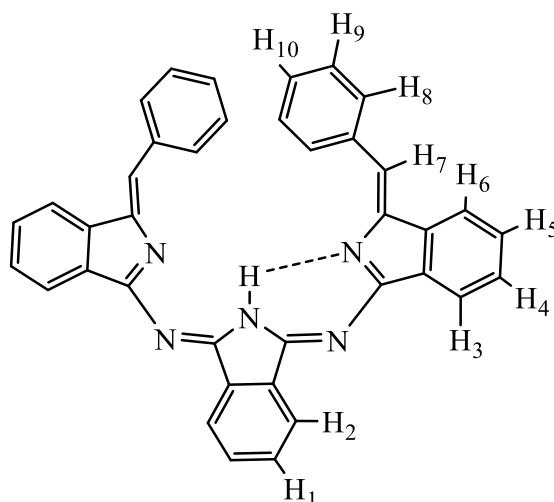
**<sup>11</sup>B-NMR** (160.5 MHz, CD<sub>2</sub>Cl<sub>2</sub>, 298 K): δ (ppm) = -14.67 (s, 1B).

**<sup>19</sup>F-NMR** (470.6 MHz, CD<sub>2</sub>Cl<sub>2</sub>, 298 K): δ (ppm) = -62.64 (s, 1F, -CF<sub>3</sub>).

**MS** (MALDI-TOF): *m/z* = 632.15 [M+H]<sup>+</sup> (100%)

**UV-Vis** (distilled CH<sub>2</sub>Cl<sub>2</sub>): λ max (nm) (ε (dm<sup>3</sup>·mol<sup>-1</sup>·cm<sup>-1</sup>)) = 547 (6.72·10<sup>4</sup>), 323 (4.64·10<sup>4</sup>).

**Fluorescence** (CH<sub>2</sub>Cl<sub>2</sub>, Excitation at 500 nm): 559 nm, Φ<sub>F</sub> = 0.37

**Trimer (152)**

Intermediate isolated during the reaction towards the synthesis of SubTBDAP-OBu **140**: A mixture of (Z)-1-(phenylmethylene)-1H-indole-3-amine **12** (0.1954 g, 0.8871 mmol, 1 eq), phthalonitrile (0.3410 g, 2.661 mmol, 3 eq) and tributyl borate (0.4124 g, 1.774 mmol, 2 eq) were placed in a sealed tube which had been previously air evacuated and filled with argon (x3), diglyme (6.5 mL) was added and the mixture was sonicated and degassed. The reaction was heated to 200 °C and aliquots were taken periodically. The aliquot taken 30 minutes after start heating the mixture was subjected to the work up described in general method H and subsequently subjected to a preparative TLC using 1:5:2 Et<sub>2</sub>O/ cyclohexane/ DCM as solvent eluent. Recrystallisation from distilled dichloromethane/ distilled hexane yielded the title compound as brown solid. Since trimer **152** was isolated from an aliquot yield could not be calculated.

**Mp** 198 -199 °C

**<sup>1</sup>H-NMR** (500.1 MHz, CD<sub>2</sub>Cl<sub>2</sub>, 263 K): δ (ppm) = 8.22 – 8.19 (m, 2H, H<sub>1</sub>), 7.98 (d, 2H, *J* = 7.1 Hz, H<sub>6</sub>), 7.87 (d, 4H, *J* = 7.5 Hz, H<sub>8</sub>), 7.74 (d, 4H, *J* = 6.3 Hz, H<sub>2</sub>, H<sub>3</sub>), 7.55 – 7.47 (m, 4H, H<sub>4</sub>, H<sub>5</sub>), 7.08 (s, 1H, -NH), 6.96 (t, 2H, *J* = 7.2 Hz, H<sub>10</sub>), 6.89 – 6.83 (m, 4H, H<sub>9</sub>), 6.65 (s, 2H, H<sub>7</sub>).

**MS** (MALDI-TOF): *m/z* = 551.71 [M]<sup>+</sup> (100%)

**HR-MS** (FTMS + p NSI) (C<sub>38</sub>H<sub>26</sub>N<sub>5</sub>) [M+H]<sup>+</sup>: Calc.: 552.2183; Found: 552.2172

**UV-Vis** (dist. CH<sub>2</sub>Cl<sub>2</sub>): λ max (nm) (ε (dm<sup>3</sup>·mol<sup>-1</sup>·cm<sup>-1</sup>)) = 334 (1.28·10<sup>4</sup>), 256 (1.16·10<sup>4</sup>).

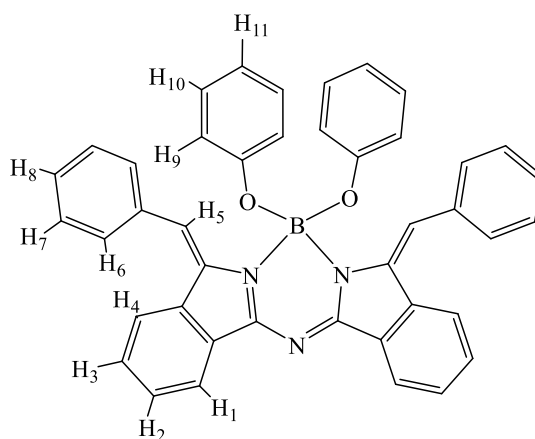


### 4.5.3 azaBODIPY derivatives

#### General procedure I for the synthesis of azaBODIPY

A mixture of aminoisoindolene derivative (1 eq) and triphenyl borate (2 eq) in *p*-xylene (2 mL), were sealed in a microwave vessel with a magnetic bar and then purged and refilled with N<sub>2</sub> three times. The mixture was irradiated in a microwave reactor at 220 °C for 1 h. After cooling, the solvent was removed under reduced pressure, and the residue was finally purified by column chromatography in silica gel using the specified solvent system to give the desired products.

#### AzaBODIPY-OPh (135)



Synthesised following general procedure I from aminoisoindolene **131** (35.0 mg, 0.159 mmol, 1 eq) and triphenyl borate (93.1 mg, 0.318 mmol, 2 eq) in *p*-xylene (2 mL). The residue was purified by column chromatography using (2:7) EtOAc/ PE as solvent system to yield pure *title compound* as yellow solid (20.1 mg, 41%).

**Rf** 0.56 Ethyl Acetate/ Cyclohexane (2:7)

**Mp** 180 – 182 °C

**<sup>1</sup>H-NMR** (500.1 MHz, CD<sub>2</sub>Cl<sub>2</sub>, 263 K): δ (ppm) = 8.36 (s, 2H, H<sub>5</sub>), 8.15 (d, 2H, *J* = 7.6 Hz, H<sub>1</sub>), 7.54 – 7.37 (m, 16H, H<sub>2</sub>, H<sub>3</sub>, H<sub>4</sub>, H<sub>6</sub>, H<sub>7</sub>, H<sub>8</sub>), 7.02 (t, 4H, *J* = 8.0 Hz, H<sub>10</sub>), 6.79 – 6.72 (m, 6H, H<sub>9</sub>, H<sub>11</sub>).

**<sup>13</sup>C-NMR** (125.7 MHz, CD<sub>2</sub>Cl<sub>2</sub>, 298 K): δ (ppm) = 164.5, 156.8, 138.4, 136.2, 135.3, 133.0, 132.3, 129.7, 129.4, 129.2, 128.7 (4), 128.7 (0), 127.5, 123.7, 123.6, 120.5, 119.3.

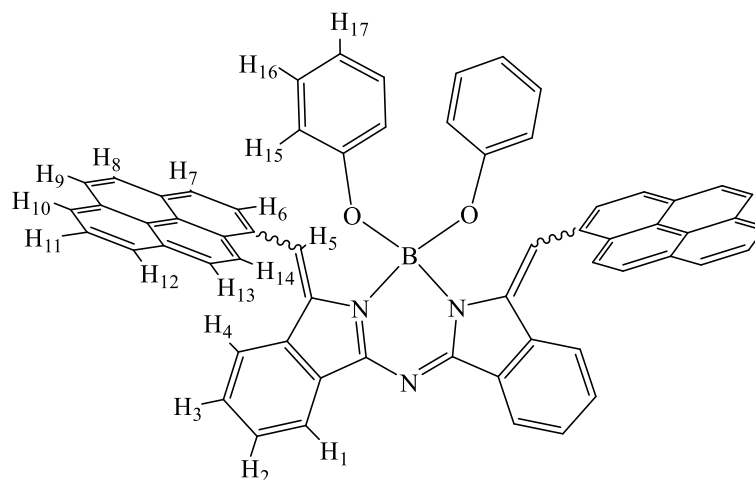
**<sup>11</sup>B-NMR** (160.5 MHz, CDCl<sub>3</sub>, 298 K): δ (ppm) = 2.34 (s, 1B).

**MS** (MALDI-TOF): *m/z* = 620.68 [M+H]<sup>+</sup> (100%)

**HR-MS** (FTMS + p NSI) (C<sub>42</sub>H<sub>30</sub>B<sub>1</sub>N<sub>3</sub>O<sub>2</sub>) [M+H]<sup>+</sup>: Calc.: 620.2511; Found: 620.2502

**UV-Vis** (distilled CH<sub>2</sub>Cl<sub>2</sub>): λ max (nm) (ε (dm<sup>3</sup>·mol<sup>-1</sup>·cm<sup>-1</sup>)) = 451 (1.82·10<sup>4</sup>), 319 (2.05·10<sup>4</sup>).

**Fluorescence** (distilled CH<sub>2</sub>Cl<sub>2</sub>, Excitation at 450 nm): 548 nm.

**AzaBODIPY-pyrene (151)**

Synthesised following general procedure I using aminoisindolene **124** (99.1 mg, 0.29 mmol, 1 eq) and triphenyl borate (93.1 mg, 166.9 mg, 0.58 mmol) in *p*-xylene (2 mL). The residue was purified by two subsequent column chromatography, the first one using (1:5:2) Et<sub>2</sub>O/Hexane/DCM as solvent system, and the second one using (3:2) DCM/PE as solvent eluent to give tittle compound as red solid (17.2 mg, 13.7 %).

**Rf** 0.32 Et<sub>2</sub>O/Hexane/DCM (1:5:2)

**Mp** 322 – 325 °C

**<sup>1</sup>H-NMR** (500.1 MHz, CD<sub>2</sub>Cl<sub>2</sub>, 263 K) (major isomer): δ (ppm) = 9.10 (s, 2H, H<sub>5</sub>), 8.24 – 7.25 (m, 20H), 7.48 (td, 2H, J = 7.7, 0.7 Hz), 7.23 – 7.18 (m, 6H, H<sub>16</sub>), 7.03 (dd, 6H, J = 8.6, 0.9 Hz, H<sub>15</sub>), 6.92 (tt, 2H, J = 7.3, 1.0 Hz, H<sub>17</sub>).

**<sup>13</sup>C-NMR** (125.7 MHz, CD<sub>2</sub>Cl<sub>2</sub>, 298 K): δ (ppm) = 164.7, 157.0, 139.6, 136.4, 133.0, 132.4, 131.9, 131.4, 131.2, 129.8, 129.7, 129.3, 129.1, 128.3, 128.2, 127.8, 127.5, 126.4, 126.0, 125.8, 125.7, 125.0, 124.8, 124.7, 123.7, 120.7, 119.6, 119.3, 118.7.

**<sup>11</sup>B-NMR** (160.5 MHz, CDCl<sub>3</sub>, 298 K): δ (ppm) = 2.76 (s, 1B, major isomer), 1.80 (s, 1B, minor isomer), ratio 4:1.

**MS** (MALDI-TOF): *m/z* = 774 [M-OPh]<sup>+</sup> (100%)

**HR-MS** (FTMS + p NSI) (C<sub>62</sub>H<sub>39</sub>B<sub>1</sub>N<sub>3</sub>O<sub>2</sub>) [M+H]<sup>+</sup>: Calc.: 868.3140; Found: 868.3135.

**UV-Vis** (distilled CH<sub>2</sub>Cl<sub>2</sub>): λ max (nm) (ε (dm<sup>3</sup>·mol<sup>-1</sup>·cm<sup>-1</sup>)) = 490 (1.26·10<sup>4</sup>), 346 (2.04·10<sup>4</sup>), 277 (2.88·10<sup>4</sup>), 267 (2.87·10<sup>4</sup>).

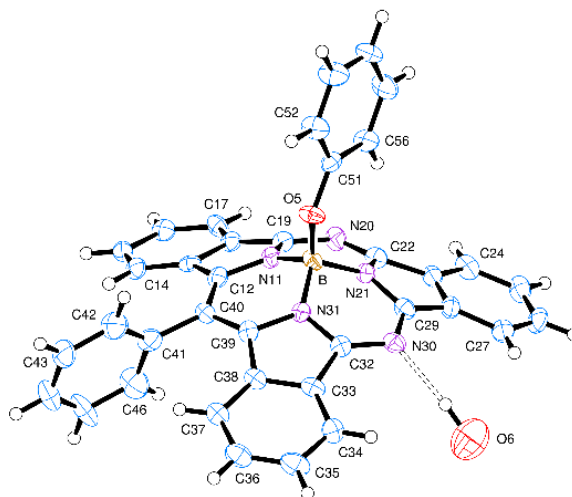
**Fluorescence** (distilled CH<sub>2</sub>Cl<sub>2</sub>, Excitation at 490 nm): 626 nm.

#### 4.5.4 X-Ray Data

*X-Ray analysis performed at University of East Anglia by Dr David Hughes*

##### *meso*-PhenylSubTBDAP-OPh (134)

A single crystal suitable for X-ray analysis was prepared by recrystallisation from a mixture of acetone/hexane.



*Crystal data:* C<sub>37</sub>H<sub>22</sub>BN<sub>5</sub>O, H<sub>2</sub>O, M = 581.42. Monoclinic, space group P2<sub>1</sub>/n (equiv. to no. 14), a = 11.0275(5), b = 13.7317(8), c = 17.8943(8) Å, β = 91.644(4)°, V = 2708.6(2) Å<sup>3</sup>. Z = 4, D<sub>c</sub> = 1.426 g cm<sup>-3</sup>, F(000) = 1208, T = 140(1) K, μ(Mo-Kα) = 0.09 cm<sup>-1</sup>, λ(Mo-Kα) = 0.71069 Å.

Crystals are red prisms. From a sample under oil, one, ca 0.05 x 0.10 x 0.41 mm, was mounted on a glass fibre and fixed in the cold nitrogen stream on an Oxford Diffraction Xcalibur-3/Sapphire3-CCD diffractometer, equipped with Mo-Kα radiation and graphite monochromator. Intensity data were measured by thin-slice ω- and φ-scans. Total no. of reflections recorded, to θ<sub>max</sub> = 21.5°, was 24461 of which 3107 were unique (R<sub>int</sub> = 0.111); 2074 were 'observed' with I > 2σ<sub>I</sub>.

Data were processed using the CrysAlisPro-CCD and -RED (1) programs. The structure was determined by the direct methods routines in the SHELXS program (2A) and refined by full-matrix least-squares methods, on F<sup>2</sup>'s, in SHELXL (2B). The non-hydrogen atoms were refined with anisotropic thermal parameters. Hydrogen atoms in the main molecule were included in idealised positions and their U<sub>iso</sub> values were set to ride on the U<sub>eq</sub> values of the parent carbon atoms. There were a number of persistent difference peaks in the neighbourhood of the solvent water oxygen atom, O(6), and four of these were included as hydrogen atoms which were refined freely; two appear close to likely sites as part of the water molecule, whilst two were further from the oxygen atom and might be indications of site disorder of the solvent molecule. At the conclusion of the refinement, wR<sub>2</sub> = 0.140 and R<sub>1</sub> = 0.098 (2B) for all 3107 reflections weighted w = [σ<sup>2</sup>(F<sub>o</sub><sup>2</sup>) + (0.0631P)<sup>2</sup>]<sup>-1</sup> with P = (F<sub>o</sub><sup>2</sup> + 2F<sub>c</sub><sup>2</sup>)/3; for the 'observed' data only, R<sub>1</sub> = 0.057.

In the final difference map, the highest peak (ca 0.23 eÅ<sup>-3</sup>) was near H(37).

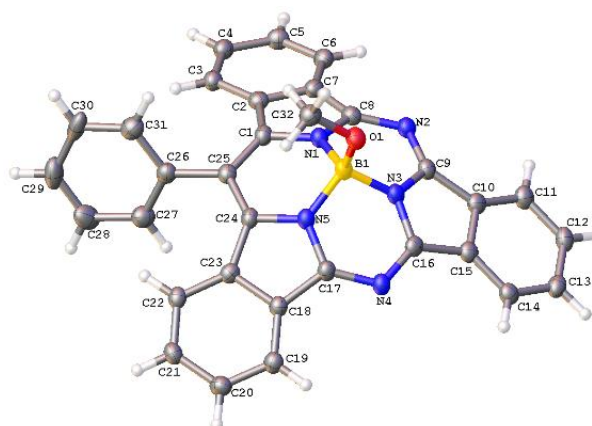
Scattering factors for neutral atoms were taken from reference (3). Computer programs used in this analysis have been noted above, and were run through WinGX (4) on a Dell Optiplex GX620 PC at the University of East Anglia.

## References

- (1) Programs CrysAlisPro, Oxford Diffraction Ltd., Abingdon, UK (2010).
- (2) 'International Tables for X-ray Crystallography', Kluwer Academic Publishers, Dordrecht (1992). Vol. C, pp. 500, 219 and 193.
- (3) L. J. Farrugia, (2012) *J. Appl. Cryst.* 45, 849–854.

***X-Ray analysis performed at the UK National Crystallography Service at Southampton by Dr Simon J. Coles and Dr Graham J. Tizzard***

### ***meso-PhenylSubTBDAP-OMe (133)***



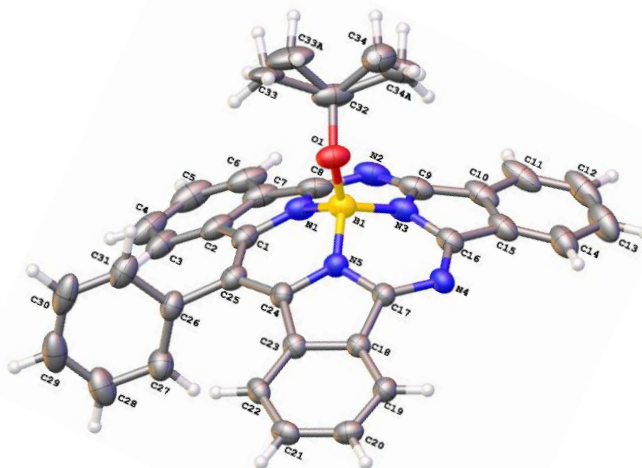
Crystals suitable for X-Ray analysis were grown dissolving SubTBDAP **133** in a mixture of dichloromethane/hexane and allowing slow diffusion with acetone.

Formula: C<sub>32</sub>H<sub>20</sub>BN<sub>5</sub>O; Mr = 501.35; crystal dimensions: 0.11 x 0.06 x 0.01 mm; crystal system: Monoclinic; space group: P2<sub>1</sub>/c; a = 11.856(2) Å, b = 8.8935(17) Å, c = 21.923(4) Å, α = 90°, β = 92.213(3)°, γ = 90°; V = 2309.9(7) Å<sup>3</sup>; Z = 4; ρ<sub>calcd</sub> = 1.442 Mg/m<sup>3</sup>; μ = 0.090 mm<sup>-1</sup>; Mo Kα radiation, λ = 0.71075 Å; T = 100 K; 2θ<sub>max</sub> = 55°; 15778/5289 measured/independent reflections; R<sub>int</sub>: 0.0601; R<sub>1</sub>[F<sub>2</sub> > 2σ(F<sub>2</sub>)] = 0.0605, wR<sub>2</sub>(all data) = 0.1675; Δρ<sub>max</sub> = 1.097 eÅ<sup>-3</sup>, Δρ<sub>min</sub> = -0.224 eÅ<sup>-3</sup>. Red plate crystals gave good diffraction. The data were collected on a Rigaku Saturn 724+ area detector mounted at the window of an FR-E+ rotating anode generator with a Mo anode and equipped with an Oxford Cryosystems cryostream device. Rigaku CrystalClear[1] was used to record images and for data integration. The structure was solved by charge-flipping methods using SUPERFLIP[2] and refined on Fo<sub>2</sub> by full-matrix least squares refinement using SHELXL-2013.[3] All non-hydrogen atoms were refined with anisotropic displacement parameters. Hydrogen atoms were added at calculated positions and refined using a riding model with isotropic displacement parameters based on the equivalent isotropic displacement parameter (U<sub>eq</sub>) of the

parent atom. The structure was deposited on the Cambridge Structural Database with the deposition number CCDC 1044583.

### **meso-PhenylSubTBDAP-O<sup>i</sup>Pr (139)**

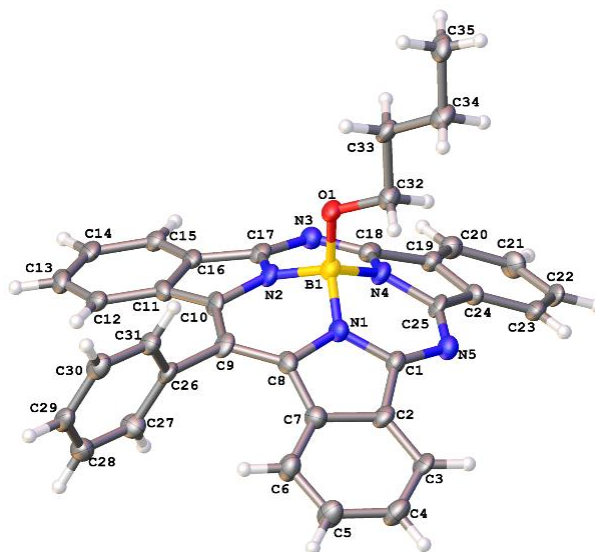
A single crystal suitable for X-Ray analysis was grown from a mixture of cyclohexane/acetone.



Formula:  $C_{34}H_{24}BN_5O$ ;  $M_r = 529.39$ ; crystal dimensions: 0.09 x 0.08 x 0.08 mm; crystal system: Monoclinic; space group:  $P2_1/c$ ;  $a = 9.391(2) \text{ \AA}$ ,  $b = 28.565(6) \text{ \AA}$ ,  $c = 10.538(3) \text{ \AA}$ ,  $\alpha = 90^\circ$ ,  $\beta = 113.175(4)^\circ$ ,  $\gamma = 90^\circ$ ;  $V = 2598.8(11) \text{ \AA}^3$ ;  $Z = 4$ ;  $\rho_{\text{calcd}} = 1.353 \text{ Mg/m}^3$ ;  $\mu = 0.084 \text{ mm}^{-1}$ ; Mo  $K\alpha$  radiation,  $\lambda = 0.71075 \text{ \AA}$ ;  $T = 100 \text{ K}$ ;  $2\theta_{\text{max}} = 50^\circ$ ; 27657/4574 measured/independent reflections;  $R_{\text{int}}: 0.0808$ ;  $R I[F^2 > 2\sigma(F^2)] = 0.0514$ ,  $wR2(\text{all data}) = 0.1281$ ;  $\Delta\rho_{\text{max}} = 0.288 \text{ e\AA}^{-3}$ ,  $\Delta\rho_{\text{min}} = -0.193 \text{ e\AA}^{-3}$ . Red block crystals were poorly diffracting with no significant data beyond  $0.84 \text{ \AA}$ . The data were collected on a Rigaku Saturn 724+ area detector mounted at the window of an FR-E+ rotating anode generator with a Mo anode and equipped with an Oxford Cryosystems cryostream device. Rigaku CrystalClear<sup>[1]</sup> was used to record images and for data integration. The structure was solved by charge-flipping methods using SUPERFLIP<sup>[2]</sup> and refined on  $F_o^2$  by full-matrix least squares refinement using SHELXL-2014.<sup>[3]</sup> All non-hydrogen atoms were refined with anisotropic displacement parameters. Hydrogen atoms were added at calculated positions and refined using a riding model with isotropic displacement parameters based on the equivalent isotropic displacement parameter ( $U_{\text{eq}}$ ) of the parent atom. The isopropoxide substituent is disordered over two positions (60:40). The structure was deposited on the Cambridge Structural Database with the deposition number CCDC 1052412.

**meso-PhenylSubTBDAP-OBu (140)**

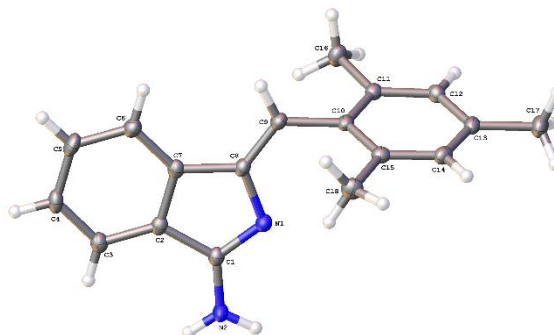
Crystals suitable for X-Ray were grown dissolving SubTBDAP **140** in a mixture of dichloromethane/acetone allowing slow diffusion of cyclohexane.



Formula: C<sub>35</sub>H<sub>26</sub>BN<sub>5</sub>O; Mr = 543.42; crystal dimensions: 0.07 x 0.04 x 0.01 mm; crystal system: Monoclinic; space group: P2<sub>1</sub>/c; a = 9.6971(8) Å, b = 30.054(3) Å, c = 9.8109(8) Å, α = 90°, β = 110.468(9)°, γ = 90°; V = 2678.8(4) Å<sup>3</sup>; Z = 4; ρ<sub>calcd</sub> = 1.347 Mg/m<sup>3</sup>; μ = 0.083 mm<sup>-1</sup>; Mo Kα radiation, λ = 0.71075 Å; T = 100 K; 2θ<sub>max</sub> = 50°; 19159/4732 measured/independent reflections; R<sub>int</sub>: 0.1086; R<sub>1</sub>[F<sub>2</sub> > 2σ(F<sub>2</sub>)] = 0.0936, wR<sub>2</sub>(all data) = 0.1924; Δρ<sub>max</sub> = 0.313 eÅ<sup>-3</sup>, Δρ<sub>min</sub> = -0.337 eÅ<sup>-3</sup>. Red plate crystals were poorly diffracting with no significant data beyond 0.84 Å. The data were collected on a Rigaku Saturn 724+ area detector mounted at the window of an FR-E+ rotating anode generator with a Mo anode and equipped with an Oxford Cryosystems cryostream device. Rigaku CrystalClear[1] was used to record images and Agilent CrysAlisPro[4] was used for data integration. The structure was solved by charge-flipping methods using SUPERFLIP[2] and refined on Fo<sup>2</sup> by full-matrix least squares refinement using SHELXL-2014.[3] All non-hydrogen atoms were refined with anisotropic displacement parameters. Hydrogen atoms were added at calculated positions and refined using a riding model with isotropic displacement parameters based on the equivalent isotropic displacement parameter (U<sub>eq</sub>) of the parent atom. The structure was deposited on the Cambridge Structural Database with the deposition number CCDC 1044584.

**Aminoisindolene (145)**

Suitable crystals for X-Ray analysis were grown from a mixture of distilled dichloromethane/ distilled petroleum ether.

**Table 1.** Crystal data and structure refinement details.

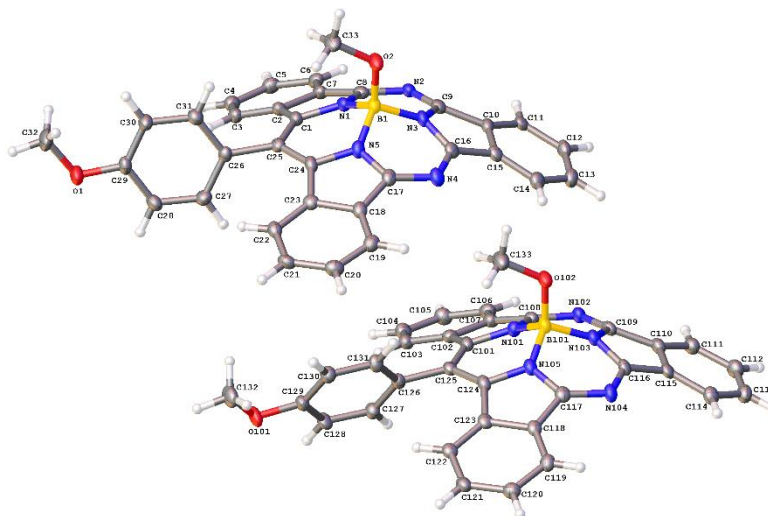
Identification code	<b>2015ncs0123za</b>	
Empirical formula	C <sub>18</sub> H <sub>18</sub> N <sub>2</sub>	
Formula weight	262.34	
Temperature	100(2) K	
Wavelength	0.71075 Å	
Crystal system	Monoclinic	
Space group	P2 <sub>1</sub> /n	
Unit cell dimensions	<i>a</i> = 8.58875(16) Å	<i>α</i> = 90°
	<i>b</i> = 11.9958(2) Å	<i>β</i> = 103.8020(19)°
	<i>c</i> = 13.9185(3) Å	<i>γ</i> = 90°
Volume	1392.60(5) Å <sup>3</sup>	
Z	4	
Density (calculated)	1.251 Mg / m <sup>3</sup>	
Absorption coefficient	0.074 mm <sup>-1</sup>	
<i>F</i> (000)	560	
Crystal	Block; colourless	
Crystal size	0.1 × 0.03 × 0.03 mm <sup>3</sup>	
<i>θ</i> range for data collection	2.270 – 27.481°	
Index ranges	−11 ≤ <i>h</i> ≤ 11, −15 ≤ <i>k</i> ≤ 15, −18 ≤ <i>l</i> ≤ 18	
Reflections collected	30463	
Independent reflections	3180 [ <i>R</i> <sub>int</sub> = 0.0508]	
Completeness to <i>θ</i> = 26.000°	100.0 %	
Absorption correction	Semi-empirical from equivalents	
Max. and min. transmission	1.00000 and 0.83398	
Refinement method	Full-matrix least-squares on <i>F</i> <sup>2</sup>	
Data / restraints / parameters	3180 / 2 / 190	
Goodness-of-fit on <i>F</i> <sup>2</sup>	1.053	
Final <i>R</i> indices [ <i>F</i> <sup>2</sup> > 2σ( <i>F</i> <sup>2</sup> )]	<i>R</i> 1 = 0.0440, <i>wR</i> 2 = 0.1123	
<i>R</i> indices (all data)	<i>R</i> 1 = 0.0509, <i>wR</i> 2 = 0.1161	
Extinction coefficient	n/a	
Largest diff. peak and hole	0.321 and −0.256 e Å <sup>-3</sup>	

**Diffraction:** Rigaku AFC12 goniometer equipped with an enhanced sensitivity (HG) Saturn724+ detector mounted at the window of an FR-E+ SuperBright molybdenum rotating anode generator with HF Varimax optics (100μm focus). **Cell determination and data collection:** CrystalClear-SM Expert 3.1 b27 (Rigaku, 2013). **Data reduction, cell refinement and absorption correction:** CrysAlisPro 1.171.37.35 (Agilent, 2014). **Structure solution SUPERFLIP** (Palatinus, L. & Chapuis, G. (2007). J. Appl. Cryst. 40, 786-790). **Structure refinement:** SHELXL-2014 (Sheldrick, G.M. (2015). Acta Cryst. C71, 3-8). **Graphics:** OLEX2 (Dolomanov, O. V., Bourhis, L. J., Gildea, R. J., Howard, J. A. K. & Puschmann, H. (2009). J. Appl. Cryst. 42, 339-341).



***meso*-(4-Methoxyphenyl)SubTBDAP-OMe (146)**

Crystals suitable for X-Ray analysis were grown by dissolving SubTBDAP **24** in a mixture of dichloromethane/acetone and allowing slow diffusion of methanol.



Formula: C<sub>33</sub>H<sub>22</sub>BN<sub>5</sub>O<sub>2</sub>; Mr = 531.36; crystal dimensions: 0.06 x 0.06 x 0.01 mm; crystal system: Monoclinic; space group: P2<sub>1</sub>/n; a = 15.0996(6) Å, b = 17.6493(8) Å, c = 18.9194(9) Å, α = 90°, β = 96.370(4)°, γ = 90°; V = 5010.9(4) Å<sup>3</sup>; Z = 8; ρ<sub>calcd</sub> = 1.409 Mg/m<sup>3</sup>; μ = 0.090 mm<sup>-1</sup>; Mo Kα radiation, λ = 0.71075 Å; T = 100 K; 2θ<sub>max</sub> = 55°; 62368/11493 measured/independent reflections; R<sub>int</sub> = 0.1519; R<sub>1</sub>[F<sub>2</sub> > 2σ(F<sub>2</sub>)] = 0.0651, wR<sub>2</sub>(all data) = 0.1445; Δρ<sub>max</sub> = 0.271 eÅ<sup>-3</sup>, Δρ<sub>min</sub> = -0.271 eÅ<sup>-3</sup>. Red plate crystals gave good diffraction. The data were collected on a Rigaku Saturn 724+ area detector mounted at the window of an FR-E+ rotating anode generator with a Mo anode and equipped with an Oxford Cryosystems cryostream device. Rigaku CrystalClear[1] was used to record images and Agilent CrysAlisPro[4] was used for data integration. The structure was solved by charge-flipping methods using SUPERFLIP[2] and refined on Fo<sub>2</sub> by full-matrix least squares refinement using SHELXL-2014.[3] All non-hydrogen atoms were refined with anisotropic displacement parameters. Hydrogen atoms were added at calculated positions and refined using a riding model with isotropic displacement parameters based on the equivalent isotropic displacement parameter (U<sub>eq</sub>) of the parent atom. The structure was deposited on the Cambridge Structural Database with the deposition number CCDC 1044585.



## Pyrene-azaBODIPY (151)

Suitable crystals for X-Ray diffraction were grown from a distilled dichloromethane/methanol.

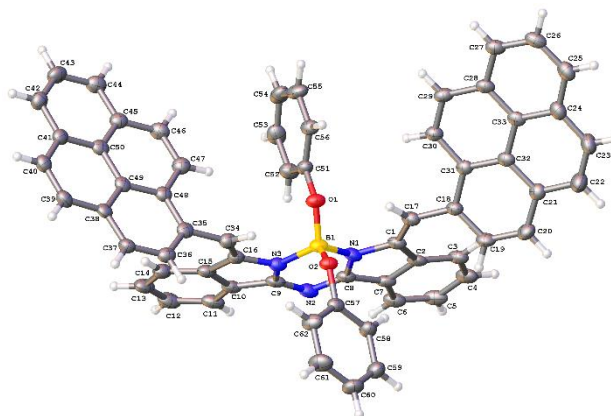


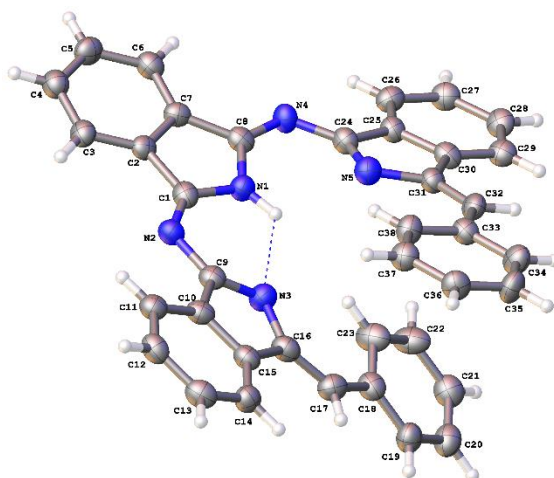
**Table 1.** Crystal data and structure refinement details.

Identification code	<b>2015ncs0224a</b>	
Empirical formula	$C_{62}H_{38}BN_3O_2$	
Formula weight	867.76	
Temperature	100(2) K	
Wavelength	0.71073 Å	
Crystal system	Monoclinic	
Space group	$P121/c1$	
Unit cell dimensions	$a = 13.897(2)$ Å	$\alpha = 90^\circ$
	$b = 20.5333(11)$ Å	$\beta = 136.17(3)^\circ$
	$c = 22.056(4)$ Å	$\gamma = 90^\circ$
Volume	4358.5(19) Å <sup>3</sup>	
Z	4	
Density (calculated)	1.322 Mg / m <sup>3</sup>	
Absorption coefficient	0.080 mm <sup>-1</sup>	
$F(000)$	1808	
Crystal	Block; red	
Crystal size	0.09 × 0.06 × 0.04 mm <sup>3</sup>	
$\theta$ range for data collection	2.337 – 27.488°	
Index ranges	–18 ≤ $h$ ≤ 17, –26 ≤ $k$ ≤ 26, –27 ≤ $l$ ≤ 28	
Reflections collected	25826	
Independent reflections	9806 [ $R_{int} = 0.2676$ ]	
Completeness to $\theta = 25.242^\circ$	99.9 %	
Absorption correction	Semi-empirical from equivalents	
Max. and min. transmission	1.00000 and 0.09354	
Refinement method	Full-matrix least-squares on $F^2$	
Data / restraints / parameters	9806 / 0 / 614	
Goodness-of-fit on $F^2$	0.945	
Final $R$ indices [ $F^2 > 2\sigma(F^2)$ ]	$R1 = 0.0611$ , $wR2 = 0.0983$	
$R$ indices (all data)	$R1 = 0.1434$ , $wR2 = 0.1176$	
Extinction coefficient	0.00111(19)	
Largest diff. peak and hole	0.262 and –0.222 e Å <sup>-3</sup>	

**Diffraction:** Rigaku AFC12 goniometer equipped with an enhanced sensitivity (HG) Saturn724+ detector mounted at the window of an FR-E+ SuperBright molybdenum rotating anode generator with VHF Varimax optics (70µm focus). **Cell determination and data collection:** CrystalClear-SM Expert 3.1 b27 (Rigaku, 2013). **Data reduction, cell refinement and absorption correction:** CrysAlisPro 1.171.37.35 (Agilent, 2014). **Structure solution:** SUPERFLIP (Palatinus, L. & Chapuis, G. (2007). J. Appl. Cryst. 40, 786-790). **Structure refinement:** SHELXL-2014 (Sheldrick, G.M. (2015). Acta Cryst. C71, 3-8). **Graphics:** OLEX2 (Dolomanov, O. V., Bourhis, L. J., Gildea, R. J., Howard, J. A. K. & Puschmann, H. (2009). J. Appl. Cryst. 42, 339-341).

**Trimer (152)**

Crystals suitable for X-Ray analysis were grown from a mixture of distilled dichloromethane/distilled petroleum ether.

**Table 1.** Crystal data and structure refinement details.

Identification code	<b>2015ncs0058a</b>	
Empirical formula	$C_{38}H_{25}N_5$	
Formula weight	551.63	
Temperature	100(2) K	
Wavelength	0.71075 Å	
Crystal system	Triclinic	
Space group	$P\bar{1}$	
Unit cell dimensions	$a = 11.538(7)$ Å	$\alpha = 115.776(6)^\circ$
	$b = 12.307(8)$ Å	$\beta = 106.207(4)^\circ$
	$c = 12.399(8)$ Å	$\gamma = 103.928(4)^\circ$
Volume	1382.6(15) Å <sup>3</sup>	
Z	2	
Density (calculated)	1.325 Mg / m <sup>3</sup>	
Absorption coefficient	0.080 mm <sup>-1</sup>	
$F(000)$	576	
Crystal	Block; Red	
Crystal size	0.03 × 0.03 × 0.01 mm <sup>3</sup>	
$\theta$ range for data collection	1.947 – 25.106°	
Index ranges	–13 ≤ $h$ ≤ 13, –13 ≤ $k$ ≤ 14, –14 ≤ $l$ ≤ 13	
Reflections collected	14752	
Independent reflections	4850 [ $R_{int} = 0.1294$ ]	
Completeness to $\theta = 25.106^\circ$	98.6 %	
Absorption correction	Semi-empirical from equivalents	
Max. and min. transmission	1.000 and 0.647	
Refinement method	Full-matrix least-squares on $F^2$	
Data / restraints / parameters	4850 / 0 / 392	
Goodness-of-fit on $F^2$	1.040	
Final $R$ indices [ $F^2 > 2\sigma(F^2)$ ]	$R1 = 0.0744$ , $wR2 = 0.1265$	
$R$ indices (all data)	$R1 = 0.1767$ , $wR2 = 0.1660$	
Extinction coefficient	n/a	
Largest diff. peak and hole	0.262 and –0.234 e Å <sup>-3</sup>	

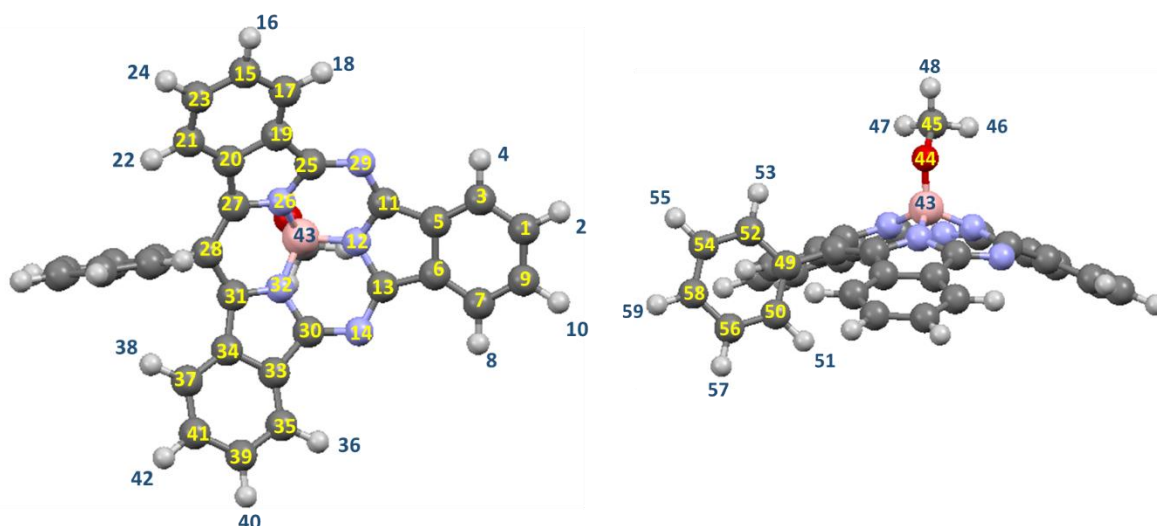
**Diffraction:** Rigaku AFC12 goniometer equipped with an enhanced sensitivity (HG) Saturn724+ detector mounted at the window of an FR-E+ SuperBright molybdenum rotating anode generator with VHF Varimax optics (70µm focus). **Cell determination and data collection:** CrystalClear-SM Expert 3.1 b27 (Rigaku, 2013). **Data reduction, cell refinement and absorption correction:** CrystalClear-SM Expert 2.1 b31 (Rigaku, 2014). **Structure solution:** SUPERFLIP (Palatinus, L. & Chapuis, G. (2007). J. Appl. Cryst. 40, 786-790). **Structure refinement:** SHELXL-2014 (Sheldrick, G.M. (2008). Acta Cryst. A64, 112-122). **Graphics:** OLEX2 (Dolomanov, O. V., Bourhis, L. J., Gildea, R. J., Howard, J. A. K. & Puschmann, H. (2009). J. Appl. Cryst. 42, 339-341).

## References

- [1] CrystalClear, 2008-2013, Rigaku Corporation, The Woodlands, Texas, U.S.A.  
 [2] L. Palatinus, G. Chapuis, *J. Appl. Cryst.* 2007, 40, 786-790.  
 [3] G. M. Sheldrick, *Acta Cryst. A*, 2008, A64, 112-122.  
 [4] CrysAlisPro Software system, version 1.171.37.31, 2014, Agilent Technologies UK Ltd, Oxford, UK

### 4.5.5 Theoretical methods and Cartesian coordinates of the DFT optimized structures

The chemical shifts of protons in SubTBDAP **133** were computed at the BP86-D3/def2-SVP level of theory. The calculations have been performed using the program TURBOMOLE version 6.4.<sup>[190]</sup> For the calculations we have used the BP86<sup>[191]</sup>functional. TMS has been calculated with the same conditions and employed as reference. It is important to notice that this calculation doesn't have into account the solvent effect, therefore the exact values will be somehow displaced, but it is assumed that this effect would affect almost equally to all signals.



NMR DFT shielding constants						
#	NO.	TYPE	MULT.	ISOTROPIC	ANISOTROPIC	dD/dB-CONTRIBUTION
1	c	1	63.28188587	178.04675584	-180.24377168	
2	h	1	24.02214523	7.89640687	2.62877853	
3	c	1	68.60255525	171.04985114	-184.37736074	
4	h	1	23.00376594	11.27591628	-10.45301495	
5	c	1	59.55756184	155.75388245	-199.34847643	
6	c	1	59.89742578	154.93229182	-198.86669387	
7	c	1	68.78087295	171.30184337	-185.20599081	
8	h	1	22.99538732	11.38600804	-11.02426394	
9	c	1	63.32288239	177.97326414	-180.39938744	
10	h	1	24.02381112	7.97395585	2.40073204	
11	c	1	44.49350072	122.29005054	-234.52447960	
12	n	1	79.61758259	206.85984173	-277.69288443	
13	c	1	43.97653429	122.63733558	-235.97112946	
14	n	1	12.02721569	409.51262632	-320.45134097	
15	c	1	64.46128043	176.56707407	-182.70178958	
16	h	1	24.10261259	8.18472832	-0.02409914	
17	c	1	69.02316349	171.24732450	-183.47783269	
18	h	1	22.91182736	11.59801873	-10.45484888	
19	c	1	59.78349173	152.89078100	-200.66271247	

20	c	1	59.00835204	153.78662884	-203.87340601
21	c	1	67.96930893	167.36508588	-194.21684141
22	h	1	23.86731244	16.17109609	-14.62546189
23	c	1	64.41368983	176.66837951	-184.00841755
24	h	1	24.28509868	9.27069282	-1.76149777
25	c	1	43.47537489	117.90015745	-237.47598280
26	n	1	75.51042935	214.60615686	-277.85059178
27	c	1	56.87932463	131.66723586	-217.90163656
28	c	1	67.70473486	129.89471754	-213.36102599
29	n	1	11.71126986	409.97232727	-319.50018810
30	c	1	42.99494623	119.16856914	-238.88000290
31	c	1	55.81020403	134.57537862	-220.35657726
32	n	1	77.26291480	213.76647187	-278.63960739
33	c	1	60.92762911	151.89460011	-199.67212832
34	c	1	59.01680977	153.81690973	-204.58150004
35	c	1	69.32274255	170.99187820	-184.06431082
36	h	1	22.97040733	11.62292944	-11.02085998
37	c	1	68.82274290	167.17711604	-193.49298915
38	h	1	24.60582559	17.00513942	-15.21835180
39	c	1	64.65542846	176.66040516	-183.54037735
40	h	1	24.20169727	8.19841130	-0.68612505
41	c	1	64.33819034	177.03529281	-185.17381126
42	h	1	24.46735557	9.49315859	-2.48536394
43	b	1	123.51059537	56.51202404	-99.70342398
44	o	1	295.44385030	96.48714715	-99.90361123
45	c	1	137.45086710	70.51403726	-108.68258519
46	h	1	30.34429595	14.87196453	0.79652183
47	h	1	30.36532196	14.75872641	-2.67254833
48	h	1	29.57008576	15.53167356	1.98734949
49	c	1	53.50100437	176.69250514	-211.62437185
50	c	1	60.37792837	177.21072624	-209.75454010
51	h	1	24.57610434	13.43357019	-21.46109616
52	c	1	58.04141762	179.65401335	-202.26677671
53	h	1	23.38698027	11.23107135	-14.75456018
54	c	1	62.96878690	182.91135039	-185.36307451
55	h	1	23.91345736	5.68205728	-2.08018287
56	c	1	63.15147200	182.09178870	-189.71328672
57	h	1	24.28232531	6.13159708	-6.20541431
58	c	1	63.08315633	182.77621288	-182.05490435
59	h	1	24.09803651	4.29073423	1.61498909

\$end

\$TMPDIR /scratch/

## List of References

- [1] a) L. Chen, Q. Chen, M. Wu, F. Jiang, M. Hong, *Acc. Chem. Res.* **2015**, *48*, 201-210; b) E. I. Zenkevich, C. von Borczyskowski, *J. Porphyrins Phthalocyanines* **2014**, *18*, 1-19.
- [2] D. V. Talapin, J.-S. Lee, M. V. Kovalenko, E. V. Shevchenko, *Chem. Rev.* **2010**, *110*, 389-458.
- [3] M. S. Skolnick, D. J. Mowbray, *Annu. Rev. Mater. Res.* **2004**, *34*, 181-218.
- [4] S. Botti, *Handbook of Nanophysics: Nanoparticles and Quantum Dots*, CRC Press. Editor: Sattler, Klaus D., **2010**.
- [5] Y. Zhang, R. A. Agbaria, I. M. Warner, *Supramol. Chem.* **1997**, *8*, 309-318.
- [6] a) K. M. Kadish, K. M. Smith, R. Guilard, *The Porphyrin Handbook, Vol. 1–20*, **2000**; b) K. M. Kadish, K. M. Smith, R. Guilard, *Handbook of Porphyrin Science, Vol. 1–20*, **2010**.
- [7] G. de la Torre, G. Bottari, M. Sekita, A. Hausmann, D. M. Guldi, T. Torres, *Chem. Soc. Rev.* **2013**, *42*, 8049-8105.
- [8] A. R. Battersby, *Nat. Prod. Rep.* **2000**, *17*, 507-526.
- [9] L. R. Milgrom, *The Colours of Life: An Introduction to the Chemistry of Porphyrins and Related Compounds*, Oxford University Press New York, United States, **1997**.
- [10] A. R. Battersby, C. J. R. Fookes, G. W. J. Matcham, E. McDonald, *Nature* **1980**, *285*, 17-21.
- [11] D. Dolphin (ed.), *The Porphyrins, Vol. 3*, Academic Press, New York, **1978**.
- [12] P. Rothmund, A. R. Menotti, *J. Am. Chem. Soc.* **1941**, *63*, 267-270.
- [13] A. D. Adler, F. R. Longo, J. D. Finarelli, J. Goldmacher, J. Assour, L. Korsakoff, *J. Org. Chem.* **1967**, *32*, 476-476.
- [14] J. S. Lindsey, *Acc. Chem. Res.* **2009**, *43*, 300-311.
- [15] A. H. Jackson, *The Porphyrins: Structure and Synthesis, Part A Vol. 1*, Academic Press New York, **1978**.
- [16] a) F. H. Moser, A. L. Thomas, *Phthalocyanine Compounds*, Reinhold publishing corporation, New York, **1963**; b) F. H. Moser, A. L. Thomas, *The Phthalocyanines: Manufacture and applications, Vol. 2*, **1983**.
- [17] N. B. Mckeown, *Phthalocyanine Materials: Synthesis, Structure and Function*, Cambridge University Press, Cambridge, **1998**.
- [18] V. N. Nemykin, S. V. Dudkin, F. Dumoulin, C. Hirel, A. Gül, V. Ahsen, *Reviews and Accounts* **2014**, *2014*, 142-204.
- [19] a) R. P. Linstead, *J. Chem. Soc.* **1934**, 1016-1017; b) C. E. Dent, R. P. Linstead, A. R. Lowe, *J. Chem. Soc.* **1934**, 1033-1039; c) R. P. Linstead, A. R. Lowe, *J. Chem. Soc.* **1934**, 1022-1027; d) G. T. Byrne, R. P. Linstead, A. R. Lowe, *J. Chem. Soc.* **1934**, 1017-1022.
- [20] I. Chambrier, M. J. Cook, P. T. Wood, *Chem. Commun.* **2000**, 2133-2134.
- [21] M. J. Gouterman, *J. Mol. Spectrosc.* **1961**, *6*, 138.
- [22] Z. Zhao, A. N. Cammidge, D. L. Hughes, M. J. Cook, *Org. Lett.* **2010**, *12*, 5138-5141.

- [23] K. M. Kadish, K. M. Smith, R. Guilard, *The Porphyrin Handbook: Applications of phthalocyanines, Vol. 19*, Elsevier, **2003**.
- [24] K. M. Kadish, K. M. Smith, R. Guilard, *The Porphyrin Handbook: Applications: past, present and future*, Academic Press, **2003**.
- [25] a) J. L. Sessler, S. J. Weghorn (Eds), *Expanded, Contracted and Isomeric Porphyrins*, Pergamon, Oxford, **1997**; b) D. Kuzuhara, Y. Sakakibara, S. Mori, T. Okujima, H. Uno, H. Yamada, *Angew. Chem. Int. Ed.* **2013**, *52*, 3360-3363; c) R. Misra, T. K. Chandrashekar, *Acc. Chem. Res.* **2008**, *41*, 265-279.
- [26] S. Saito, A. Osuka, *Angew. Chem. Int. Ed.* **2011**, *50*, 4342-4373.
- [27] V. J. Bauer, D. L. J. Clive, D. Dolphin, J. B. Paine, F. L. Harris, M. M. King, J. Loder, S. W. C. Wang, R. B. Woodward, *J. Am. Chem. Soc.* **1983**, *105*, 6429-6436.
- [28] J. Mack, N. Kobayashi, *Chem. Rev.* **2010**, *111*, 281-321.
- [29] V. W. Day, T. J. Marks, W. A. Wachter, *J. Am. Chem. Soc.* **1975**, *97*, 4519-4527.
- [30] C. G. Claessens, D. González-Rodríguez, M. S. Rodríguez-Morgade, A. Medina, T. Torres, *Chem. Rev.* **2013**, *114*, 2192-2277.
- [31] A. Meller, A. Ossko, *Monatshefte für Chemie / Chemical Monthly* **1972**, *103*, 150-155.
- [32] C. G. Claessens, D. González-Rodríguez, T. Torres, *Chem. Rev.* **2002**, *102*, 835-854.
- [33] M. Hanack, M. Geyer, *J. Chem. Soc., Chem. Commun.* **1994**, 2253-2254.
- [34] K. M. Kadish, K. M. Smith, R. Guilard, *The Porphyrin Handbook: Phthalocyanines : spectroscopic and electrochemical characterization*, Academic Press, **2003**.
- [35] E. R. L. Brisson, A. S. Paton, G. E. Morse, T. P. Bender, *Ind. Eng. Chem. Res.* **2011**, *50*, 10910-10917.
- [36] D. González-Rodríguez, T. Torres, E. L. G. Denardin, D. Samios, V. Stefani, D. S. Corrêa, *J. Organomet. Chem.* **2009**, *694*, 1617-1622.
- [37] Y. Bernhard, P. Winckler, R. Chassagnon, P. Richard, E. Gigot, J.-M. Perrier-Cornet, R. A. Decreau, *Chem. Commun.* **2014**, *50*, 13975-13978.
- [38] Y. Bernhard, P. Winckler, J.-M. Perrier-Cornet, R. A. Decreau, *Dalton Trans.* **2015**, *44*, 3200-3208.
- [39] G. E. Morse, T. P. Bender, *ACS Appl. Mater. Interfaces* **2012**, *4*, 5055-5068.
- [40] S. Zhang, R. Guoa, B. Xua, C. Songa, Z. Lia, J. Zhaoa, *ECS Electrochem. Lett.* **2014**, *3*, A36-A38.
- [41] J. Guilleme, J. Arago, E. Orti, E. Cavero, T. Sierra, J. Ortega, C. L. Folcia, J. Etxebarria, D. Gonzalez-Rodriguez, T. Torres, *J. Mater. Chem. C* **2015**, *3*, 985-989.
- [42] a) P. Sullivan, G. E. Collis, L. A. Rochford, J. F. Arantes, P. Kemppinen, T. S. Jones, K. N. Winzenberg, *Chem. Commun.* **2015**; b) C.-F. Lin, S.-W. Liu, C.-C. Lee, T. Sakurai, M. Kubota, W.-C. Su, J.-C. Huang, T.-L. Chiu, H.-C. Han, L.-C. Chen, C.-T. Chen, J.-H. Lee, *Sol. Energy Mater. Sol. Cells* **2015**, *137*, 138-145; c) B. Ebenhoch, N. B. A. Prasetya, V. M. Rotello, G. Cooke, I. D. W. Samuel, *J. Mater. Chem. A* **2015**; d) C.-F. Lin, V. M. Nichols, Y.-C. Cheng, C. J. Bardeen, M.-K. Wei, S.-W. Liu, C.-C. Lee, W.-C. Su, T.-L. Chiu, H.-C. Han, L.-C. Chen, C.-T. Chen, J.-H. Lee, *Sol. Energy Mater. Sol. Cells* **2014**, *122*, 264-270;



- e) F. Jin, B. Chu, W. Li, Z. Su, X. Yan, J. Wang, R. Li, B. Zhao, T. Zhang, Y. Gao, C. S. Lee, H. Wu, F. Hou, T. Lin, Q. Song, *Org. Electron.* **2014**, *15*, 3756-3760.
- [43] K. Cnops, B. P. Rand, D. Cheyons, B. Verreert, M. A. Empl, P. Heremans, *Nat Commun* **2014**, *5*.
- [44] M. Kouhnavard, S. Ikeda, N. A. Ludin, N. B. Ahmad Khairudin, B. V. Ghaffari, M. A. Mat- Teridi, M. A. Ibrahim, S. Sepeai, K. Sopian, *Renewable and Sustainable Energy Reviews* **2014**, *37*, 397-407.
- [45] P. Malik, J. Singh, R. Kakkar, *Adv. Mater. Lett.* **2014**, *5*, 612-628.
- [46] M. G. Bawendi, M. L. Steigerwald, L. E. Brus, *Annu. Rev. Phys. Chem.* **1990**, *41*, 477-496.
- [47] V. I. Klimov, *Nanocrystal Quantum Dots*, Second ed., CRC Press, **2010**.
- [48] A. J. Nozik, M. C. Beard, J. M. Luther, M. Law, R. J. Ellingson, J. C. Johnson, *Chem. Rev.* **2010**, *110*, 6873-6890.
- [49] J. N. Freitas, A. S. Goncalves, A. F. Nogueira, *Nanoscale* **2014**, *6*, 6371-6397.
- [50] D. Bera, L. Qian, T.-K. Tseng, P. H. Holloway, *Materials* **2010**, *3*, 2260-2345.
- [51] D. Bera, L. Qian, P. H. Holloway, in *Drug Delivery Nanoparticles Formulation and Characterization, Vol. 191* (Ed.: First), **2009**, pp. 349-366.
- [52] X. Xia, Z. Liu, G. Du, Y. Li, M. Ma, *J. Lumin.* **2010**, *130*, 1285-1291.
- [53] Y. Yin, A. P. Alivisatos, *Nature* **2005**, *437*, 664-670.
- [54] a) E. Hao, H. Sun, Z. Zhou, J. Liu, B. Yang, J. Shen, *Chem. Mater.* **1999**, *11*, 3096-3102; b) S. K. Pradhan, Z. T. Deng, F. Tang, C. Wang, Y. Ren, P. Moeck, V. Petkov, *J. Appl. Phys.* **2007**, *102*, 044304.
- [55] a) C. Bullen, P. Mulvaney, *Langmuir* **2006**, *22*, 3007-3013; b) X. Luo, P. Liu, N. T. N. Truong, U. Farva, C. Park, *J. Phys. Chem. C* **2011**, *115*, 20817-20823.
- [56] a) M. Wang, J. K. Oh, T. E. Dykstra, X. Lou, G. D. Scholes, M. A. Winnik, *Macromolecules* **2006**, *39*, 3664-3672; b) R. Sharma, G. P. Holland, V. C. Solomon, H. Zimmermann, S. Schiffenhaus, S. A. Amin, D. A. Buttry, J. L. Yarger, *J. Phys. Chem. C* **2009**, *113*, 16387-16393.
- [57] X.-Q. Li, J. Mu, F. Li, X.-B. Gao, *Colloids and Surfaces A: Physicochemical and Engineering Aspects* **2005**, *260*, 239-243.
- [58] E. I. Zenkevich, T. Blaudeck, A. M. Shulga, F. Cichos, C. von Borczyskowski, *J. Lumin.* **2007**, *122-123*, 784-788.
- [59] a) J. Ning, Y. Wang, Q. Wu, X. Zhang, X. Lin, H. Zhao, *RSC Advances* **2015**, *5*, 21153-21160; b) B. N. Le, O. Mermut, Google Patents, **2010**.
- [60] C.-S. Chu, C.-Y. Chuang, *Sensors and Actuators B: Chemical* **2015**, *209*, 94-99.
- [61] S. Jin, H.-J. Son, O. K. Farha, G. P. Wiederrecht, J. T. Hupp, *J. Am. Chem. Soc.* **2013**, *135*, 955-958.
- [62] A. J. Shaikh, F. Rabbani, T. A. Sherazi, Z. Iqbal, S. Mir, S. A. Shahzad, *J. Phys. Chem. A* **2015**.

- [63] S. Jin, M. Tagliazucchi, H.-J. Son, R. D. Harris, K. O. Aruda, D. J. Weinberg, A. B. Nepomnyashchii, O. K. Farha, J. T. Hupp, E. A. Weiss, *J. Phys. Chem. C* **2015**, *119*, 5195-5202.
- [64] C. M. Lemon, E. Karnas, M. G. Bawendi, D. G. Nocera, *Inorg. Chem.* **2013**, *52*, 10394-10406.
- [65] S. Silvi, A. Credi, *Chem. Soc. Rev.* **2015**.
- [66] Q. Liu, R. Zhu, Y. Jiang, Q. Jia, S. Yang, Q. Shao, D. Wang, P. Cui, *Mater. Sci. Eng., B* **2014**, *188*, 106-113.
- [67] a) S. Dayal, J. Li, Y.-S. Li, H. Wu, A. C. S. Samia, M. E. Kenney, C. Burda, *Photochem. Photobiol.* **2008**, *84*, 243-249; b) S. Dayal, Y. Lou, A. C. S. Samia, J. C. Berlin, M. E. Kenney, C. Burda, *J. Am. Chem. Soc.* **2006**, *128*, 13974-13975.
- [68] S. Nyoni, T. Nyokong, *Electroanalysis* **2014**, *26*, 2261-2272.
- [69] Y. Choi, S. Kim, M.-H. Choi, S.-R. Ryoo, J. Park, D.-H. Min, B.-S. Kim, *Adv. Funct. Mater.* **2014**, *24*, 5781-5789.
- [70] O. Adegoke, T. Nyokong, *Synth. Met.* **2014**, *188*, 35-45.
- [71] S. Dayneko, A. Tameev, M. Tedoradze, I. Martynov, M. Artemyev, I. Nabiev, A. Chistyakov, *Appl. Phys. Lett.* **2013**, *103*, 063302.
- [72] V. M. Blas-Ferrando, J. Ortiz, V. Gonzalez-Pedro, R. S. Sanchez, I. Mora-Sero, F. Fernandez-Lazaro, A. Sastre-Santos, *Chem. Commun.* **2015**, *51*, 1732-1735.
- [73] G. Obaid, I. Chambrier, M. J. Cook, D. A. Russell, *Photochem. Photobiol. Sci.* **2015**, *14*, 737-747.
- [74] T. Stuchinskaya, M. Moreno, M. J. Cook, D. R. Edwards, D. A. Russell, *Photochem. Photobiol. Sci.* **2011**, *10*, 822-831.
- [75] G. Obaid, I. Chambrier, M. J. Cook, D. A. Russell, *Angew. Chem. Int. Ed.* **2012**, *51*, 6158-6162.
- [76] C. G. Claessens, M. J. Vicente-Arana, T. Torres, *Chem. Commun.* **2008**, 6378-6380.
- [77] C. G. Claessens, T. Torres, *Chem. Commun.* **2004**, 1298-1299.
- [78] I. Sánchez-Molina, B. Grimm, R. M. Krick Calderon, C. G. Claessens, D. M. Guldi, T. Torres, *J. Am. Chem. Soc.* **2013**, *135*, 10503-10511.
- [79] D. González-Rodríguez, M. V. Martínez-Díaz, J. Abel, A. Perl, J. Huskens, L. Echegoyen, T. s. Torres, *Org. Lett.* **2010**, *12*, 2970-2973.
- [80] C. B. Murray, D. J. Norris, M. G. Bawendi, *J. Am. Chem. Soc.* **1993**, *115*, 8706-8715.
- [81] W. W. Yu, X. Peng, *Angew. Chem. Int. Ed.* **2002**, *41*, 2368-2371.
- [82] Z. A. Peng, X. Peng, *J. Am. Chem. Soc.* **2000**, *123*, 183-184.
- [83] C. Banerjee, University of East Anglia ,PhD Thesis **2013**.
- [84] J. Jasieniak, L. Smith, J. v. Embden, P. Mulvaney, M. Califano, *J. Phys. Chem. C* **2009**, *113*, 19468-19474.
- [85] W. W. Yu, L. Qu, W. Guo, X. Peng, *Chem. Mater.* **2003**, *15*, 2854-2860.
- [86] *AIST: Integrated Spectral Database System of Organic Compounds. (Data were obtained from the National Institute of Advanced Industrial Science and Technology (Japan)).*



- [87] X. Ji, D. Copenhaver, C. Sichmeller, X. Peng, *J. Am. Chem. Soc.* **2008**, *130*, 5726-5735.
- [88] J. R. Sachleben, E. W. Wooten, L. Emsley, A. Pines, V. L. Colvin, A. P. Alivisatos, *Chem. Phys. Lett.* **1992**, *198*, 431-436.
- [89] G. P. Holland, R. Sharma, J. O. Agola, S. Amin, V. C. Solomon, P. Singh, D. A. Buttry, J. L. Yarger, *Chem. Mater.* **2007**, *19*, 2519-2526.
- [90] J. Taylor, T. Kippeny, S. Rosenthal, *J. Cluster Sci.* **2001**, *12*, 571-582.
- [91] B. Fritzing, R. K. Capek, K. Lambert, J. C. Martins, Z. Hens, *J. Am. Chem. Soc.* **2010**, *132*, 10195-10201.
- [92] M. Green, *J. Mater. Chem.* **2010**, *20*, 5797-5809.
- [93] Christian G. Claessens, D. González-Rodríguez, B. del Rey, T. Torres, G. Mark, H.-P. Schuchmann, C. von Sonntag, J. G. MacDonald, Ronald S. Nohr, *Eur. J. Org. Chem.* **2003**, *2003*, 2547-2551.
- [94] B. Noziere, R. Lesclaux, M. D. Hurley, M. A. Dearth, T. J. Wallington, *J. Org. Chem.* **1994**, *98*, 2864-2873.
- [95] S. Dabak, A. Gül, ö. Bekaroğlu, *Chem. Ber.* **1994**, *127*, 2009-2012.
- [96] C. D. Zyskowski, V. O. Kennedy, *J. Porphyrins Phthalocyanines* **2000**, *4*, 707-712.
- [97] J. G. Macdonald, R. S. Nohr, Novel subphthalocyanine colorants, ink compositions, and methods of making the same. Google Patents, **2000**.
- [98] C. G. Claessens, D. González-Rodríguez, C. M. McCallum, R. S. Nohr, H.-P. Schuchmann, T. Torres, *J. Porphyrins Phthalocyanines* **2007**, *11*, 181-188.
- [99] J. R. Stork, R. J. Potucek, W. S. Durfee, B. C. Noll, *Tetrahedron Lett.* **1999**, *40*, 8055-8058.
- [100] N. Kobayashi, R. Kondo, S. Nakajima, T. Osa, *J. Am. Chem. Soc.* **1990**, *112*, 9640-9641.
- [101] H. Ali, S. K. Sim, J. E. van Lier, *J. Chem. Res., Synop.* **1999**, 496-497.
- [102] S. I. Vagin, A. Frickenschmidt, B. Kammerer, M. Hanack, *Chem. Eur. J.* **2005**, *11*, 6568-6573.
- [103] Ł. Łapok, C. G. Claessens, D. Wöhrle, T. Torres, *Tetrahedron Lett.* **2009**, *50*, 2041-2044.
- [104] J. Guilleme, L. Martínez-Fernández, D. González-Rodríguez, I. Corral, M. Yáñez, T. Torres, *J. Am. Chem. Soc.* **2014**, *136*, 14289-14298.
- [105] J. Guilleme, D. González-Rodríguez, T. Torres, *Angew. Chem. Int. Ed.* **2011**, *50*, 3506-3509.
- [106] D. González-Rodríguez, T. Torres, D. M. Guldi, J. Rivera, L. Echegoyen, *Org. Lett.* **2002**, *4*, 335-338.
- [107] Y. Nishihara, *Applied Cross-Coupling Reactions*, Springer Berlin Heidelberg, **2012**.
- [108] R. D. Stephens, C. E. Castro, *J. Org. Chem.* **1963**, *28*, 3313-3315.
- [109] K. Sonogashira, Y. Tohda, N. Hagihara, *Tetrahedron Lett.* **1975**, *16*, 4467-4470.
- [110] K. Sonogashira, *J. Organomet. Chem.* **2002**, *653*, 46-49.
- [111] J. Gonzalo Rodriguez, R. Martin-Villamil, F. H. Cano, I. Fonseca, *J. Chem. Soc., Perkin Trans. 1* **1997**, 709-714.
- [112] I. Bertini, C. Luchinat, G. Parigi, *Solution NMR of Paramagnetic Molecules: Applications to metalloproteins and models*, Elsevier Science, **2001**.

- [113] Z. Rappoport, I. Marek, *The Chemistry of Organocopper Compounds*, John Wiley & Sons, **2010**.
- [114] J. S. Valentine, E. B. Gralla, *Copper-Containing Molecules*, Elsevier Science, **2002**.
- [115] I. Bertini, P. Turano, A. J. Vila, *Chem. Rev.* **1993**, *93*, 2833-2932.
- [116] W. Maketon, C. Z. Zenner, K. L. Ogden, *Environ. Sci. Technol.* **2008**, *42*, 2124-2129.
- [117] D. González-Rodríguez, T. Torres, *Eur. J. Org. Chem.* **2009**, *2009*, 1871-1879.
- [118] N. Miyaura, T. Yanagi, A. Suzuki, *Synth. Commun.* **1981**, *11*, 513-519.
- [119] A. Suzuki, *Angew. Chem. Int. Ed.* **2011**, *50*, 6722-6737.
- [120] A. N. Cammidge, V. H. M. Goddard, H. Gopee, N. L. Harrison, D. L. Hughes, C. J. Schubert, B. M. Sutton, G. L. Watts, A. J. Whitehead, *Org. Lett.* **2006**, *8*, 4071-4074.
- [121] N. Miyaura, T. Ishiyama, H. Sasaki, M. Ishikawa, M. Sato, A. Suzuki, *J. Am. Chem. Soc.* **1989**, *111*, 314-321.
- [122] M. Gouterman, *J. Chem. Phys.* **1959**, *30*, 1139-1161.
- [123] R. Gomes, A. Hassinen, A. Szczygiel, Q. Zhao, A. Vantomme, J. C. Martins, Z. Hens, *J. Phys. Chem. Lett.* **2011**, *2*, 145-152.
- [124] V. M. Dzhagan, I. Lokteva, C. Himcinschi, J. Kolny-Olesiak, M. Y. Valakh, S. Schulze, D. R. T. Zahn, *J. Appl. Phys.* **2011**, *109*, 084334.
- [125] M. Ince, A. Medina, J.-H. Yum, A. Yella, C. G. Claessens, M. V. Martínez-Díaz, M. Grätzel, M. K. Nazeeruddin, T. Torres, *Chem. Eur. J.* **2014**, *20*, 2016-2021.
- [126] N. M. T. Lourenço, C. M. Monteiro, C. A. M. Afonso, *Eur. J. Org. Chem.* **2010**, *2010*, 6938-6943.
- [127] W. Zhu, D. Ma, *Org. Lett.* **2006**, *8*, 261-263.
- [128] A. J. J. Lennox, G. C. Lloyd-Jones, *Chem. Soc. Rev.* **2014**, *43*, 412-443.
- [129] J. M. Khurana, S. Chauhan, G. Bansal, *Monatsh. Chem.* **2004**, *135*, 83-87.
- [130] P. G. M. Wuts, T. W. Greene, *Greene's Protective Groups in Organic Synthesis*, Wiley, **2006**.
- [131] T. D. Nelson, R. D. Crouch, *Synthesis-Stuttgart* **1996**, *1996*, 1031-1069.
- [132] E. R. Zubarev, J. Xu, J. D. Gibson, A. Sayyad, *Org. Lett.* **2006**, *8*, 1367-1370.
- [133] S. Vettel, P. Knochel, *Tetrahedron Lett.* **1994**, *35*, 5849-5852.
- [134] S. T. A. Shah, P. J. Guiry, *Org. Biomol. Chem.* **2008**, *6*, 2168-2172.
- [135] M. Wang, C. Li, D. Yin, X.-T. Liang, *Tetrahedron Lett.* **2002**, *43*, 8727-8729.
- [136] A. B. Smith, C. A. Risatti, O. Atasoylu, C. S. Bennett, J. Liu, H. Cheng, K. TenDyke, Q. Xu, *J. Am. Chem. Soc.* **2011**, *133*, 14042-14053.
- [137] A. N. Cammidge, I. Chambrier, M. J. Cook, L. Sosa-Vargas, *Synthesis and Properties of the Hybrid Phthalocyanine- Tetrabenzoporphyrin Macrocycles in Handbook of Porphyrin Science, Vol. 16*, World Scientific Publishing Company, Singapore, **2012**.
- [138] E. G. Nikolay, P. S. Gennady, I. K. Oskar, *Russ. Chem. Rev.* **2013**, *82*, 412.
- [139] N. Alharbi, A. Díaz-Moscoso, G. J. Tizzard, S. J. Coles, M. J. Cook, A. N. Cammidge, *Tetrahedron* **2014**, *70*, 7370-7379.
- [140] C. M. B. Carvalho, T. J. Brocksom, K. T. de Oliveira, *Chem. Soc. Rev.* **2013**, *42*, 3302-3317.

- [141] C. E. Dent, *J. Chem. Soc.* **1938**, 1-6.
- [142] P. A. Barrett, R. P. Linstead, G. A. P. Tuey, J. M. Robertson, *J. Chem. Soc.* **1939**, 1809-1820.
- [143] A. N. Cammidge, I. Chambrier, M. J. Cook, L. Sosa-Vargas, in *Handbook of Porphyrin Science, Vol. 16*, **2012**, pp. 331-404.
- [144] V. V. Kalashnikov, V. E. Pushkarev, L. G. Tomilova, *Russ. Chem. Rev.* **2014**, *83*, 657.
- [145] a) J. Heinr. Helberger, *Justus Liebigs Annalen der Chemie* **1937**, *529*, 205-218; b) J. H. Helberger, A. von Rebay, *Justus Liebigs Annalen der Chemie* **1937**, *531*, 279-287.
- [146] G. P. 494738A, **1938**.
- [147] P. A. Barrett, R. P. Linstead, F. G. Rundall, G. A. P. Tuey, *J. Chem. Soc.* **1940**, 1079-1092.
- [148] A. N. Cammidge, M. J. Cook, D. L. Hughes, F. Nekelson, M. Rahman, *Chem. Commun.* **2005**, 930-932.
- [149] A. N. Cammidge, I. Chambrier, M. J. Cook, D. L. Hughes, M. Rahman, L. Sosa-Vargas, *Chem. Eur. J.* **2011**, *17*, 3136-3146.
- [150] C. C. Leznoff, N. B. McKeown, *J. Org. Chem.* **1990**, *55*, 2186-2190.
- [151] Y.-H. Tse, A. Goel, M. Hu, A. B. P. Lever, C. C. Leznoff, J. E. Van Lier, *Can. J. Chem.* **1993**, *71*, 742-753.
- [152] a) W. B. Dandliker, M. L. Hsu, Google Patents, **1993**; b) W. B. Dandliker, M. L. Hsu, Google Patents, **1999**.
- [153] N. Alharbi, G. J. Tizzard, S. J. Coles, M. J. Cook, A. N. Cammidge, *Tetrahedron* **2015**, *in press*.
- [154] A. Díaz-Moscoso, G. J. Tizzard, S. J. Coles, A. N. Cammidge, *Angew. Chem. Int. Ed.* **2013**, *52*, 10784-10787.
- [155] D. S. Andrianov, V. B. Rybakov, A. V. Cheprakov, *Chem. Commun.* **2014**, *50*, 7953-7955.
- [156] S. M. Borisov, G. Zenkl, I. Klimant, *ACS Appl. Mater. Interfaces* **2010**, *2*, 366-374.
- [157] A. N. Cammidge, I. Chambrier, M. J. Cook, A. K. Ray, N. B. Chaure, *ECS J. Solid State Sci. Technol.* **2015**, *4*, 3086-3090.
- [158] a) Y. Takeuchi, A. Matsuda, N. Kobayashi, *J. Am. Chem. Soc.* **2007**, *129*, 8271-8281; b) N. Kobayashi, Y. Takeuchi, A. Matsuda, *Angew. Chem. Int. Ed.* **2007**, *46*, 758-760.
- [159] Y. Inokuma, Z. S. Yoon, D. Kim, A. Osuka, *J. Am. Chem. Soc.* **2007**, *129*, 4747-4761.
- [160] E. Tsurumaki, Y. Inokuma, S. Easwaramoorthi, J. M. Lim, D. Kim, A. Osuka, *Chem. Eur. J.* **2009**, *15*, 237-247.
- [161] A. Osuka, E. Tsurumaki, T. Tanaka, *Bull. Chem. Soc. Jpn.* **2011**, *84*, 679-697.
- [162] M. Pawlicki, K. Hurej, L. Szterenber, L. Latos-Grazynski, *Angew. Chem. Int. Ed.* **2014**, *53*, 2992-2996.
- [163] R. Myśliborski, L. Latos-Grażyński, L. Szterenber, T. Lis, *Angew. Chem.* **2006**, *118*, 3752-3756.
- [164] Y. Inokuma, A. Osuka, *Dalton Trans.* **2008**, 2517-2526.
- [165] T. Torres, *Angew. Chem. Int. Ed.* **2006**, *45*, 2834-2837.

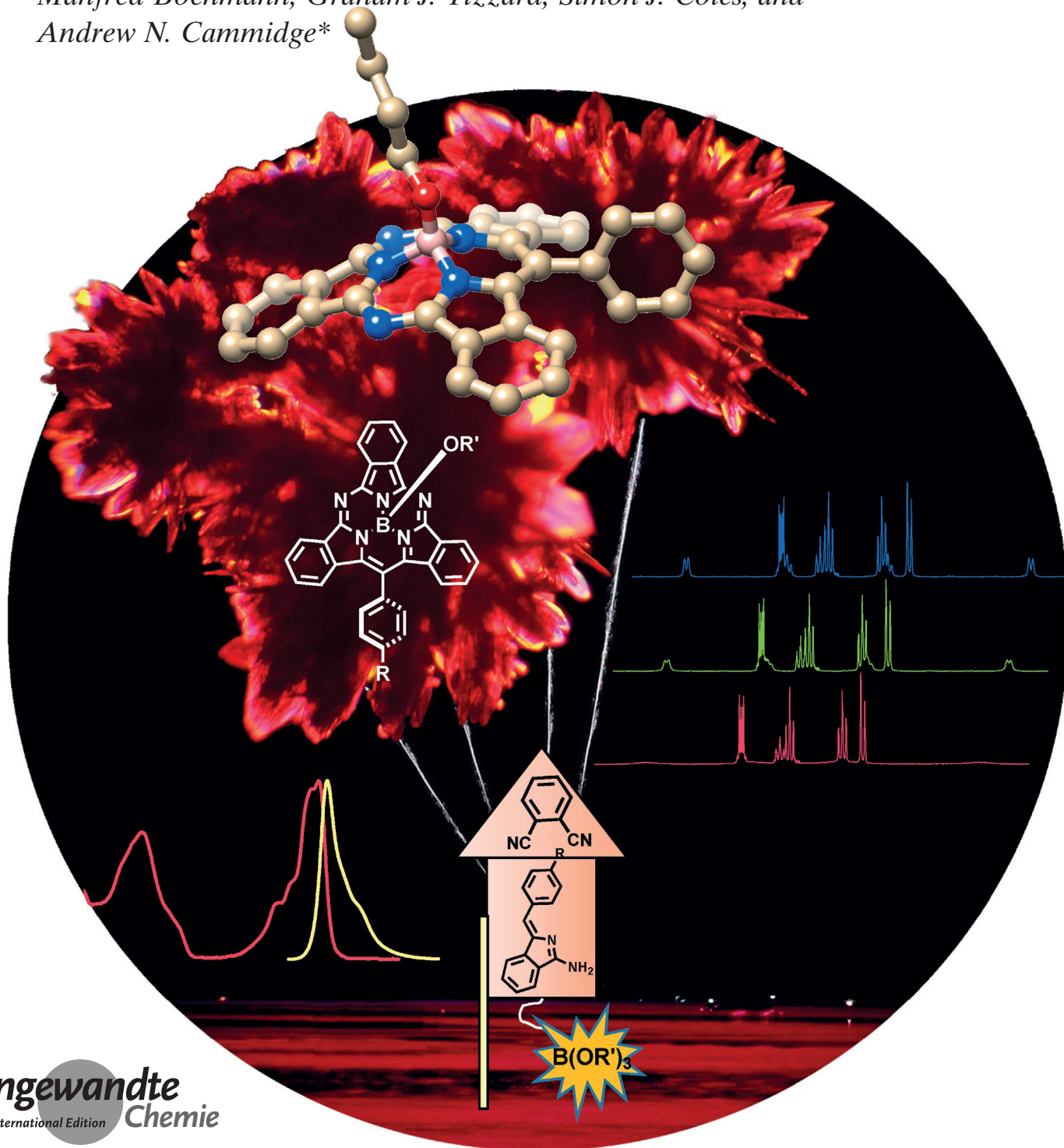
- [166] Y. Inokuma, J. H. Kwon, T. K. Ahn, M.-C. Yoo, D. Kim, A. Osuka, *Angew. Chem. Int. Ed.* **2006**, *45*, 961-964.
- [167] L. Edwards, M. Gouterman, C. B. Rose, *J. Am. Chem. Soc.* **1976**, *98*, 7638-7641.
- [168] E. A. Makarova, S. Shimizu, A. Matsuda, E. A. Luk'yanets, N. Kobayashi, *Chem. Commun.* **2008**, 2109-2111.
- [169] S. Dalai, V. N. Belov, S. Nizamov, K. Rauch, D. Finsinger, A. de Meijere, *Eur. J. Org. Chem.* **2006**, 2753-2765.
- [170] M. Hellal, G. D. Cuny, *Tetrahedron Lett.* **2011**, *52*, 5508-5511.
- [171] R. Chinchilla, C. Najera, *Chem. Soc. Rev.* **2011**, *40*, 5084-5121.
- [172] A. Díaz-Moscoso, E. Emond, D. L. Hughes, G. J. Tizzard, S. J. Coles, A. N. Cammidge, *J. Org. Chem.* **2014**, *79*, 8932-8936.
- [173] G. Ulrich, R. Ziessel, A. Harriman, *Angew. Chem. Int. Ed.* **2008**, *47*, 1184-1201.
- [174] A. Harriman, G. Izzet, R. Ziessel, *J. Am. Chem. Soc.* **2006**, *128*, 10868-10875.
- [175] L. Li, J. Han, B. Nguyen, K. Burgess, *J. Org. Chem.* **2008**, *73*, 1963-1970.
- [176] P. J. Dyson, J. S. McIndoe, *Transition Metal Carbonyl Cluster Chemistry*, Taylor & Francis, **2000**.
- [177] J. H. Simpson, *Organic Structure Determination Using 2-D NMR Spectroscopy: A Problem-based Approach*, Elsevier/AP, **2012**.
- [178] M. Bruch, *NMR Spectroscopy Techniques, Second Edition*, Taylor & Francis, **1996**.
- [179] D. Pavia, G. Lampman, G. Kriz, J. Vyvyan, *Introduction to Spectroscopy*, Cengage Learning, **2008**.
- [180] G. Ulrich, C. Goze, M. Guardigli, A. Roda, R. Ziessel, *Angew. Chem. Int. Ed.* **2005**, *44*, 3694-3698.
- [181] M. S. Newman, D. Lednicer, *J. Am. Chem. Soc.* **1956**, *78*, 4765-4770.
- [182] M. Yamaguchi, M. Shigeno, N. Saito, K. Yamamoto, *Chem. Rec.* **2014**, *14*, 15-27.
- [183] R. Amemiya, M. Yamaguchi, *Org. Biomol. Chem.* **2008**, *6*, 26-35.
- [184] R. Velapoldi, H. Tønnesen, *J. Fluoresc.* **2004**, *14*, 465-472.
- [185] Y. Inokuma, A. Osuka, *Chem. Eur. J.* **2009**, *15*, 6863-6876.
- [186] A. Weitemeyer, H. Kliesch, D. Woehrlle, *J. Org. Chem.* **1995**, *60*, 4900-4904.
- [187] C. G. Claessens, T. Torres, *Tetrahedron Lett.* **2000**, *41*, 6361-6365.
- [188] K. Adachi, H. Watarai, *Chem. Eur. J.* **2006**, *12*, 4249-4260.
- [189] C. Leblanc, R. A. Pulz, N. J. Stiefl, in *PCT Int. Appl.*, Novartis AG, Switz., **2009**, p. 146.
- [190] a) R. Ahlrichs, M. Bär, M. Häser, H. Horn, C. Kölmel, *Chem. Phys. Lett.* **1989**, *162*, 165-169; b) J. P. Perdew, *Physical Review B* **1986**, *33*, 8822-8824.
- [191] A. D. Becke, *Phys. Rev. A* **1988**, *38*, 3098-3100.

## **Appendix – Publication**

**“Synthesis of Meso-Substituted Subphthalocyanine–Subporphyrin Hybrids: Boron Subtribenzodiazaporphyrins”**

# Synthesis of Meso-Substituted Subphthalocyanine–Subporphyrin Hybrids: Boron Subtribenzodiazaporphyrins\*\*

Sonia Remiro-Buenamañana, Alejandro Díaz-Moscoso, David L. Hughes, Manfred Bochmann, Graham J. Tizzard, Simon J. Coles, and Andrew N. Cammidge\*





**Abstract:** The first syntheses of hybrid structures that lie between subphthalocyanines and subporphyrins are reported. The versatile single-step synthetic method uses a preformed aminoisindolene to provide the bridging methine unit and its substituent while trialkoxyborates simultaneously act as Lewis acid, template, and provider of the apical substituent. The selection of each component therefore allows for the controlled formation of diverse, differentially functionalized systems. The new hybrids are isolated as robust, pure materials that display intense absorption and emission in the mid-visible region. The new compounds are further characterized in solution and solid state by variable-temperature NMR spectroscopy and X-ray crystallography, respectively.

Macrocyclic oligopyrrole structures are ubiquitous in both nature and everyday life. The general class is exemplified by the two symmetric frameworks of porphyrin **1** (4 pyrrole units linked by methine bridges) and phthalocyanine **2** (4 isoindole units linked by nitrogen bridges; Figure 1). Many thousands of studies have been published covering their design, synthesis, properties, and applications, and research effort continues to increase.<sup>[1]</sup>

Of particular importance are recent synthetic efforts to prepare modified structures where the macrocyclic core (usually aromatic) itself is perturbed, yielding derivatives with fundamentally different properties and uses.<sup>[2–5]</sup> Studies have focused separately on ring-expanded<sup>[6]</sup> and -contracted<sup>[7]</sup> analogues. The manipulation of porphyrin-like structures has proved most straightforward for ring-expanded systems, with synthetic strategies building on established polypyrrole construction methods. Expanded phthalocyanine structures include the uranyl derivative **3**,<sup>[8]</sup> which comprises five indole-type units. Ring-contracted phthalocyanines<sup>[7]</sup> are especially intriguing and have been the subject of growing research efforts since the serendipitous formation of boron subphthalocyanine (SubPc, **4**) by Meller and Ossko in 1972.<sup>[9]</sup>

SubPcs<sup>[7,10]</sup> adopt a bowl-like conformation. The central boron atom bears a further apical group (X in **4**), which can be interchanged under appropriate conditions.<sup>[7]</sup> The optical properties of SubPcs are distinctive as they show intense absorption and emission around 550 nm, leading to a particular focus on their application as components in photovoltaic cells.<sup>[7,11–13]</sup> A small number of subporphyrins are also known, the most notable examples being the synthetic breakthroughs

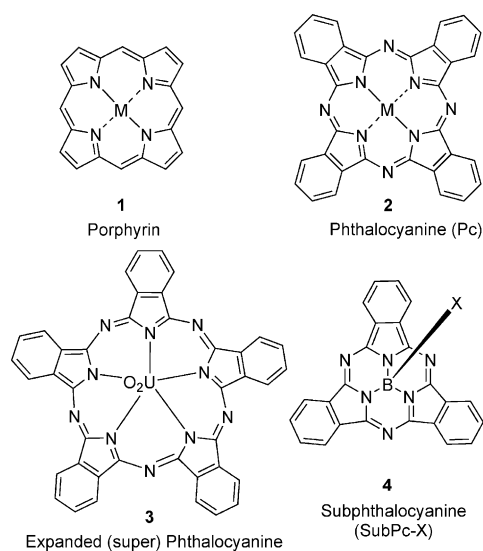


**Figure 1.** The parent structures porphyrin **1**, phthalocyanine **2**, expanded phthalocyanine **3**, and subphthalocyanine **4** (M = metal or H, H).

reported by Osuka and Kobayashi leading to the first syntheses of boron tribenzosubporphyrins **5**<sup>[14]</sup> and **6**<sup>[15]</sup> (Figure 2).

The most challenging core modification of the oligopyrrole/indole macrocycles is arguably the generation of hybrid structures<sup>[16]</sup> that lie between the classic porphyrin and phthalocyanine parent structures. The challenge posed by these systems is perhaps best illustrated by the limited number of studies to date,<sup>[16]</sup> despite their first identification being reported in the late 1930s by Dent<sup>[17]</sup> and the Linstead group.<sup>[18]</sup> The greatest drawback to the investigation of the hybrid structures is the limited synthetic possibilities available to access modified and bespoke derivatives. Nevertheless, interest in the hybrid structures has accelerated rapidly over the last decade even though most syntheses have relied on the original procedures, albeit with some improvements.<sup>[16,19,20]</sup> We recently reported a significant breakthrough in this area,<sup>[21]</sup> disclosing a new, versatile procedure that gives controlled access to functionalized TBTAPs (TBTAP = tetrabenzotriazaporphyrin, a phthalocyanine–tetrabenzoporpyrin hybrid in which a single aza bridge of the Pc ring is replaced by carbon). Importantly, the synthesis allows for the introduction of substituents at the “new” meso site. Cheprakov and co-workers<sup>[22]</sup> have subsequently reported a complementary approach to a second member of the hybrid series,

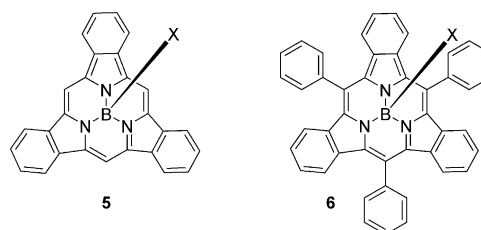


**Figure 2.** Tribenzosubporphyrins reported by the Osuka (**5**) and Kobayashi (**6**) groups.

[\*] S. Remiro-Buenamañana, Dr. A. Díaz-Moscoso, Dr. D. L. Hughes, Prof. M. Bochmann, Prof. A. N. Cammidge  
School of Chemistry, University of East Anglia  
Norwich Research Park, Norwich NR4 7TJ (UK)  
E-mail: a.cammidge@uea.ac.uk

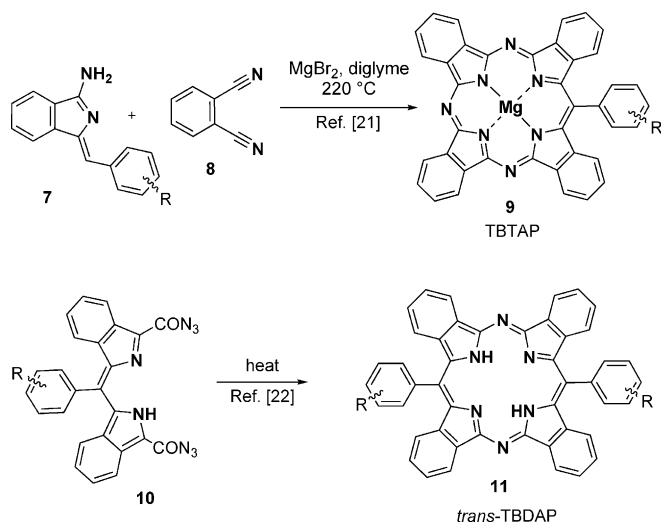
Dr. G. J. Tizzard, Dr. S. J. Coles  
UK National Crystallography Service, School of Chemistry  
University of Southampton, Southampton SO17 1BJ (UK)

[\*\*] Support from the UEA (S.R.-B.), the EU (A.D.-M.), and the EPSRC (the National Crystallography and Mass Spectrometry Services) is gratefully acknowledged. We thank Dr. C. MacDonald and Prof. P. Ballester for help with NMR measurements and calculations, respectively.



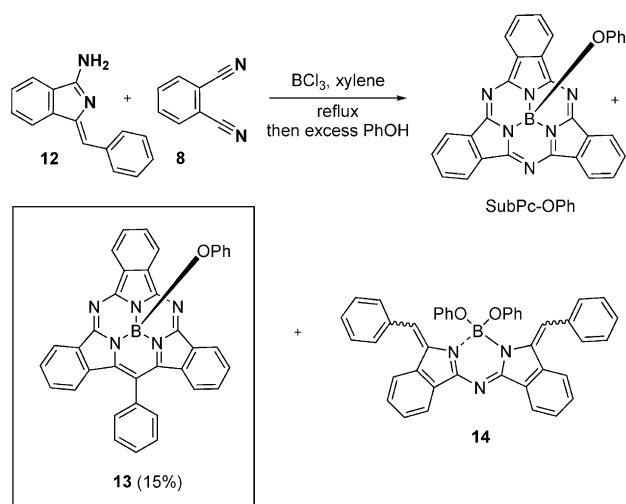
Supporting information for this article is available on the WWW under <http://dx.doi.org/10.1002/anie.201502662>.

the *trans*-TBDAPs (Scheme 1). Until now, hybrid structures based on the ring-contracted systems, SubPc and tribenzo-SubPn, are unknown. Herein, we report a versatile method that provides access to the first examples of such hybrids, alongside a preliminary examination of their properties.



**Scheme 1.** Synthetic breakthroughs giving straightforward access to functionalized porphyrin–phthalocyanine hybrids.

The optimized synthesis of SubPc **4** (X = Cl) typically involves the reaction of phthalonitrile (**8**) with BCl<sub>3</sub> at elevated temperature (xylene at reflux).<sup>[7,23]</sup> In these reactions, the boron reagent acts as a Lewis acid and as a template. In our recently developed synthesis of TBTAP hybrids **9**, we employed aminoindolene precursor **7** to initiate the macrocyclization process around a magnesium template ion, and we therefore reasoned that the same precursor could potentially initiate macrocyclization in the presence of a boron template leading to a hybrid in which a (functionalized) meso carbon atom formally replaces one of the bridging nitrogen atoms present in the SubPc parent. The target product is a boron subtribenzodiazaporphyrin (SubTBDAP). Consequently, in the initial set of successful reactions, aminoindolene **12**<sup>[24]</sup> was reacted with phthalonitrile in the presence of BCl<sub>3</sub> in xylene at reflux. Three distinct, highly colored products were formed. The first product was identified as the simple, symmetric SubPc-Cl, formed by the expected homomacrocyclization of phthalonitrile. MALDI-MS studies strongly implied that the other two new compounds were the required SubTBDAP-Cl and the azaBO-DIPY-type compound formed from self-condensation<sup>[25]</sup> of the aminoindolene precursor **12** followed by complexation with boron. However, attempts to isolate and characterize the new products were impeded by the reactivity of the labile B–Cl bond present in all components of the mixture. Therefore, in a subsequent reaction (Scheme 2), macrocyclization was performed again, but followed directly by treatment of the crude product mixture with an excess amount of phenol to convert all B–Cl fragments into stable B–OPh moieties. Separation of the mixture could then be achieved by



**Scheme 2.** Synthesis of a boron subphthalocyanine–subporphyrin hybrid, a so-called SubTBDAP (**13**).

chromatography, allowing for the isolation of the first pure SubTBDAP **13** as a bright pink material with intense yellow fluorescence ( $\phi \approx 0.5$ , Stokes shift ca. 15 nm). The yield (15%) is impressive, especially when compared to typical yields of both simple SubPcs and unsymmetric phthalocyanines. The absorption and emission spectra are compared to those of the parent SubPc (**4**, X = OPh) in Figure 3. The

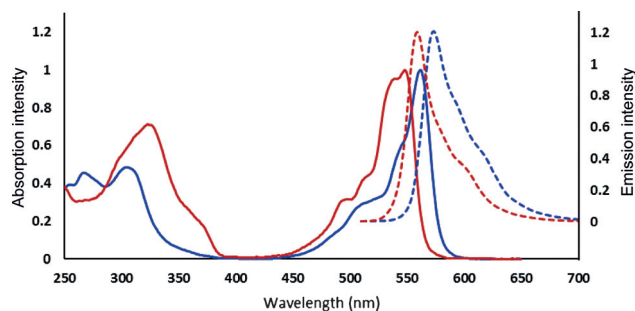


**Figure 3.** Absorption (—) and emission (---) spectra of hybrid SubTBDAP **13** (red) and SubPc-OPh (blue).

absorbance and fluorescence maxima are both blue-shifted by approximately 10–20 nm compared to those of SubPc, reflecting the change towards a more porphyrin-like character in the hybrid **13**. The absorption spectrum of SubTBDAP also shows the main band to be split—a consequence of the reduced symmetry in the macrocyclic chromophore core. The blue shift also indicates that as expected, the appended meso phenyl substituent does not contribute to the main  $\pi$ -system, lying essentially perpendicular to the SubTBDAP core. This parallels the arrangement in both the well-known meso-phenyl porphyrins and the meso-aryl TBTAPs.

The <sup>1</sup>H NMR spectrum for hybrid **13** at room temperature shows the expected signals for the macrocyclic core and the apical O–Ph group (signals for the O–Ph group are shielded by the core ring current). However, the signals for the *ortho*- and *meta*-hydrogen atoms of the meso phenyl substituent are



very broad and featureless, indicating slow rotation of the group. Lowering the temperature leads to sharpening and resolution of the signals (Figure 4). A large chemical shift difference is observed for the two doublets corresponding to the *ortho*-hydrogen atoms, and they were assigned based on their sensitivity to interchange of the apical alkoxide substituent.  $H_o$ , which lies under the conical macrocycle, appears at approximately 6.9 ppm in all cases, whereas the resonance

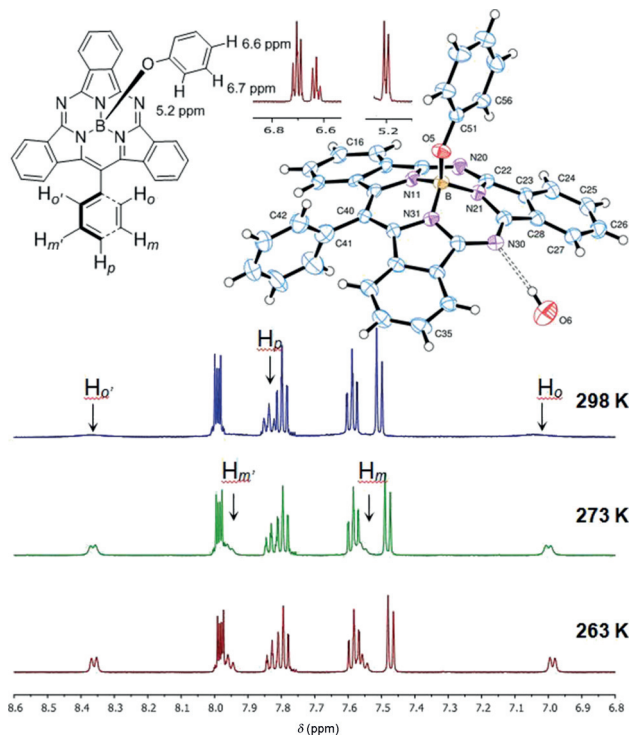
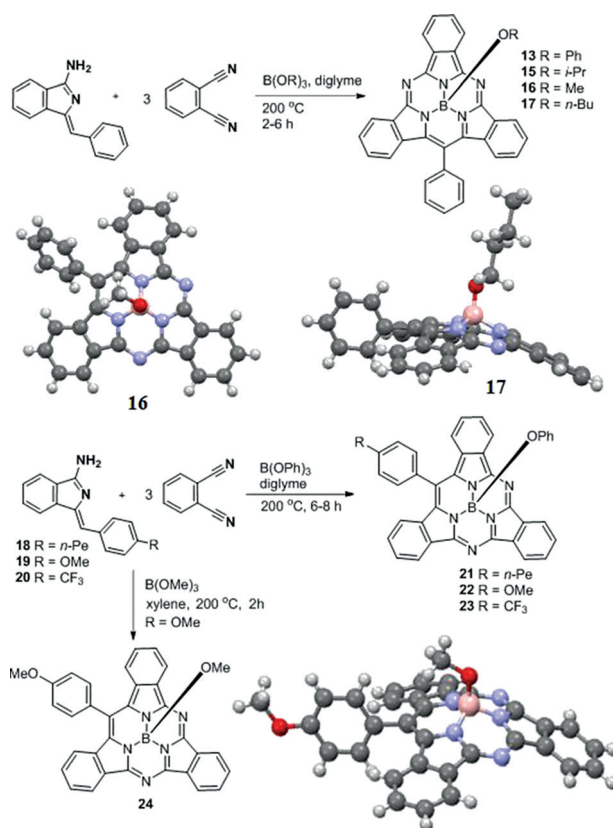


**Figure 4.** Variable-temperature  $^1\text{H}$  NMR spectra of hybrid **13** and its crystal structure.

for  $H_o$ , the proton lying on the same side as the alkoxide, is sensitive to its nature and is seen in the range of 8.2–8.6 ppm. The assignment was further supported by calculations (see the Supporting Information). Crystals suitable for X-ray diffraction were eventually grown from a mixture of acetone and hexane allowing for the determination of the solid-state structure.<sup>[26]</sup> In the crystal, the boron atom is bonded to the three pyrrole nitrogen atoms and the phenoxy oxygen atom (which is in the apical site of the pyramidal arrangement) in a tetrahedral (or trigonal pyramidal) arrangement (Figure 4). The boron atom is displaced 0.614(5) Å from the plane of the three N atoms, and the SubTBDAP ring system is wrapped around the base; each benzene ring plane is tilted by approximately 20° with respect to the plane of the three pyrrole N atoms away from the phenoxy group. The meso phenyl group was confirmed to be lying essentially perpendicular to the SubTBDAP core.

The SubTBDAP molecules are arranged in pairs with the overlapping, centrosymmetrically related N21/C29 isindole rings approximately 3.62 Å apart; these groups are also bridged by a pair of solvent water molecules, which appear to form hydrogen bonds to the nitrogen atoms N20 and N30.

The synthesis outlined above allowed for the isolation of a SubTBDAP hybrid. However, the versatility of the procedure suffers from the practical drawback of the simultaneous formation of a symmetric SubPc. The formation of the SubPc is of course expected because these initial conditions are known to lead to the macrocyclization of phthalonitrile alone. We therefore turned our attention to the development of reaction conditions that would lead to the formation of the hybrid structures (macrocyclization initiated by aminoisindolenes **7**) without competing formation of the SubPc. This was achieved by employing less reactive boronate esters as the Lewis acid/template, recognizing that phthalonitrile itself requires a more reactive boron source for SubPc formation. The use of boronate esters ( $\text{B}(\text{OR})_3$ ) has the added advantage of leading directly to the stable SubTBDAP-OR variants in a single operation (Scheme 3). Diglyme was found to be



**Scheme 3.** Versatile syntheses of TBDAP hybrids enabling the selective functionalization at the meso aryl and apical sites.

a convenient and suitable solvent, and the reaction between the aminoisindole precursor and phthalonitrile (1:3) proceeded smoothly at 200 °C in three hours. SubPc was not formed, and the hybrid SubTBDAPs were easily isolated. Yields were marginally lower than for the stepwise procedure (typically around 10%) but compensated by synthetic convenience and versatility. Excess phthalonitrile can be recovered from the reaction alongside the hydrolysis products (phthalimide). The main side products are the expected azadipyrromethene (from self-condensation) and polar/oligo-

meric baseline material. The reactions can also be performed in xylene or indeed in the absence of solvent.

The scope of the method has been demonstrated by the derivatives prepared to date (Scheme 3). The selection of a boronate ester template leads to control over the apical substituent (**13**, **15–17**). Most significant, however, is the ability to engineer the new “meso” substituents at will—synthetic control that makes this new class of hybrid structures uniquely attractive. Aminoisoindolones **7** are easily prepared from acetylenic precursors,<sup>[24]</sup> and the macrocyclization reaction tolerates the manipulation of this group, which was exemplified by the formation of **21–23**, examples of hybrid SubTBDAPs bearing alternative aryl substituents. All of the products were isolated as pure, freely soluble, crystalline solids. Crystal structures have been obtained for **15–17** (see the Supporting Information for that of **15**) and also for **24** (Scheme 3).<sup>[26]</sup>

In conclusion, we have reported the first examples of a new class of hybrid macrocyclic systems whose core structure lies between those of subphthalocyanines and subporphyrins. The synthesis is controlled, allowing for the manipulation of the functional groups at both the central boron atom and importantly at the new meso site. Of particular significance is the synthetic ease and versatility that will permit imaginative design of bespoke materials to exploit the intrinsic potential of the intriguing core structure.

**Keywords:** dyes/pigments · heterocycles · phthalocyanines · porphyrinoids · synthetic methods

**How to cite:** *Angew. Chem. Int. Ed.* **2015**, *54*, 7510–7514  
*Angew. Chem.* **2015**, *127*, 7620–7624

- [1] a) *The Porphyrin Handbook*, Vols. 1–20 (Eds.: K. M. Kadish, K. M. Smith, R. Guilard), Academic Press, **2000–2003**; b) *Handbook of Porphyrin Science*, Vols. 1–20 (Eds.: K. M. Kadish, K. M. Smith, R. Guilard), World Scientific Publishing, **2010–2012**.
- [2] *Expanded, Contracted and Isomeric Porphyrins* (Eds.: J. L. Sessler, S. J. Weighorn), Pergamon, Oxford, **1997**.
- [3] D. Kuzuhara, Y. Sakakibara, S. Mori, T. Okujima, H. Uno, H. Yamada, *Angew. Chem. Int. Ed.* **2013**, *52*, 3360–3363; *Angew. Chem.* **2013**, *125*, 3444–3447.
- [4] R. Misra, T. K. Chandrashekar, *Acc. Chem. Res.* **2008**, *41*, 265–279.
- [5] O. Matsushita, V. M. Derkacheva, A. Muranaka, S. Shimizu, M. Uchiyama, E. A. Luk'yanets, N. Kobayashi, *J. Am. Chem. Soc.* **2012**, *134*, 3411–3418, and references therein.
- [6] S. Saito, A. Osuka, *Angew. Chem. Int. Ed.* **2011**, *50*, 4342–4373; *Angew. Chem.* **2011**, *123*, 4432–4464.
- [7] C. G. Claessens, D. Gonzalez-Rodriguez, M. S. Rodriguez-Morgade, A. Medina, T. Torres, *Chem. Rev.* **2014**, *114*, 2192–2277.
- [8] V. W. Day, T. J. Marks, W. A. Wachter, *J. Am. Chem. Soc.* **1975**, *97*, 4519–4527.
- [9] A. Meller, A. Ossko, *Monatsh. Chem.* **1972**, *103*, 150–155.
- [10] a) C. G. Claessens, D. Gonzalez-Rodriguez, T. Torres, *Chem. Rev.* **2002**, *102*, 835–853; b) P. J. Brothers, *Inorg. Chem.* **2011**, *50*, 12374–12386.
- [11] K. L. Mutolo, E. I. Mayo, B. P. Rand, S. R. Forrest, M. E. Thompson, *J. Am. Chem. Soc.* **2006**, *128*, 8108.
- [12] H. Kumar, P. Kumar, R. Bhardwaj, G. D. Sharma, S. Chand, S. C. Jain, V. Kumar, *J. Phys. D* **2009**, *42*, 015103.
- [13] H. Gommans, T. Aernouts, B. Verreet, P. Heremans, A. Medina, C. G. Claessens, T. Torres, *Adv. Funct. Mater.* **2009**, *19*, 3435–3439.
- [14] Y. Inokuma, J. H. Kwon, T. K. Ahn, M.-C. Yoo, D. Kim, A. Osuka, *Angew. Chem. Int. Ed.* **2006**, *45*, 961–964; *Angew. Chem.* **2006**, *118*, 975–978.
- [15] E. A. Makarova, S. Shimizu, A. Matsuda, E. A. Luk'yanets, N. Kobayashi, *Chem. Commun.* **2008**, 2109–2111.
- [16] “Synthesis and Properties of the Hybrid Phthalocyanine-Tetrazobenzoporphyrin Macrocycles”: A. N. Cammidge, I. Chambrier, M. J. Cook, L. Sosa-Vargas in *Handbook of Porphyrin Science*, Vol. 16 (Eds. K. M. Kadish, K. M. Smith, R. Guilard), World Scientific Publishing Company, Singapore, **2012**, pp. 331–404.
- [17] C. E. Dent, *J. Chem. Soc.* **1938**, 1–6.
- [18] P. A. Barrett, R. P. Linstead, G. A. P. Tuey, J. M. Robertson, *J. Chem. Soc.* **1939**, 1809–1820.
- [19] A. N. Cammidge, I. Chambrier, M. J. Cook, D. L. Hughes, M. Rahman, L. Sosa-Vargas, *Chem. Eur. J.* **2011**, *17*, 3136–3146.
- [20] a) N. E. Galanin, E. V. Kudrik, G. P. Shaposhnikov, *Russ. J. Gen. Chem.* **2004**, *74*, 282–285; b) N. E. Galanin, L. A. Yakubov, E. V. Kudrik, G. P. Shaposhnikov, *Russ. J. Gen. Chem.* **2008**, *78*, 1436–1440.
- [21] A. Díaz-Moscoso, G. J. Tizzard, S. J. Coles, A. N. Cammidge, *Angew. Chem. Int. Ed.* **2013**, *52*, 10784–10787; *Angew. Chem.* **2013**, *125*, 10984–10987.
- [22] D. S. Andrianov, V. B. Rybakov, A. V. Cheprakov, *Chem. Commun.* **2014**, *50*, 7953–7955.
- [23] C. G. Claessens, D. Gonzalez-Rodriguez, B. del Ray, T. Torres, G. Mark, H.-P. Schuchmann, C. von Sonntag, J. G. MacDonald, R. S. Nohr, *Eur. J. Org. Chem.* **2003**, 2547–2551.
- [24] M. Hellal, G. D. Cuny, *Tetrahedron Lett.* **2011**, *52*, 5508–5511.
- [25] A. Díaz-Moscoso, E. Emond, D. L. Hughes, G. J. Tizzard, S. J. Coles, A. N. Cammidge, *J. Org. Chem.* **2014**, *79*, 8932–8936.
- [26] CCDC 1046860 (**13**), 1052412 (**15**), 1044583 (**16**), 1044584 (**17**), and 1044585 (**24**) contain the supplementary crystallographic data for this paper. These data can be obtained free of charge from The Cambridge Crystallographic Data Centre via [www.ccdc.cam.ac.uk/data\\_request/cif](http://www.ccdc.cam.ac.uk/data_request/cif).

Received: March 23, 2015

Published online: May 15, 2015